INVESTIGATING THE PERFORMANCE OF GENERATOR PROTECTION RELAYS USING A REAL-TIME SIMULATOR

by

Yu-Ting Huang

Submitted in the fulfilment of the academic requirement for the degree of Master of Science in Engineering, in the School of Electrical, Electronic and Computer Engineering, University of KwaZulu-Natal, Durban, South Africa.

November 2013

DECLARATION 1 – PLAGIARISM

I ,Yu-Ting Huang, declare that:

1. The research reported in this thesis, except where otherwise indicated, is my original research.

2. This thesis has not been submitted for any degree or examination at any other university.

3. This thesis does not contain other persons' data, pictures, graphs or other information, unless specifically acknowledged as being sourced from other persons.

4. This thesis does not contain other persons' writing, unless specifically acknowledged as being sourced from other researchers. Where other written sources have been quoted, then:

    a. Their words have re-written but the general information attributed to them has been referenced;
    b. Where their exact words have been used, then their writing has been placed in italics and inside quotation marks, and referenced.

5. This thesis does not contain text, graphics or tables copied and pasted from the Internet, unless specifically acknowledged, and the source being detailed in the thesis and in the References sections.

Yu-Ting Huang ....
(BScEng) Signature Date

As the candidate's Supervisor I agree to the submission of this thesis.

Supervisor: Bruce Rigby ....
(BScEng, MScEng, PhD (Natal), MIEEE) Signature Date

DECLARATION 2 – PUBLICATIONS

DETAILS OF CONTRIBUTION TO PUBLICATIONS that form part and/or include research presented in this thesis (include publications in preparation, submitted, *in press* and published and give details of the contributions of each author to the experimental work and writing of each publication).

Publication 1:

Y-T Huang, B S Rigby, A B Dehkordi: "Using a new faulted synchronous machine model for hardware-in-loop testing of a generator protection relay", Southern African Power System Protection Conference, 2012.

Publication 2:

Y-T Huang, B S Rigby: "Design and Real-Time Simulator Testing of Generator Protection Schemes for Low- and High-Impedance Grounding Methods", PAC World Conference, Cape Town, 2013.

This thesis is dedicated to my family.

ABSTRACT

Real-time simulators have been utilized to perform hardware-in-loop testing of protection relays and power system controllers for some years. However, hardware-in-loop testing of generator protection relays has until recently been limited by a lack of suitable dynamic models of synchronous generators in the real-time simulation environment. Historically, the Park transformation has been chosen as the mathematical approach for dynamic modelling of electrical machines in simulation programs, since it greatly simplifies the dynamic equations. However, generator internal winding faults could not be represented faithfully with the aforementioned modelling approach due to its mathematical limitations. Recently, a new real-time phase-domain, synchronous machine model has become available that allows representation of internal winding faults in the stator circuits of a synchronous machine as well as faults in the excitation systems feeding the field circuits of these machines. The development of this phase-domain synchronous machine model for real-time simulators opens up the scope for hardware-in-loop testing of generator protection relays since the performance of various generator protection elements can now be examined using the advanced features provided by the new machine model.

This thesis presents a thorough, research-based analysis of the new phase-domain synchronous generator model in order to assess its suitability for testing modern generator protection schemes. The thesis reviews the theory of operation and settings calculations of the various elements present in a particular representative modern numerical generator protection relay and describes the development of a detailed, real-time digital simulation model of a multi-generator system suitable for studying the performance of the protection functions provided within this relay. As part of the development of this real-time model, the thesis presents a custom-developed real-time modelling approach for representing the load-dependent third-harmonic voltages present in the windings of a large synchronous generator which are needed in order to test certain types of stator-winding protection schemes.

The thesis presents the results of detailed, closed-loop testing of the representative generator protection relay hardware and its settings using the developed models on a real-time digital simulator. The results demonstrate the correctness of the modelling and testing approach and show that using the phase-domain synchronous machine model, together with the supplementary models presented in the thesis, it is possible to evaluate the performance of various generator protective functions that could not otherwise have been analysed using conventional machine models and testing techniques.

ACKNOWLEDGEMENTS

I would like to express my immense gratitude towards Professor Rigby, for supervising my work during this thesis and providing valuable guidance time and time again; furthermore the efforts put into the correction of the thesis and provision of funds are much appreciated.

Some of the modelling approaches used in this thesis came from the ideas of Dr Ali Dehkordi of RTDS Technologies, Canada. I am grateful to Dr Dehkordi for these ideas, as well as for a number of example cases he provided for the RTDS simulators that were most helpful when learning the SEL 300G protection relay.

I would also like to thank the staff at Durban University of Technology, especially F. D'Almaine and Regina Naidoo for their support and encouraging words during my studies.

Thanks go to my many friends and colleagues, who over the years offered their kindness and encouragement, especially Chenal Palhad from the Postgraduate Research Laboratory, for his valuable advice and encouragement.

The University of KwaZulu-Natal, Durban University of Technology and Schweitzer Engineering Laboratory South Africa are gratefully acknowledged for providing equipment and facilities to conduct my research in; the work could not have been completed to a high standard without them.

Finally, I wish to thank my family for their patience, love and support during the years of my studies.

TABLE OF CONTENTS

CHAPTER 3

STUDY SYSTEM

CHAPTER 4

THEORY AND SETTINGS FOR LOW-RESISTANCE GROUNDED GENERATOR PROTECTION STUDIES

CHAPTER 5

HIL TESTING OF LOW-RESISTANCE GROUNDED GENERATOR PROTECTION STUDY SYSTEM

CHAPTER 6

100% STATOR GROUND PROTECTION FOR HIGH-RESISTANCE GROUNDED GENERATORS

LIST OF FIGURES

LIST OF TABLES

LIST OF SYMBOLS

Acronyms

RTDS	Real-Time Digital Simulator
DSP	Digital Signal Processor
GUI	Graphical User Interface
DAC	Digital to Analogue Converter
WIF	Workstation Interface
IRC	Inter-Rack Communication
A/D	Analogue to Digital Converter
IED	Intelligent Electronic Devices
RAM	Random Access Memory
CPU	Central Processing Unit
TCC	Time-Current Characteristic
MWFA	Modified Winding Function Approach
AVR	Automatic Voltage Regulator
PSS	Power System Stabilizer
DFT	Discrete Fourier Transform

CHAPTER 1

INTRODUCTION

1.1 General Background

New generation and transmission facilities are being constructed due to the increasing power demand from both society and industry. Since electricity is one of the basic necessities nowadays, fast growing population leads to higher demand for power. Rapid economic development prompts industrial activities and hence also increases the power demand. Since both society and industry rely heavily on electricity, unexpected power outages are not desirable. From past experiences, numerous large-scale black-outs have been caused by incorrect setting of protection relays and bad coordination between different protection elements [1],[2]. In order to minimize the disruption to the system and loss of supply to customers as a result of these problems in future, better modelling and testing tools are required for engineers to design more secure protection systems. Power system protection is important in all aspects of the power system such as generation, transmission and distribution. The objective of the protection relay is to isolate the faulted section of the power system in a fast manner. The time taken for the protection relay to remove the fault is known as fault clearing time. The fault clearing time can have a significant influence on the system's stability. In the case of some generator and transmission system faults, if the fault is not cleared sufficiently quickly (within the critical clearing time), one or more generators may lose synchronism and eventually be tripped out by their generator protection relays. Loss of generation capacity during or after a fault puts more stress on other generators still connected to the system, and on the system as a whole; therefore it can also have adverse knock-on effects on system stability such as voltage collapse due to insufficient reactive power support [3].

It is a great challenge for protection engineers to design a protection system with high security since the complexity of interconnected power systems has increased due to the increasing demand for power. In order to understand the behaviour of complex power systems under steady-state or transient conditions, different power system simulators have typically been used such as PSCAD, EMTP/ATP, PSS/E and DIgSILENT [4],[5]. These power system simulators are used to simulate different system scenarios and contingencies, and the results can be used for protection relay settings or design of power system controllers.

The development of real-time digital simulation opened up a whole new approach for protection relay testing and power system controller testing. Before the advent of real-time simulation, protection relays and power system controllers were often tested using open-loop injection of test currents and voltages into the physical equipment. Open-loop testing has a significant disadvantage

since the protection relays can only be tested under pre-simulated test scenarios and their interaction with the power system cannot be predicted. Due to this limitation, the performance of some protection elements could not be verified via open-loop tests. However, these limitations of open-loop relay and controller testing were greatly reduced after real-time simulators became available. Over the years, use of real-time simulators became more and more widespread because they possess certain capabilities which conventional power system simulation lacks [5],[6]. Real-time simulators provide the capability to conduct detailed closed-loop testing of physical protection hardware that allows live interaction between the power system simulation model and the physical equipment under test.

It has been possible to conduct highly-detailed closed-loop testing of most types of protection relays and system controllers using real-time simulators for some years [7],[8],[9]. However, generator protection is one area where the full potential of real-time simulator testing could not initially be realised because the mathematical models used to represent the electrical machines in simulation studies have had some limitations. The dynamic equations of electrical machines are typically recast into a two-axis (dq) coordinate frame using the Park transform for more convenient solution in power system simulation programs. This two-axis mathematical model of the generator is highly detailed and well-suited for use in power system stability studies in which the dynamic response of the generators to external disturbances is of interest. However, it is not suitable for testing most generator protection relay functions because of the two-axis structure of the model's dynamic equations, with which it has not historically been possible to represent internal winding faults accurately. However, the recent development of phase-domain real-time synchronous machine models has opened up new scope for generator protection relay testing [10].

The settings of generator controllers and protection systems and the margin between generator operating points and their capability limits all have important influences on the stability of the system as a whole. If the generators have tight operating margins, the stress of the power system increases and therefore the system is more susceptible to disturbances. The coordination between different generator controllers and generator protection elements is also important. Poorly coordinated protection systems can trip the generator during the post-fault period [1],[2]. Misoperation of the protection systems on any item of electrical equipment, but especially of those protecting a generator, will pose a large disturbance to the system and threaten the stability of the power system. The study of generator protection systems and their performance is closely linked to the area of power system stability because generators play such a big role in the stability of the power system as a whole. Furthermore, the operation of a generator's protection schemes will influence the power system's stability, and power system stability issues will in turn affect the performance of individual generator protection schemes. Hence, the study of generator protection

requires some understanding of both generator and system stability. The diagram shown in Figure 1.1 illustrates how different stability issues in the power system are classified within the broad subject area of power system stability.

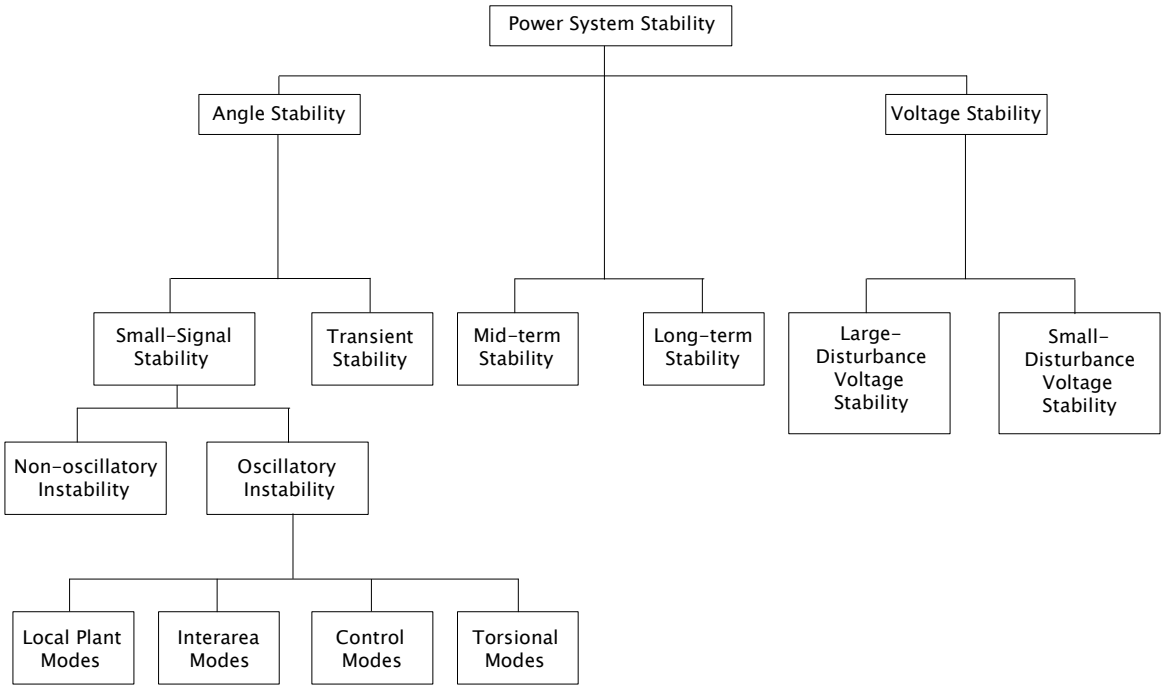

Figure 1.1. Classification of power system stability (reproduced from [11]).

1.2 The Real-Time Simulator

The work presented in this thesis was carried out on a RTDS Technologies real-time digital simulator (RTDS^{TM}). Although the RTDS is a type of power system simulator, its philosophy is somewhat different from conventional power system simulators. The principal purpose of the real-time simulator is not just to execute the simulation in real time but also to allow physical equipment under study to be connected to it, thereby allowing advanced testing of protection relays and system controllers to be carried out relatively easily.

The technology used to implement protection functions has developed from electromechanical relays to sophisticated microprocessor-based relays. Modern protection relays are highly complex systems and it is very difficult to represent the detailed characteristics of an individual manufacturer's relays in a power system simulation by means of mathematical models [12]. This is one of the reasons why the real-time simulator is a favourable option for protection engineers since it can be used for hardware-in-loop testing of actual protection relays and system controllers. The equipment that is connected to the real-time simulator for testing can interact with the power

system simulation in real time. The hardware-in-loop testing can be used for the verification of the equipment performance under different system scenarios and contingencies.

RSCAD is the software for the real-time simulator which comprises a group of sub-programs (DRAFT, RUNTIME, TLINE, CABLE and MULTIPLOT) that are used to program, run and control the real-time simulator. Both DRAFT and RUNTIME are Graphical User Interface (GUI) based sub-programs. Detailed models of the power system can be developed in DRAFT while the development of the visual interface for monitoring and interaction purposes is done in RUNTIME [13]. Over the years, the environment of RSCAD has been improved due to collaboration between the manufacturer of the simulator and some well-known companies in the field of electrical engineering [14],[15],[16]. The real-time simulator is usually used for hardware-in-loop testing of physical equipment. However, it is not always necessary to connect a specific manufacturer's physical equipment to the real-time simulator if the user wants to perform closed-loop analysis of a category of protection or control equipment and its interaction with the power system under study. The control system modelling software in RSCAD offers various control system component models which can be used for the development of real-time simulation models of the test equipment [12]. The software also provides different pre-developed generic models of protection relays for real-time simulation studies [17]. These generic relay models are highly-detailed and possess all the principal functional elements typically found in actual protection relay hardware. In the protection studies carried out in this thesis, the generic dynamic model of a generator protection relay provided within RSCAD was used in parallel with an actual manufacturer's protection relay hardware (SEL 300G) in order to gain further insight into the hardware relay's behaviour during the tests.

1.3 Thesis background and objectives

The performance of many protection relays can, and has been, successfully evaluated by conducting hardware-in-loop testing using a real-time simulator. However, the performance of some generator protection elements could not previously be evaluated in this way due to certain limitations of the mathematical approach normally used for dynamic modelling of synchronous machines in simulation programs. The well-known two-axis synchronous machine model had a limited ability to represent internal winding faults in the stator circuits of the machine and therefore none of the generator stator winding protection schemes could be evaluated using such models.

A recently-developed phase-domain synchronous machine model has the ability to represent internal winding faults on the stator circuit of a generator. This new machine model also allows detailed electrical circuit representation of the generator's excitation input. The research in this thesis has been motivated by the development of this machine model, since its capabilities now

enable important additional elements of generator protection relays to be tested which technically could not be achieved in the past.

Although some proof-of-principle studies have been carried out by using the generic RSCAD generator protection relay model in order to demonstrate the capabilities of the new phase-domain synchronous machine model [18], there is very little experience on the real-time closed-loop testing of any actual generator protection relay hardware using this new machine model. The aim of this thesis was to carry out a thorough, research-based analysis of the new synchronous generator model and its application in generator protection and control studies using an actual manufacturer's protection relay hardware (SEL 300G), with the objective being to gain a better understanding of the strengths and limitations of the newly developed phase-domain synchronous machine model. At the same time, the performance of particular protection elements provided by the generator protection relay, and the most appropriate way to set them, can be better understood through such a study as a result of the ability to test these elements in a realistic manner using the new generator model.

1.4 Thesis layout

This thesis has eight main chapters. Chapter One provides the introduction and background to the thesis and the motivation behind the work.

Chapter Two provides an overview of general power system protection concepts together with different protection philosophies and technologies. A general review of all the different types of protection element commonly used in generator protection is also presented in this chapter. Finally, the chapter provides some background to the generator modelling and testing approaches that are followed in the thesis.

Chapter Three reviews the main functional elements and theory of operation of both the RSCAD generic real-time model of a generator protection relay and the actual hardware protection relay (SEL 300G), both of which are used in the studies of the thesis. The chapter then presents the details of the chosen study system and development of the real-time model of this system used in later chapters. The details of the interfacing of this real-time model to the testing equipment are also included in order to demonstrate how hardware-in-loop testing is carried out for this particular research project.

Chapter Four focuses in more detail on the theory of operation and setting calculations of the particular generator protection elements that are actually used in the research study, namely phase

percentage restrained differential protection (87P), loss-of-field protection (40) and out-of-step protection (78). Different setting considerations for each element are also discussed within this chapter.

Chapter Five contains different hardware-in-loop testing results under various fault scenarios for each of the generator protection elements described in Chapter Four. The results of these tests are used to assess the performance and limitations of each of the studied protection elements.

In the detailed theory and studies presented in Chapter Four and Five of the thesis, the generator is assumed to be grounded using a low-resistance grounding scheme for which differential protection of the stator winding is appropriate. The alternative method of grounding a generator is by means of some form of high-resistance grounding technique which then requires the use of very different types of protection against ground faults in the stator windings. Two distinct protection schemes are commonly used for generator stator winding protection when the generator is grounded through high resistance: either a neutral injection scheme (64S) or a 100% stator ground fault protection scheme (64G) can be used to provide full protection coverage for the generator winding. However, a 100% stator ground fault protection scheme is the focus in this thesis since this is the protection scheme provided by the particular hardware relay (SEL 300G) that was available for this work. Chapter Six describes the recommended practice and procedures followed in the thesis to design a high-resistance grounding scheme for the generators in the study system and the modelling of this system in the real-time simulation environment so that the subsequent testing of the SEL 300G's 100% stator ground fault protection scheme would be carried out on a system with representative parameters and practical characteristics.

Chapter Seven contains the results of detailed hardware-in-loop testing of the relay's 100% stator ground fault protection scheme using the detailed real-time model of the generator and its grounding scheme described in Chapter Six. The results are used to assess the suitability of using real-time simulation models of synchronous generators for hardware-in-loop testing of 100% stator ground fault schemes by comparing the measured performance (stator winding coverage) of the sub-elements making up the scheme against the performance of these elements expected from theory.

Chapter Eight presents the conclusions of the thesis research as well as recommendations for further studies.

1.5 Thesis contributions

Detailed real-time models have been developed to carry out hardware-in-loop studies for particular generator protection elements. The generators were represented using phase-domain synchronous machine models in the simulation studies. Through this research project, the validity of testing an industrial generator protection relay using the phase-domain synchronous machine model has been established.

Although the phase-domain synchronous machine model provided to general users of RSCAD allows realistic representation of internal winding faults on a generator, it does not represent phase-belt harmonics in the generator stator winding. Consequently, this machine model is not able, on its own, to represent the third-harmonic voltages in the stator windings that are relied upon by some forms of 100% stator ground fault protection schemes to detect stator winding faults. In this thesis, extra modelling effort was therefore put into developing a custom real-time model to simulate the generated third-harmonic voltages in the stator windings in order to supplement the RSCAD faulted generator model with the characteristics that it lacks for the purposes of 100% stator ground fault protection relay testing.

The performances of the phase percentage restrained differential protection (87P), loss-of-field protection (40), out-of-step protection (78) and 100% stator ground fault protection schemes (64G) of the SEL 300G generator protection relay have been evaluated by conducting hardware-in-loop testing of the device. Hardware-in-loop studies can be carried out to test other, different generator protection relays following a similar approach in the future.

1.6 Research publications

Some of the research findings of this thesis have been presented at local conferences [19],[20].

CHAPTER 2

BACKGROUND AND LITERATURE REVIEW

2.1 Introduction

The broad objectives of this thesis have been presented in the previous chapter, specifically the use of real-time digital simulators for studying generator protection relay performance. However, before considering the specific issues associated with generator protection, one must have some background knowledge on the broader subject of power system protection generally.

Power system protection is a critical branch in the field of electrical engineering. A properly designed protection system must be able to clear faults as reliably as possible when there is a fault on the protected equipment, and to remain inactive if the protected equipment is in a healthy operating state, or if the fault is outside of the protection system's zone of responsibility.

The fundamentals of power system protection are presented in this chapter in order to explain different functions and importance of a protection system. Different protection philosophies and relay technologies are also presented to provide background knowledge on the subject. Since generator protection is the main focus of the thesis, an overview of the protection elements provided by modern industrial generator protection relays is also presented. Finally, the chapter discusses the generator modelling and testing approaches which are followed in this thesis.

2.2 Attributes of power system protection systems

The purpose of a protection system is to detect and remove the faulted section of the power system network as quickly as possible. The type and location of a fault determines the magnitude of the disturbance it causes to the power system. The speed of response of a protection relay to a fault also determines the severity of the disturbance imposed on the system as a result of the fault. Therefore fast and reliable protection systems are required for fault isolation in order to maintain the integrity and stability of the power system and to minimize the damage to the faulted plant itself. This section provides definitions of some terms which are typically used in the field of power system protection.

2.2.1 Reliability

The reliability of a protection system indicates the correctness of its operation. Dependability and security are two aspects of the reliability. Complete dependability can be understood as the relay always operating for faults on the plant it is supposed to protect, while complete security can be understood as the relay never operating for faults that are not on the plant it is supposed to protect.

Reliability of the relays in a protection scheme is extremely important from the perspective of power system protection [21],[22],[23].

2.2.2 Sensitivity

A protection system must have the ability to discriminate between a healthy system condition and a faulty system condition. During an abnormal system condition, measured system quantities will exceed pre-determined threshold values in order to initiate corrective action to be taken by the protection system [23]. The margin between trip and restraint regions determines the sensitivity of the protection system. A protection system with a smaller margin between its trip and restraint regions will have a higher sensitivity and vice versa [22].

2.2.3 Selectivity

Different protection relays are installed and configured to protect different parts of the power system. The purpose of protection coordination is to determine graded settings for different protective relays in order to achieve selectivity in the way that they respond to faults [23]. If the relay settings are coordinated properly, the primary relay will operate as quickly as possible when there is a fault within its protection zone and it also provides backup protection with a delay time for faults outside its protection zone [21]. The backup relay is used in order to try to ensure that the fault will be isolated if the primary relay fails to operate correctly. Therefore selectivity is also known as relay coordination which defines the zones of operation of different relays.

2.2.4 Speed

A protection system is required to remove a fault after it has been detected. The time taken by the protection system to implement this corrective action determines the severity of the equipment damage and can also influence the stability of the power system. The magnitude of the disturbance to the power system and the damage to its equipment can be reduced if the fault is isolated in a short period of time [22].

2.3 Background of protection relays

The principle purpose of protection relays is to discriminate between normal and faulted system operating conditions. The faulted section of the power system is then isolated from the rest of the healthy power system. The fault clearing speed can have a significant impact on the system stability and the severity of the equipment damage. The faster the fault clearing time, the less damage there will be to the equipment, and the more likely the system will be able to remain in a stable condition. The time taken to remove a fault is known as the clearing time which is defined

by the summation of the comparison time, decision time and the action time of the protection systems involved [23].

$$T_c = T_p + T_d + T_a \quad (2.1)$$

Where T_c = clearing time [s]

T_p = comparison time [s]

T_d = decision time [s]

T_a = action time, including circuit breaker operating time [s]

The block diagram in Figure 2.1 illustrates the functional elements of a protective device. The actual system quantities are measured by means of instrument transformers such as voltage transformers and current transformers. The settings of the protection relay are the threshold quantities which are compared to the measured quantities. The protection relay will make a decision based on the measured system quantities and the threshold quantities. The outcome of the decision sent to the circuit breaker can be either a close signal or a trip signal. The circuit breaker will take appropriate action based on the control signal received.

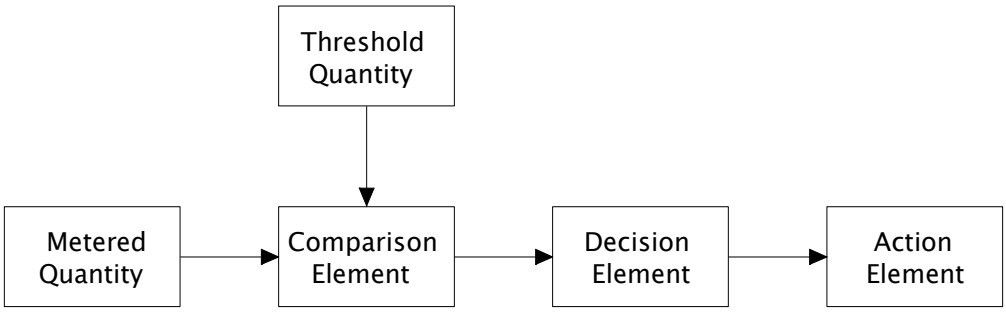

Figure 2.1. Protective device functional elements.

Sections 2.3.1 to 2.3.4 illustrate different protective equipment that was developed using different types of technology available at different periods of relay development.

2.3.1 Fuses

The fuse was the earliest form of protective device which was designed based on the overcurrent principle. The fuse is installed in series with the protected equipment and it only responds to the overcurrent condition. The fuse has a fusible link which will be melted when the current exceeds the rating of the fuse. The melting time for the fusible link is inversely proportional to the fault current. The fuse possesses both current sensing and circuit isolation capabilities. Fuses can be used in different applications such as overload protection or short-circuit protection. When the current drawn by the protected equipment exceeds the rating of the fuse, the fusible link will be melted

which leads to an open circuit and hence isolates the protected equipment. Fuses are still widely used due to their simplicity and low cost. Usually each fuse has a chart for coordination purposes.

2.3.2 Electromechanical relays

There are two types of electromechanical relays: the plunger-type and induction-type relays. The structure of the plunger-type electromechanical relays is a moving solenoid plunger placed inside a stationary electromagnet as illustrated in Figure 2.2. The mass of the plunger determines the operating time of the relay; therefore it can be adjusted to suit the need of the specific application. When the current flow through the coil exceeds a threshold value (also known as the pick-up setting), there will be an upward force developed on the solenoid plunger that causes the solenoid plunger to overcome downward forces (i.e. the weight of the plunger and the restraining influence of the return spring) and close the normally open contact. The operation speed of the plunger-type electromechanical relays is fast, usually within few cycles of the AC power system, and they do not have intentional delay. They are therefore known as instantaneous relays [23],[24].

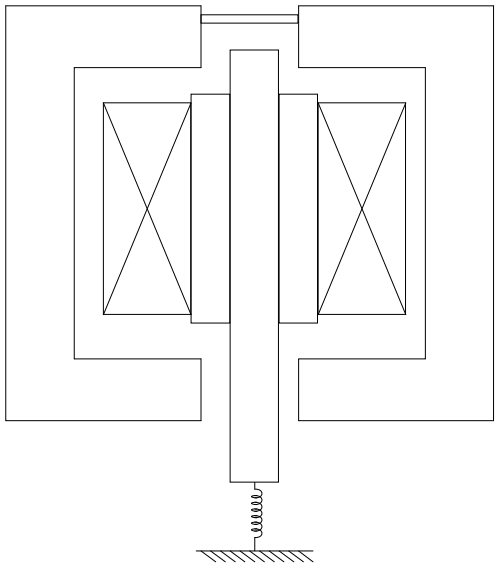

Figure 2.2. Plunger-type relay.

The operating principle of the induction-type relays is similar to the single-phase AC motor. Figure 2.3 illustrates an induction disc relay. Figure 2.4 illustrates a moving cup induction relay. The electromagnetic field produced by the magnetic poles will induce eddy currents in the moving element (either the disc or cup). The field on the moving element produced by the eddy currents tries to align with the field produced by the coils, which causes rotational movement. The angle of rotation required for the movable contact to reach the fixed contact is adjusted by the time lever. The time required for the relay to trip is hence determined by the time lever. The induction-type electromechanical relays can be configured for different applications such as overcurrent, distance,

differential and directional protection functions. For many applications, the electromechanical relays are still being used due to their reliability and low cost [23],[24].

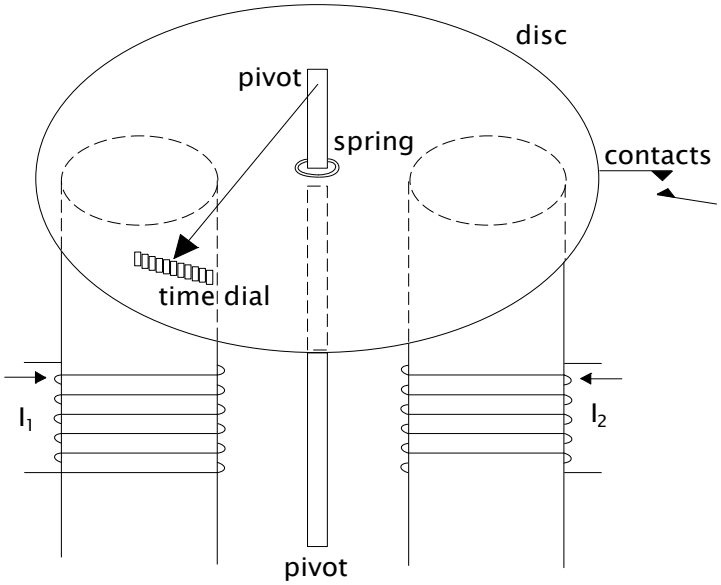

Figure 2.3. Induction disc relay.

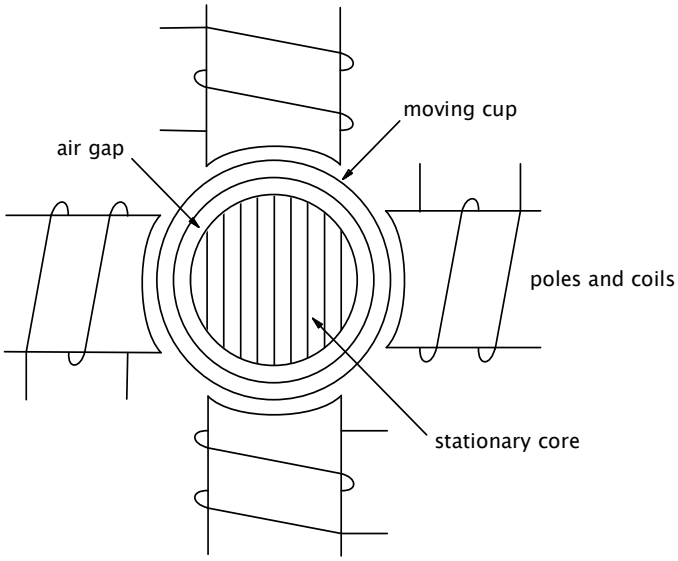

Figure 2.4. Moving cup induction relay.

2.3.3 Solid-state relays

Due to the increasing complexity of power systems, protection relays are designed to handle more and more sophisticated problems. The advancement in semiconductor technology has led to the evolution of protection relay designs. Solid-state relays (also known as static relays) were introduced in the early 1960s [23]. In contrast with electromechanical relays, solid-state relays do not have any moving mechanical parts and they need auxiliary power supplies in order to operate.

Solid-state relays consist of two main circuitries: digital logic circuits for logical variable operations and analogue circuits for both measuring circuits and fault sensing. The intention of the solid-state relay development was to replace electromechanical relays; therefore all the characteristics associated with existing electromechanical relays can be implemented using solid-state relays [24]. However, while the characteristics of a particular type of electromechanical relay are fixed, in solid-state relays, these characteristics can be modified. Solid-state relays have higher accuracy and faster operating speed than electromechanical relays. The reduced size of solid-state relays is one of their advantages since less mounting space is required; they also do not have to be mounted in a certain orientation compared to electromechanical relays. Solid-state relays also have better immunity against dust and vibration, but higher electromagnetic interference susceptibility is one of their disadvantages, and therefore shielding is required in the installation. Solid-state relays are very sensitive to environmental factors such as humidity and temperature and therefore their operating ranges are narrower than those of electromechanical relays [23],[24].

2.3.4 Digital microprocessor-based relays

The concept of using digital devices to perform protection functions was proposed by George Rockefeller in 1969 [23]. However, the concept was not realized due to the high cost of the digital computer at the time. The limited processing power of early digital computers was another reason to initially discard the concept of digital relay implementation. However, subsequent development of faster digital computers and microprocessors led to a re-evaluation of George Rockefeller's concept on implementation of the digital relay. The price for both digital computers and the associated memory chips has decreased significantly due to maturity of the technology. As a result, microprocessor-based relays became commercially available in the 1980s. These microprocessor-based relays are distinct from the other types of relays since they are fully implemented using digital technology. The reliability of the protection system can be improved by using digital relays since their status can be monitored. The programmable nature of their functions is another important feature of digital relays: many different relay characteristics can be provided within one device so that the protection engineer can select different characteristics and modify them for different applications without changing the physical device. Because the processing power of available microprocessors increases over time, more sophisticated algorithms can be implemented on digital relays as the technology advances. Digital relays also have the ability to record the data measured on the power system. This is a significant advantage for protection engineers since the recorded data can be used for system dynamic study or fault analysis. Modern digital relays are more versatile than earlier microprocessor-based relays and therefore they are also being referred to as Intelligent Electronic Devices (IEDs) rather than simple protective relays. These digital relays also have the ability to communicate with each other and hence allow a better coordination between their protective functions [23].

Figure 2.5 illustrates a functional block diagram of a digital relay. The inputs to the digital relay are analogue quantities measured from the power system. The analogue quantities at the input to the digital relay are digitized or sampled by an analogue-to-digital (A/D) converter at a sampling frequency that can vary from 240 Hz to 2 kHz (between, approximately, 4 to 40 samples per cycle of the power system's AC waveforms). The sampled data remains in the device's scratchpad, which is the Random Access Memory (RAM), for the Central Processing Unit (CPU) to process. Digital filters are used to filter out the unwanted noise in the sampled data. The comparison between the sampled data and the threshold values is done in the relay logic and a decision is made based on the result of the comparison. The outcome is sent to the circuit breaker in order to control the circuit breaker. The status of the circuit breaker is also often monitored by the digital relay [23].

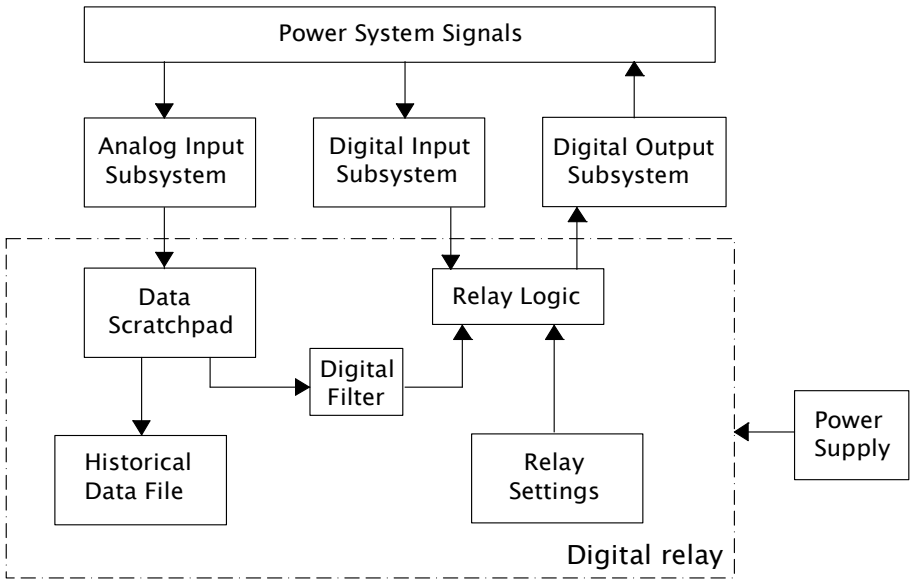

Figure 2.5. Functional block diagram of a digital relay.

2.4 Protection relay principles

This section provides a broad overview of different protective relaying principles. Different relays have different characteristics and hence are intended to be used for different applications. The same protective function can often be implemented by using different relays, and therefore an understanding of different relay characteristics is very important. Often the same piece of plant (e.g. generator and transformer, etc.) is protected by more than one type of relay or more than one type of element in one relay at the same time for various reasons. If there is more than one relay in the protection system, the reliability of the protection system as a whole will not be compromised if the primary protection relay fails to operate correctly since there is backup protection available in the protection scheme from other relays. In some applications, especially generator protection, different relay characteristics are required in order to provide complete protection for the plant

from various types of fault and for various locations of faults. The available relay options are listed below:

1) Overcurrent relay
2) Differential relay
3) Directional relay
4) Distance relay

2.4.1 Overcurrent relay

The relay based on overcurrent principle was developed around 1902 [25]. The principle of the overcurrent relay is to isolate the protected equipment when the operating current exceeds a pre-set threshold value. In order to operate the overcurrent relay, only currents have to be measured from the system. The overcurrent relay can be used for overload protection and short-circuit fault protection. It can also be used as a backup protection if the primary protection fails to operate. However, if it is used as a backup protection, the relay's operating time must be coordinated with the primary protection to prevent its operation before the primary protection. Overcurrent relays can be classified into several categories: instantaneous, definite-time and inverse-time overcurrent relays.

Figure 2.6 illustrates time-current characteristics for a definite time and different inverse-time relays. For a definite-time overcurrent relay to operate, two conditions must be satisfied: the fault current must exceed the predetermined value and the duration of the fault must be longer than the time setting of the relay. When these two conditions are met, the definite time overcurrent relay will issue a trip signal to the circuit breaker. In contrast to a definite-time overcurrent relay, an instantaneous overcurrent relay operates with no intentional time delay when the measured current is greater than the threshold setting [23].

The purpose of the inverse-time overcurrent relay is to isolate higher-current faults with a higher clearing speed. The magnitude of the fault current determines the speed of the fault clearing action taken by inverse-time overcurrent relays. Different inverse-time relays possess different types of time-current characteristics (TCCs) and therefore different inverse-time relays can be chosen based on the requirements of the specific application. Examples of some of the available options are listed below:

1) Standard inverse
2) Very inverse
3) Extremely inverse

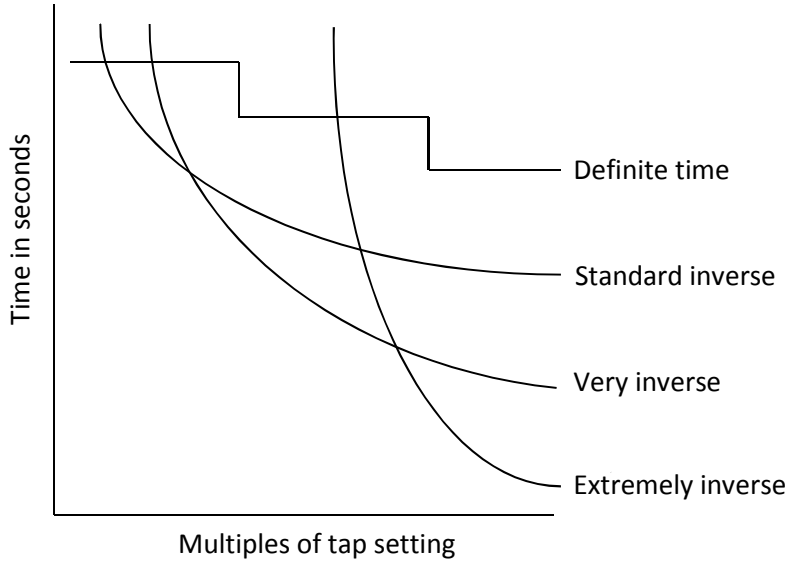

Figure 2.6. Definite time and inverse time characteristics of the overcurrent relay.

The characteristic equations for the aforementioned types of inverse-time overcurrent relays are defined as follows.

Standard inverse overcurrent relays:

$$t_{op} = \frac{0.14}{M^{0.02} - 1} \times TM \tag{2.2}$$

Very inverse overcurrent relays:

$$t_{op} = \frac{13.5}{M - 1} \times TM \tag{2.3}$$

Extremely inverse overcurrent relays:

$$t_{op} = \frac{80}{M^2 - 1} \times TM \tag{2.4}$$

Where t_{op} = operating time [s]

M = ratio of the input current to the pickup current

TM = time multiplier or time dial setting

2.4.2 Differential relay

The current differential relay was introduced in 1905 [25]. The philosophy underlying current differential protection schemes is based on Kirchhoff's current law. Measurements of current are made at both ends of the protected equipment and the differential relay only operates when there is

a difference in current entering and leaving the device. In practice, the differential current (also known as the operating current) must exceed a small set threshold value of current. The differential relay can only detect faults within the specific equipment being protected and it cannot be used as backup protection for other equipment therefore it is often referred to as unit protection.

2.4.3 Directional relay

The directional relay was developed in 1909 [25]. The directional relay is designed to respond to the relative phase angle between a current and another current or voltage reference [23]. A directional relay is typically used in conjunction with some other form of relay such as an overcurrent relay or a distance relay. The use of a directional relay together with an overcurrent relay or a distance relay does not change the original characteristics of either of these relays but rather it provides an additional feature for these relays: because a directional relay has the ability to sense the direction of the power flow at a specific location, it can add selectivity to these forms of protection so that the overcurrent or distance relay then responds only to faults in one direction relative to the relay (forward or reverse). A directional relay requires a reasonably constant reference quantity (also known as the polarizing quantity). During a fault, the phase angle of the system voltages does not change significantly, whereas the phase angle of the line current can undergo significant changes of up to 180°. Therefore in most applications, system voltages are used as a reference quantity [21].

2.4.4 Distance relay

The distance relay was developed in 1923 [25]. In distance relaying, the voltage and current measured from the system are used to determine the total impedance seen by the relay. The relay operates when the impedance seen by the relay is less than its threshold setting.

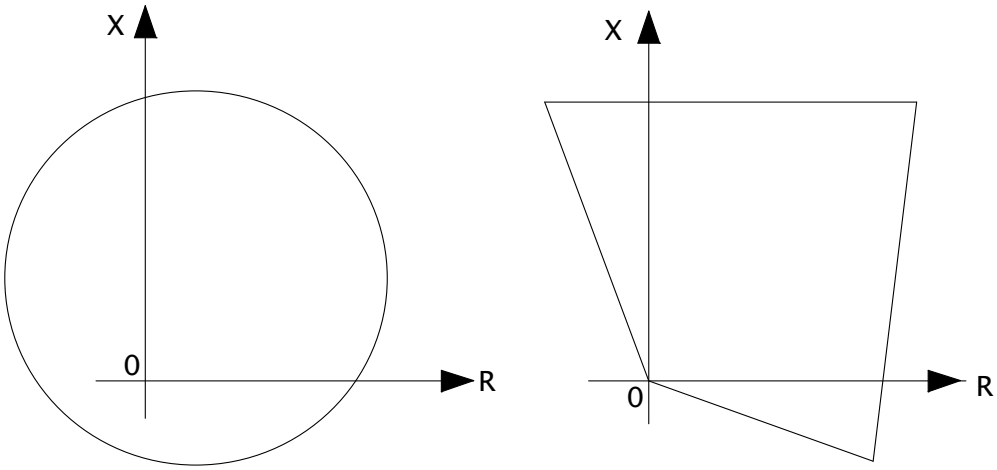

Figure 2.7. Offset mho and quadrilateral tripping characteristics.

A distance relay's tripping characteristic is a two-dimensional area defined on the R-X impedance plane in order to allow coordination of different protection zones. There are two commonly used tripping characteristics in distance protection relays, namely the offset mho and quadrilateral characteristics [26]. Figure 2.7 illustrates offset mho and quadrilateral tripping characteristics. Often a directional relay is added to the distance relay in order to provide directionality to the relay's tripping characteristic in the R-X plane. When there is a fault in the system, the impedance seen by the relay will change. The distance relay will operate when the impedance it sees crosses into the tripping characteristic of the relay defined on the R-X plane.

2.5 Generator protection

Generators are important assets of a power utility and they also play an important role in the power system's stability. A number of different protective elements are employed to protect a generator from damage during system contingencies and abnormal operating conditions. The generator protection system can also be used to prevent occurrence of disastrous events due to misoperation by utility personnel. In order to understand abnormal operating conditions or malfunctions that are possible on a generator, one must know the characteristics and limits of the generator during its normal operation. Every generator has operational limits, and these limits depend on the rating of the generator.

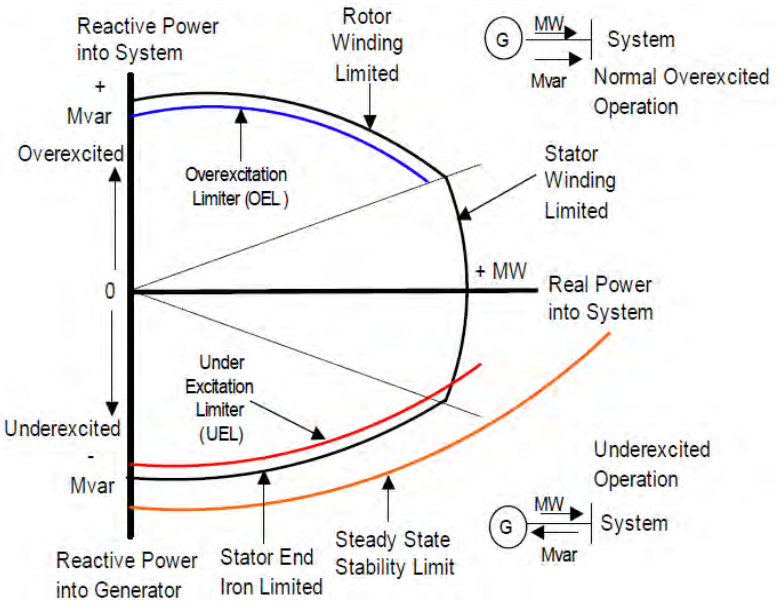

Figure 2.8. Generator capability curve [2].

Figure 2.8 shows an example of a capability curve typical of large synchronous generators used in utility power stations. The generator capability curve defines the operational limits for the generator and it is used to coordinate between the generator's excitation system and its protection systems. Poor coordination between generator controllers and protection elements will lead to

misoperation of the protection systems during system disturbances. Unnecessary tripping of generators is highly undesirable: any unnecessary loss of generation capacity is a large disturbance to the system. In a more stressed power system, loss of generation capacity can have an adverse cascading effect that could eventually lead to regional blackout. The sensitivity and time coordination of a generator's protection elements require particular attention because sometimes generator protection relays respond to the normal action taken by the excitation controller during the fault-clearing period. Therefore utilizing the generator capability curve for coordination of the protection elements will enhance the reliability and reduce the possibility of misoperation of the generator protection system.

Figure 2.9 shows a functional block diagram of the excitation control system of a large synchronous generator. The excitation system controls are used to regulate the generator's terminal voltage and reactive power output, while the governor controls its active power output and frequency. On a synchronous generator, the turbine governor is a load controller which controls the input mechanical power in order to match the required output active electrical power. There are two different types of turbine governor control: Isochronous control and droop governor control.

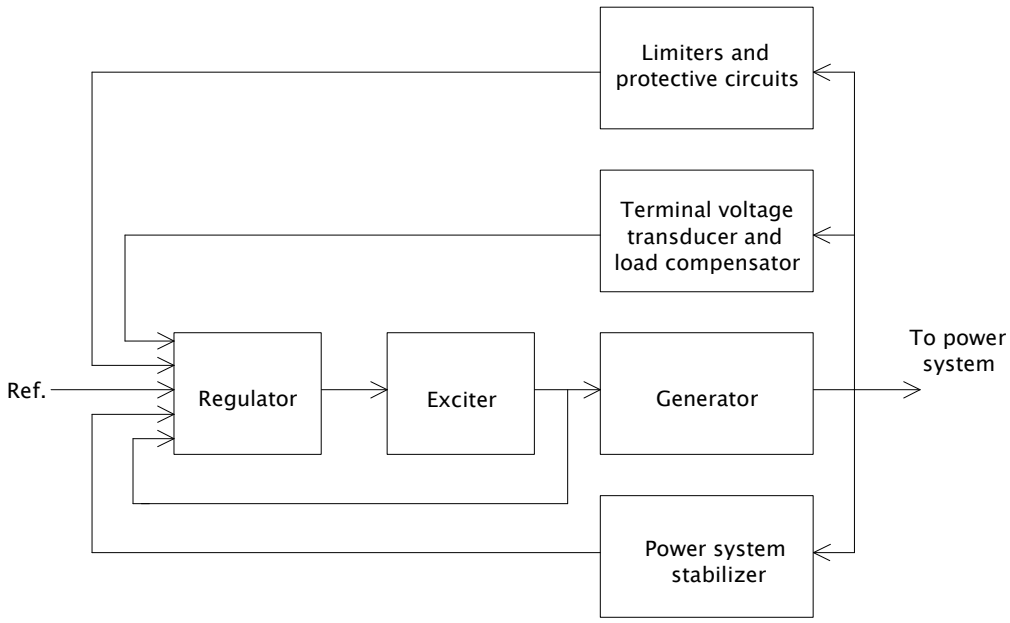

Figure 2.9. Functional block diagram of a synchronous generator excitation control system (reproduced from [11]).

The purpose of the isochronous mode of governor control is to maintain a constant pre-settable speed as the active power output of a generator increases or decreases. Isochronous governor control is typically applied to single, islanding generator applications in order to maintain constant system frequency during islanding conditions [1], [27].

If the governor control is set to droop mode, an increase in active power output of the generator will lead to a linear decrease in generator speed. This mode of governor control is typically applied to generators that are connected to the power system in order to regulate their speed versus load characteristic. If all generators have the same droop setting, they will share load proportional to their full load capacity [1],[27]. This control topology can avoid excessive loading and unloading between the interconnected generators when they are operating in parallel.

2.5.1 Generator excitation systems

The purpose of the excitation system is to provide the current needed to establish the rotor magnetic field so as to maintain the generator in synchronism. In so doing the excitation system also determines the amount of reactive power to be generated or absorbed at the generator AC terminals. There are many different types of excitation system: DC excitation, AC excitation and static excitation systems [11]. Automatic voltage regulation (AVR), constant power factor regulation, and constant reactive power regulation are the options available for the excitation control [1]. As mentioned previously, different generators have different capabilities and therefore their operational limits are different. There are different limiters that restrict the excitation controller in order to avoid operation beyond the generator's capabilities.

The purpose of the overexcitation limiter (OEL) is to prevent a prolonged excess of excitation current supply to the generator field [28]; however, brief overcurrent is allowed and is highly desirable on the field in order to maintain stability after faults. A prolonged overload condition must be avoided since it will cause insulation deterioration due to thermal damage and hence lead to insulation failure. Misoperation of the field protection may occur if the overexcitation limiter is not properly coordinated with the field protection.

The function of the underexcitation limiter (UEL) is to prevent heating of the stator end region during the underexcitation operation. It also prevents the excitation current commanded by the automatic voltage regulator from reducing to a level where the loss-of-field protection operates [28], as well as preventing the generator from losing synchronism due to insufficient synchronizing torque.

From the above mentioned excitation limiters, one can see the importance of the coordination between the excitation limiters and the generator protection elements. Misoperation of the generator protection system may be a result of the poor coordination between the excitation limiters and the generator protection elements.

2.5.2 Generator grounding scheme

In practice, there are many grounding schemes available to ground a generator. The particular generator grounding scheme used will be chosen based on the following factors: cost of the grounding scheme, implementation complexity and the rating of the generator.

The grounding schemes can be classified into the following categories:

1) Ungrounded
2) Solidly grounded
3) Low-impedance grounded
4) High-impedance grounded

For an ungrounded generator, there is no physical connection between the generator neutral and the system ground. During a stator winding to ground (stator-ground) fault, there will be a small flow of fault current as a result of the shunt capacitance between the stator windings and ground. The ground fault current is not a concern in the case of the ungrounded generator; however the overvoltage will be a threat [29]. Therefore it is not recommended to implement this grounding scheme for a generator due to the overvoltage condition encountered during a ground fault on the generator stator winding.

A solidly grounded generator has a physical connection between the generator neutral and the system ground. There will be no other resistor or reactor inserted between the generator neutral and the system ground except for an earthing conductor. A stator-ground fault that occurs under this grounding configuration will produce a large ground fault current [29].

Low-impedance generator grounding can be classified into two types: low-resistance or low-reactance grounding configuration. A resistor or a reactor with low-ohmic value is usually used for the connection between the generator neutral and the system ground for this grounding scheme. The resistor value for a low-resistance grounding scheme is selected to limit the current through the neutral resistor to 1.5 times nominal generator rated current during a stator-ground fault [29]. Where this form of grounding scheme is used, either a ground differential protection or phase percentage differential protection scheme is usually implemented to protect the generator stator windings.

High-impedance grounding schemes can also be classified into two types: high-resistance or high-reactance grounding configuration. There are different practical ways to implement this type of grounding scheme. A resistor with high-ohmic value can be inserted directly between the generator

neutral and the system ground. The alternative approach is to connect the generator neutral and the system ground through the primary winding of a grounding transformer, with the grounding resistor connected to the secondary winding of the grounding transformer [29]. A detailed discussion of this grounding method is contained in Chapter Six of the thesis. For high-resistance grounded generators, 100% stator ground fault protection (64G) and neutral injection schemes (64S) are two of the protection schemes that have the ability to provide full stator winding protection coverage.

2.5.3 Generator protection elements

This section provides a broad overview of the protection elements provided by typical industrial generator protection relays. Before the detailed discussion on the settings of the generator protection elements, one must understand the motivation behind the development of such protection functions. Table 2.1 illustrates a list of different protective elements that are available in the particular generator protection relay used in this thesis, namely the SEL 300G. As seen in Table 2.1, every protection element has a unique ANSI/IEEE standardized power system device function number with an appropriate suffix. The development of such device function numbers is to assist engineers to conveniently identify the basic functions of electrical plant in a circuit diagram. The device function numbers are to be used in drawing, elementary and connection diagrams, instruction books, publications, and specifications [21], [30].

Table 2.1: Generator protection elements [31]

Device	Description
87P	Phase percentage restrained differential, can include unit step-up transformer, and unit auxiliary transformer
87N	Ground differential for low impedance grounded generators
50/51N	Neutral Overcurrent Protection
50/51P	Phase Overcurrent Protection
64G	100% Stator Ground Detection for high impedance and resistance grounded generators
40	Loss-of-Field Protection
32	Loss of Prime Mover Protection
AE	Accidental Energization Protection
24	Volts per Hertz Protection
46	Negative Sequence Overcurrent Protection
27	Undervoltage Element
59	Overvoltage Element
81	Over and Under Frequency Protection
81AC	Off Nominal Frequency Time Accumulators for Steam Turbines
78	Out-of-Step Protection
21	Distance Backup with Load Encroachment
25	Synchro-Check Element for Breaker Close Supervision
60	Loss- of-Potential Logic

2.5.3.1 Phase percentage restrained differential protection: Device 87P

Short-circuit faults may occur anywhere in the power system. The occurrence of such a fault within a generator winding is due to insulation deterioration or insulation failure. Depending on the type of grounding scheme employed, the generator may produce a large amount of current during the short-circuit fault, and the system voltage may be depressed. Large short-circuit current will also cause severe damage to the generator stator winding and the insulation and create a large magnetic force that will lead to winding deformation and subject the shaft and couplings to mechanical shock [32]. It is important to isolate the faulted generator from service when a winding short-circuit fault occurs in order to reduce both electrical and mechanical damage to the generator.

Differential protection is a type of protection scheme that is often used to protect the windings of a particular piece of equipment (e.g. generator windings, transformer windings or motor windings). Differential protection schemes can also be used to protect transmission lines (also known as line differential protection). Figure 2.10 illustrates one possible configuration of a differential protection scheme. The fundamental principle of the differential protection scheme is based on Kirchhoff's current law. This protection scheme uses currents measured on both sides of the winding and checks whether the sum of the currents entering the winding is equal to the sum of the currents leaving that winding. When the differential current (also known as the operating current) is not equal to zero, the relay will trip the protected equipment. The operating principle described above is the ideal situation.

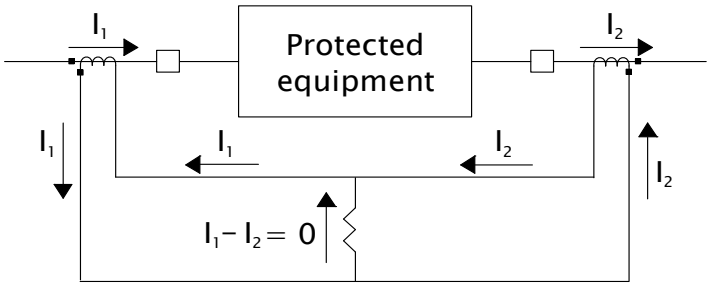

Figure 2.10. Differential protection scheme.

In practice, the differential current will have some small non-zero value even under healthy conditions due to the current transformer manufacturing tolerances. There are many other factors that can influence the operation of generator differential protection when a generator step-up transformer is included in the differential protection zone [33]:

1) Inrush current during transformer energization
2) Steady state magnetizing current of the transformer
3) CT ratio mismatch

4) Phase shift between primary and secondary side of the transformer
5) Current variation due to on-load tap changer of the transformer (OLTC)

In order to accommodate these factors, which result in a non-zero differential current that varies with operating conditions under un-faulted conditions, a percentage differential protection scheme was introduced. The percentage differential protection scheme takes into account all the factors that will affect the operation of the differential protection. The percentage differential relay characteristic is referred to as the slope of the relay. The slope setting of the relay can be adjusted by the user. There are two types commonly available: single-slope or dual-slope percentage differential relay characteristics.

The operating principle of the percentage differential protection scheme is based on comparison between the differential current and the threshold setting at a specific calculated restraint current. The percentage differential relay will operate when the differential current exceeds the threshold setting at a specific calculated restraint current. The sensitivity of the percentage differential protection can be adjusted by changing the slope of the relay characteristic. This type of protection scheme greatly reduces the possibility of misoperation and therefore the protection system is more reliable. A detailed discussion of this protection scheme is contained in Chapter Four.

2.5.3.2 Ground differential protection for low impedance grounded generators: Device 87N

Ground differential protection is one form of generator protection scheme implemented to protect generator stator windings when the generator is low-resistance grounded. Figure 2.11 illustrates a ground differential protection scheme. On the terminal side of the generator, there are three current transformers connected in parallel. Under healthy operating conditions, the vector sum of the line currents through the secondaries of these three current transformers will be zero. Similarly, there will be no current flowing in the secondary side of the current transformer placed in the generator neutral under normal operating conditions. Thus there will be no differential current to trip the relay since there is no difference in current from the input measurements under normal conditions.

When a fault occurs outside the unit protection zone, the vector sum of the generator line currents will be equal to the current flowing through the generator neutral. Again, there will be no differential current to trip the relay since the input measurements are the same in this case. If a fault occurs within the unit protection zone, the vector sum of the generator line currents will not be the same as the current flowing through the generator neutral and therefore the relay will trip.

The concept of the ground differential protection scheme is the same as the percentage differential protection scheme explained in Section 2.5.3.1. The device number will be the same since they have the same functionality; however the suffix changes depending on their application.

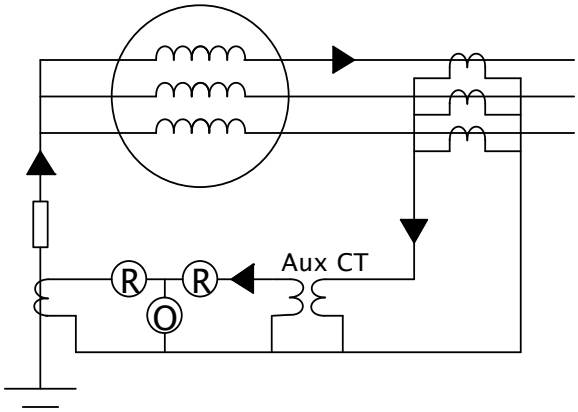

Figure 2.11. Ground differential relays (reproduced from [32]).

Figure 2.12 illustrates a combination of phase percentage differential protection and ground percentage differential protection for stator winding protection.

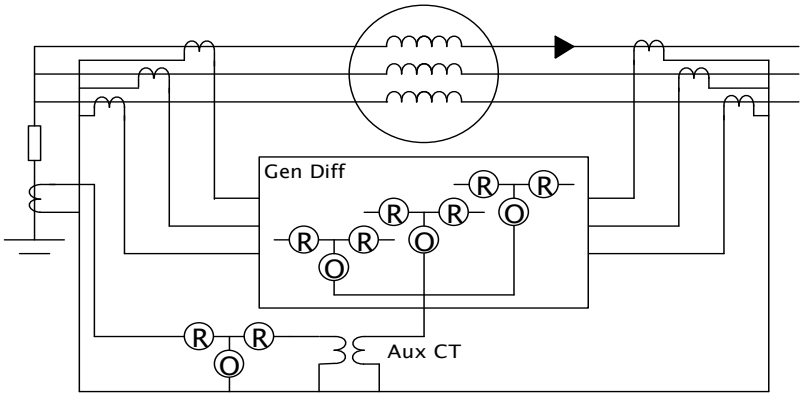

Figure 2.12. Combined phase percentage differential and ground percentage differential protection scheme (reproduced from [32]).

2.5.3.3 100% stator ground detection for high impedance and resistance grounded generators: Device 64G

As discussed earlier, there are many grounding schemes available to ground a generator neutral. For generators with high MVA rating, a high-impedance or high-resistance grounding scheme is recommended. The advantage of this grounding configuration is its ability to limit the fault current when there is a stator winding to ground (stator-ground) fault on the generator. Under this type of grounding scheme, the risk of severe damage on generator stator windings during a stator-ground fault is greatly reduced.

For a high-impedance grounded generator, differential protection is no longer capable of detecting a stator-ground fault on the generator due to the limited fault current. Under this type of grounding system, alternative protection schemes are required to detect stator-ground faults on the generator.

The Protection schemes shown in Figures 2.13 to 2.15 utilize a distinct practical characteristic of generators to detect the presence of ground faults in their windings, namely the non-sinusoidal components in their output voltages: generators typically produce harmonic voltages such as the 3^{rd}, 9^{th}, 15^{th} harmonics (also known as triplen harmonics). Of these harmonic voltages, the 3^{rd} harmonic voltage has the highest magnitude and it is the one chosen for use in generator protection schemes [32].

The particular 100% stator ground fault protection scheme shown in Figure 2.13 contains two sub-elements, namely a fundamental-frequency neutral overvoltage element (59GN) and a third-harmonic undervoltage element (27H). The fundamental-frequency neutral overvoltage element (59GN) is connected across the grounding impedance to sense zero-sequence voltage. When there is a stator-ground fault on the generator, the magnitude of fundamental frequency voltage across the grounding resistor increases. The (59GN) element utilizes this characteristic to detect stator-ground faults on the generator. However, the (59GN) element cannot detect stator-ground faults near generator neutral due to insufficient sensitivity of the element. In order to cover this protection blind region of the (59GN) element, the third harmonic undervoltage element (27H) is introduced. When there is a ground-fault near the generator neutral, the measured third-harmonic voltage across the grounding resistor decreases. The (27H) element utilizes this characteristic to detect stator-ground faults near the generator neutral.

Figure 2.14 illustrates another form of 100% stator ground fault protection scheme. This scheme also contains two sub-elements, namely a fundamental-frequency neutral overvoltage element (59GN) and a third-harmonic overvoltage element (59T). The third-harmonic overvoltage element (59T) is an alternative method to detect stator-ground faults near generator neutral. When there is a stator-ground fault near the generator neutral, the magnitude of the measured third-harmonic voltage at the generator terminal increases. The (59T) element utilizes this characteristic to detect stator-ground faults near the generator neutral.

It is important to note that the generator loading condition influences the amplitude of the third-harmonic voltage that is induced in the generator stator winding. If a stator-ground fault occurs on the generator during a light load condition, both the third-harmonic undervoltage element (27H) and the third-harmonic overvoltage element (59T) are unable to perform satisfactorily. Therefore

the protection schemes shown in Figures 2.13 and 2.14 can only provide 100% stator winding protection under certain system operating conditions.

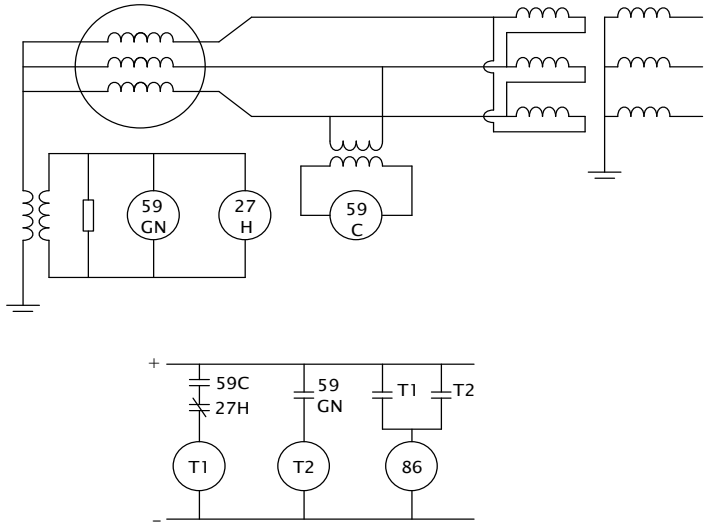

Figure 2.13. 100% stator protection: Undervoltage scheme (reproduced from [34]).

27H: Undervoltage relay tuned to respond to third-harmonic frequency (150 Hz)

59C: Voltage supervision relay, block tripping by 27H during start-up

59GN: Time delay overvoltage relay tuned to fundamental frequency (50 Hz)

86: Lock-out relay, requires a manual reset when actuated

T1, T2: Timers

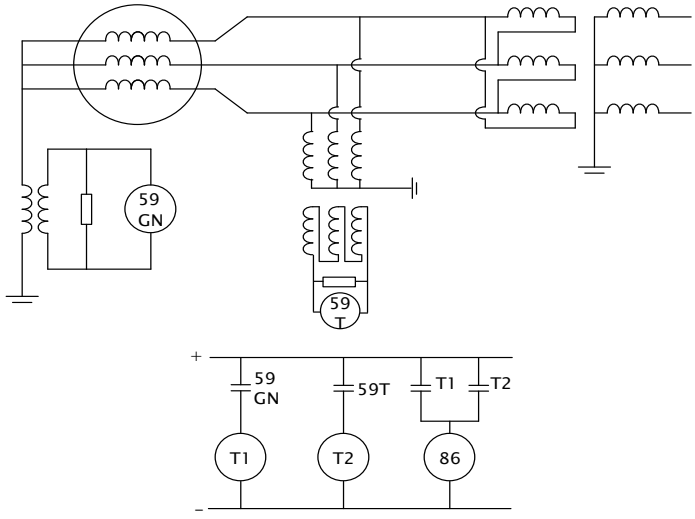

Figure 2.14. 100% stator protection: overvoltage scheme (reproduced from [34]).

59GN: Time delay overvoltage relay tuned to fundamental frequency (50 Hz)

59T: Instantaneous overvoltage relay tuned to third harmonic frequency (150 Hz)

86: Lock-out relay, requires a manual reset when actuated

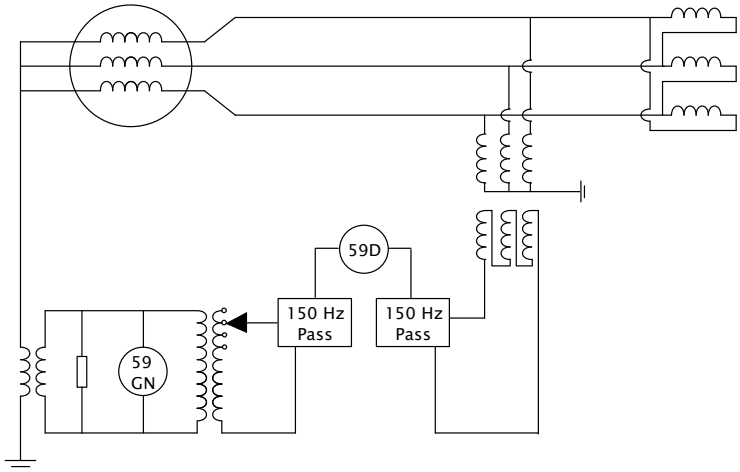

Figure 2.15. Third-harmonic voltage differential scheme (reproduced from [34]).

59GN: Time delay overvoltage relay tuned to fundamental frequency (50 Hz)
59D: Instantaneous third-harmonic voltage differential relay

Figure 2.15 illustrates another form of 100% stator ground fault protection scheme. This protection scheme contains two sub-elements, namely a fundamental-frequency neutral overvoltage element (59GN) and an instantaneous third-harmonic voltage differential element (59D). The ratio between the third-harmonic terminal voltage and the third-harmonic neutral voltage of a generator should remain the same during normal operation, but the ratio changes when a stator-ground fault occurs. The instantaneous third-harmonic voltage differential element (59D) uses this characteristic to detect stator-ground faults on the generator. Unlike the third-harmonic undervoltage element (27H) and third-harmonic overvoltage element (59T), the (59D) element can detect stator-ground faults on a generator under various generator loading conditions. A detailed discussion of this particular protection scheme is contained in Chapter Six.

Figure 2.16 illustrates a neutral injection scheme (device: 64S) which is an alternative option to provide 100% stator winding protection [35]. This protection scheme utilizes an injection transformer in order to apply an AC voltage signal to the neutral. The injection transformer is in series with the grounding transformer. The injected AC voltage signal is usually at a sub-harmonic of the normal system frequency. The magnitude of the sub-harmonic current will be determined by the overall system impedance. An overcurrent relay is tuned to monitor this sub-harmonic current in the neutral circuit. When there is a stator ground fault, the winding capacitance will be bypassed and hence the overall system impedance decreases. The sub-harmonic current increases as a result of the reduction of the overall system impedance. The overcurrent relay will operate when the sub-harmonic current increases to a level that exceeds the threshold setting [32]. An alternative way to detect stator-ground faults is to calculate the resultant impedance using the subharmonic injection voltage and current, and to compare this impedance with a threshold setting [35].

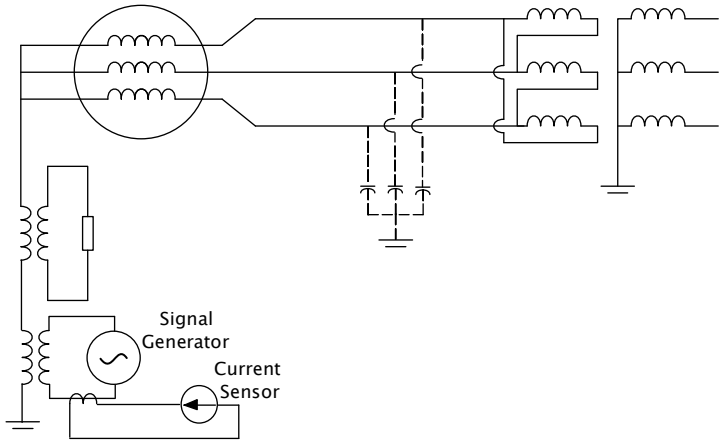

Figure 2.16. Neutral injection scheme (reproduced from [32]).

2.5.3.4 Loss of field protection: Device 40

The generator excitation system is extremely important from the system dynamic point of view since it controls the reactive power flow and is essential for maintaining the synchronism of the generator and hence continued active power transfer. A loss of field happens when there is a failure between the excitation system and the generator field. Misoperation of the field circuit breaker, short-circuit or open-circuit conditions in the excitation system are some of the possible causes for a loss-of-field condition. When the field is lost, the decay of the rotor current is inevitable [32]. This decay in the rotor current leads to decay in the internal generator voltage which ultimately reduces the reactive power output. At some stage of the decay process, synchronism between the stator and the rotor will be lost due to weakening of the magnetic coupling. During a loss-of-field condition, the output of active electrical power is also affected.

Figure 2.17 illustrates the relationship between a generator's active power versus angle curve and its field current. As one can see from Figure 2.17, the output of active electrical power decreases as a result of the reduction in the internal generator voltage which is caused by the reduction of the rotor current. When the input mechanical power exceeds the active output electrical power, the generator will lose synchronism, and accelerate in an attempt to dissipate the excess mechanical power.

During a loss of field condition, the rotor speed will exceed synchronous speed and the generator will operate as an induction generator, and start drawing reactive power from the power system for the purpose of excitation under the asynchronous operating condition. The intake of reactive power under these conditions may exceed the operational limit of the generator. A large amount of reactive power consumption poses a threat to both neighbouring generators and transmission lines [36]. The transmission lines can be overloaded due to the large reactive power flow in the system

and the overloaded condition may cause the transmission lines to be tripped. The neighbouring generators will have to increase their excitation to maximum capacity (as known as ceiling excitation) in order to support the large amount of reactive power consumption. However, the generator field will suffer from thermal damage if a prolonged excess of excitation current is supplied to the field continuously. If the system fails to support the required reactive power, the system voltage will collapse.

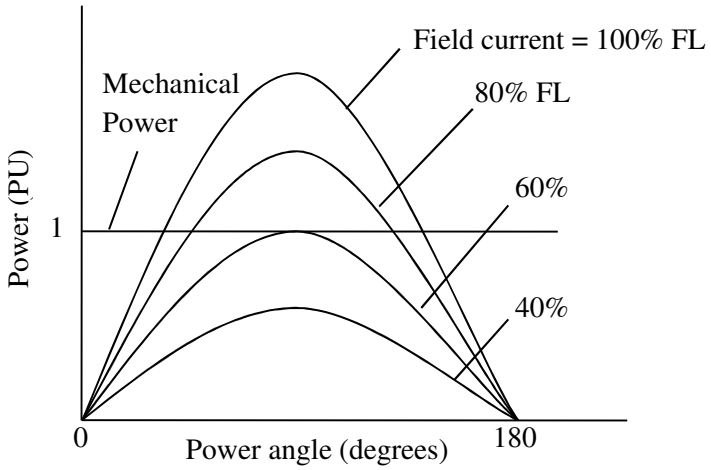

Figure 2.17. Power angle curves at different field currents.

High stator current, rotor damage, torque pulsation and end-core heating are the concerns that arise in generators operating with loss of field conditions [32]. Some irreversible damages can occur from the above described phenomena. Therefore extensive asynchronous operation is undesirable and generators suffering a loss-of-field condition should be isolated before it leads to excessive damage on the generator and system wide instability [37].

Loss-of-field protection must be able to identify faults properly and also coordinate with the normal generator controller operations. The tripping characteristic of a loss-of-field protection scheme is a two-dimensional area defined on an R-X impedance plane. A directional-distance relay is typically used for loss-of-field protection since it can discriminate between sudden loss of excitation and purposely reduced excitation [34]. A detailed discussion of loss-of-field protection is contained in Chapter Four.

2.5.3.5 Out-of-step protection: Device 78

Power systems are quite often subjected to transient disturbances. These transient disturbances such as major load switching or faults may cause an out-of-step condition between two interconnected systems. During an out-of-step condition, generator stator windings may be damaged due to

winding stresses caused by high peak currents and off-nominal frequency operation. The mechanical structure of a generator and its shaft may also be damaged due to excited mechanical resonances caused by pulsating torques [11],[32],[34]. A generator or a group of generators that has pole slipped must be isolated from the rest of the system in order to maintain the integrity and stability of the system, as well as for the protection of the generator itself.

In the past, the electrical centre during an out-of-step condition was usually out in the transmission system. Therefore transmission line relays could detect out-of-step conditions between two interconnected systems and separate them without the need for tripping generators. However, system and generator impedance characteristics have changed considerably over the years: system impedances have decreased significantly due to continuous expansion of transmission systems, while generator impedances have increased due to improved generator cooling methods [32],[34]. Due to these changes in system and generator impedance characteristics, the electrical centre during an out-of-step condition can appear in a generator or a generator step up transformer. Therefore a separate out-of-step protection function is required at the generator terminals to detect out-of-step conditions when the electrical centres of swings are close to the generator zone. A detailed discussion of the swing characteristics of a generator during an out-of-step condition is contained in Chapter Four.

Protection schemes that can be applied for detecting generator out-of-step conditions are essentially the same as the ones that are applied for detecting transmission line out-of-step conditions. The tripping characteristic of the various types of out-of-step protection schemes is a two-dimensional area defined on an R-X impedance plane. Examples of some of the available out-of-step protection schemes are listed below [38]:

1) Simple mho scheme;
2) Single blinder scheme;
3) Double blinder scheme;
4) Double lens and concentric circle scheme.

A detailed discussion of the single blinder protection scheme is contained in Chapter Four.

2.5.3.6 Volts per hertz protection: Device 24

The volts per hertz protection function on a generator protection relay is provided to protect against excessive overexcitation of the generator and, optionally, also the generator step up transformer. An excessive overexcitation condition occurs when the flux levels in the magnetic circuits of the generator and transformer exceed the design limit, which can result in damage to the equipment. It

is a challenge to perform a direct measurement of the magnetic flux; however the magnetic flux is quantifiable from the output voltage magnitude and the frequency. A volts per hertz relay uses the ratio of voltage and frequency to estimate the flux in the magnetic path. If the ratio of voltage and frequency (or estimated flux) exceeds the pre-determined value, the volts per hertz relay will operate. The tripping characteristic of a volts per hertz relay can be definite-time, inverse-time or a combination of definite-time and inverse-time [1],[34].

The following derivation demonstrates why the ratio of voltage and frequency can be used to estimate the flux in a magnetic core. Both generators and transformers operate based on Faraday's law of electromagnetic induction as shown in equation (2.5). The magnitude of the induced voltage in the stator windings of a generator or in the secondary windings of a transformer depends on the rate-of-change of the flux ($d\varphi/dt$) linking the windings and the number of winding turns (N) [32].

$$e = N\frac{d\varphi}{dt} \tag{2.5}$$

The flux required to produce a given voltage can be derived from equation (2.5) and the outcome of the derivation is shown in equation (2.6).

$$\varphi_{max} = \frac{\sqrt{2}E_{RMS}}{N * 2\pi f} \tag{2.6}$$

Where φ_{max} = maximum value of core flux required to produce E_{RMS}

E_{RMS} = RMS output voltage

N = number of turns in the output winding

f = frequency [Hz]

From equation (2.6), one can see that the magnetic flux required to produce a certain output voltage is directly proportional to the ratio of the output voltage over frequency and therefore this characteristic is utilized by volts per hertz relays.

$$\varphi \propto \frac{V}{f} \tag{2.7}$$

Core heating is one of the concerns when designing the magnetic core of an AC machine and it is caused by eddy current and hysteresis losses. Both eddy current and hysteresis losses are dependent on the magnetic flux density of the circuit and the frequency. In order to reduce the heating effect caused by eddy currents, the generator stator and transformer cores are laminated [32].

Eddy current loss:

$$P_e = K_e f^2 B_m^2 t^2 \ (W/kg) \tag{2.8}$$

Hysteresis loss:

$$P_h = K_h f B_m^{1.5 \ to \ 2.5} \ (W/kg) \tag{2.9}$$

Excessive flux can be a result of the high output voltage or low operating frequency. Saturation occurs when there is excessive flux in the magnetic circuit. During normal operation, the magnetic flux is at its rated, design value and the permeability of the magnetic circuit is higher than that of the surrounding structures. When saturation of the magnetic circuit occurs, both eddy current and hysteresis losses will be increased due to the increase in the magnetic flux density. Increase in losses will lead to increase in temperature of the generator stator and the transformer cores. When the temperature exceeds the design thermal limit, the inter-lamination insulation material will be damaged [32]. The increase in core temperature ultimately decreases the permeability of the magnetic circuit and therefore the excess flux will be spilled into the surrounding structures. The non-laminated surrounding structures will be subjected to damage due to thermal runaway caused by induced eddy currents.

One of the main causes of excessive overexcitation on generators and transformers is operation of a generator unit under automatic voltage regulator control at reduced frequencies during start-up and shutdown [32],[34]. With the automatic voltage regulator maintaining rated voltage while the generator is operating at 95% of its rated speed or lower, the ratio of V/Hz at the generator terminals will be 1.05 pu or greater. Excessive overexcitation can also occur when the feedback signal from the terminal voltage transducer to the automatic voltage regulator is suddenly lost [32],[34]. Under this system contingency, the generator terminal voltage seen by the automatic voltage regulator is zero volts. The regulator will boost the field voltage to its ceiling limit in an attempt to restore the generator terminal voltage. In this case, ratio of V/Hz is much higher than the limit as a result of high generator terminal voltage.

2.5.3.7 Negative-sequence overcurrent protection: Device 46

Balanced three-phase loading is the ideal operating condition for a generator. However, it is difficult to achieve due to the nature of the power system. Open phases, faults and unbalanced loads are some of the causes of unbalanced loading conditions on a generator [32],[34]. From symmetrical component representation of unbalanced system conditions, generator stator currents can be resolved into positive, negative and zero sequence components as shown in equations (2.10) to (2.12), respectively.

$$I_1 = \frac{I_a + I_b\angle 120° + I_c\angle 240°}{3} \tag{2.10}$$

$$I_2 = \frac{I_a + I_b\angle 240° + I_c\angle 120°}{3} \tag{2.11}$$

$$I_0 = \frac{I_a + I_b + I_c}{3} \tag{2.12}$$

The magnetic field produced by the positive sequence generator current I_1 rotates in the same direction as the rotor. Both the rotor and the magnetic fields are rotating at the same speed which is known as synchronous speed. The resultant field retains a fixed position with respect to the rotor since the speed and direction of rotation of both are the same, and hence there will be no current induced into the rotor [32].

Negative sequence current I_2 appears when there is an unbalanced generator loading condition. Negative sequence current will produce a magnetic field which also rotates at synchronous speed; however, the direction of rotation is opposite to that of the power system. If negative sequence current exists, a double-frequency current will be induced into the rotor windings. The double-frequency currents induced in the rotor can cause a drastic rotor temperature increase in a very short time. Excessive rotor heating can result in insulation failure or deterioration of mechanical structures [32].

A generator can accommodate a certain amount of negative sequence current during its operation without consequences of severe damage. Both the continuous and short-time negative sequence current capabilities of a generator are clearly defined in [39]. An overcurrent relay is typically employed to detect negative sequence current that exceeds the defined capability limit of a generator.

2.5.3.8 Synchronism check relays: Device 25

During normal operation of a power system, generators will be isolated from service from time to time for maintenance or damage repair work. It is also the case that only some generators run continuously to supply the base load while the other generators are deployed only during peak load conditions. When a generator is returning to service, synchronization must be performed. The purpose of the synchronization is to match the magnitude, frequency and phase of the voltages on either side of the generator circuit breaker to within the set thresholds. The synchronism check relay performs a check on the voltage level and the operating frequency on both sides of the open circuit breaker and makes sure that they are within the acceptable limits before it issues a close

signal for the circuit breaker. The synchronism check is very important when the generator is returning to service. If the synchronization is not done properly before the closure of the circuit breaker, it can create large electrical and mechanical transients that can damage the generator, generator-step-up transformer and prime mover. In order to avoid these electrical and mechanical transients, the voltage and the frequency should ideally be matched perfectly. However, in practice, there will be small intentional mismatches, within the allowed tolerances, between the voltage magnitude and frequency of the generator and those of the system. The frequency of the generator will be set slightly higher than the system frequency and the generator output voltage will be set higher and leading the system voltage on the other side of the open circuit breaker. The above settings ensure that active and reactive power will flow out of the generator upon synchronisation. This will prevent the generator from operating as a motor due to reverse power flow after closure of the circuit breaker. The higher generator output voltage will avoid the intake of reactive power due to voltage dips during the period of synchronization [32].

2.5.3.9 Abnormal voltage protection: Devices 27 & 59

Abnormal voltage protection is provided to prevent the generator from operating beyond its design limit, and will operate under the following two situations: overvoltage conditions and undervoltage conditions. The undervoltage condition is not harmful to the generator since it will not cause any damage to it, but overheating of the auxiliary motors is an adverse effect for the undervoltage condition. The undervoltage relay is used to prevent extended operation at low voltages in order to protect the auxiliary motors. When the generator is operated at a voltage level much higher than its design limit, there will be excessive dielectric stress on the generator which will lead to insulation failure [1]. An overvoltage relay is used to protect the generator from overvoltage conditions.

2.5.3.10 Abnormal frequency protection: Device 81

The system frequency is 50 Hz under normal operation. The system frequency depends on the operating speed of the generator.

$$n_s = \frac{120 * f}{p} \tag{2.14}$$

Where n_s = synchronous speed [rpm]
f = system frequency [Hz]
p = number of magnetic poles

The mismatch between the generation of active power and the system load can lead to either acceleration or deceleration of the generator. Sudden loss of a major load or a transmission facility leads to the acceleration of the generators. Under this circumstance, mechanical power input to the

generators exceeds the electrical power transferred out of them and the imbalance causes acceleration of the generator rotors and an increase in the system frequency. When the generation is less than the system load, the generators will decelerate. This may be caused by sudden loss of major generation capacity. Under this circumstance, some of the kinetic energy stored in the rotors of the remaining generators connected to the system is converted to the electrical energy in order to sustain the system load. Off-frequency operation is not desirable since it will affect many aspects of the power system. Some of the system loads (i.e. induction motors) are very sensitive to the supply frequency; therefore any variation in the supply frequency will affect the performance of the loads. Abnormal frequency operation will also affect these types of sensitive load that are operating within the power stations themselves and therefore jeopardize the reliability and security of the entire generation plant [32]. Damage to the generating plant equipment is one of the major concerns during abnormal frequency operation. For example, the natural frequency of a turbine blade is designed to be sufficiently removed from rated speed and multiples of rated speed (i.e. the rated fundamental frequency and its harmonics) so as to avoid mechanical resonances. Excessive mechanical stress could be exerted on the turbine blades due to mechanical resonances if the turbine runs at non-rated speeds which could eventually lead to turbine cracking [40].

The National Energy Regulator of South Africa (NERSA) clearly indicates that the acceptable frequency deviation is ± 2% (± 1 Hz) for the grid network and ± 2.5% (± 1.25 Hz) for an island network. The limit for maximum frequency deviation is ± 2.5% (± 1.25 Hz) for the grid network and ± 5% (± 2.5 Hz) for the island network [41].

2.6 Generator modelling

The dynamic equations of synchronous machine windings are normally transformed into a two-axis (dq) coordinate frame using the Park Transformation [10]. This approach simplifies the structure of the mathematical model of the synchronous machine significantly. The two-axis form of the synchronous machine model is quite suitable for power system stability studies; however, it is not ideally suited to the requirements of most generator protection studies. Although the two-axis approach to modelling the synchronous machine greatly reduces the structural complexity of the machine model, certain details on the machine cannot be represented as a result of this simplification. For instance, generator internal winding faults (i.e. short circuits between the windings and ground) cannot readily be represented in the simulation model.

On the other hand, the use of a phase-domain dynamic model of the synchronous machine does allow internal winding faults to be represented more realistically in the simulation model. In the phase-domain generator model provided in RSCAD, the faulted winding has been included in the

inductance matrix calculation so that short circuits between the windings and ground can be simulated in the synchronous machine model. Another important feature of this model is that it allows a detailed electric representation of the external supply to the generator field circuit. In other words, this model allows the excitation input to the generator to be represented using power system components so that short circuit and open circuit faults on the excitation system, and even faults within the power electronics of an exciter, can be represented more realistically.

The phase-domain synchronous machine model has two different approaches for solving its inductance matrix, namely a two-axis (dq) based approach and a modified winding function approach [13]. The complete (modified winding function approach) version of the phase-domain synchronous machine model is capable of representing phase-belt harmonics induced in the generator stator winding. However, some specific generator details (i.e. the exact distribution of the stator windings and the actual shape of the rotor-pole arc) are required as inputs to the machine model when using the modified winding function approach [10]. It is a great challenge to acquire these specific generator details required for the complete version of the machine model and therefore only the simplified version (two-axis based approach) is provided in RSCAD for use on the real-time simulator. The simplified version of this machine model accepts standard parameters from the two-axis form of the synchronous machine equations rather than requiring knowledge of the physical geometry of an actual machine. However, this simplified version of the phase-domain synchronous machine model ignores certain details of the full phase-domain model as it assumes sinusoidal variation of all inductances with rotor position [10]. As a result, the simplified version of the machine model does not represent phase-belt harmonics in the generator stator winding, and so it is not able to represent the third-harmonic voltages in these windings that are relied upon by some forms of 100% stator ground fault protection scheme to detect stator winding faults. The simplified version of the phase-domain synchronous machine model that is available [13] does nevertheless allow internal stator winding faults and external field circuit faults to be represented accurately, at least with respect to the fundamental frequency behaviour of the generator variables. With additional modelling effort, it may be possible to supplement the characteristics of this simplified version of the faulted synchronous machine model to allow testing of 100% stator ground schemes that rely on detection of third-harmonic voltages. This issue is examined in detail in Chapter Six of the thesis.

2.7 Testing methods

In the past, real-time simulations were performed using analogue simulators. These analogue simulators were made from scaled down power system components [4], with each component physically connected in a similar fashion as in the real system. Equipment such as power system controllers and protection relays can be connected to analogue simulators in order to evaluate their

dynamic performance. However, the complexity and costs of an analogue simulator increases as the system model under study becomes more complex [4].

In contrast to analogue simulators, software-based simulators can be used to study power system transients based on mathematical representations of the system and its dynamics rather than scaled down physical components [4],[5]. Using this type of approach, a much more detailed power system network under study can be readily represented in the simulation. However, most of the software-based simulators cannot execute their simulations in real-time due to limited processing power of the computer workstations [5]. Because of non-real-time operation of these software-based simulators, interaction between hardware equipment (e.g. power system controllers and protection relays) and simulated plant is not possible. Nevertheless, different fault scenarios of the power system can be simulated using non-real-time software-based simulators and particular voltage and current waveforms required as relay inputs can be recorded during the simulation study. Alternatively, voltage and current waveforms can be generated by test-sets or obtained from actual fault records taken from system contingencies. These voltage and current waveforms can then be played back in real time using digital to analogue converters [4]. The protection relay under study is then injected with secondary voltages and currents in order to observe the relay's response to a particular fault scenario. This type of approach is often referred to as open-loop injection testing. Using this testing method, a quick validation of protection relay settings can be achieved, however, the performance of some relays' protective functions cannot be evaluated.

Real-time simulation technology has been realised due to advances in digital signal processing and improved efficiency of power system component models [5]. Power system simulations are carried out on the real-time digital simulator which consists of many high-speed digital signal processors operating in parallel. The real-time digital simulator differs from traditional non-real-time system simulation in many aspects. The real-time simulator not only can execute the simulation in real time but also allows physical equipment to be connected to, and interact with, the simulated plant. The performance of physical protection relays with full settings can be studied and the interaction between the simulated power system and the protection relays can be observed using this real-time, closed-loop testing approach [4],[5],[6]. This now well-established and advanced relay testing methodology has been adopted by relay manufacturers and researchers at various institutions. The main objective of this research project was to perform hardware-in-loop testing on one of the industrial generator protection relays (SEL 300G) which was donated to the research centre where the work was to be carried out. A detailed discussion of hardware setup for real-time closed-loop testing is contained in Chapter Three.

2.8 Conclusion

This chapter has presented some background material to illustrate the role and the importance of power system protection in general. Reviews on specific generator protection functions and their applications have also been presented.

The chapter further discussed different modelling approaches for the synchronous machine in power system simulation studies. The advantages and disadvantages of each modelling approach were discussed. It is concluded that the phase-domain category of synchronous machine model has many advantages when it comes to the area of generator protection studies, especially for studies of stator winding protection schemes. Therefore the performance of phase percentage restrained differential protection (87P) and 100% stator ground fault protection (64G) can be evaluated using this type of machine model. Furthermore, this machine model allows detailed and realistic representation of the generator field supply circuitry and therefore the performance of loss-of-field protection (40) can also be evaluated. As discussed earlier, generators play an important role in a power system's stability and therefore a generator or a group of generators that is pole slipped must be isolated in order to maintain stability of the remaining interconnected generators. Thus the performance of out-of-step protection (78) is critical in terms of a power system's stability. Each of the aforementioned generator protection functions is focused on in the protection studies carried out in the later chapters of the thesis.

The next chapter describes the study system used in this thesis to investigate the use of phase-domain generator models on the real-time simulator for testing generator protection relays and explains how the hardware-in-loop studies used to test these relays are carried out.

CHAPTER 3

STUDY SYSTEM

3.1 Introduction

In the previous chapter, overviews of some general protection concepts and particular generator protection elements have been presented. Different modelling approaches for synchronous machines and various testing methods for hardware equipment were also reviewed. The conclusion reached was that the dynamic performance of particular generator protective functions can be evaluated using the real-time simulator with phase-domain synchronous machine models.

This chapter reviews the particular study system used in this research project. The study system comprises four generators at a power station connected to a remote system via two transmission lines. A real-time simulation model was developed in the simulation package RSCAD, based on this study system, for the purpose of hardware-in-loop testing of a SEL 300G generator protection relay. Using this type of approach, generator protection studies can be carried out in a more realistic testing environment. In addition, the hardware generator protection relay can interact with the simulated plant (i.e. one of four generators in the power station): for instance, it can send trip signals to associated generator circuit breakers or receive breaker status from the simulated plant.

This chapter also provides an overview of the actual hardware generator protection relay (SEL 300G) that is used throughout this research project. Details of the closed-loop connections between the real-time simulator and the SEL 300G relay hardware are given to provide the background to the actual test set up for this particular project.

Finally, the chapter discusses the purpose of using RSCAD's generic, real-time model of a generator protection relay in parallel with the actual generator protection relay hardware under test during particular types of protection study such as loss-of-field protection (40) and out-of-step protection (78).

3.2 Overview of the study system

Before proceeding to the hardware-in-loop testing of the generator protection relay, a real-time simulation model had to be developed and it was based on the chosen study system shown in Figure 3.1. This system was selected for the following reasons. Firstly, the system is a well-known benchmark model [11] for conducting generator stability studies. Secondly, it has documented parameters that are representative of both large generators and their associated controllers. In studies of generator protection, it is extremely important to have detailed and realistic information

on the generator controllers since these controllers have a significant influence on generator and power system stability, and hence on some of the generator protection elements during system disturbances.

Figure 3.1 illustrates the single line diagram of the study system being simulated in RSCAD. In this original study system example, all four generators in the power station are commonly represented using a single lumped generator and step-up transformer model of MVA rating equal to the combined rating of the four individual units [11]. In this study system, the total capacity of the generating plant is 2220 MVA with a terminal voltage of 24 kV. The primary side of the generator step-up transformer was connected at the terminals of the generator and the voltage on the secondary side of the transformer was stepped up to 400 kV for connection to the HV bus which feeds two transmission lines. These two transmission lines were then connected to a remote system which is represented as an infinite bus in the real-time simulation model.

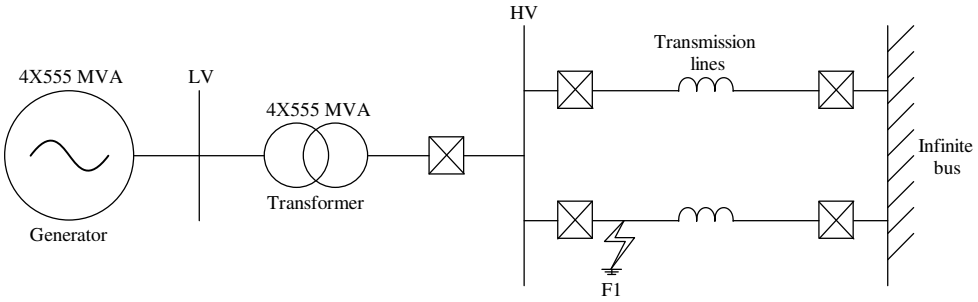

Figure 3.1. Single line diagram of the study system with all four generators represented using a lumped generator model (4LG).

However, the study system as described above was not the final representation of the system used for the hardware-in-loop testing of the generator protection relay since it required further modifications to suit the specific requirements of generator protection studies. The purpose of modifying the real-time model was to allow the external generator protection relay to be connected in a hardware-in-loop configuration so as to be able to provide specific protection functions for a single one of the generators in the study system.

Figure 3.2 illustrates a modified version of the study system in Figure 3.1. The system is electrically the same as the representation shown in Figure 3.1 but employs a slightly different approach to lumping the multiple generators in the power station. In this modified version, three of the generating units are represented using one lumped synchronous machine and step-up transformer model (of 1665 MVA rating), and the fourth generating unit is represented separately by means of a single 555 MVA synchronous machine and transformer model. With this modified representation of the study system, generator internal winding faults and various field

contingencies can be considered on a single generator in the station. This approach not only allows for more realistic interfacing between the real-time model of the generator and the external relay in terms of the required current transformer turns ratios, but also, in the case of certain protection functions such as loss-of-field (40) it is important that the behaviour of the neighbouring, healthy generators in the station during such an event, and their influence on the response of the faulted generator and its protection, are represented properly.

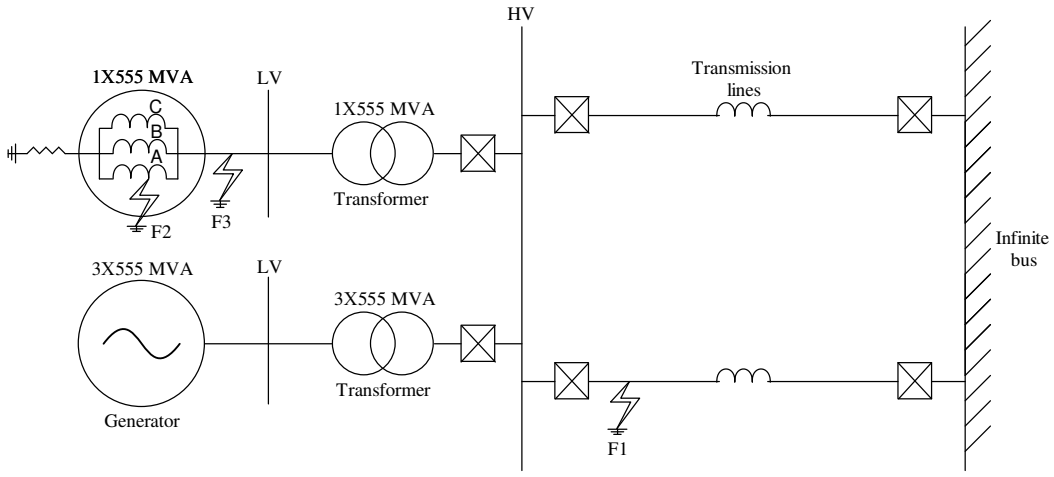

Figure 3.2. Single line diagram of the study system with three of the units represented using a lumped generator model (3LG) and one unit represented using a single generator model (1G).

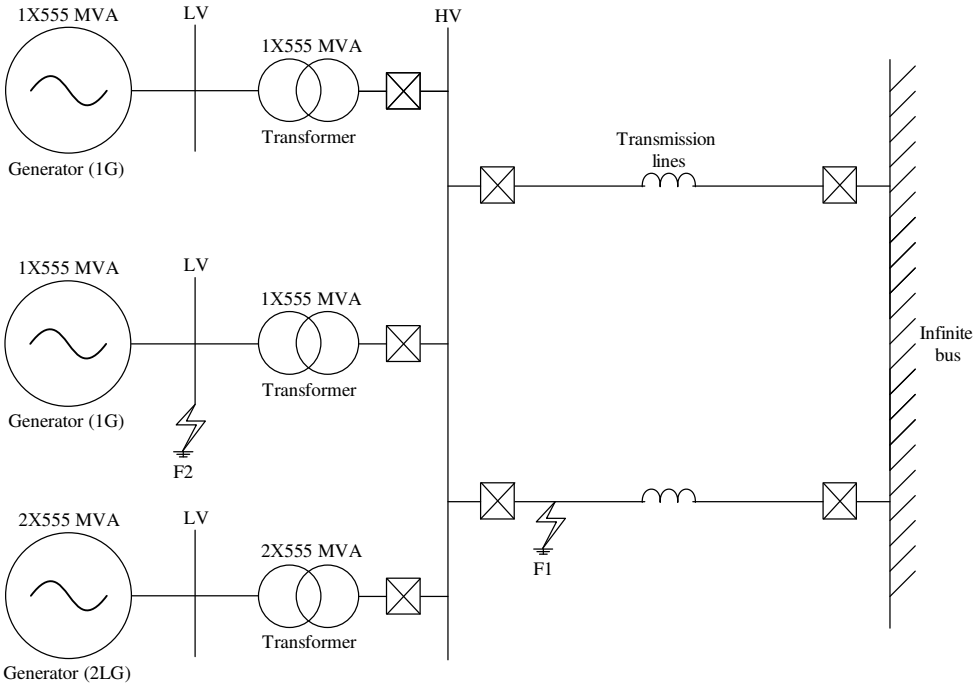

Figure 3.3. Single line diagram of the study system with two of the units represented using a lumped generator model (2LG) and two units each represented using a single generator model (1G).

A generator's stability can be significantly influenced when a large system disturbance occurs inside or near the power station. For this reason, out-of-step protection (78) is employed to detect and isolate unstable generators that cannot return to steady-state operation after a system disturbance. For the purpose of examining the performance of an out-of-step protection (78) function that is implemented to protect a particular 555 MVA generator within the power station of the chosen study system, another modified version of the study system was developed in order to allow a large system disturbance inside the power station to be represented.

Figure 3.3 illustrates this second modified version of the original study system in Figure 3.1. The system is again electrically the same as the representation shown in Figure 3.1 but now employs another approach to lumping the multiple generators in the power station. In this representation, two of the generating units are represented using one lumped synchronous machine and step up transformer model (of 1110 MVA rating), while the third and fourth generating units are represented separately by means of single 555 MVA synchronous machine and transformer models. Including this level of detail in the model of the study system makes it possible to study the response of out-of-step protection functions on one generator unit to a severe fault at the terminal of a single, neighbouring unit in the same station that may, or may not be tripped out as a result of the contingency and may not have been operating at the same steady-state operating conditions of active and reactive power output prior to the disturbance.

3.3 Real-time model of study system for low-resistance grounded generator protection studies

As discussed in the previous chapter, there are many grounding schemes available for generators. This section presents the real-time simulation model of the study system just described which was developed for the particular requirements of studying the protection of low-resistance grounded generators in Chapters Four and Five.

Figure 3.4 shows the new phase-domain synchronous machine model available for the real-time simulator platform in RSCAD. This new model differs from the more regular form of machine model used on the real-time simulator and in other simulation programmes in many respects. The major difference is that this new synchronous machine model has the ability to represent realistic internal winding faults on the stator circuit. This new feature provided by the phase-domain synchronous machine model allows the user to apply an internal winding fault on the stator winding at a user-settable location from end of the winding all the way to the generator stator terminals. The model therefore offers the facility to test the performance of generator winding protection schemes such as generator differential protection (87P) or (87N), 100% stator ground fault protection (64G) and neutral injection (64S). Figure 3.4 also illustrates two different modes in which the phase-domain synchronous machine model can be employed in real-time studies. The

appearance of the model on the left hand side of Figure 3.4 illustrates one of these simulation modes in which the generator model only requires a control-signal type of input from an adjacent excitation control system model. In the second mode, shown on the right hand side of Figure 3.4, the phase-domain synchronous machine model allows the adjacent excitation system to be modelled explicitly as an electrical circuit which then forms part of the electromagnetic transient solution. This is another advantage of the phase-domain synchronous machine model: since the electrical equipment supplying the generator field circuit can now be represented in detail using power system components, more realistic contingencies and fault scenarios can be considered when conducting generator protection studies.

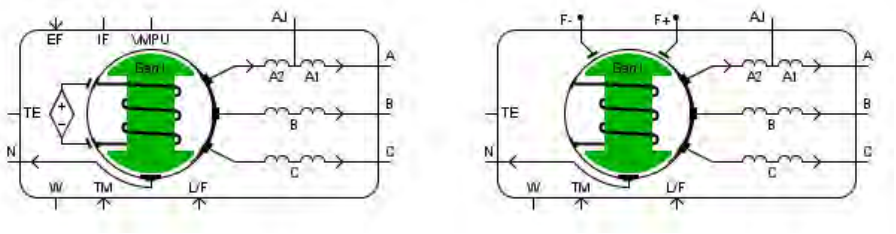

Figure 3.4. Phase-domain synchronous machine model.

Figure 3.5 shows the detailed real-time simulation model of the modified version of the study system shown in Figure 3.2 that has been developed for the studies in Chapters Four and Five of this thesis. As mentioned in the previous section, for these particular studies three of the four generators in the power station were represented using a lumped generator model of 1665 MVA rating so that a SEL 300G generator protection relay could be connected to a model of the remaining, single generator of 555 MVA rating. In the RSCAD representation of the study system shown in Figure 3.5, the machine model and its excitation controls used to represent the three lumped generators, and the machine model and excitation controls used to represent the single generator are each grouped within the hierarchy block component boxes seen on the left-hand side of the diagram. The real-time models grouped within the hierarchy component box for the single generator to be interfaced to the protection relay are shown in more detail in the diagram of Figure 3.6.

Figure 3.6 shows the full details of the real-time modelling of the particular 555 MVA generator in the study system that is represented individually for the purposes of studying low-resistance grounding protection systems (i.e. Figure 3.6 shows the contents of the hierarchy box labelled UNIT 1 in Figure 3.5).

As mentioned earlier, generator controllers have a significant influence on system stability, and consequently on the performance of some of the generator protection elements during system

disturbances. For this reason, detailed representations of the generator's automatic voltage regulator (AVR) and power system stabilizer (PSS) are included in the real-time simulation model as shown in Figure 3.6.

A phase-domain synchronous machine model was used to represent the particular 555 MVA generator in the study system that was to be interfaced to protection relays during the studies as shown in Figure 3.6. This machine model allows the user to apply an internal winding fault on phase A of the stator winding at user-settable location. This advanced feature provided by the phase-domain synchronous machine model allows the performance of different types of generator winding protection scheme to be evaluated. For low-resistance grounded generators, phase percentage restrained differential protection (87P) is one form of generator protection scheme that can be employed to protect generator stator windings, and this form of protection was to be studied using the real-time simulation model developed.

The phase percentage restrained differential protection (87P) function provided by the SEL 300G generator protection relay being studied also allows the generator step up transformer to be included in the differential protection zone. In order to carry out this particular protection study, a faulted transformer model is required to represent the generator step up transformer. However, a faulted three-phase transformer model was not available in the real-time simulation package (RSCAD) and therefore the generator step up transformer is represented using three individual faulted single-phase transformer models as shown in Figure 3.6. The faulted single-phase transformer model has the ability to represent realistic transformer internal winding faults such as turn-to-turn faults or turn-to-ground faults. As can be seen in Figure 3.6, internal winding faults can be represented on the primary winding of the generator step up transformer. A similar transformer model was developed to represent the internal winding faults on the secondary winding of the generator step up transformer.

When a stator winding to ground (stator-ground) fault occurs on a generator, different circuit breakers (i.e. generator's main circuit breaker, field circuit breaker and neutral circuit breaker) need to be opened in order to clear the fault. All the aforementioned circuit breakers are included in the real-time simulation model shown in Figure 3.6. The operation of these circuit breakers is controlled by a binary signal sent by the SEL 300G hardware relay. The purpose of opening the generator's main circuit breaker is to isolate the faulted generator from the system, while the generator field is de-energized by opening the field circuit breaker to disconnect the field source from the generator field winding. The purpose of opening the neutral circuit breaker is to interrupt the stator-ground fault current rapidly otherwise the fault current would flow for several seconds due to the slow decay of the generator voltage after the field has been de-energized.

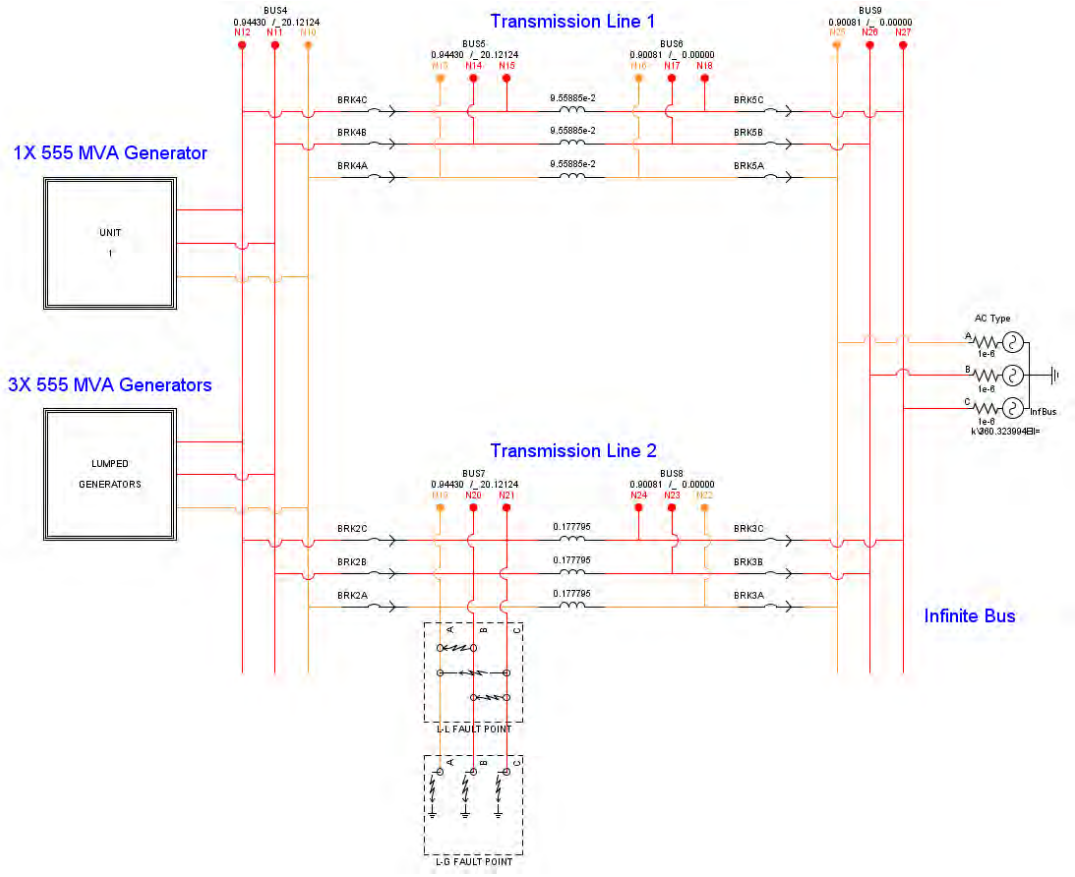

Figure 3.5. Real-time simulation model of the study system using the representation shown in Figure 3.2.

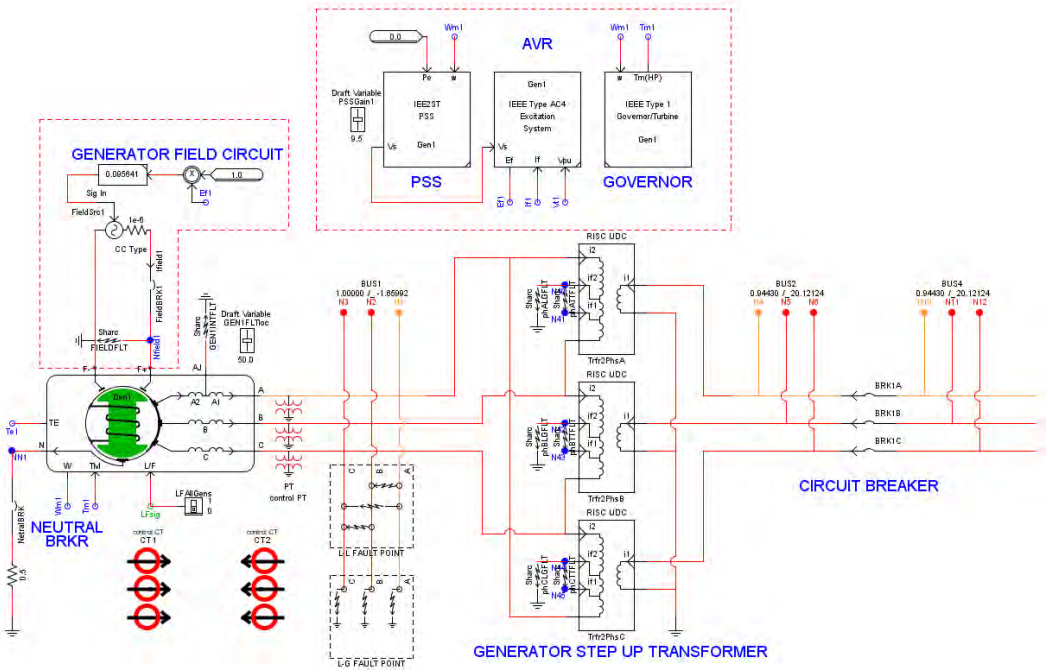

Figure 3.6. Real-time modelling details of one generator in the study system for low-resistance grounding protection tests.

As mentioned earlier, the phase-domain synchronous machine model provides another important feature which allows the generator field circuit to be modelled explicitly. As can be seen in Figure 3.6, an external source and a field circuit breaker are included in the generator field circuit. Using the phase-domain synchronous machine model in this mode, different system contingencies on the generator field circuit can now be considered. For instance, contingencies such as the inadvertent opening of the field breaker or a short-circuit across the field winding can be included in the studies to evaluate the performance of the loss-of-field protection (40) function.

Figure 3.6 also shows that voltage and current transformers are included in the real-time simulation model to measure the system variables that are required as inputs to the relay under study. The measured secondary quantities from these instrument transformers are to be injected into the SEL 300G generator protection relay in order for the protection functions to make their tripping decisions.

3.4 SEL 300G Relay

The SEL 300G is the particular relay to be connected in closed-loop with the real-time simulator, in a hardware-in-loop configuration, in order to provide specific protection functions for the particular 555 MVA generator under study. The SEL 300G relay is a multifunctional digital microprocessor based relay and it is representative of the class of device typically used to protect the large generators found in power stations. This relay contains different protective functions that are implemented to protect the generator from various types of fault and system contingency. The available protective functions of SEL 300G relay are listed in Table 2.1 in Chapter Two.

AcSELerator QuickSet is the software tool used to configure the different protection element settings within the SEL 300G generator protection relay. Figure 3.7 illustrates the AcSELerator QuickSet software setting window. The user can activate or deactivate any protection elements provided by the SEL 300G relay according to the requirements of the designed protection system. However, one particular protection function, namely protection against loss-of-potential (60), cannot be deactivated since its purpose is to detect any loss of signal from the voltage transformers used to measure generator terminal voltages. This loss-of-potential element is usually used to trigger an alarm in order to notify the system operators in such an emergency situation. The loss-of-potential element is also used to block the relay from tripping when there is a situation of lost voltage transformer signal. Some of the other generator protection functions (i.e. loss-of-field protection, out-of-step protection and backup distance protection) require the signals measured by the voltage transformers at the generator terminals in order to determine the trajectory of the impedance locus upon which they base their tripping decisions. In order to avoid misoperation of

the relay during a loss-of-potential condition, the loss-of-potential element always has to be included when the user is designing the tripping logic for generator protection.

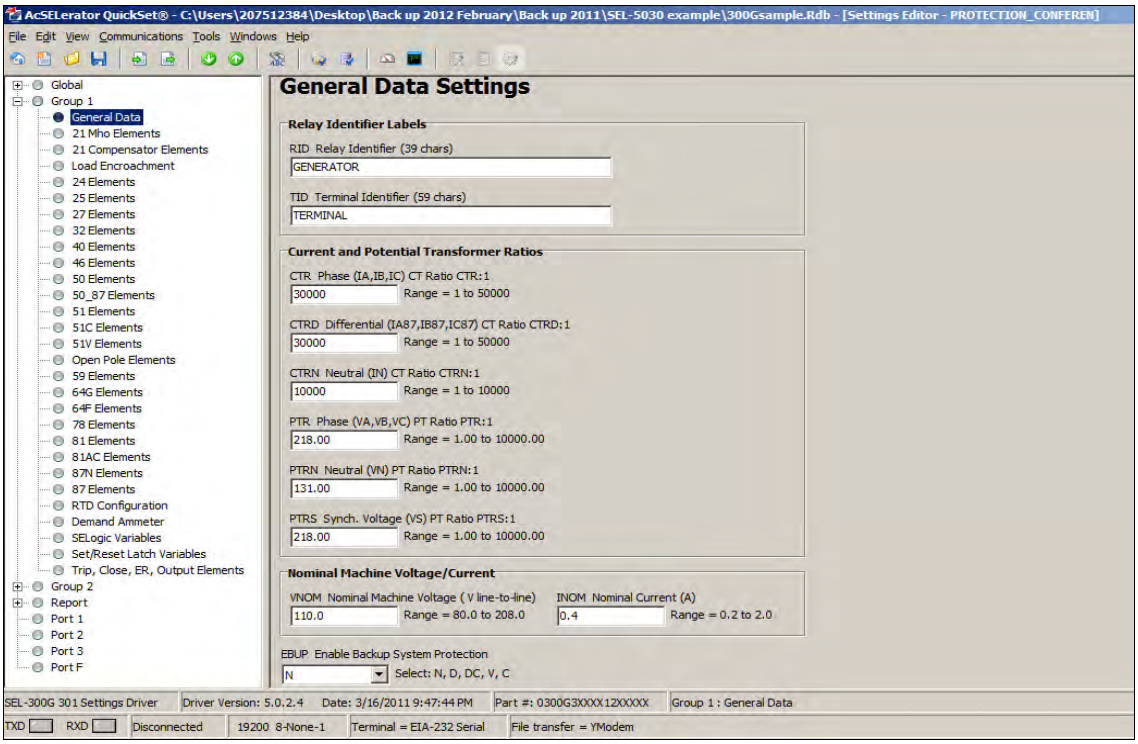

Figure 3.7. AcSELerator QuickSet software setting window.

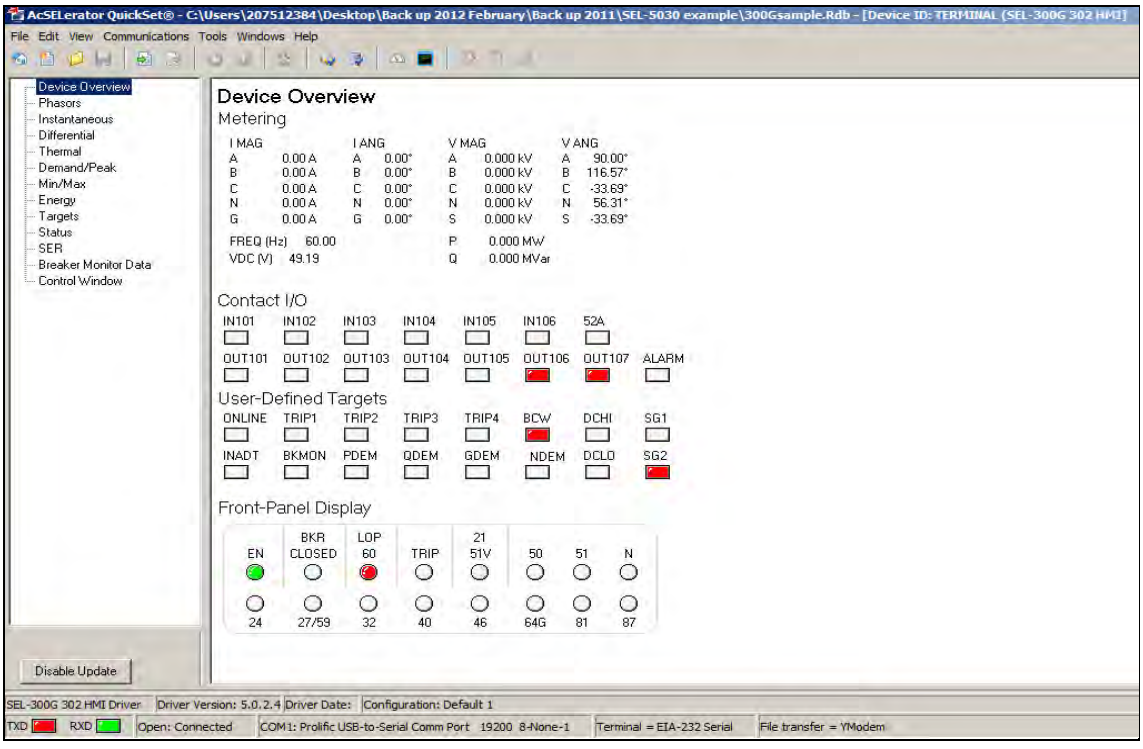

Figure 3.8a. HMI of the SEL 300G relay: Device overview.

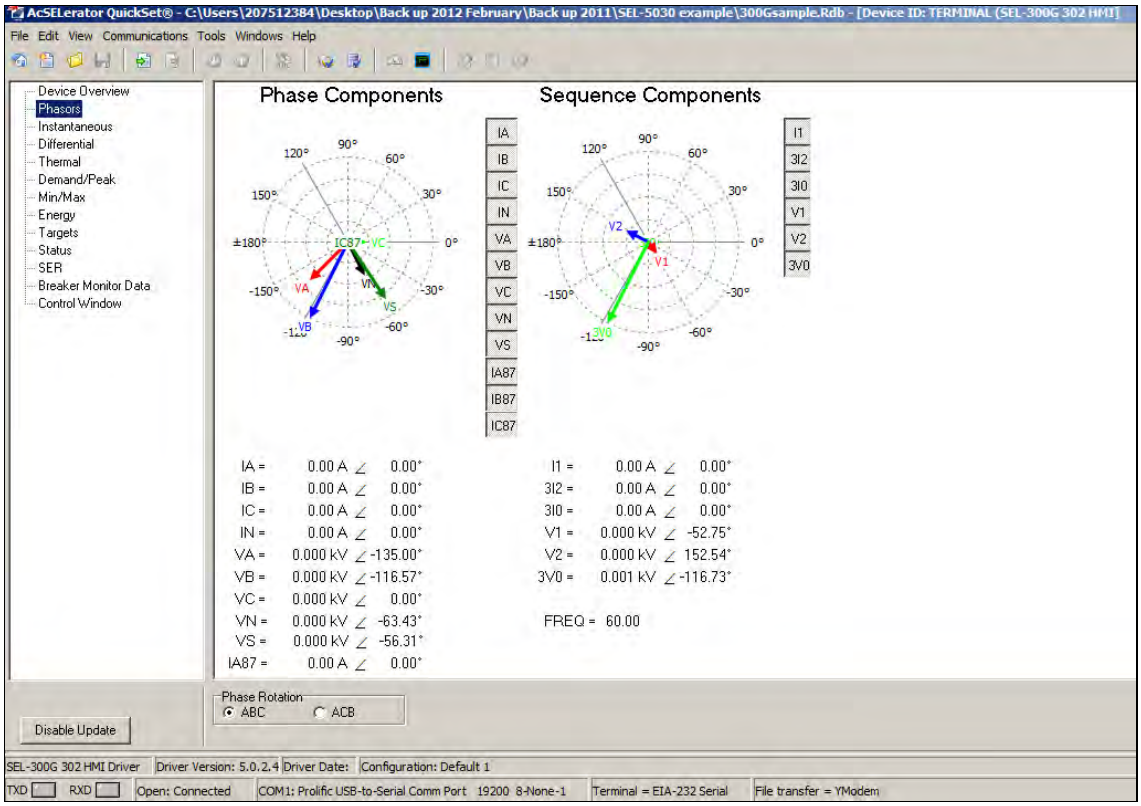

Figure 3.8b. HMI of the SEL 300G relay: Phasors.

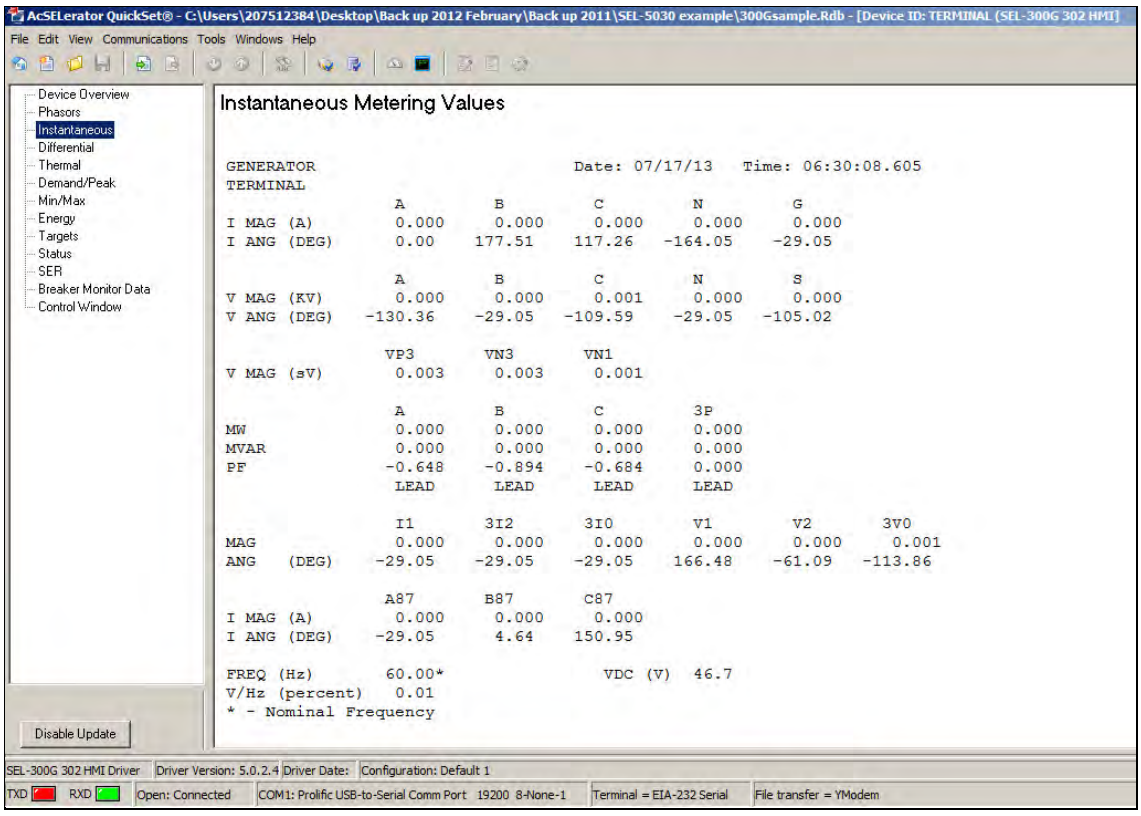

Figure 3.8c. HMI of the SEL 300G relay: Instantaneous metering values.

The AcSELerator QuickSet software also provides other features besides relay setting functionality. Logic functions for tripping and closing the protected generator can be designed within the software. The software also allows real-time monitoring of the system variables as shown in Figures 3.8a to 3.8c (i.e. measured voltages, measured currents and different sequence components calculated by the relay) when the generator is in service. One of the important features of modern digital microprocessor based relays is their event recording capability. This is a very useful feature for post-fault analysis since protection engineers can now analyse the system contingency associated with a fault from the data recorded by the relay during the disturbance. Improvements of the settings or new operating procedures can be recommended from the post-fault analysis in order to achieve a more secure protection system and a more reliable power system.

3.5 HIL connection of generator protection relay

The study system plant is modelled in detail mathematically using the real-time simulation package (RSCAD) and the real-time simulator executes the solution of the dynamic behaviour of this plant in real time. Figure 3.9 illustrates how hardware-in-loop testing is conducted on the real-time simulator for the particular protection studies carried out in the thesis.

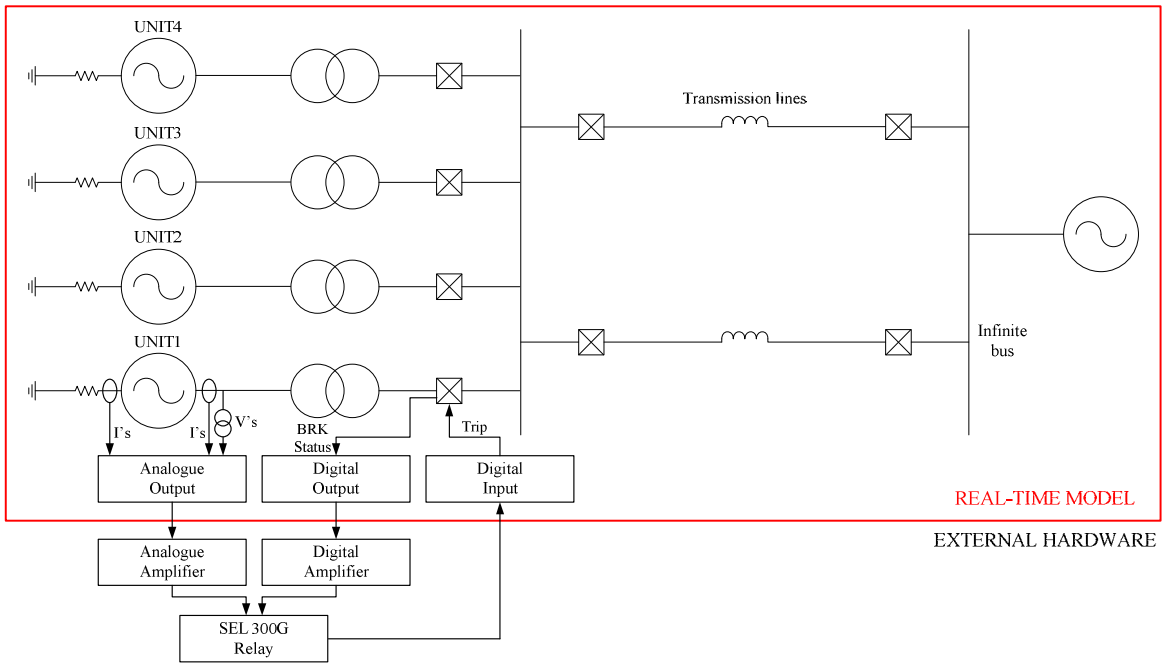

Figure 3.9. Schematic diagram showing real-time closed-loop testing of a SEL 300G generator protection relay connected to one of the low-resistance grounded generators in the study system.

As discussed in Section 3.3, instrument transformers are included in the simulation model of the protected plant for the purpose of measurement and their secondary quantities are exported to analogue output cards that form part of the real-time simulator hardware. Analogue amplifiers then amplify the analogue signals at the output of the simulator to the magnitudes which correspond to

the secondary output variables of the instrument transformers within the real-time model. The outputs of these amplifiers, representing the secondary voltages from voltage transformers and secondary currents from current transformers within the real-time model, are injected into the normal measurement inputs of the SEL 300G generator protection relay that is under study.

A similar approach can be followed if digital signals need to be exported to the external protection hardware under test. For instance, the status of the circuit breaker is required by the external hardware relay in order to implement a breaker failure protection scheme. In the real-time simulation, the status of any of the generator's circuit breakers (open or closed) can be exported to a digital output card on the simulator in the form of binary logic variables (1 or 0). A digital amplifier (also known as a high voltage digital interface panel) is used to boost the TTL-level logic at the output of the simulator to the appropriate logic level required for connection to a binary logic input of the SEL 300G generator protection relay hardware.

Various protection elements are implemented inside the SEL 300G generator protection relay in order to respond to different system contingencies and fault scenarios. When the protection relay makes a decision to trip the generator in response to a fault on the generator or some other stability issue, the relay's trip signal is sent back to the real-time model via a digital input panel on the simulator in order to open the corresponding circuit breakers to clear the fault. For example, in the event of a stator winding to ground fault on the generator, depending on the grounding arrangement of the generator, the trip signal sent by the protection relay can be used to open the generator's main circuit breaker, field circuit breaker and the neutral circuit breaker as required.

Figure 3.10 shows a schematic representation of the connections required for hardware-in-loop closed-loop testing of a protection relay using photographs of the actual equipment involved in practice.

Finally, Figure 3.11 shows a photograph of the actual test set up used during the work in this thesis, showing the detailed electrical connections between the inputs and outputs of the hardware relay (SEL 300G), the real-time simulator and the amplifiers as well as the host computer used to run the studies.

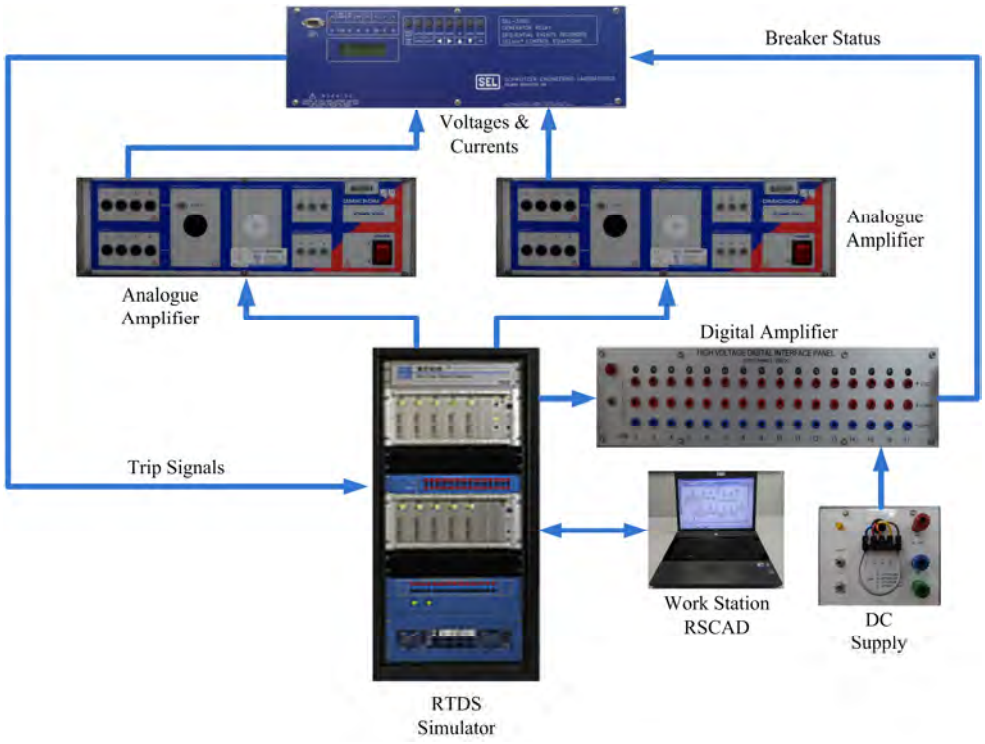

Figure 3.10. Schematic representation of hardware setup for real-time closed-loop testing.

Figure 3.11. Photograph of the actual test set up.

3.6 Generic real-time model of generator protection relay

As mentioned in Chapter One, the RSCAD programme provides various pre-developed generic models of protection relays for real-time simulation studies. There are several advantages to using these software protection relay models. Firstly, users can familiarise themselves with the protection philosophies and setting calculations using software relay models. Secondly, various protection studies can be conducted using these software relay models if hardware relays are not available.

In the studies of loss-of-field protection (40) and out-of-step protection (78), RSCAD's pre-developed generic real-time model of a generator protection relay was included in the real-time simulation model to run in parallel with the hardware generator protection relay (SEL 300G). This highly-detailed software generator protection relay is a multifunctional relay which possesses features that are similar to actual generator protection relay hardware. The purpose of using the software generator protection relay was to gain more insight into the dynamic behaviour of the actual hardware generator protection relay during particular protection studies rather than to predict the performance of the actual hardware relay. In other words, the software relay model was only used to display the trajectory of the positive sequence impedance in the R-X impedance plane during studies of loss-of-field protection (40) and out-of-step protection (78). The tripping characteristics of the aforementioned protection functions can then be overlaid onto the recorded impedance's trajectory in the R-X impedance plane for explaining the behaviour of the actual hardware relay during these particular protection studies.

3.7 Conclusion

This chapter has presented an overview of the study system to be used for real-time closed-loop testing of a SEL 300G generator protection relay. The development of the real-time simulation model, based on a well-known study system, and the reasons for certain modifications in the representation of the generators in the system were also discussed in detail.

The functionalities for both the SEL 300G generator protection relay and RSCAD's software generator protection relay model were reviewed in order to provide some background to the equipment under test. Furthermore, the equipment set up used for this particular project was presented in order to illustrate how real-time closed-loop testing is conducted for the SEL 300G generator protection relay. This chapter, in short, has presented all the preparation work that was required before conducting the actual hardware-in-loop tests on the SEL 300G generator protection relay.

Chapter Four focuses on the theory behind, and setting calculations for, the particular generator protective functions that are to be studied in the hardware-in-loop tests to be presented in Chapter Five, namely phase percentage restrained differential protection (87P), loss-of-field protection (40) and out-of-step protection (78).

CHAPTER 4

THEORY AND SETTINGS FOR LOW-RESISTANCE GROUNDED GENERATOR PROTECTION STUDIES

4.1 Introduction

In the previous chapter, the details of the particular study system selected for conducting real-time closed-loop studies were reviewed. In addition, different real-time simulation models of the selected study system were introduced to suit the particular requirements when testing a range of different protection functions available on the SEL 300G relay. The approach used in practice to interconnect the real-time simulator and the SEL 300G relay hardware was also demonstrated to provide some background to the work performed in the thesis.

Before evaluating the particular protection functions of interest on the SEL 300G generator protection relay using the real-time closed-loop testing approach, full settings for these protection elements have to be configured on the relay. This chapter focuses on the theory of operation and setting calculations for the particular generator protective functions to be studied in the hardware-in-loop tests to be presented in Chapter Five, namely phase percentage restrained differential protection (87P), loss-of-field protection (40) and out-of-step protection (78). In addition, different practical setting considerations for each of the aforementioned protection elements are discussed in detail.

4.2 Phase percentage restrained differential protection (87P)

There are different types of fault that can occur on the stator windings of a generator. The main types of stator winding fault are: phase to earth faults, phase to phase faults, and inter-turn faults involving turns of the same phase winding. Of these faults, a phase to earth fault is the most common occurrence on the stator winding [42]. When a phase to earth fault occurs on the stator winding of a low-resistance grounded generator, it will produce a large fault current that flows in the stator winding which can cause severe damage to both stator winding and stator core. For this reason, the generator must be tripped as quickly as possible in order to avoid severe damage during a stator winding to ground (stator-ground) fault in low-resistance grounded units.

The phase percentage restrained differential protection function (87P) provided by the SEL 300G relay is one form of protection scheme that can be implemented to protect the stator windings of a low-resistance grounded generator. This protection scheme relies on measurement of the currents at both ends of the stator winding of the protected generator in order to calculate differential and

restraint currents which are then utilized to make tripping decisions. Equations (4.1) and (4.2) show the mathematical definition of the differential and restraint currents respectively.

$$I_{DIFF} = |I_1 - I_2| \tag{4.1}$$

$$I_{RT} = \frac{|I_1 + I_2|}{2} \tag{4.2}$$

The tripping characteristic of a phase percentage restraint differential protection scheme (87P) is a two-dimensional area defined on a Cartesian plane. Figure 4.1 illustrates one type of tripping criterion known as a dual-slope differential characteristic. The vertical axis on the Cartesian plane shown in Figure 4.1 represents the differential current while the horizontal axis represents the restraint current. The boundary conditions of the dual-slope differential characteristic are defined by the following user-adjustable settings:

1) Restrained Differential Element Pickup Setting (O87P)
2) Restrained Differential Element Slope 1 Setting (SLP1)
3) Restraint Current at Intersection of Slope 1 and Slope 2 (IRS1)
4) Restrained Differential Element Slope 2 Setting (SLP2)
5) Unrestrained Differential Element Pickup Setting (U87P)

The purpose of these user-adjustable settings is to accommodate different factors that can influence the differential current under normal operating conditions. A detailed discussion of these factors is contained in Sections 4.2.1 and 4.2.2. These adjustable settings of the dual-slope differential characteristic clearly define the regions for the phase percentage restrained differential protection (87P) to operate or to restrain.

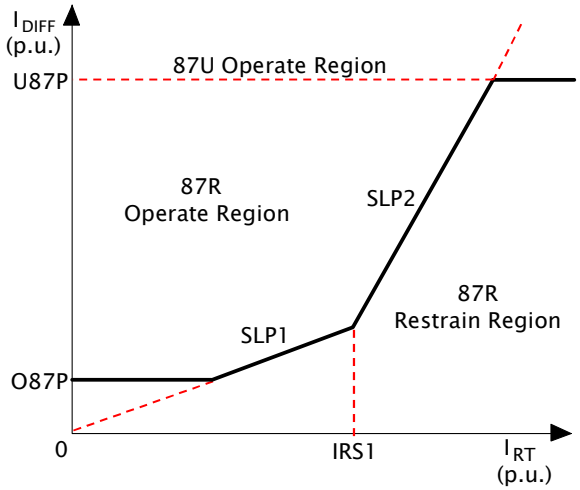

Figure 4.1. Dual-slope differential characteristic (reproduced from [31]).

The logic diagram shown in Figure 4.2 illustrates the algorithm implemented by the SEL 300G generator protection relay for the phase percentage differential protection scheme. For the phase percentage restrained differential protection (87P) to operate, there must be sufficient differential current to cause the differential versus restraint current trajectory to pass into the tripping area of the dual-slope differential characteristic.

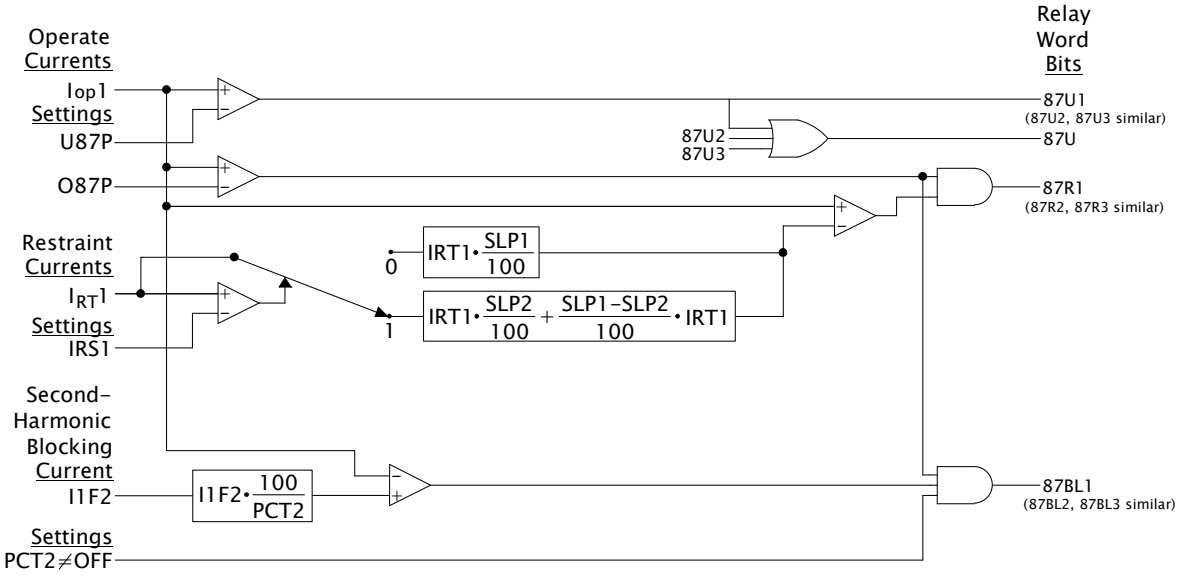

Figure 4.2. Logic diagram of phase percentage differential protection (reproduced from [31]).

As discussed earlier, phase percentage restrained differential protection (87P) is implemented to protect the stator windings of a low-resistance grounded generator. However, the SEL 300G relay also allows the option for the generator step up (GSU) transformer to be included in the differential protection zone. Sections 4.2.1 and 4.2.2 illustrate different setting calculations and considerations for each of these different protection arrangement options.

4.2.1 Settings of the 87P element without GSU transformer included

In this section, only the single, 555 MVA, low-resistance grounded generator shown in Figure 3.2 is considered when calculating the settings for the phase percentage restrained differential protection scheme.

The first step is to calculate the full-load secondary outputs of the current transformers used to measure the currents in the generator stator windings since this information is required as a relay input setting. Under healthy generator operating conditions, the full-load stator current of the protected generator can be calculated as follows.

$S_{base} = 555\ MVA$

$V_{base} = 24\ kV$

$$I_{base} = \frac{S_{base}}{\sqrt{3} \cdot V_{base}} = \frac{555 * 10^6}{\sqrt{3} \cdot (24 * 10^3)} = 13.351\ kA$$

The current transformers represented in the real-time simulation model have turns ratio of 30000:1 and therefore the secondary outputs of the current transformers are:

$$I_{sec} = \frac{I_{base}}{CT\ ratio} = \frac{13.351 * 10^3}{30000/1} = 0.45\ A$$

Restrained Differential Element Slope 1 Setting (SLP1):

As discussed in Section 2.5.3.1 in Chapter Two, there are many factors that can result in a differential current under un-faulted conditions that is not only non-zero, but that also varies with operating conditions. The purpose of the SLP1 setting is to increase the differential current required for tripping in direct proportion to the measured restraint current in order to enhance the security of the protection scheme during normal operating conditions. The following factors are considered when calculating the Restrained Differential Element Slope 1 Setting value.

1) Measurement accuracies for the current transformers.
2) Pick-up accuracy for the protection relay.
3) Sufficient operating margin.

Different classes of current transformers have different measurement accuracies and therefore the measurement accuracy must be obtained from the nameplate of that specific current transformer. In this case, the current transformer measurement accuracy is assumed to be 10%. The relay pickup accuracy can be obtained from the instruction manual of the relay. In this case, the relay pickup accuracy is 5% [31]. An operating margin of 5% is typically provided in order to increase the security of the differential protection scheme. Based on the information given above, the Slope 1 setting can be calculated as follows.

$SLP1 = 10\% + 10\% + 5\% + 5\% = 30\%$

Restrained Differential Element Pickup Setting (O87P):

The restrained differential element pickup setting (O87P) defines the minimum pickup value of the differential current shown in Figure 4.1. The O87P setting is calculated using the guidance shown in equation (4.3).

$$O87P = 0.5 * SLP1 + P' \quad (4.3)$$

Where P' = no-load losses of the transformer at maximum voltage [%]

P' represents the core loss component of current in the transformer equivalent circuit which is expressed as a percentage of nominal current. This value will only be included in the O87P setting calculation when the GSU transformer is included in the differential protection zone [43]. In this case, P' is equal to zero.

$$O87P = 0.5 * \frac{30}{100} = 0.15\ p.u.$$

Restrained Differential Element Slope 2 Setting (SLP2):

The purpose of the SLP2 setting is to increase the security of the differential protection scheme during heavy through-fault conditions. A heavy through-fault condition can result in severe saturation of a current transformer. When a current transformer saturates, it can no longer faithfully reproduce the primary current with a scale factor on the secondary side of the current transformer. As a result, a very high differential current can be obtained under heavy through-fault conditions. The SLP2 setting is typically set higher than the SLP1 setting in order to further increase the differential current required for tripping in direct proportion to the measured restraint current during heavy through-fault conditions. When phase percentage restrained differential protection (87P) is configured to protect a generator without including the GSU transformer, the SLP2 setting is fixed to 100%.

Restraint Current at Intersection of Slope 1 and Slope 2 (IRS1):

When the 87P element is configured to protect a generator without including the GSU transformer, the turning point between slope 1 and slope 2 defined by the value IRS1 is fixed to 3.0 per unit.

Unrestrained Differential Element Pickup Setting (U87P):

The purpose of the Unrestrained Differential Element Pickup Setting (U87P) is to detect very high differential current that clearly indicates a fault inside the differential protection zone. The U87P setting is set to 10 per unit as recommended by the relay manufacturer [31].

Table 4.1 summarizes the settings that were used to configure the SEL 300G generator protection relay when conducting protection studies of the 87P element in which the GSU transformer was excluded from the differential protection zone.

Table 4.1. Settings for the 87P element without GSU transformer included

Element	Description	Setting
E87	Enable differential protection	G
VWDGD XFMR	Hi-side winding L-L voltage (kV)	*
TRCON XFMR	Protection configuration	*
CTCON	87 input CT connection	*
TAP1	Phase input TAP value (A)	*
TAPD	87 input TAP value (A)	*
U87P	Unrestrained element pickup (p.u.)	10
O87P	Restrained element pickup (p.u.)	0.15
SLP1	Restraint slope 1 percentage (%)	30
SLP2	Restraint slope 2 percentage (%)	100 (Fixed)
IRS1	Restraint slope 1 limit (p.u.)	3.0 (Fixed)
PCT2	Second harmonic blocking percent	*
IHBL	Independent harmonic blocking	*
87B	Restrained element block (SELogic Equation)	0

* Denotes settings required only when GSU transformer is included.

4.2.2 Settings of the 87P element with GSU transformer included

In order to include a GSU transformer in the differential protection zone, one set of current transformers is required to measure currents on the high voltage side of the GSU transformer while the other set measures the currents at the neutral end of each phase of the generator stator windings. In this section, both the low-resistance grounded 555 MVA generator and the 555 MVA step up transformer shown in Figure 3.2 are considered when calculating the settings for the phase percentage restrained differential protection scheme.

The first step is to calculate the full-load secondary outputs of the current transformers used to measure the currents at each end of the differential zone since this information is required as relay input settings. The rated secondary output of the current transformers that measure the currents at the neutral end of the generator stator windings is 0.45 A as already outlined in Section 4.2.1. The full-load secondary outputs of the current transformers that measure the currents on the high voltage side of the GSU transformer can be calculated as follows.

$$S_{base} = 555\ MVA$$

$$V_{base} = 400\ kV$$

$$I_{base} = \frac{S_{base}}{\sqrt{3} \cdot V_{base}} = \frac{555 * 10^6}{\sqrt{3} \cdot (400 * 10^3)} = 801.07\ A$$

The current transformers on the high voltage side of the GSU transformer in the real-time simulation model are each of turns ratio 2000:1 and therefore the secondary outputs of these current transformers are:

$$I_{sec} = \frac{I_{base}}{CT\ ratio} = \frac{801.07}{2000/1} = 0.40\ A$$

CT ratio mismatch

From the above calculations, one can see that the secondary outputs of the current transformers at the two ends of the differential protection zone are not exactly the same. Since current transformers have standard ratios, sometimes it is difficult to select CT ratios that can perfectly match the currents on the high and low voltage sides of the GSU transformer. This is one of the factors that results in a non-zero differential current during un-faulted operating conditions.

In modern numerical protection relays, CT ratio mismatch can be compensated for mathematically by introducing a CT ratio correction factor (also known as an amplitude-matching factor). The purpose of the CT ratio correction factor is to re-scale input current measurements from different current transformers in order to minimize the differential current during normal operating conditions.

In the SEL 300G generator protection relay, the settings TAP1 and TAPD represent the CT ratio correction factors on the low and high voltage sides of the GSU transformer respectively. The TAP1 setting is typically set equal to the nominal secondary current of the protected generator [31], while the TAPD setting can be calculated as follows.

$$TAPD = \frac{VNOM \cdot INOM \cdot PTR \cdot CTR \cdot C2}{1000 \cdot VWDGD \cdot CTRD}$$

$$= \frac{110 * 0.45 * 218 * 30000 * 1}{1000 * 400 * 2000} = 0.40$$

Where VNOM = generator nominal voltage in secondary volts

INOM = generator nominal current in secondary amps

VWDGD = rated line-to-line voltage on the high voltage side of the transformer in kV

PTR = ratio of the potential transformer at the generator terminal

CTR = ratio of the CT at the neutral end of the generator winding

CTRD = ratio of the CT which is located on the high voltage side of the transformer

C2 = 1.732 if CT configuration = DAB or DAC

C2 = 1 for all other combinations of transformer and CT configuration

Phase shift compensation

In the real-time simulation model shown in Figure 3.6, the GSU transformer is connected in a delta-star configuration. With this transformer configuration, the measured currents on the low and

high voltage sides of the GSU transformer are not in phase. In the past, different current transformer configurations were utilized to compensate for the phase shift between the currents on the low and high voltage sides of the GSU transformer so that the secondary current measurements actually input to the protection relay would be in phase. However, with modern numerical protection relays, any phase shift between the low and high voltage sides of the GSU transformer can be compensated for mathematically. The SEL 300G relay requires two settings inputs from the user in order to compute the corresponding vector group for phase shift compensation, namely the transformer configuration (TRCON XFMR) and the current transformer configuration (CTCON).

Restrained Differential Element Pickup Setting (O87P):

There is one setting change required on the dual-slope differential characteristic when the GSU transformer is included in the differential protection zone, namely the restrained differential element pickup setting (O87P). As discussed earlier, the transformer's core loss current component must be taken into consideration when the GSU transformer is included in the differential protection zone.

In the real-time simulation model shown in Figure 3.6, the transformer's core loss current component was chosen to be 1% of its nominal current. If the transformer's core loss component is not known, P' is typically assumed to be 10% of the nominal current [43]. The O87P setting is calculated using the same guidance shown in equation (4.3).

$$O87P = 0.5 * slope\ 1 + P'$$

$$= 0.5 * \frac{30}{100} + \frac{1}{100} = 0.16$$

Table 4.2. Settings for the 87P element with GSU transformer included

Element	Description	Setting
E87	Enable differential protection	T
VWDGD XFMR	Hi-side winding L-L voltage (kV)	OFF
TRCON XFMR	Protection configuration	DACY
CTCON	87 input CT connection	Y
TAP1	Phase input TAP value (A)	0.45
TAPD	87 input TAP value (A)	0.4
U87P	Unrestrained element pickup, multiple of TAP	10
O87P	Restrained element pickup, multiple of TAP	0.16
SLP1	Restraint slope 1 percentage (%)	30
SLP2	Restraint slope 2 percentage (%)	100
IRS1	Restraint slope 1 limit, multiple of TAP	3
PCT2	Second harmonic blocking percent	15
IHBL	Independent harmonic blocking	N
87B	Restrained element block (SELogic Equation)	0

Table 4.2 summarizes the settings that were used to configure the SEL 300G generator protection relay when conducting protection studies of the 87P element in which the GSU transformer was included in the differential protection zone.

4.3 Loss-of-field protection (40)

The purpose of a generator excitation system is to control reactive power flow and also to maintain the synchronism of the generator so as to ensure continuous active power transfer. If there is a failure between the excitation system and the generator field due to a particular contingency (e.g. misoperation of the field circuit breaker, short- or open-circuit conditions in the excitation system), the generator will start to draw a large amount of reactive power from the interconnected system. Before the excitation failure, the generator may be delivering reactive power to the system. Consequently, a loss-of-field condition can result in a large reactive load being imposed on the power system which can cause widespread voltage reduction if there is not enough reactive power support available in the system, which in turn may lead to system-wide instability [11],[32]. In addition, a generator may suffer from high stator current, high induced rotor currents and torque pulsations due to asynchronous operation during loss-of-field conditions [32]. Since a loss-of-field condition is such an undesirable event in the power system, a generator that operates without field excitation must be detected and isolated as quickly as possible in order to avoid severe generator damage as well as to maintain the stability of the power system.

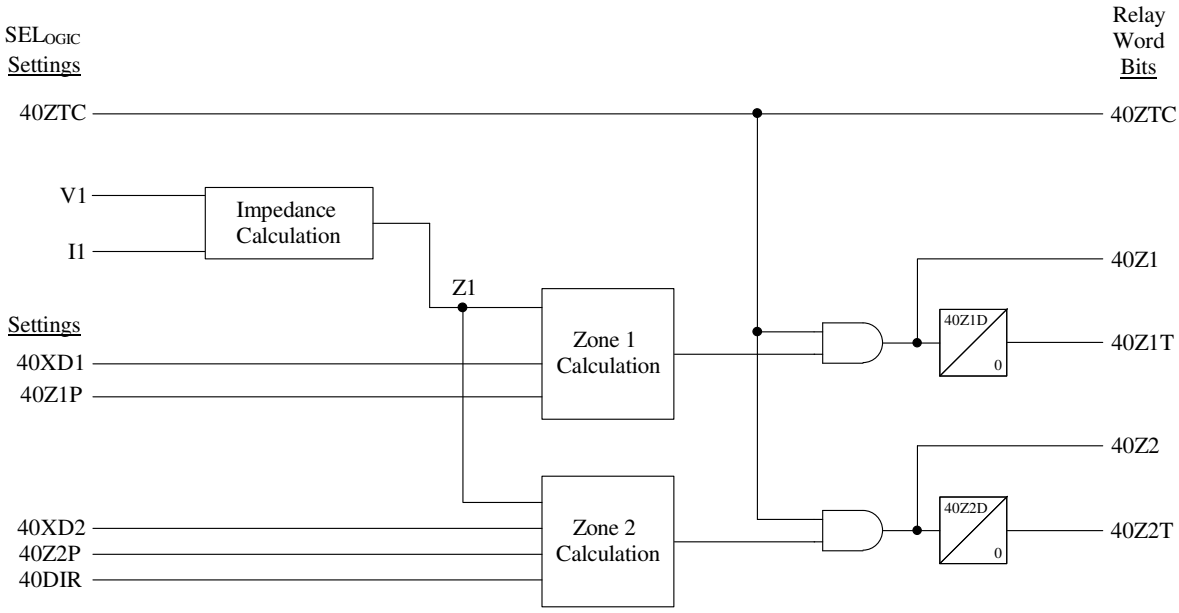

Figure 4.3. Logic diagram of loss-of-field protection element (reproduced from [31]).

The logic diagram shown in Figure 4.3 illustrates the algorithm implemented by the SEL 300G generator protection relay for loss-of-field protection schemes. The SEL 300G relay provides two types of loss-of-field protection scheme and their setting calculations are contained in Sections

4.3.1 and 4.3.2. In both types of loss-of-field protection scheme, two offset-mho elements are applied at the generator terminals and they are each set to look into the machine. Both types of protection scheme rely on the measurements taken by the voltage and current transformers at the generator terminals in order to determine the trajectory of the impedance seen looking back into the generator, upon which they base their tripping decisions: when excitation on the field of a generator is lost, the trajectory of this seen impedance will pass into the defined tripping characteristics of the offset-mho elements on the R-X plane and cause the relay to trip.

It is important to note that the impedance seen by the protection relay has units of ohms in secondary impedance since the inputs to the relay are the secondary quantities from the voltage and current transformers at the generator terminals. Therefore the tripping characteristics of loss-of-field protection schemes are likewise defined in terms of secondary impedance. As such, all primary impedances must be converted into secondary impedances with consideration for the current and voltage transformation ratios as shown in equation (4.4).

$$Z_{secondary} = Z_{primary} \cdot \frac{CT\ ratio}{VT\ ratio} \tag{4.4}$$

4.3.1 Loss-of-field protection with negative zone 2 offset

Figure 4.4 illustrates one type of loss-of-field protection scheme provided by the SEL 300G relay that is typically employed to protect generators. This protection scheme contains two offset mho circles (labelled as zone 1 and zone 2) as shown in Figure 4.4.

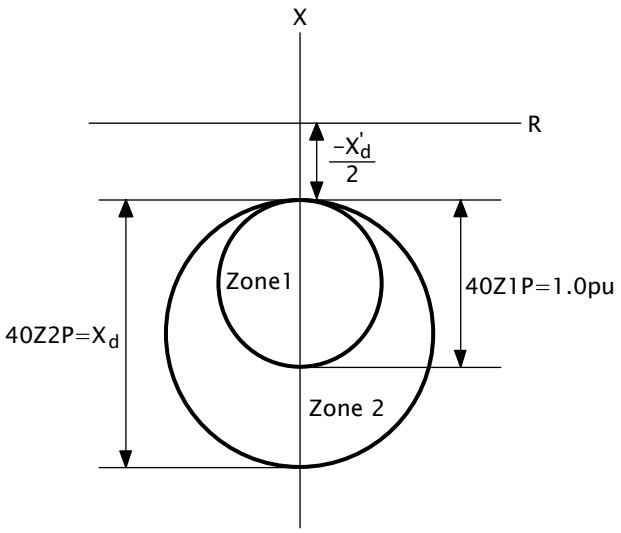

Figure 4.4. Operating characteristic of loss-of-field element with negative zone 2 offset (reproduced from [31]).

Before calculating the settings of these tripping characteristics, the base impedance value for the system must be calculated. The following value of base impedance is calculated from the generator's primary quantities using the information presented earlier in Section 4.2.1.

$$Z_{base\ primary} = \frac{V_{base}}{\sqrt{3} \cdot I_{base}} = \frac{24 * 10^3}{\sqrt{3} * 13.351 * 10^3} = 1.0379\ \Omega$$

As discussed earlier, this primary base impedance must be converted into a secondary base impedance using equation (4.4). In the real-time simulation model, the voltage transformer ratio is 24000/110 and the current transformer ratio is 30000/1, from which the secondary base impedance can be calculated as follows.

$$Z_{base\ secondary} = Z_{base\ primary} \cdot \frac{CT\ ratio}{VT\ ratio}$$

$$= 1.0379 * \frac{30000/1}{24000/110} = 142.8\ \Omega$$

Zone 1 setting calculation

The zone 1 mho characteristic is offset from the origin by one half of the value of the generator's direct-axis transient reactance ($X'_d/2$) as shown in Figure 4.4. The purpose of offsetting the mho characteristic is to avoid misoperation during system disturbances and faults other than loss-of-field conditions. The diameter of the zone 1 mho circle is typically set to 1 pu. The zone 1 mho element is typically set to operate without any intentional time delay [31],[32]. If the positive sequence impedance encroaches the zone 1 mho circle during the worst-case stable generator swing, either the diameter of the zone 1 mho circle needs to be reduced, or a small time delay needs to be inserted [31].

$$Mho\ diameter = 1\ pu$$

$$Offset\ reactance = -\frac{X'_d}{2} = -\frac{0.3}{2} = -0.15\ pu$$

The above per unit quantities are then converted into ohms using the value of base secondary impedance ($Z_{base\ secondary}$) calculated earlier.

$$Mho\ diameter = 1 * 142.8 = 142.8\ \Omega$$

$$Offset\ reactance = -0.15 * 142.83 = -21.4\ \Omega$$

In the studies considered in this thesis no intentional time delay was set for zone 1.

$$Time\ delay = 0.0\ second$$

Zone 2 setting calculation

The offset of the zone 2 mho characteristic is set to be the same as that for zone 1 as shown in Figure 4.4. The diameter of the zone 2 mho circle is typically set to the value of the generator's direct-axis synchronous (steady-state) reactance (X_d). The time delay in this zone is typically set between 0.5 and 0.6 seconds [31],[32],[34]. The purpose of the time delay inserted in this zone is to avoid any misoperation of loss-of-field protection for a worst-case stable swing of the generator caused by contingencies other than a loss-of-field condition, which may also be expected to pass through the characteristic of this zone.

$$Mho\ diameter = X_d = 1.81\ pu$$

$$Offset\ reactance = -\frac{X'_d}{2} = -\frac{0.3}{2} = -0.15\ pu$$

The above per unit quantities are then converted into ohms using the value of base secondary impedance ($Z_{base\ secondary}$) calculated earlier.

$$Mho\ diameter = 1.81 * 142.8 = 258.5\ \Omega$$

$$Offset\ reactance = -0.15 * 142.8 = -21.4\ \Omega$$

$$Time\ delay = 0.5\ second$$

Table 4.3 summarizes the settings that were used to configure the SEL 300G generator protection relay for real-time closed-loop studies of the aforementioned loss-of-field protection scheme and the testing results are to be presented in Chapter Five. The results are then utilized to examine the dynamic performance of such protection schemes under different field contingencies.

Table 4.3. Settings of loss-of-field protection scheme (Negative offset zone 2)

Element	Description	Setting
E40	Enable loss-of-field protection	Y
Zone 1 settings		
40Z1P	Zone 1 mho diameter (ohms)	142.8
40XD1	Zone 1 offset reactance (ohms)	-21.4
40Z1D	Zone 1 pickup time delay (seconds)	0.0
Zone 2 settings		
40Z2P	Zone 2 mho diameter (ohms)	258.5
40XD2	Zone 2 offset reactance (ohms)	-21.4
40Z2D	Zone 2 pickup time delay (seconds)	0.5
40DIR	Zone 2 directional Supervising Angle (degree)	*
40ZTC	40Z element torque control (SELogic Equation)	!60LOP

* Denotes setting required only when the other type of loss-of-field protection scheme in the SEL 300G relay is employed.

4.3.2 Loss-of-field protection with positive zone 2 offset

Figure 4.5 illustrates the other type of loss-of-field operating characteristic available in the SEL 300G relay that is typically employed for the purpose of compatibility with some existing electromechanical loss-of-field relays [31]. In this case the scheme comprises two offset-mho elements (labelled as zone 1 and zone 2), a directional element and an undervoltage element. The tripping characteristics of the mho elements are defined with extended diameters and the zone 2 mho element is positively offset in this protection scheme compared to the one shown in Section 4.3.1.

The procedure for calculating the secondary base system impedance required to determine the settings for this type of scheme is the same as that described in Section 4.3.1.

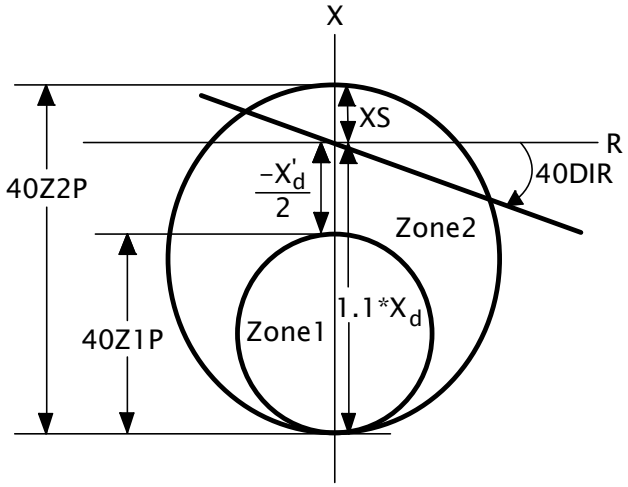

Figure 4.5. Operating characteristic of loss-of-field element with positive zone 2 offset (reproduced from [31]).

Zone 1 setting calculation

As can be seen from Figure 4.5, the zone 1 mho circle is negatively offset by $X'_d/2$ from the origin.

$$Offset\ reactance = -\frac{X'_d}{2}$$

$$= -\frac{0.3}{2} = -0.15\ pu$$

The diameter of zone 1 mho circle is calculated as follows.

$$Mho\ diameter = 1.1 * X_d - \frac{X'_d}{2}$$

$$= 1.1 * 1.81 - \frac{0.3}{2} = 1.841\ pu$$

The above per unit quantities are then converted into ohms using the value of base secondary impedance ($Z_{base\ secondary}$) calculated in Section 4.3.1.

$Offset\ reactance = -0.15 * 142.8 = -21.4\ \Omega$

$Mho\ diameter = 1.841 * 142.8 = 262.9\ \Omega$

Since the diameter of the zone 1 mho circle is larger in this type of loss-of-field scheme, the possibility of the generator's positive sequence impedance encroaching into zone 1 during power swings or out-of step conditions is increased. Therefore a small time delay is typically inserted in this zone in order to avoid misoperation during power swings or out-of-step conditions.

$Time\ delay = 0.25\ second$

Zone 2 setting calculation

The offset of the zone 2 mho circle is set to XS as shown in Figure 4.5. XS represents the sum of the GSU transformer impedance ($X_{transformer}$) and the total system impedance (X_{system}). For the study system considered in this thesis, the total system impedance (X_{system}) beyond the generator step up transformer is calculated as follows.

$X_{system} = 0.5\ //\ 0.93 = 0.325\ pu$

$XS = X_{transformer} + X_{system}$

$= 0.15 + 0.325 = 0.475\ pu$

$Offset\ reactance = XS = 0.475\ pu$

The diameter of the zone 2 mho circle is calculated as follows.

$Mho\ diameter = 1.1 * X_d + XS$

$$= 1.1 * 1.81 + 0.475 = 2.466\ pu$$

The above per unit quantities are then converted into ohms using the value of base secondary impedance ($Z_{base\ secondary}$) calculated in Section 4.3.1.

$Offset\ reactance = 0.475 * 142.8 = 67.8\ \Omega$

$Mho\ diameter = 2.466 * 142.8 = 352.2\ \Omega$

In the case of the zone 2 element, a time delay of 1.0 second is typically inserted to avoid relay misoperation during system disturbances.

$$Time\ delay = 1.0\ second$$

Undervoltage element

When using this type of loss-of-field protection scheme, accelerated zone 2 tripping can be realized by including an undervoltage element. In other words, when the trajectory of the generator's positive sequence impedance passes into the zone 2 characteristic and the measured generator terminal voltage is below the undervoltage setting threshold, the relay trips immediately regardless of the time delay inserted in this zone. The undervoltage element is typically set to 80% of the nominal voltage for a unit-connected generator and 87% of nominal voltage for multiple generators bussed together at their terminals [31].

$$V = \frac{0.8 * VNOM}{\sqrt{3}}$$

$$= \frac{0.8 * 110}{\sqrt{3}} = 50.8\ V$$

Where VNOM = rated secondary generator line-to-line voltage [V]

Directional element

Due to the increased diameter and positive offset of the zone 2 mho circle in this type of scheme, the trajectory of the generator's positive sequence impedance may pass into the zone 2 characteristic under certain normal generator operating conditions and hence be incorrectly considered as a loss-of-field condition. The purpose of the directional element in this protection scheme is to discriminate between normal generator operating conditions and loss-of-field conditions. When the positive sequence impedance is located above the directional element in the R-X impedance plane, any trip action issued by the loss-of-field protection element will be restrained. The angle of the directional element 40DIR is typically set equal to the arccosine of the generator's rated power factor; however, the minimum angle at which 40DIR can be set is $-20°$ [31].

Table 4.4 summarizes the settings that were used to configure the SEL 300G generator protection relay for real-time closed-loop studies of the aforementioned loss-of-field protection scheme and the testing results are to be presented in Chapter Five. The results are then utilized to examine the dynamic performance of the aforementioned loss-of-field protection scheme as well as to compare

it with the performance of the loss-of-field protection scheme discussed in Section 4.3.1 under the same types of field contingencies.

Table 4.4. Settings for loss-of-field protection (Positive offset zone 2)

Element	Description	Setting
E40	Enable loss-of-field protection	Y
Zone 1 settings		
40Z1P	Zone 1 mho diameter (ohms)	262.9
40XD1	Zone 1 offset reactance (ohms)	-21.4
40Z1D	Zone 1 pickup time delay (seconds)	0.25
Zone 2 settings		
40Z2P	Zone 2 mho diameter (ohms)	352.2
40XD2	Zone 2 offset reactance (ohms)	67.8
40Z2D	Zone 2 pickup time delay (seconds)	1
40DIR	Zone 2 directional Supervising Angle (degree)	-20
40ZTC	40Z element torque control (SELogic Equation)	!60LOP

In both loss-of-field protection schemes discussed in Sections 4.3.1 and 4.3.2, misoperation due to a loss-of-potential condition (i.e. signals lost from the voltage transformer at the generator terminals) can be avoided by setting the logic 40ZTC to (!60LOP) as shown in Table 4.3. This allows the relay to block the trip signal issued by the loss-of-field element during a loss-of-potential condition.

4.4 Generator out-of-step protection (78)

When an out-of-step condition occurs between two interconnected systems due to transient disturbances, these systems must be separated as quickly as possible in order to avoid severe generator damage and adverse cascading tripping effects which may lead to system wide instability. In the past, the electrical centre during an out-of-step condition was usually out in the transmission system. However, as a result of significant changes in system and generator impedance characteristics over the years, the electrical centre can appear in a generator or a generator step up transformer during an out-of step condition. For this reason, a separate out-of-step protection function may be employed at the generator terminals to detect out-of-step conditions in which the electrical centres of the electromechanical swings are close to generator zone.

4.4.1 Generator swing characteristics

Figure 4.6 shows an illustration of a simple power system network and its equivalent circuit diagram in order to demonstrate the typical behaviour of a system during out-of-step conditions, and how such conditions can be detected from the variations that take place in the apparent impedance measured by a relay at the terminal of a generator.

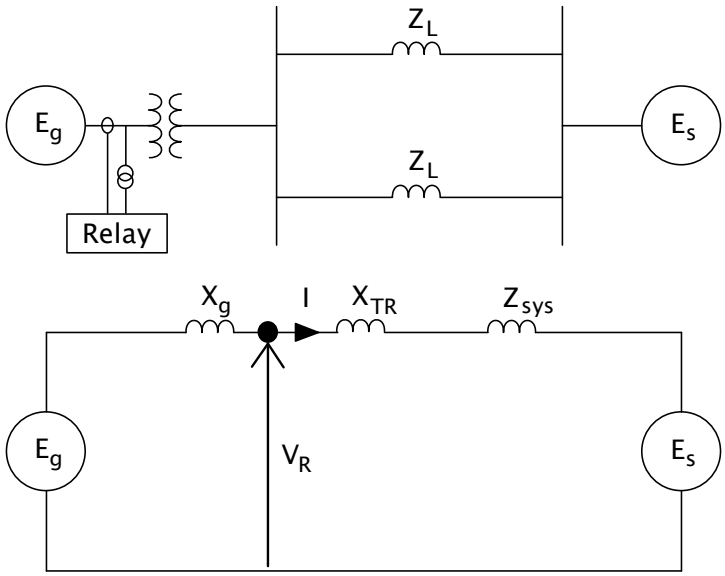

Figure 4.6. Simple power system network and its equivalent circuit diagram.

Using the equivalent circuit diagram shown in Figure 4.6, the current measured at the generator terminals can be calculated as follows.

$$\mathrm{I} = \frac{E_g \angle \delta - E_s}{X_g + X_{TR} + Z_{sys}} \tag{4.5}$$

And the voltage measured at the generator terminals is calculated as follows.

$$V_R = E_g \angle \delta - I * X_g \tag{4.6}$$

Letting $n = E_g/E_s$ and $1\angle\delta = cos\delta + jsin\delta$, the generalized equation for the impedance seen by the relay can be derived as follows.

$$Z_R = \frac{V_R}{I} = \frac{E_g \angle \delta - \dfrac{E_g \angle \delta - E_s}{X_g + X_{TR} + Z_{sys}} * X_g}{\dfrac{E_g \angle \delta - E_s}{X_g + X_{TR} + Z_{sys}}}$$

After simplification of the above equation, the generalized equation becomes

$$Z_R = \left(X_g + X_{TR} + Z_{sys}\right) * n * \frac{(n - cos\delta) - jsin\delta}{(n - cos\delta)^2 + sin^2\delta} - X_g \tag{4.7}$$

When the special case in which $E_g = E_s$ $(n = 1)$ is evaluated, equation (4.7) becomes

$$Z_R = \frac{X_g + X_{TR} + Z_{sys}}{2}\left(1 - jcot\frac{\delta}{2}\right) - X_g \tag{4.8}$$

Equations (4.7) and (4.8) show that, for given values of voltage magnitude at the two ends of the system, the apparent impedance seen by the relay is a function of a number of physical impedance parameters associated with the generator and the external system, and the phase angle δ between the voltages E_g and E_s at the two ends of the system. During the electromechanical swings that follow system disturbances, the angle δ across the system varies with time, as therefore does the apparent impedance Z_R seen by the relay, so that the relay is able to detect the presence of an out-of-step condition from the trajectory of this apparent impedance on a two-dimensional R-X plane.

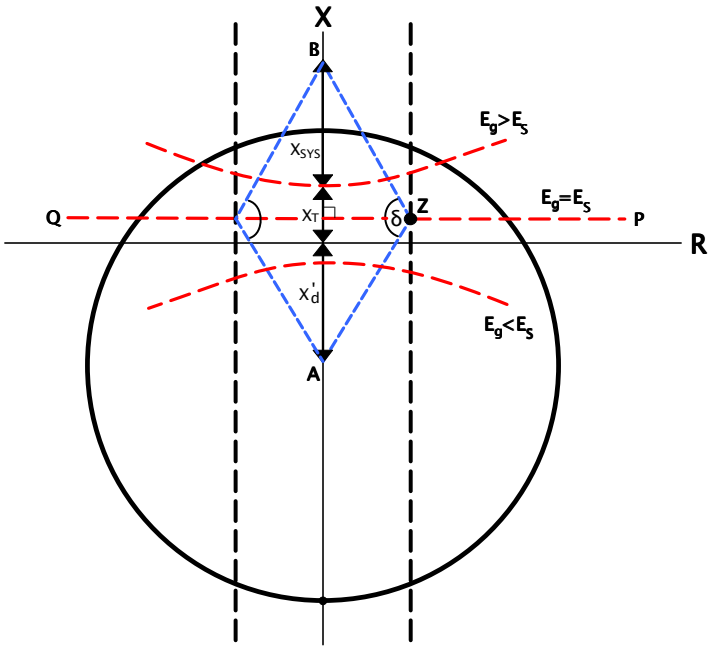

Figure 4.7.Out-of-step impedance loci on the R-X plane.

Figure 4.7 shows three distinct out-of-step impedance trajectories (loci of Z_R on the R-X plane), each for a different ratio $n = E_g/E_s$ of the system voltages. Figure 4.7 shows that in the special case when the ratio of the system voltages $E_g/E_s = 1$, the impedance locus during an out-of-step condition is a straight line labelled PQ, that is a perpendicular bisector of the total system impedance characteristic, represented by the line drawn between points A and B on the R-X plane. At any point Z on the locus of the apparent impedance, the angle between the straight lines drawn from point Z to the points A and B at each end of the system impedance characteristic corresponds to the angular separation δ between the voltages E_g and E_s at each end of the system. Following a system disturbance, as the angle δ between E_g and E_s increases during the resulting electromechanical swing, the trajectory of the impedance locus travels in the direction from point P towards point Q. When the impedance locus intersects the total impedance line AB, the systems are 180° out of phase. As the trajectory of the impedance travels to the left of the system impedance line, the angular separation increases beyond 180° and eventually the systems will be in phase

again. When the trajectory of the apparent impedance travels back to the point on the locus where the swing started, it constitutes completion of one full slip cycle.

If the ratio of the system voltages is greater than one ($E_g/E_s > 1$) during an out-of-step condition, the impedance locus will be a circle with its centre located on the extension of line AB above line PQ. However, if the ratio of the system voltages is smaller than one ($E_g/E_s < 1$) during an out-of-step condition, then the impedance locus will be a circle with its centre located on the extension of line AB below line PQ.

Based on these known characteristics of the generator's impedance trajectories during electromechanical swing conditions, out-of-step protection schemes are able to discriminate between stable and unstable swings using well-established techniques from impedance relaying, such as the use of a mho characteristic together with blinders.

4.4.2 Single blinder scheme

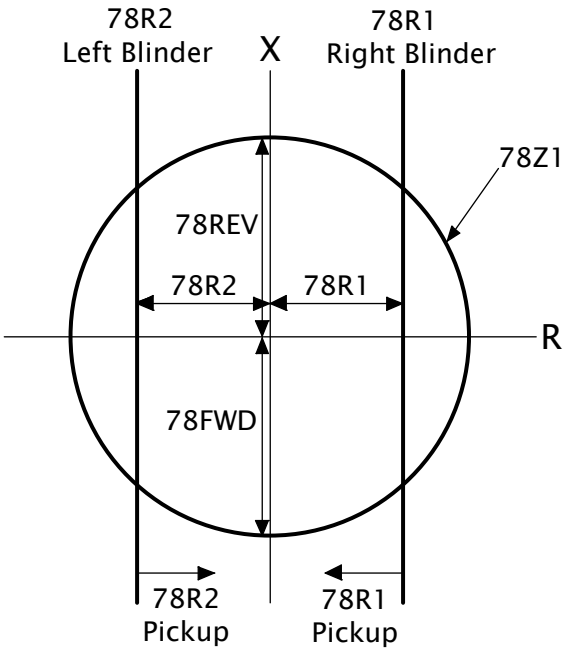

Figure 4.8. Operating characteristic of single blinder scheme for out-of-step protection on the R-X plane.

Figure 4.8 illustrates the operating characteristic of a single blinder scheme defined on the R-X impedance plane for out-of-step protection. This protection scheme contains a supervisory offset-mho element (78Z1) and one set of blinders, 78R1 and 78R2, also known as an impedance element which are located at equal distances on either side of the reactance axis. The purpose of adding blinders in the out-of-step protection scheme is to avoid relay misoperation during recoverable

swings. Also, these blinders can be controlled to allow the circuit breaker to open at a more favourable angle for arc interruption during an out-of-step condition.

The logic diagram shown in Figure 4.9 illustrates the algorithm implemented by the SEL 300G generator protection relay for the single blinder out-of-step protection scheme. When the trajectory of the positive sequence impedance of the generator travels from right to left during an out-of-step condition, it encroaches the offset mho circle (78Z1) first. At this stage, the internal logic of the relay indicates that there is a power swing condition in the system. When the swing impedance travels further into the offset mho circle, it crosses the blinder 78R1 on the positive side of the reactance axis which causes the internal logic to latch the state of a logic variable associated with 78R1 to one. When the swing impedance subsequently crosses the blinder 78R2 on the negative side of the reactance axis, the internal logic will latch the state of 78R2 to one. After the internal logic of the relay has latched the states of both 78R1 and 78R2 to one and the swing impedance has exited the offset-mho circle, the internal logic of the relay then indicates that an out-of-step condition has been detected. At this stage, a user-settable delay timer (78TD) is triggered. When the inserted delay time has elapsed, the relay will issue a trip signal to open the generator's main circuit breaker in order to isolate the unstable generator from the system.

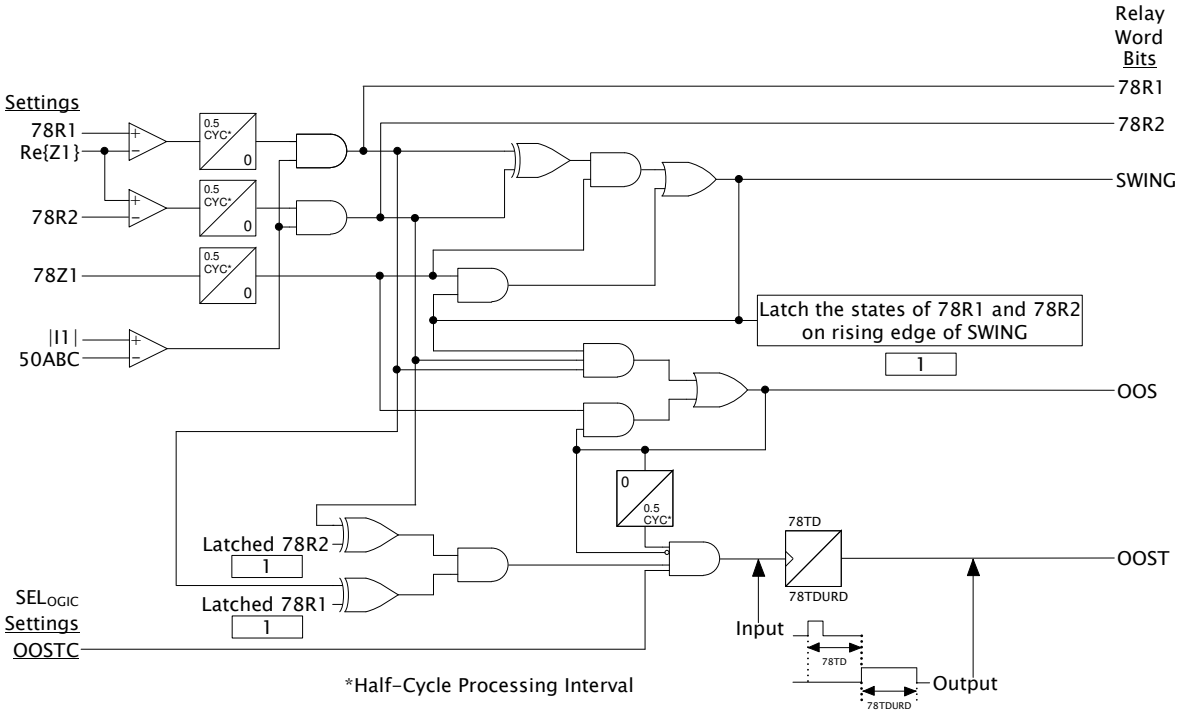

Figure 4.9. Logic diagram of single blinder scheme for out-of-step protection (reproduced from [31]).

It is important to note that an unstable generator does not need to be shut down completely. In other words, only the generator's main circuit breaker is required to be opened during an out-of-step condition. When the system stabilizes, the generator can then be resynchronized and connected back on to the grid without requiring a long start up process.

Single blinder scheme setting calculations

The forward reach 78FWD of the 78Z1 element shown in Figure 4.8 is typically set at 2.0 to 3.0 times the value of the generator's direct-axis transient reactance X'_d.

$$78FWD = 3 * X'_d$$

$$= 3 * 0.3 = 0.9\ pu$$

The reverse reach 78REV of the 78Z1 element shown in Figure 4.8 is typically set at 1.5 to 2.0 times the transformer reactance $X_{transformer}$ in order for the element to have an adequate coverage plus some margin.

$$78REV = 2 * X_{transformer}$$

$$= 2 * 0.15 = 0.3\ pu$$

The above per unit quantities are then converted into ohms using the value of base secondary impedance ($Z_{base\ secondary}$) calculated in Section 4.3.1.

$$Forward\ reach = 0.9 * 142.8 = 128.5\ \Omega$$

$$Reverse\ reach = 0.3 * 142.8 = 42.8\ \Omega$$

In order to calculate the blinder setting of this type of out-of-step protection scheme, transient studies are typically carried out to investigate the maximum angular separation between systems that may occur without loss of synchronism. Based on the experience described in [11], the maximum angular separation between a generator and a system that may occur without loss of synchronism is $\delta_{max} = 120°$. Based on the assumption of $\delta = 120°$ being the largest possible angle before the generator pole-slips, the horizontal distance of the blinder from the origin to the particular point on the impedance locus that corresponds to the angle $\delta = 120°$ can be calculated by drawing two straight lines from point Z to the points A and B at each end of the system impedance characteristic as shown in Figure 4.7.

The blinder setting is calculated as follows.

$$blinder\ setting\ (78R1) = \left(\left(\frac{X'_d + X_T + X_{sys}}{2}\right) * \tan(90° - \frac{\delta}{2})\right)$$

$$= \left(\left(\frac{0.3 + 0.15 + 0.325}{2}\right) * \tan(90° - \frac{120}{2})\right) = 0.224\ pu$$

The above per unit quantity is then converted into ohms using the value of base secondary impedance ($Z_{base\ secondary}$) calculated in Section 4.3.1.

$$d = 0.224 * 142.8 = 32.0\ \Omega$$

Table 4.5 summarizes the protection settings of the single blinder scheme calculated in this section. These settings were used to configure SEL 300G generator protection relay when conducting real-time closed-loop studies of the out-of-step protection function in Chapter Five of the thesis.

Table 4.5. Settings for out-of-step protection (Single blinder scheme)

Element	Description	Setting
E78	Enable out-of-step protection	1B
78FWD	Forward reach reactance (ohms)	128.5
78REV	Reverse reach reactance (ohms)	42.8
78R1	Right hand blinder (ohms)	32.0
78R2	Left hand blinder (ohms)	32.0
78D	Out-of-step delay (seconds)	*
78TD	Out-of-step trip delay	0.0
78TDURD	Out-of-step trip duration	3.0
50ABC	Positive sequence current supervision (A)	0.05
OOSTC	78 element torque control (SELogic Equation)	1

4.5 Conclusion

In this chapter, the theory of operation of the particular generator protective functions whose performance is to be studied in the thesis have been discussed in detail in order to provide some background to their operation in response to a fault. In addition, setting calculations for these protection elements were thoroughly demonstrated with detailed discussions of their setting considerations. Using the protection settings calculated in this chapter, a thorough analysis of the performance of these particular generator protective functions can be carried out using the real-time closed-loop testing approach.

The generator protective functions covered in this chapter are those employed to protect the 555 MVA generator and GSU transformer shown in the example study system of Figure 3.2 for the particular case of low-resistance grounding of the generator. Chapter Five presents the results

obtained from the hardware-in-loop tests of these particular generator protective functions and analyses their performance during different fault scenarios and system contingencies.

CHAPTER 5

HIL TESTING OF LOW-RESISTANCE GROUNDED GENERATOR PROTECTION STUDY SYSTEM

5.1 Introduction

The previous chapter discussed the theory of operation and settings calculations for the particular generator protective functions to be applied for protection of the low-resistance grounded 555 MVA generator in the study system considered in the thesis.

Using the closed-loop testing approach described in Chapter Three, the SEL 300G generator protection relay under study was connected to the real-time simulator to protect one of the four low-resistance grounded 555 MVA generators represented in the real-time simulation model of the study system. The SEL 300G relay was configured with the settings calculated in Chapter Four for the particular generator protective functions under study.

This chapter presents the results of the hardware-in-loop (HIL) tests carried out using the real-time simulator on the performance of the phase percentage restrained differential protection (87P), loss-of-field protection (40) and out-of-step protection (78) of the studied generator. In addition, the chapter presents the results of studies into the impact on the protected generator of different circuit breaker failures (i.e. field circuit breaker and neutral circuit breaker) while attempting to clear a stator winding to ground (stator-ground) fault.

5.2 HIL test results of phase percentage restrained differential protection (87P)

The purpose of the studies presented in this section was to evaluate the performance of the 87P element under different types of fault scenario when employed to protect the particular low-resistance grounded 555 MVA generator and the generator step-up (GSU) transformer. As discussed in Chapter Three, the studies into the performance of the 87P element were carried out using the real-time simulation model shown in Figure 3.5. Section 5.2.1 shows the HIL test results when the 87P element was configured to protect the generator only, while Section 5.2.2 shows the HIL test results when the 87P element was configured to protect both the generator and the GSU transformer.

5.2.1 Performance of the 87P element when configured to protect the generator only

The studies into the performance of the 87P element were conducted under the following operating conditions: all four generators in the power station represented in the real-time simulation model were loaded to 90% of full load capacity and operated with 0.9 lagging power factor.

Figures 5.1 to 5.5 show the responses of selected variables recorded by the SEL 300G generator protection relay when a phase-to-earth fault was applied on the phase A winding of the generator at a position 20% along the winding from the neutral end. When the 87P element detected the phase-to-earth fault inside the differential protection zone, the relay issued a trip signal to open the following circuit breakers to clear the fault: the generator's main circuit breaker, its field circuit breaker, and the neutral circuit breaker. Figure 5.1 shows the slowly-decaying generator instantaneous voltages when the excitation source was disconnected from the field winding after the relay issued a trip signal. Figure 5.2 shows that the fault was successfully cleared after opening all the required circuit breakers to interrupt the fault current.

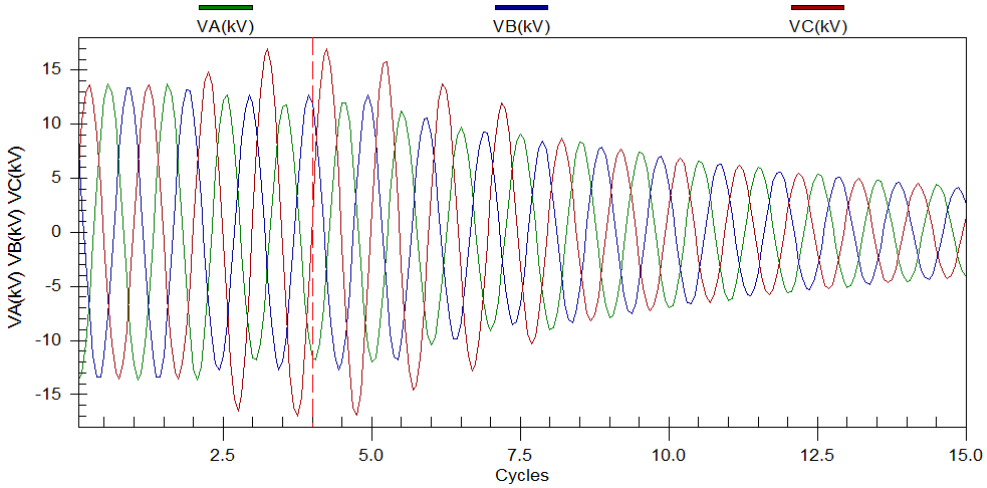

Figure 5.1. Generator instantaneous voltages during the recorded 15 cycles.

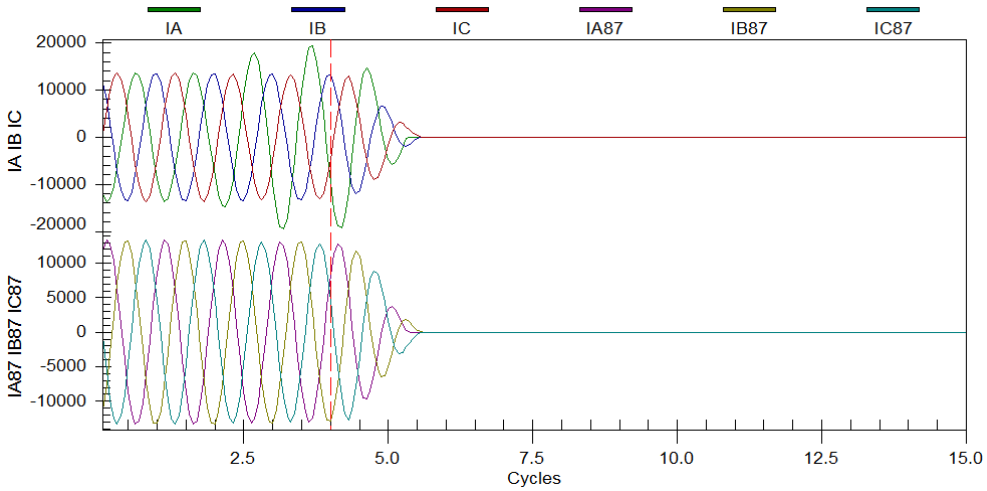

Figure 5.2. Generator instantaneous currents during the recorded 15 cycles.

Figures 5.3 to 5.5 show the differential and restraint currents for phases A, B and C respectively as calculated by the SEL 300G relay from the measurements of the current transformers located at each end of the generator stator windings. These calculated quantities (both the differential and restraint currents) associated with the faulted phase were plotted against each other on an XY plot

in order to determine the differential versus restraint current trajectory upon which the 87P element based its tripping decisions.

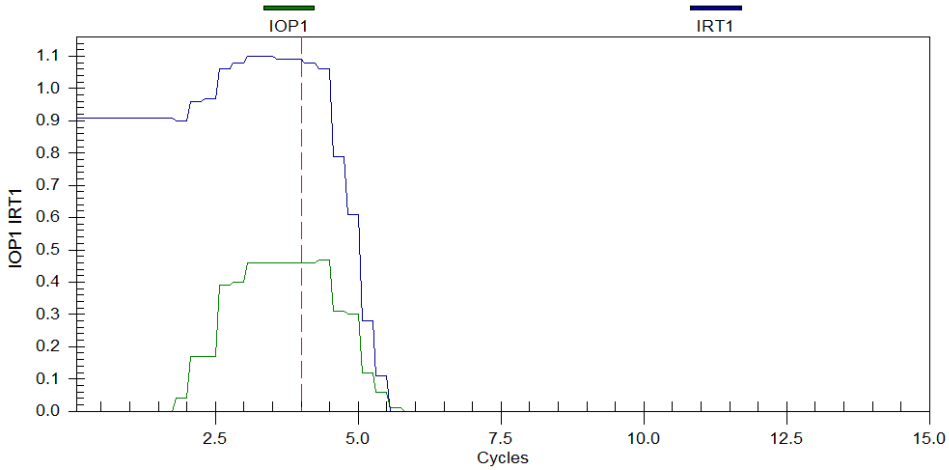

Figure 5.3. Phase A operating and restraint currents during a phase A internal winding fault.

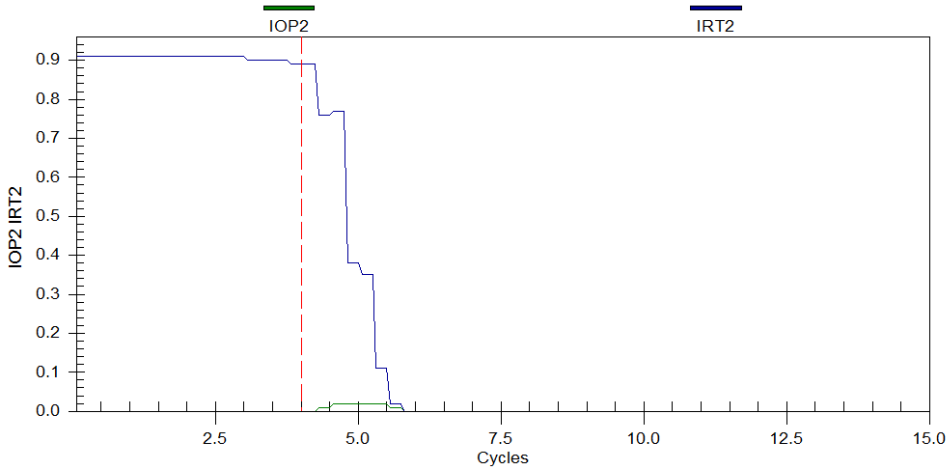

Figure 5.4. Phase B differential and restraint currents during a phase A internal winding fault.

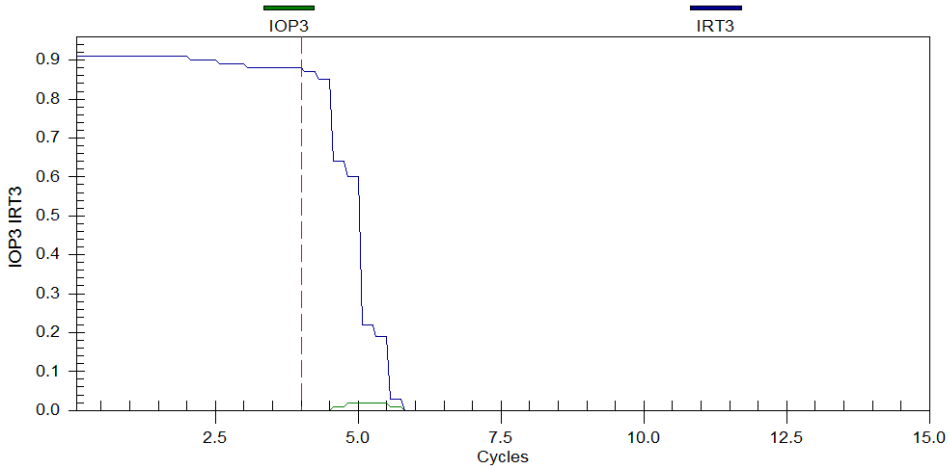

Figure 5.5. Phase C differential and restraint currents during a phase A internal winding fault.

Figure 5.6 shows the plot of the differential versus restraint current trajectory for phase A during the fault, overlaid on to the dual slope differential characteristic settings chosen for the 87P element in this case. As can be seen from Figure 5.6, the differential versus restraint current trajectory passed into the tripping area of the dual slope differential characteristic during the fault which caused the relay to issue a trip signal. After the fault was cleared, the differential versus restraint current trajectory returned to the origin on the XY plot. Plots similar to Figure 5.6 can be created for phase B and C using the method described above. However, since these two phases were healthy, the differential versus restraint current trajectory remained in the restraining area of the dual slope differential characteristic.

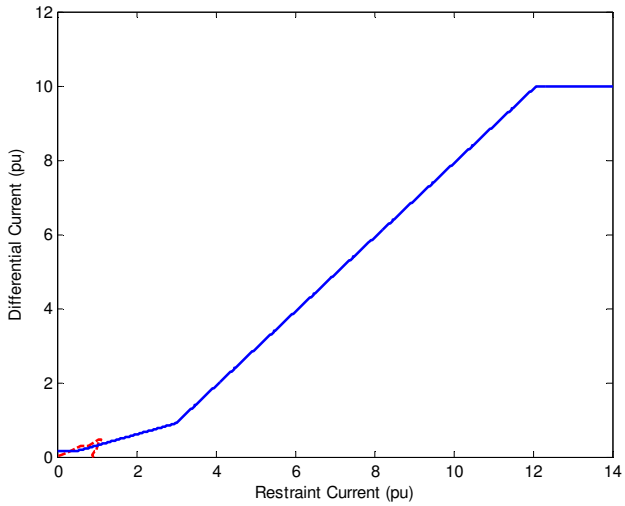

Figure 5.6. Plot of phase A differential versus restraint current during a phase A fault (Internal winding fault at 20% of the stator winding from generator neutral).

Figures 5.7 and 5.8 show plots of the differential versus restraint current trajectories for phase A when phase-to-earth faults were applied on the phase A winding at positions 95% and 10% from the neutral end respectively. These two plots demonstrate the different magnitudes of the differential current obtained when a phase-to-earth fault occurs at different locations along the stator winding. As can be seen from Figure 5.7, when the phase-to-earth fault occurred near the generator terminal, the magnitude of the differential current was sufficient to cause the differential versus restraint current trajectory to pass into the tripping area of the dual slope differential characteristic. However, when the location of the phase-to-earth fault on the stator winding was moved towards the neutral end, the phase-to-neutral voltage imposed on the faulted section of the winding became smaller, which resulted in smaller current that flowed into the faulted section of the winding. As a result, there was insufficient differential current to cause the differential versus restraint current trajectory to pass into the tripping area of the dual slope differential characteristic as shown in Figure 5.8. For this reason, the 87P element could not detect a phase-to-earth fault on the stator winding that occurred at or near the generator neutral.

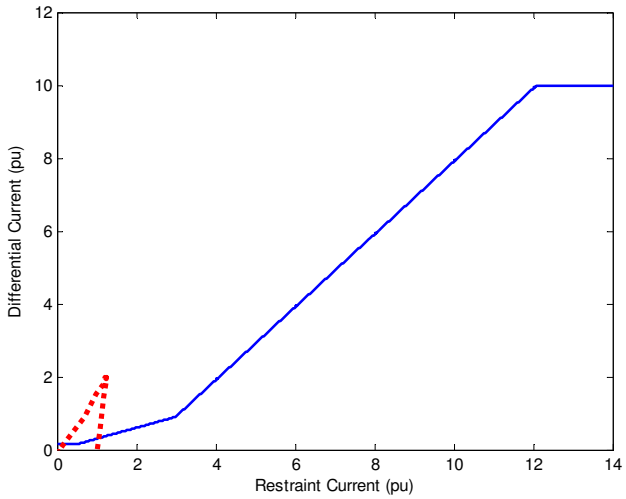

Figure 5.7. Differential characteristic for Phase A (Internal winding fault at 95% of the winding).

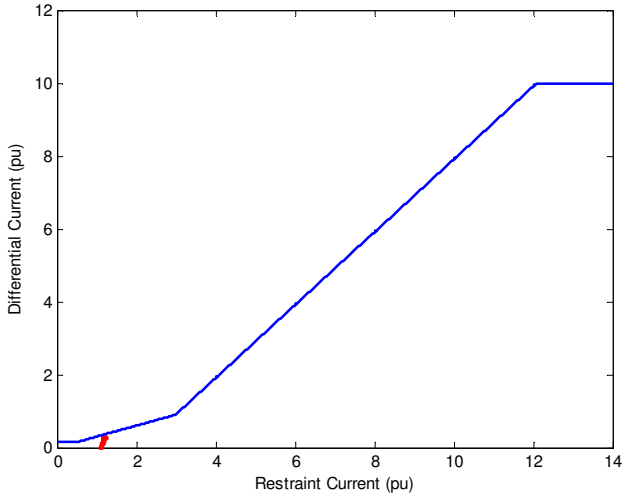

Figure 5.8 Differential characteristic for Phase A (Internal winding fault at 10% of the winding).

Table 5.1 shows the responses obtained from the SEL 300G generator protection relay under study when a phase-to-earth fault was applied at different user settable locations along the stator winding of the phase-domain synchronous machine model used to represent the protected generator in the real-time simulation. The results tabulated in Table 5.1 clearly indicate the region of the stator winding where the 87P element is unable to detect a phase-to-earth fault on the low-resistance grounded generator being protected. The size of the region of the winding that is not covered by the 87P element is influenced by the particular value of the grounding resistor chosen for the generator and by the settings of the 87P element itself [42]. For the particular grounding resistor value selected for the generator in this part of the study and the protection settings calculated in Chapter Four, the 87P element could not detect a phase-to-earth fault which occurred below 14% of the stator winding from the neutral end.

Table 5.1. Relay response to internal winding faults on the generator stator

% Winding fault	Fault duration (cycles)	Point on wave (°)	Relay response	Trip time (ms)
5	5	0	No trip	-
10	5	0	No trip	-
13	5	0	No Trip	-
14	5	0	Tripped	48.00
20	5	0	Tripped	40.32
30	5	0	Tripped	40.32
40	5	0	Tripped	36.48
50	5	0	Tripped	35.52
60	5	0	Tripped	34.56
70	5	0	Tripped	31.68
80	5	0	Tripped	33.60
95	5	0	Tripped	30.72

As can be seen from Figure 3.4, the phase-domain synchronous machine model only allows phase-to-earth faults to be applied on one phase of the generator stator winding. For this reason, the response of the relay to other types of internal fault such as phase-to-phase and turn-to-turn faults could not be studied using this machine model. However, other types of fault were considered at the terminals of the protected generator in the real-time simulation model (fault location at point F3 as shown in Figure 3.2). The purpose of these protection studies was to examine the dependability of the 87P element under different types of fault scenario that occurred inside the differential protection zone. Table 5.2 illustrates the responses obtained from the SEL 300G generator protection relay under study when different types of fault were applied at the terminals of the protected generator. Since these faults were applied inside the differential protection zone, the relay tripped and cleared the faults as expected.

Table 5.2. Relay response to faults applied at location F3 on the study system

Fault type	Fault duration (cycles)	Point on wave (°)	Relay response	Trip time (ms)
AG	5	0	Tripped	30.72
BG	5	0	Tripped	28.80
CG	5	0	Tripped	32.64
ABG	5	0	Tripped	29.76
BCG	5	0	Tripped	30.72
ACG	5	0	Tripped	31.68
ABCG	5	0	Tripped	27.84

Theoretically, the 87P element should not respond to faults that occur outside the differential protection zone if the settings of the differential characteristic are calculated correctly. Further studies were therefore carried out in order to examine the security of the 87P element for different types of fault situated outside the differential protection zone. Table 5.3 illustrates the responses obtained from the SEL 300G generator protection relay under study when different types of fault

were applied at the end of the transmission line closest to the power station (fault location at point F1 as shown in Figure 3.2). The results tabulated in Table 5.3 indicate no misoperation under different through-fault conditions and hence the protection settings of the differential characteristic were verified. Any relay misoperation under through-fault conditions would indicate incorrect settings of the differential characteristic and re-evaluation of the protection settings would then be necessary.

Table 5.3. Relay response to faults applied at location F1 on the study system

Fault type	Fault duration (cycles)	Point on wave (°)	Relay response	Trip time (ms)
AG	5	0	No trip	-
BG	5	0	No trip	-
CG	5	0	No trip	-
ABG	5	0	No trip	-
BCG	5	0	No trip	-
ACG	5	0	No trip	-
ABCG	5	0	No trip	-

A more realistic CT magnetizing curve would be required in order to study the effect of CT saturation during heavy through-fault conditions. When a CT saturates, it can no longer faithfully reproduce the primary current with a scale factor on the secondary side of the CT. As a result, very high differential current can be obtained that can cause misoperation of the 87P element if the second slope of the differential characteristic is not set correctly.

5.2.2 Performance of the 87P element when configured to protect both the generator and GSU transformer

The purpose of the protection studies conducted in this section was to examine the performance of the 87P element when both the low-resistance grounded 555 MVA generator and the GSU transformer were included in the differential protection zone. For the protection studies carried out in this section, the operating conditions of the generators in the power station were the same as described in Section 5.2.1.

As discussed in Chapter Four, there are more setting considerations for the 87P element when the GSU transformer is included in the differential protection zone, namely CT ratio correction factor and phase shift compensation. Incorrect settings of these two relay inputs may result in high differential current that could cause misoperation of the 87P element. Figure 5.9 shows the differential and restraint currents recorded by the SEL 300G relay on the healthy phase C during a phase-to-earth fault on the phase A winding of the protected generator. This figure demonstrates that both the CT ratio mismatch and phase shift between the primary and secondary currents of the GSU transformer due to its delta-star configuration were correctly compensated by the relay. The

differential current of 0.01 pu seen in Figure 5.9 corresponds to the value of the magnetizing current of the GSU transformer (1%) that was represented in the real-time simulation model.

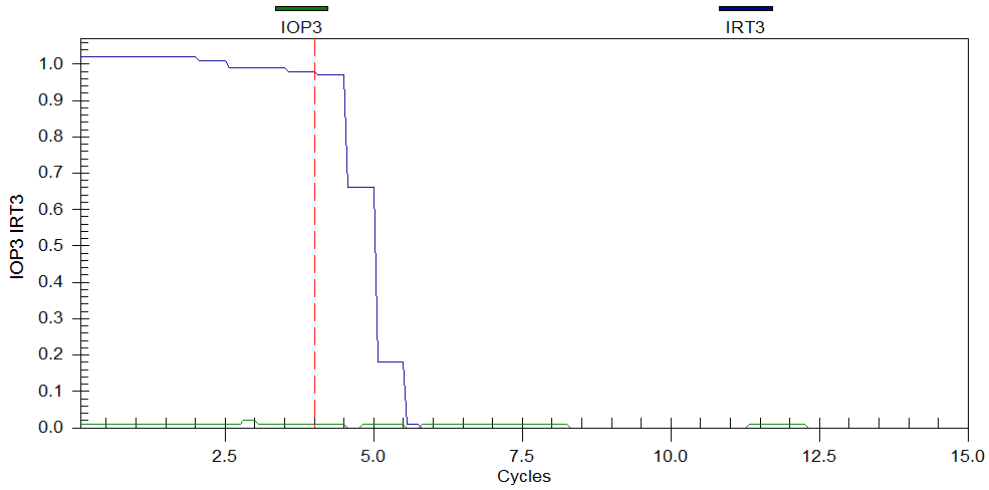

Figure 5.9. Phase C differential and restraint currents during a phase A internal winding fault.

Table 5.4 illustrates the responses obtained from the SEL 300G generator protection relay under study when a phase-to-earth fault was applied at different locations along the stator winding of the generator. By comparing Table 5.1 and Table 5.4, one can see that the performance of the 87P element was not influenced by including the GSU transformer in the differential protection zone.

Table 5.4. Relay response to internal winding faults on the generator stator

% Winding fault	Fault duration (cycles)	Point on wave (°)	Relay response	Trip time (ms)
5	5	0	No trip	-
10	5	0	No trip	-
13	5	0	No Trip	-
14	5	0	Tripped	47.00
20	5	0	Tripped	43.20
30	5	0	Tripped	40.32
40	5	0	Tripped	40.32
50	5	0	Tripped	35.52
60	5	0	Tripped	31.68
70	5	0	Tripped	34.56
80	5	0	Tripped	32.64
95	5	0	Tripped	32.64

Using the three-phase faulted transformer model represented in the real-time simulation model shown in Figure 3.6, the performance of the SEL 300G generator protection relay in response to different types of transformer internal winding fault could also be studied. Tables 5.5 and 5.6 show the HIL test results of the SEL 300G generator protection relay when turn-to-ground faults and turn-to-turn faults were applied at different locations on the primary winding of the GSU transformer respectively. As can be seen from Table 5.6, the 87P element was not able to detect a

turn-to-turn fault at the bottom of the transformer winding. Similar protection studies were carried out on the secondary winding of the GSU transformer and the HIL test results are tabulated in Tables 5.7 and 5.8.

Table 5.5. Relay response to turn-to-ground faults on the transformer primary side winding

% Winding fault	Fault duration (cycles)	Point on wave (°)	Relay response	Trip time (ms)
50	5	0	Tripped	43.2
40	5	0	Tripped	44.16
30	5	0	Tripped	35.52
20	5	0	Tripped	35.52
10	5	0	Tripped	29.76
0.1	5	0	Tripped	28.80

Table 5.6. Relay response to turn-to-turn faults on the transformer primary side winding

% Fault winding 1	% Fault winding 2	Fault duration (cycles)	Point on wave (°)	Relay response	Trip time (ms)
49.9	50.0	5	0	Tripped	28.80
49.0	50.0	5	0	Tripped	28.80
24.9	25.0	5	0	Tripped	29.76
24.0	25.0	5	0	Tripped	32.64
9.9	10.0	5	0	Tripped	33.60
9.0	10.0	5	0	Tripped	34.56
2.9	3.0	5	0	Tripped	43.2
0.1	2.7	5	0	No trip	-

Table 5.7. Relay response to turn-to-ground faults on the transformer secondary side winding

% Winding fault	Fault duration (cycles)	Point on wave (°)	Relay response	Trip time (ms)
50	5	0	Tripped	31.68
40	5	0	Tripped	28.80
30	5	0	Tripped	28.80
20	5	0	Tripped	30.72
10	5	0	Tripped	32.64
2.3	5	0	No trip	-

Table 5.8. Relay response to turn-to-turn faults on the transformer secondary side winding

% Fault winding 1	% Fault winding 2	Fault duration (cycles)	Point on wave (°)	Relay response	Trip time (ms)
49.9	50.0	5	0	Tripped	30.72
49.0	50.0	5	0	Tripped	31.68
24.9	25.0	5	0	Tripped	29.76
24.0	25.0	5	0	Tripped	31.68
9.9	10.0	5	0	Tripped	30.72
9.0	10.0	5	0	Tripped	33.60
2.9	3.0	5	0	Tripped	42.24
0.1	2.5	5	0	No trip	-

Additional tests were then carried out in order to examine the security of the 87P element for different types of fault occurring outside the differential protection zone. Table 5.9 illustrates the

responses obtained from the SEL 300G relay when different types of fault were applied at the end of the transmission line closest to the power station (fault location F1 shown in Figure 3.2). The results show no relay misoperation under any through-fault conditions which indicate that the settings of the differential characteristic are secure.

Table 5.9. Relay response to faults applied at location F1 on the study system

Fault type	Fault duration (cycles)	Point on wave (°)	Relay response	Trip time (ms)
AG	5	0	No trip	-
BG	5	0	No trip	-
CG	5	0	No trip	-
ABG	5	0	No trip	-
BCG	5	0	No trip	-
ACG	5	0	No trip	-
ABCG	5	0	No trip	-

5.2.3 Consequences of breaker failure

When the 87P element of the SEL 300G generator protection relay detects a phase-to-earth fault on the stator winding of a low-resistance grounded generator, the relay sends a trip signal to open various circuit breakers (i.e. generator's main circuit breaker, field circuit breaker and neutral circuit breaker) in order to clear the high-magnitude earth fault current. As discussed in Chapter Three, the phase-domain synchronous machine model provides many advanced features, one of which is to allow detailed electric representation of the external supply to the generator field circuit. Thus, the field circuit breaker was able to be included in the real-time simulation model as shown in Figure 3.6. Using the realistic and detailed real-time simulation model of the plant described in Chapter Three, different scenarios of circuit breaker failure during the fault clearing process can be studied in detail and the results can be used to understand and analyse the impact on the faulted generator under such circumstances. Sections 5.2.3.1 to 5.2.3.3 show the results obtained from the real-time closed-loop studies under different circuit breaker failure scenarios when clearing a phase-to-earth fault in one phase of the stator winding of the protected generator, located 95% along the stator winding from its neutral end.

5.2.3.1 Neutral and field breaker failure

Figures 5.10 to 5.14 show selected variables recorded during the real-time closed-loop studies when both the neutral and field circuit breakers failed to respond to the trip signal issued by the 87P element to clear the earth fault.

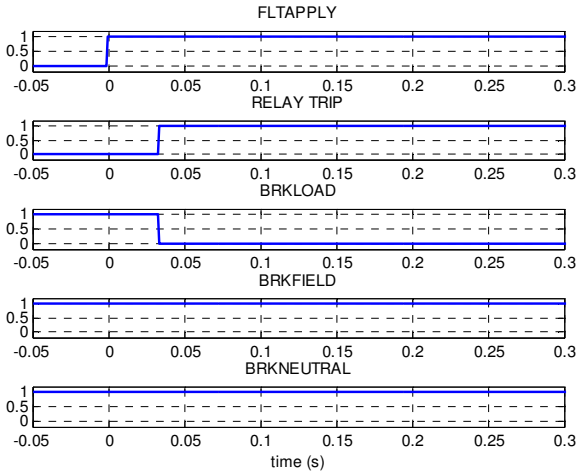

Figure 5.10. Binary control signals: neutral and field breaker failure when clearing a stator-ground fault.

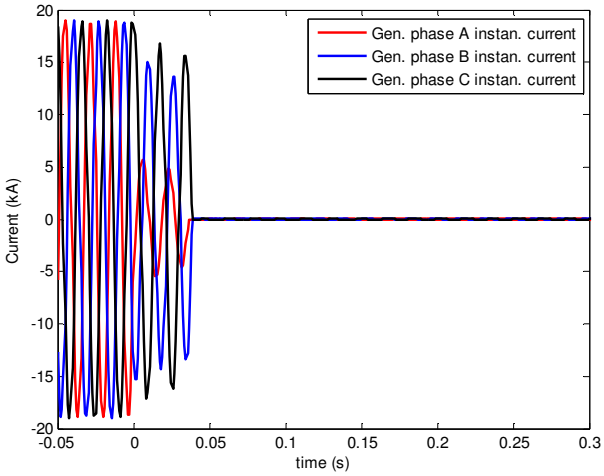

Figure 5.11. Generator winding currents at stator terminal end: neutral and field breaker failure when clearing a stator-ground fault.

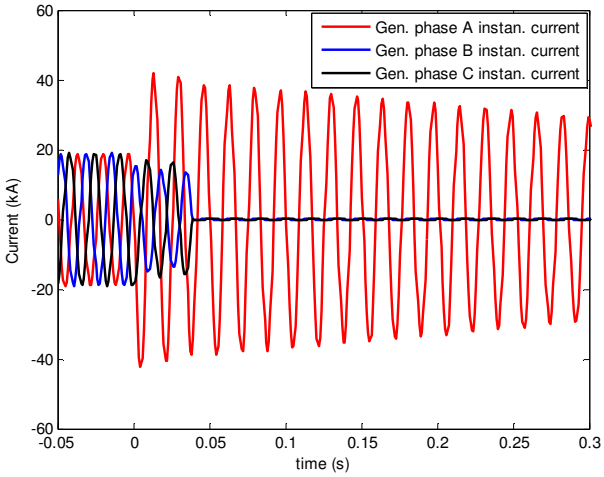

Figure 5.12. Generator winding currents at neutral end: neutral and field breaker failure when clearing a stator-ground fault.

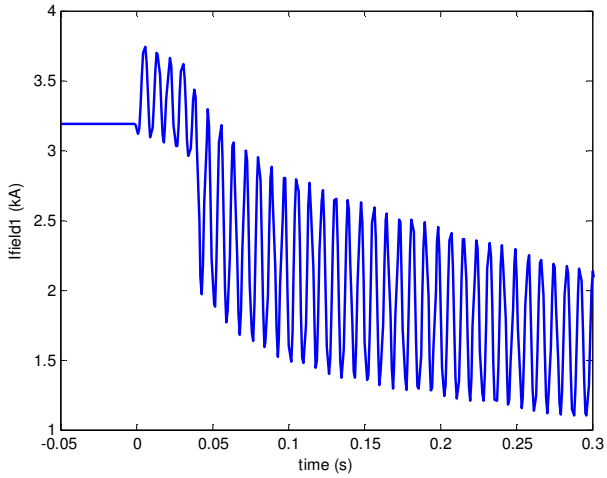

Figure 5.13. Generator field current: neutral and field breaker failure when clearing a stator-ground fault.

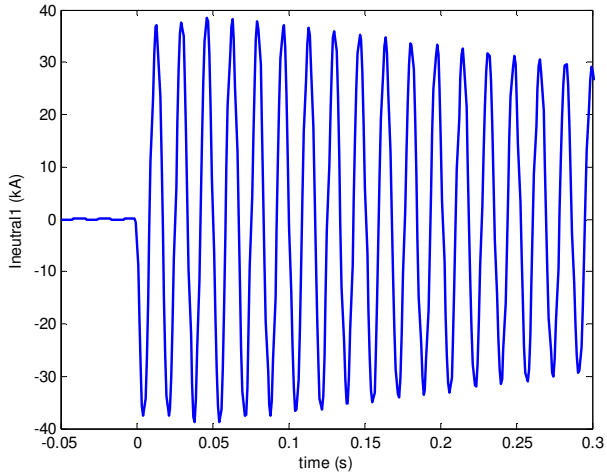

Figure 5.14. Generator neutral current: neutral and field breaker failure when clearing a stator-ground fault.

As can be seen from Figures 5.10 and 5.11, the generator's main circuit breaker was opened to isolate the faulted generator from the power system and also to prevent current being fed into the fault winding from the system. From Figure 5.12, one can see that substantial current (tens of kiloamps) nevertheless continued to flow into the fault winding since the generator field was still being energized by the excitation source due to field breaker failure. The generator stator winding could be severely damaged as a result of this high fault current continuing to flow in the stator winding.

5.2.3.2 Neutral breaker failure

Figures 5.15 to 5.19 show selected variables recorded during the real-time closed-loop studies when the neutral circuit breaker failed to respond to the trip signal issued by the 87P element to clear the earth fault.

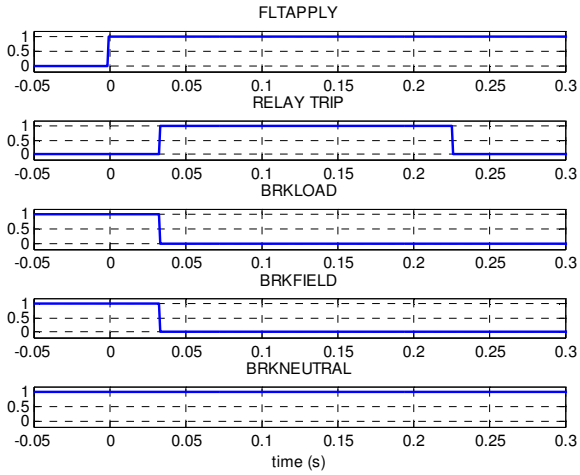

Figure 5.15. Binary control signals: neutral breaker failure when clearing a stator-ground fault.

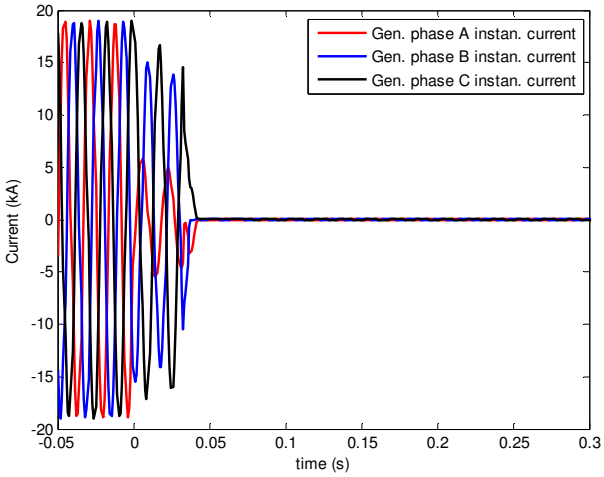

Figure 5.16. Generator winding currents at stator terminal end: neutral breaker failure when clearing a stator-ground fault.

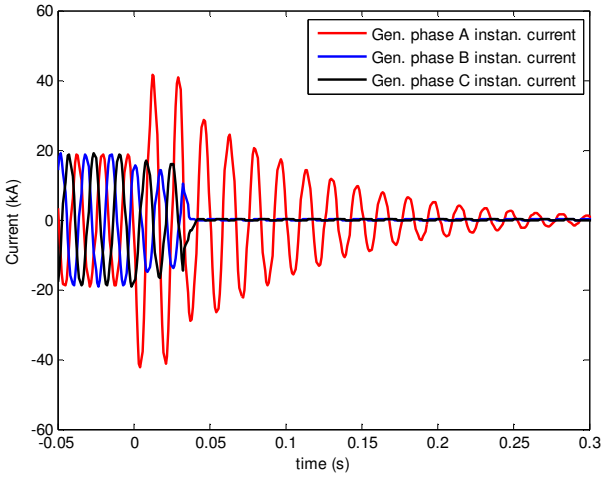

Figure 5.17. Generator winding currents at neutral end: neutral breaker failure when clearing a stator-ground fault.

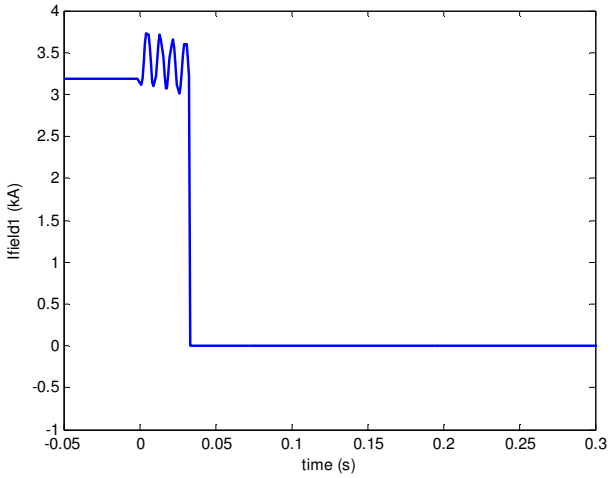

Figure 5.18. Generator field current: neutral breaker failure when clearing a stator-ground fault.

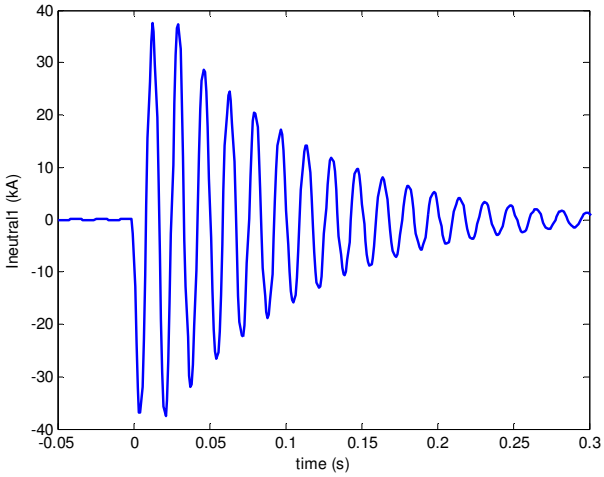

Figure 5.19. Generator neutral current: neutral breaker failure when clearing a stator-ground fault.

Figure 5.15 shows that in this case, the field breaker was correctly opened to disconnect the excitation source from the generator field winding during the fault clearing procedure. The removal of the field current causes the generator voltage to decay at a rate depending on the field time constant, with a corresponding decrease in the stator current flowing in the faulted section of the winding as seen in Figure 5.17. The results indicate that fault current on the order of tens of kiloamps nevertheless continues to flow for several hundred milliseconds after the breakers are opened due to the slow decay of the generator voltage after field de-energization.

5.2.3.3 No breaker failure

Figures 5.20 to 5.24 show selected variables recorded during the real-time closed-loop studies when all circuit breakers were operated correctly in response to the trip signal issued by the 87P element.

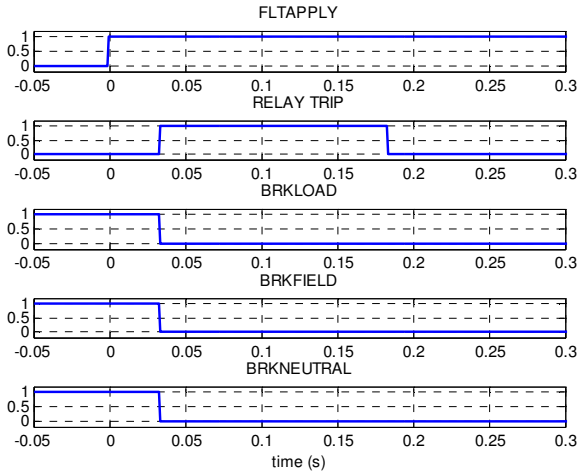

Figure 5.20. Binary control signals: correct clearing of stator-ground fault by all three breakers.

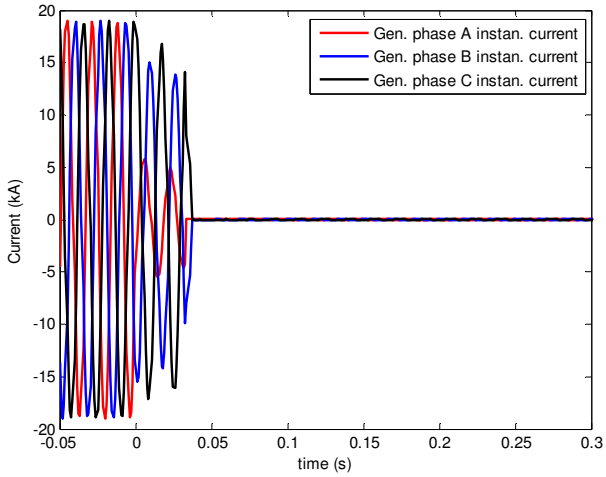

Figure 5.21. Generator winding currents at stator terminal end: correct clearing of stator-ground fault by all three breakers.

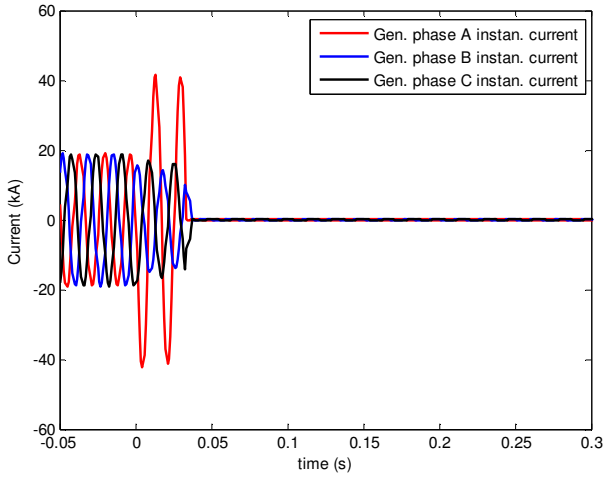

Figure 5.22. Generator winding currents at neutral end: correct clearing of stator-ground fault by all three breakers.

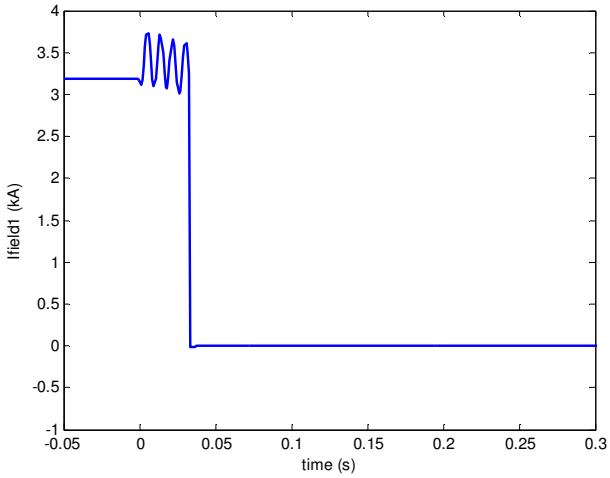

Figure 5.23. Generator field current: correct clearing of stator-ground fault by all three breakers.

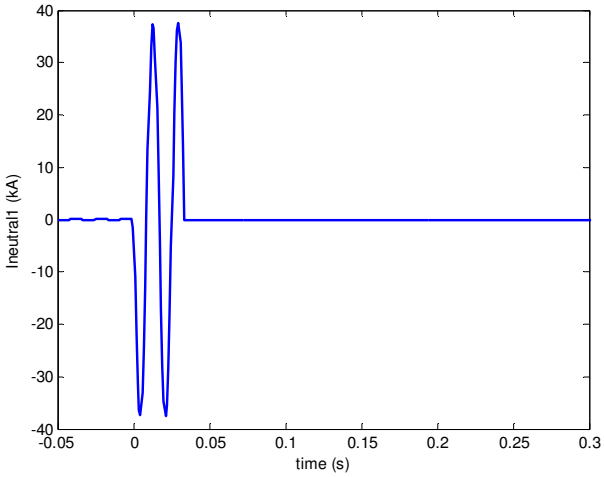

Figure 5.24. Generator neutral current: correct clearing of stator-ground fault by all three breakers.

The results in Figures 5.20 to 5.24 show that the fault current is reduced rapidly when all three circuit breakers are correctly opened during the fault clearing process. Since the zero-sequence path of the earth fault current is interrupted by opening the neutral breaker, the current in the faulted phase can no longer flow from the neutral end of the stator winding into the fault. As a result, the likelihood of damage to the stator winding of the faulted generator can be reduced significantly.

5.3 HIL test results of loss-of-field protection (40)

As just discussed, because the phase-domain synchronous machine model allows detailed electric representation of the generator field circuit using power system components, more realistic fault scenarios can be considered on the field circuit. In this section, further tests were carried out in order to investigate the performance of the SEL 300G relay's loss-of-field protection under different types of field contingency. In the following protection studies, two types of field

contingency were considered, namely a short circuit in the excitation system and an inadvertent open circuiting of the field.

The studies into the performance of the loss-of-field protection element were carried out using the realistic and detailed real-time simulation model shown in Figure 3.6 which allows the aforementioned field contingencies to be studied in detail. The studies were conducted under the following operating conditions: all four generators in the power station represented in the real-time simulation model were loaded to 90% of full load capacity and operated with 0.9 lagging power factor.

5.3.1 Excitation system short circuit

One of the limitations of the phase-domain synchronous machine model is the inability to represent internal faults within the generator field winding. Therefore in this protection study, a short-circuit fault was applied at the terminals of field winding of the protected generator. In order to observe the behaviour of the affected generator after a loss of excitation due to a short-circuited field, the trip signal issued by the 40 element of the SEL 300G generator protection relay was initially blocked. Figures 5.25 to 5.32 show selected variables obtained from the real-time closed-loop studies for the aforementioned generator field contingency.

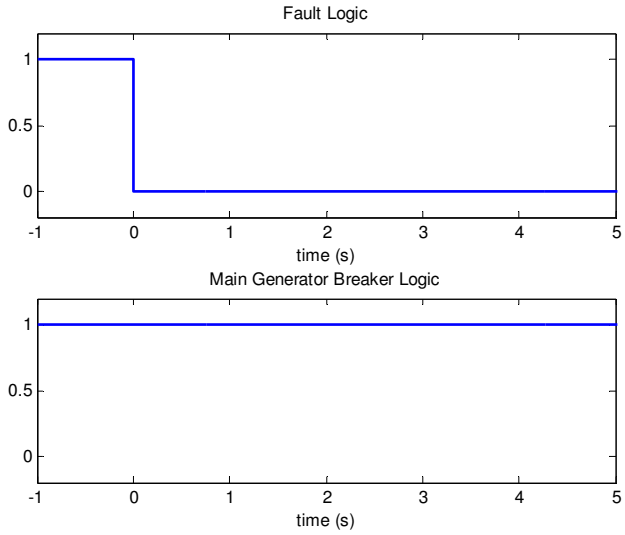

Figure 5.25. Fault and breaker logic during loss-of-field event (Shorted field circuit).

Figure 5.26 shows that when the protected generator lost the DC excitation, the field current started to decay at a rate determined by its field circuit time constant. As a result, the field flux linkage and the internal generator voltage decayed at the same rate as the field current which led to a gradual decrease in the generator terminal voltage as shown in Figure 5.27. As can be seen from Figure 5.28, the protected generator was initially supplying reactive power into the power system.

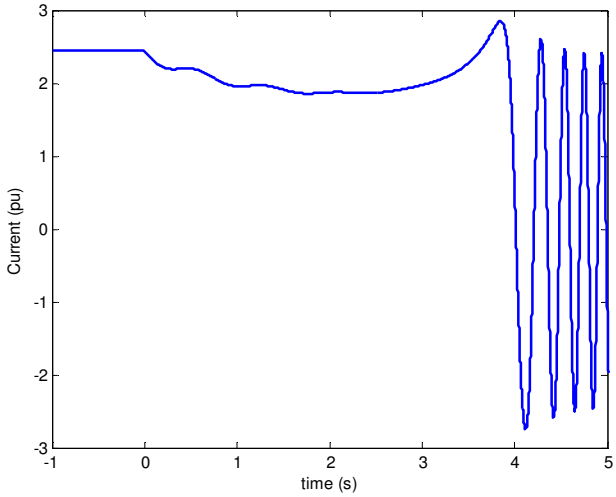

Figure 5.26. Field current during loss-of-field event (Shorted field circuit).

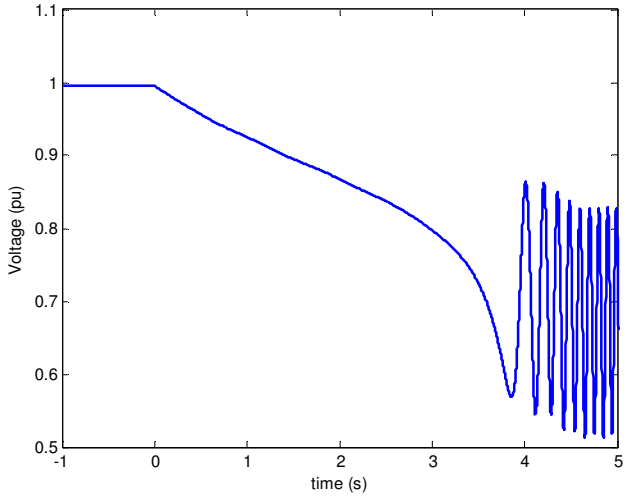

Figure 5.27. Generator terminal voltage during loss-of-field event (Shorted field circuit).

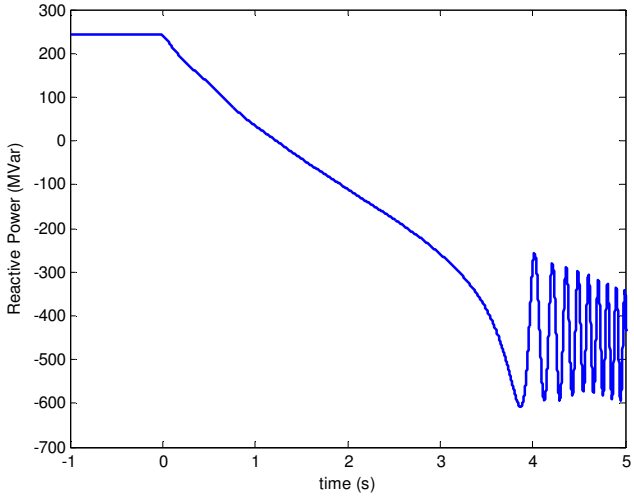

Figure 5.28. Reactive power output during loss-of-field event (Shorted field circuit).

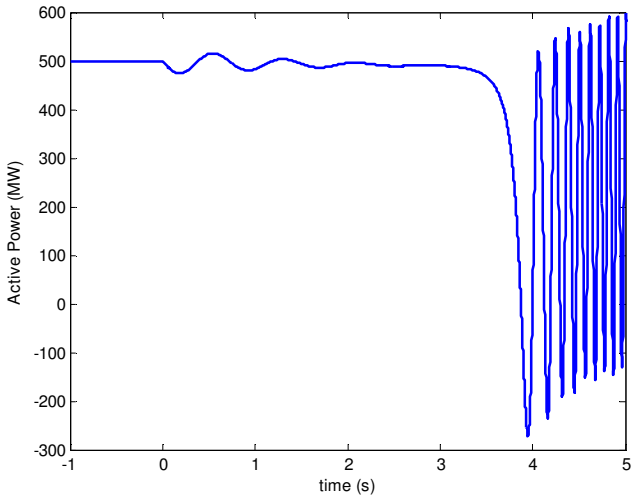

Figure 5.29. Active power output during loss-of-field event (Shorted field circuit).

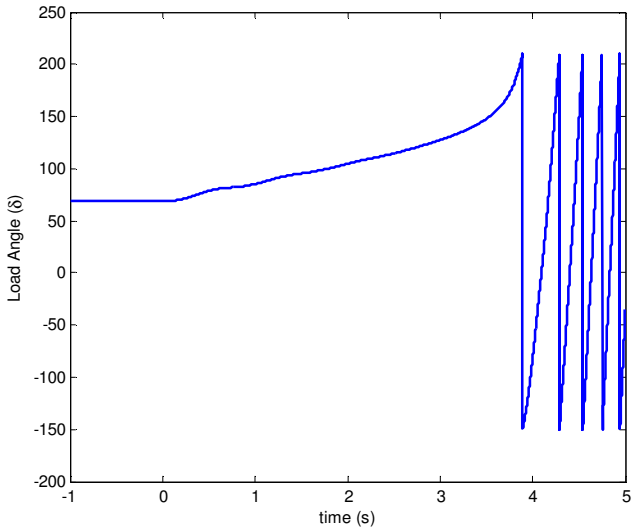

Figure 5.30. Generator load angle during loss-of-field event (Shorted field circuit).

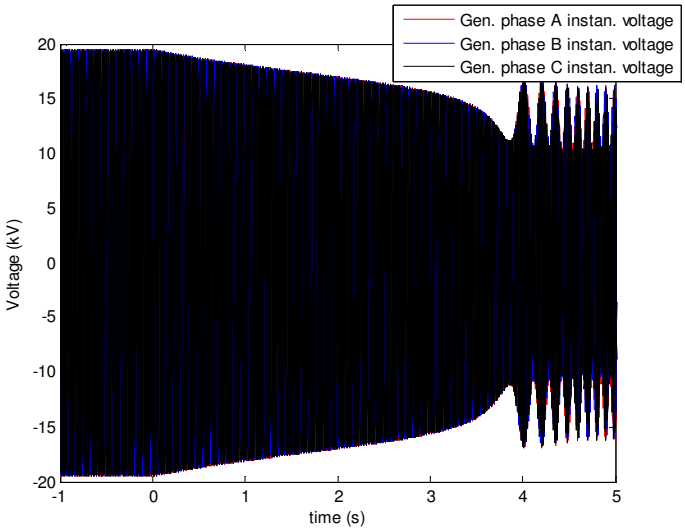

Figure 5.31. Generator instantaneous voltages during loss-of-field event (Shorted field circuit).

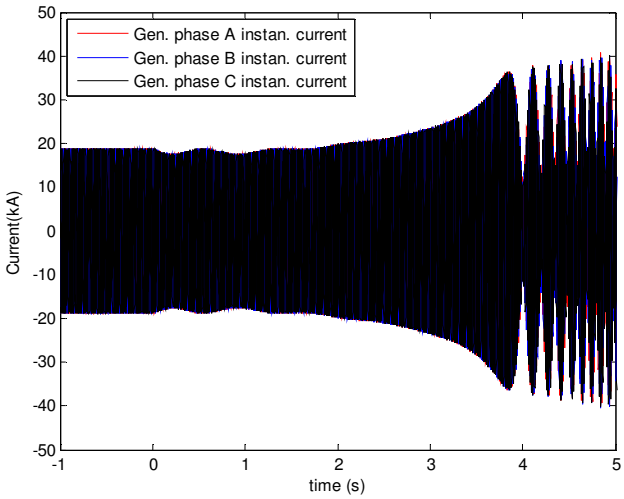

Figure 5.32. Generator instantaneous currents during loss-of-field event (Shorted field circuit).

However, the reactive power supply from the generator into the power system decayed to zero after the generator field was shorted, following which the generator started to draw a significant quantity of reactive power from the power system as a result of its loss of DC excitation. During the loss-of-field condition, the reactive power consumed by the protected generator was several times higher than the amount associated with the generator underexcitation limit. A generator operated under this condition in practice could suffer from the excessive end-core heating which would result in damage of the end-core structure, burning of stator winding insulation and failure of the insulation material between laminations [32].

During the loss-of-field condition, the ability of the protected generator to transfer active power into the power system was also affected due to the reduction in the generator terminal voltage. The generator rotor angle initially increases as the machine attempts to maintain the same amount of active power transfer into the power system as seen in Figure 5.30. Eventually, as a result of the loss-of-field event, the generator pole slips since the magnetic coupling between the stator and the rotor becomes so weak that the generator can no longer remain in synchronism with the rest of the power system. After the generator has pole-slipped, the generator instantaneous voltages and currents exhibit large cyclic variations as seen after 4.0 seconds in Figures 5.31 and 5.32 respectively.

In order to visualize and understand how the relay detects loss-of-field conditions, the variations in the apparent impedance with time viewed at the generator terminals were analysed. As discussed in Chapter Three, the RSCAD generic software generator protection relay was included in the loss-of-field protection studies in order to obtain the positive sequence resistance and reactance variations with time viewed at the generator terminals. Figure 5.33 shows the results of these measurements

during the loss-of-field event already seen in the results of Figures 5.26 to 5.32. Using the data points in Figure 5.33, the trajectory of the apparent impedance was then plotted on the R-X impedance plane as shown in Figure 5.34.

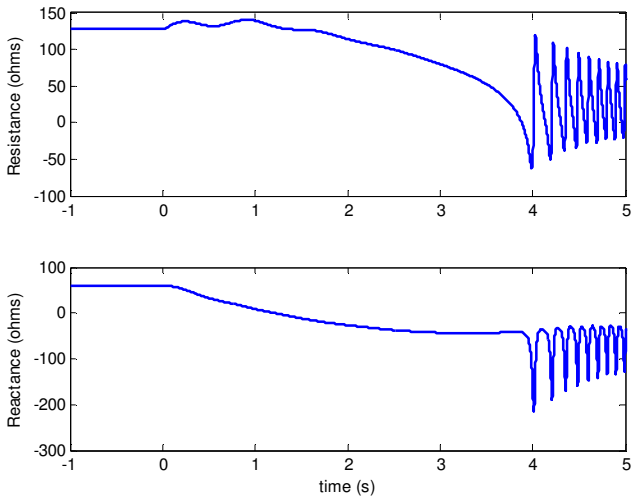

Figure 5.33. Positive sequence resistance and reactance during loss-of-field event (Shorted field circuit).

Figure 5.34 shows the trajectory of the apparent impedance overlaid onto the operating characteristics of the particular loss-of-field protection scheme shown in Figure 4.4. It is clear that the trajectory of the apparent impedance would enter both the zone 2 and zone 1 mho circles during the loss-of-field condition. The spiralling impedance locus seen in Figure 5.34 indicates that the generator had pole-slipped which typically occurs following a loss-of-field event.

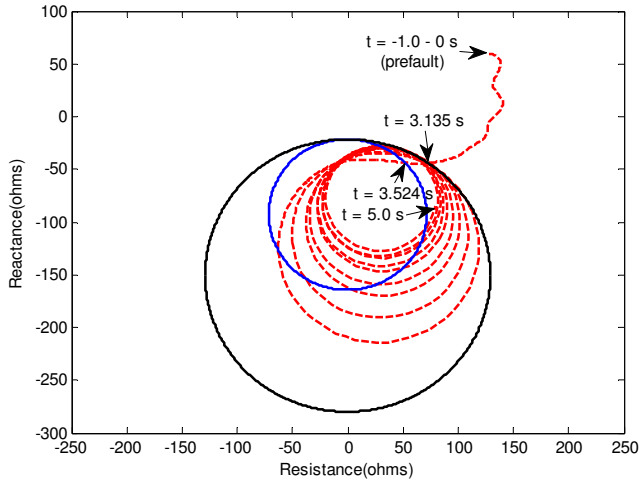

Figure 5.34. Impedance locus during loss-of-field event (Shorted field circuit).

Figures 5.35 and 5.36 show the results obtained from the real-time closed-loop studies when the 40 element of the SEL 300G generator protection relay was re-enabled. As can be seen from Figure

5.36, the relay did not trip when the positive sequence impedance entered the zone 2 mho circle because there was a time delay of 0.5 second inserted in this zone to discriminate between loss-of-field events and stable generator swings, caused by other events, that may also enter this zone. The relay tripped almost immediately once the impedance locus entered the zone 1 mho circle at time $t = 3.524$ seconds since there was no intentional time delay inserted for this zone.

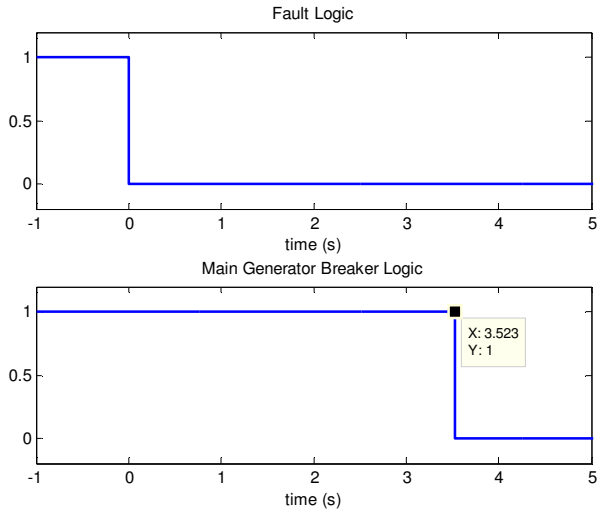

Figure 5.35. Fault and breaker logic during loss-of-field event (Shorted field circuit).

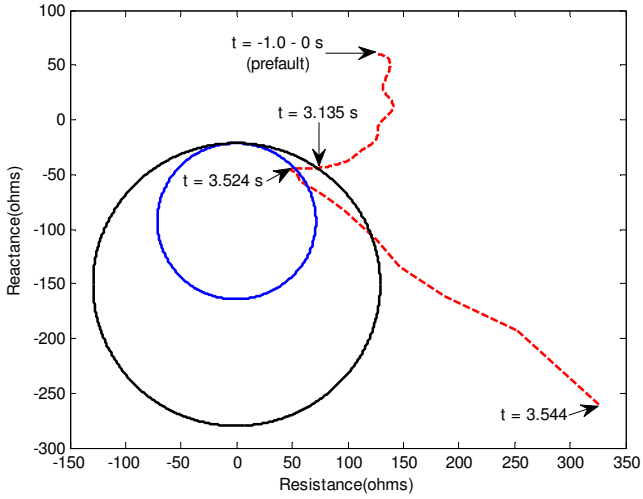

Figure 5.36. Impedance locus during loss-of-field event (Shorted field circuit).

Figures 5.37 and 5.38 show the real-time closed-loop test results for the same loss-of-field contingency when the second type of loss-of-field protection scheme available on the SEL 300G relay, shown in Figure 4.5, was employed at the terminals of the protected generator. As one can see from Figure 5.38, the impedance locus entered the zone 2 mho characteristic at $t = 1.110$ seconds after the field circuit was shorted. As discussed in Chapter Four, any trip signal issued by the 40 element of the SEL 300G relay will be blocked when the measured apparent impedance is located above the directional element. For this reason, the 40 element of the SEL 300G relay only

issued a trip signal after the impedance had passed into the zone 1 mho characteristic and the zone 1 time delay of 0.25 seconds has elapsed.

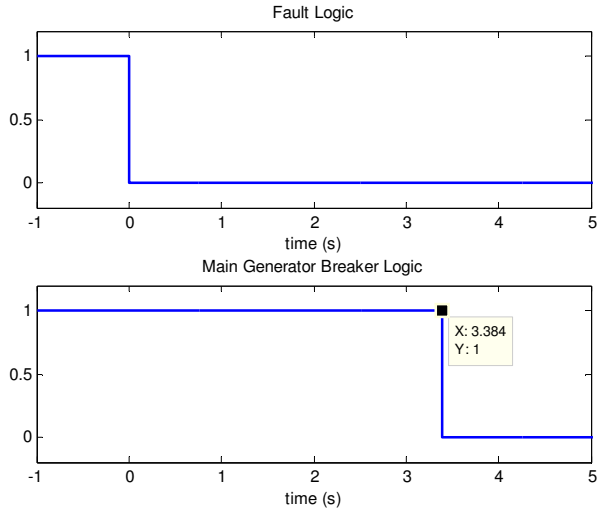

Figure 5.37. Fault and breaker logic during loss-of-field event (Shorted field circuit).

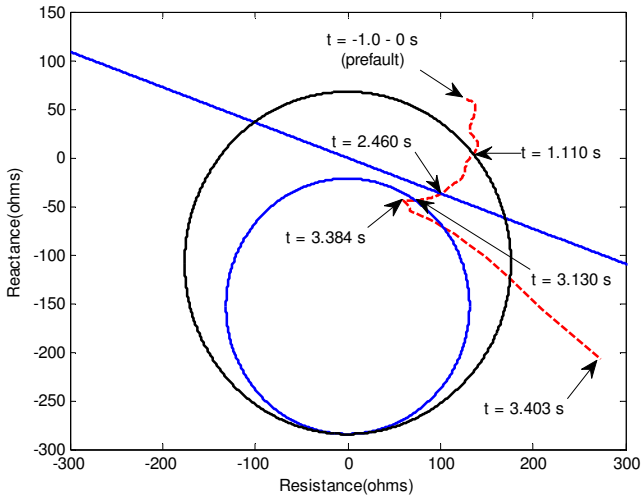

Figure 5.38. Impedance locus during loss-of-field event (Shorted field circuit).

5.3.2 Inadvertent open circuiting of the field

Open circuiting of the generator field is another type of contingency that results in loss-of-field conditions. In order to test the response of the relay to such a contingency, the field circuit breaker of the protected generator represented in the real-time simulation model shown in Figure 3.6 was deliberately opened to simulate field breaker misoperation under normal generator operating conditions. Once again, the trip signal issued by the 40 element of the SEL 300G relay was initially blocked in order to observe the behaviour of the affected generator during this type of field

contingency. Figures 5.39 to 5.46 show selected variables obtained from the real-time closed-loop studies during the aforementioned field contingency.

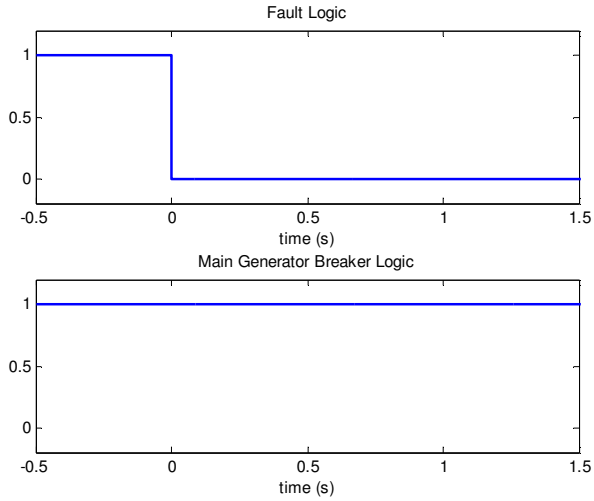

Figure 5.39. Fault and breaker logic during loss-of-field event (opened field circuit).

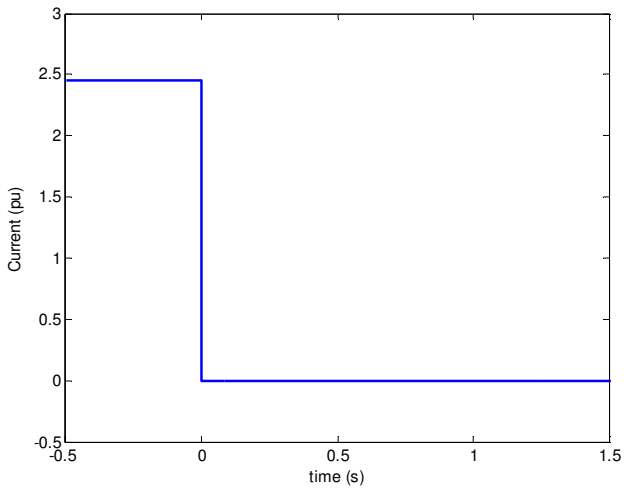

Figure 5.40. Field current during loss-of-field event (opened field circuit).

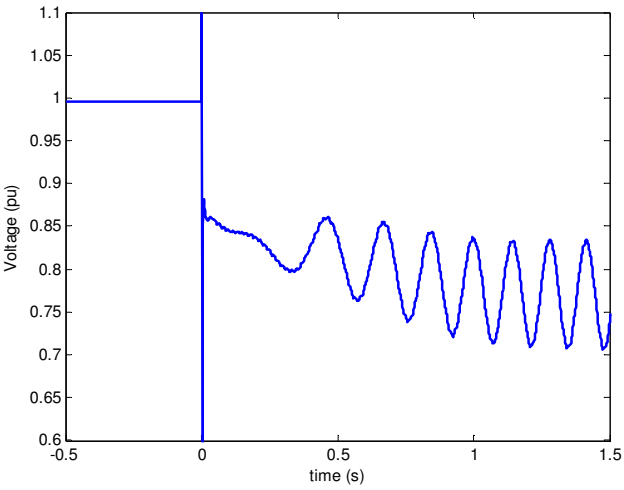

Figure 5.41. Generator terminal voltage during loss-of-field event (opened field circuit).

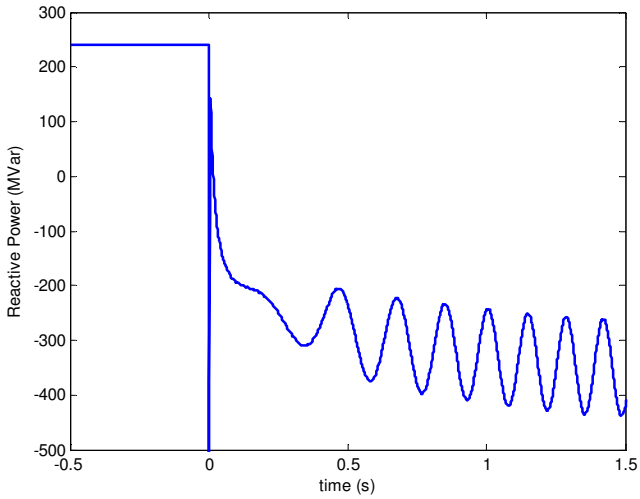

Figure 5.42. Reactive power output during loss-of-field event (opened field circuit).

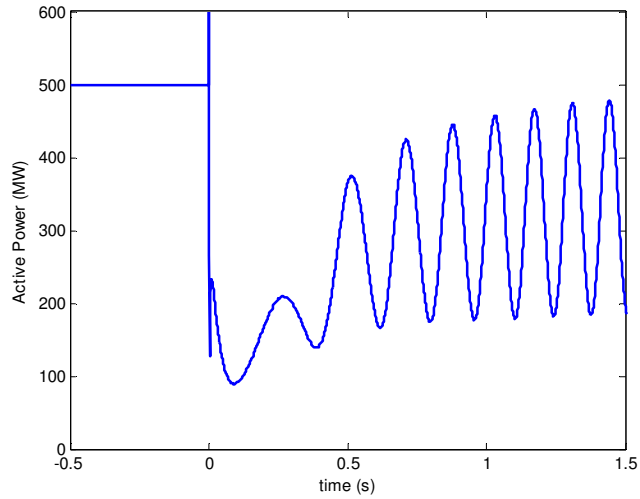

Figure 5.43. Active power output during loss-of-field event (opened field circuit).

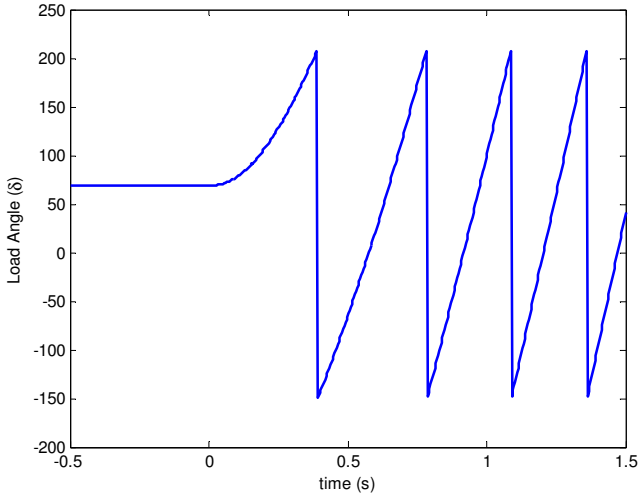

Figure 5.44. Generator load angle during loss-of-field event (opened field circuit).

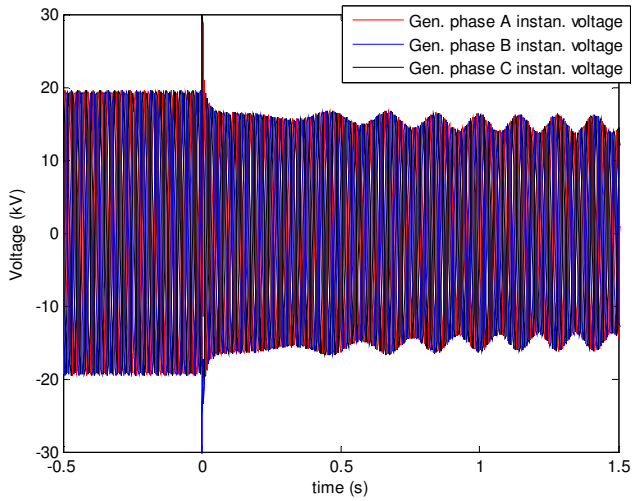

Figure 5.45. Generator instantaneous voltages during loss-of-field event (opened field circuit).

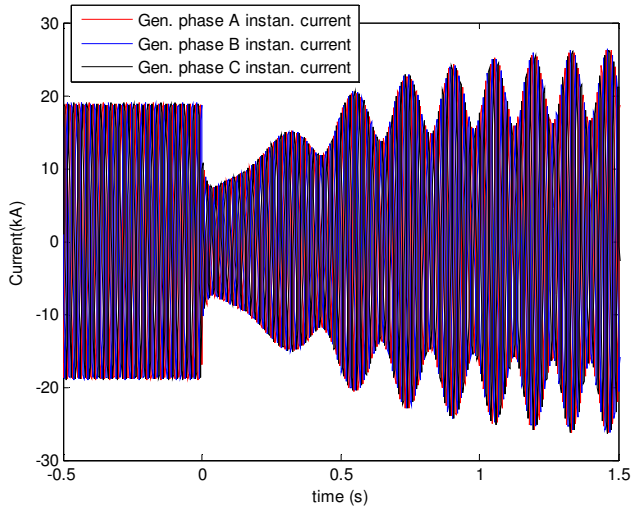

Figure 5.46. Generator instantaneous currents during loss-of-field event (opened field circuit).

The results indicate that the sudden interruption in the field current would cause drastic changes in the generator terminal voltage as shown in Figure 5.41, which in turn, would affect both the reactive and active power transferred into the power system as shown in Figures 5.42 and 5.43 respectively. In comparison with the field short circuiting incident shown in Section 5.3.1, the generator instantaneous voltages and currents change much more abruptly upon open circuiting of the field as shown in Figures 5.45 and 5.46. As a result, in the case of this field open circuiting event, one would expect a very different trajectory of the apparent impedance compared to that seen in Figure 5.34 for the field short circuit, since the protected generator responds more dramatically in this case.

Figure 5.47 shows the variations in positive sequence resistance and reactance with time seen at the terminals of the protected generator that were obtained from the RSCAD generic software generator protection relay during the field open circuit event.

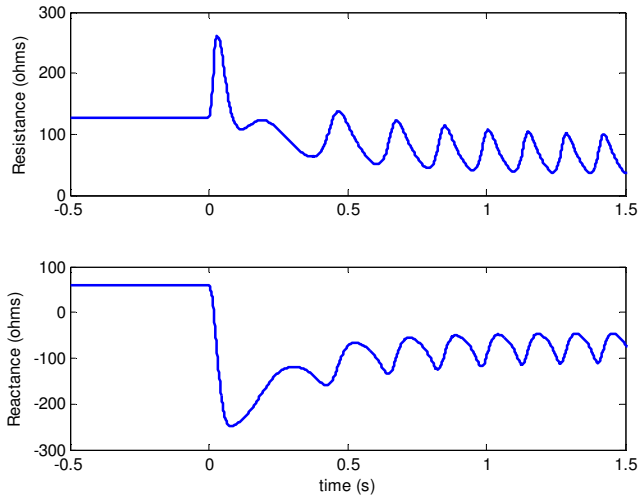

Figure 5.47. Positive sequence resistance and reactance during loss-of-field event (opened field circuit).

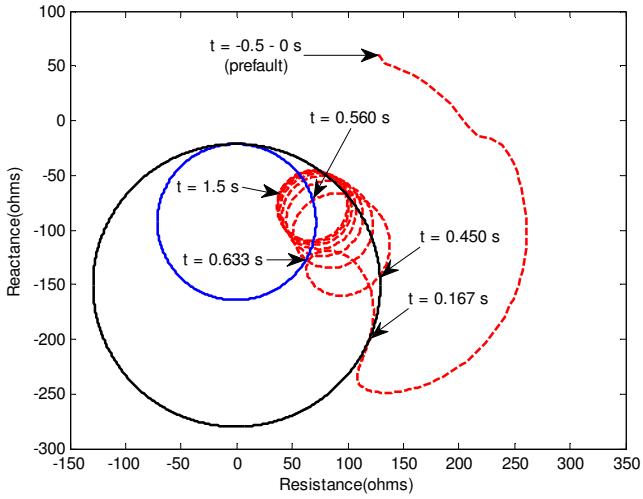

Figure 5.48. Impedance locus during loss-of-field event (opened field circuit).

Figure 5.48 shows the positive sequence resistance and reactance values from Figure 5.47 plotted against one another in the R-X impedance plane in order to visualize the impedance locus overlaid onto the operating characteristics of the loss-of-field protection scheme. In the case of this contingency, one can see that the impedance entered the operating characteristics of the 40 element much more rapidly in comparison with the field short circuiting incident shown in Figure 5.34.

Figures 5.49 and 5.50 show the results obtained from the real-time closed-loop studies when the 40 element of the SEL 300G generator protection relay was re-enabled. As can be seen from Figure 5.50, the impedance entered the zone 2 mho circle at $t = 0.167$ seconds after the field circuit breaker had been deliberately opened. However, the relay did not issue a trip signal since there was a 0.5 seconds time delay inserted in the zone 2 mho circle. The impedance subsequently exited and re-entered the zone 2 mho circle and then travelled further into the zone 1 mho circle at $t = 0.56$

seconds. The relay tripped almost immediately after the impedance entered the zone 1 mho circle since there was no intentional time delay inserted in this protective zone.

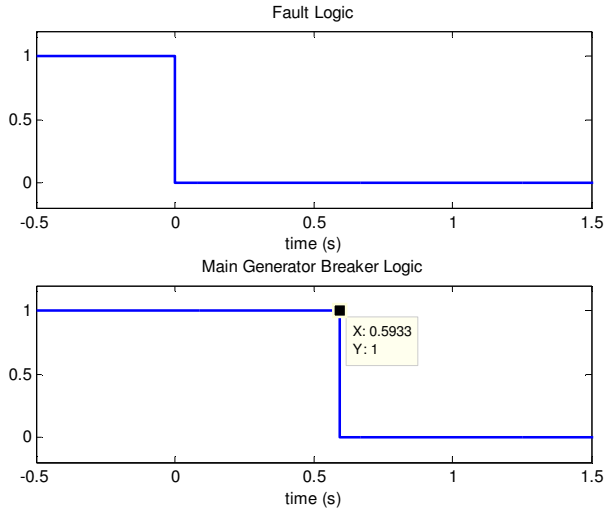

Figure 5.49. Fault and breaker logic during loss-of-field event (opened field circuit).

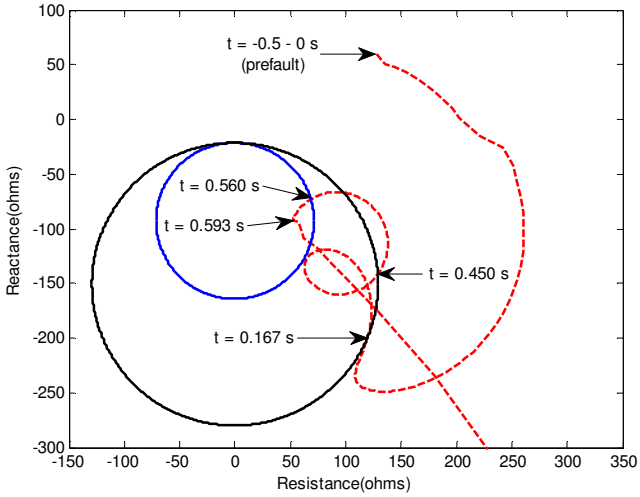

Figure 5.50. Impedance locus during loss-of-field event (opened field circuit).

Figures 5.51 and 5.52 show the real-time closed-loop test results for the same loss-of-field contingency when the second type of loss-of-field protection scheme available on the relay, shown in Figure 4.5, was employed at the terminals of the protected generator. As can be seen from Figure 5.52, the measured impedance entered the zone 2 mho characteristic at $t = 0.102$ seconds after the field circuit breaker was opened inadvertently. However, the relay did not issue a trip signal since there is a 1 second time delay inserted in zone 2 mho circle. The measured impedance then travelled further inwards, into the zone 1 mho characteristic, and eventually caused the relay to trip after the zone 1 time delay of 0.25 seconds had elapsed. The loss-of-field protection scheme shown in Figure 4.5 has therefore demonstrated its ability to trip the protected generator, for two different types of loss-of-field event, one cycle faster than the protection scheme shown in Figure 4.4

because of the extended diameters of its mho circles. However, because of these extended mho circle diameters, suitable time delays have to be selected in order to prevent misoperation under stable generator swing conditions.

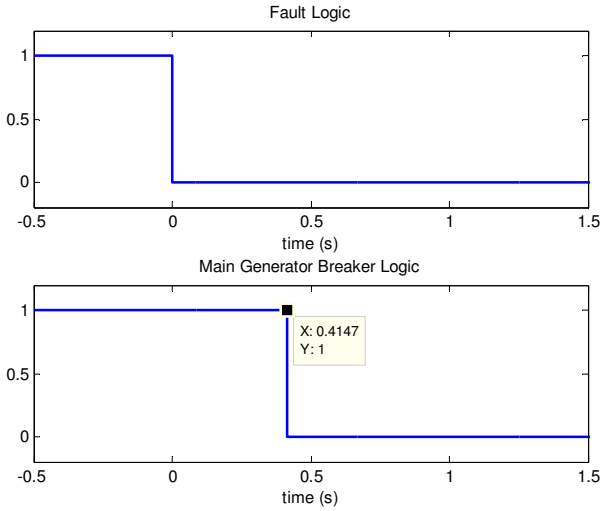

Figure 5.51. Fault and breaker logic during loss-of-field event (opened field circuit).

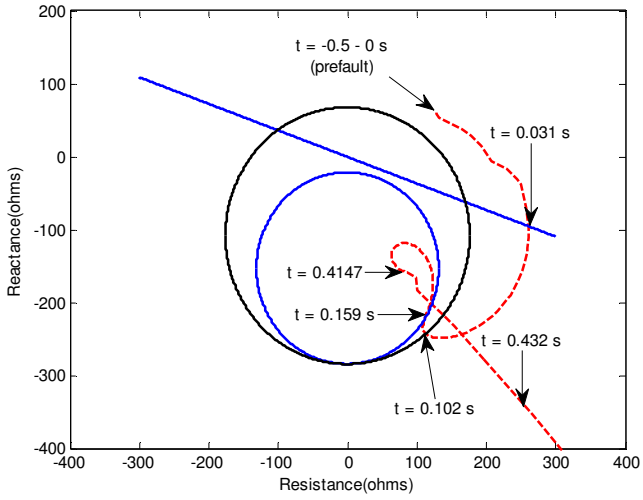

Figure 5.52. Impedance locus during loss-of-field event (opened field circuit).

5.3.3 Effect of different generator loading conditions during loss-of-field events

It is important to note that the trajectory of the positive sequence impedance during loss-of-field conditions depends on the relative rates of change of the generator internal voltage and rotor angle, which in turn, depends on the field circuit time constant and the initial generator loading condition. For this reason, additional loss-of-field protection studies were carried out in order to investigate the effects of generator initial loading conditions on the apparent impedance measured at the terminals of the protected generator under different types of field contingencies.

Table 5.10. Operating conditions of the particular generator under study

Curve	Initial Loading (per unit)	Power Factor
a	0.8	0.9 Lagging
b	0.5	0.9 Lagging
c	0.3	0.9 Lagging

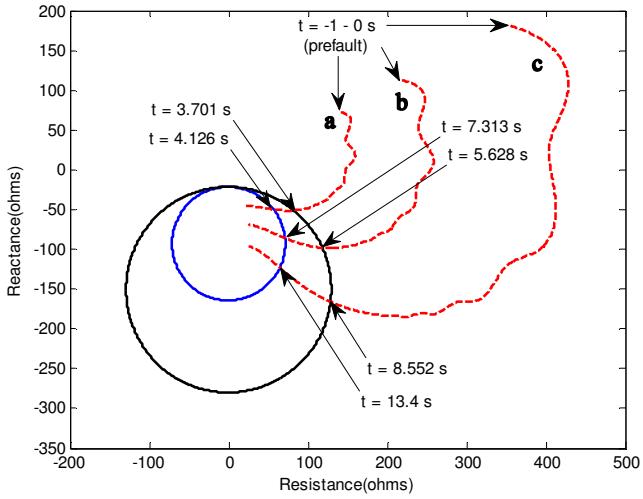

Figure 5.53. Impedance loci for different loading conditions during loss-of-field event (shorted field circuit).

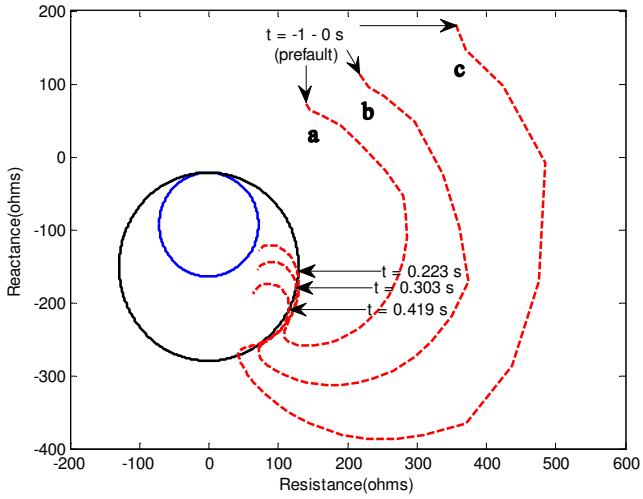

Figure 5.54. Impedance loci for different loading conditions during loss-of-field event (opened field circuit).

Figure 5.53 shows the impedance loci measured at the terminals of the protected generator during an excitation short circuit event for the three different generator initial loading conditions shown in Table 5.10. Figure 5.54 shows the measured impedance loci during an inadvertent field open circuiting event for the same three loading conditions. In both studies, one can see that the

impedance locus moved more quickly into the loss-of-field mho characteristics as the initial steady-state loading on the generator was increased.

5.4 HIL test results of out-of-step protection (78)

Different types of faults occurring at different locations on the power system can have different effects on a generator's stability. The duration of the faults can also have a significant influence on the stability of the system as a whole. When a generator loses synchronism with the system, it should be isolated from the system as quickly as possible. Fast isolation of an unstable generator can allow the stability of the remaining generators in the interconnected system to be maintained and can also prevent substantial damage to the unstable generator from high-amplitude currents, off-nominal frequency operation and pulsating torques.

This section presents the real-time closed-loop test results of the SEL 300G relay's single-blinder out-of-step protection scheme (78). As discussed in Chapter Three, a specific version of the real-time simulation model of the chosen study system, shown in Figure 3.3, was developed specifically for use in carrying out protection studies of the 78 element. By using this highly detailed real-time simulation model, different fault scenarios can be considered when examining the performance of the 78 element.

5.4.1 Faults on transmission line

The real-time closed-loop studies of the 78 element were conducted under the following operating conditions: all four generators in the power station represented in the simulation model were loaded to 90% of full load capacity and operated with 0.9 lagging power factor. A solid three-phase fault was then applied at point F1 on one of the transmission lines shown in Figure 3.3. In this particular study, the fault was then cleared by opening circuit breakers on both sides of the faulted transmission lines at different time periods after the initiation of the fault in order to be able to investigate both stable generator swing conditions and out-of-step conditions after a severe system disturbance. The test results for a stable generator swing condition and for an out-of-step condition following severe system disturbances are presented in Sections 5.4.1.1 and 5.4.1.2 respectively.

5.4.1.1 Stable swing after a system disturbance

Figures 5.55 to 5.61 show selected variables obtained from the real-time closed-loop study of the 78 element for a stable generator swing (fault F1 cleared after 0.07 seconds). The results indicate that the protected generator remained in synchronism with the system after the system disturbance and therefore the 78 element of the relay did not issue a trip signal to open the generator's main circuit breaker as shown in Figure 5.55.

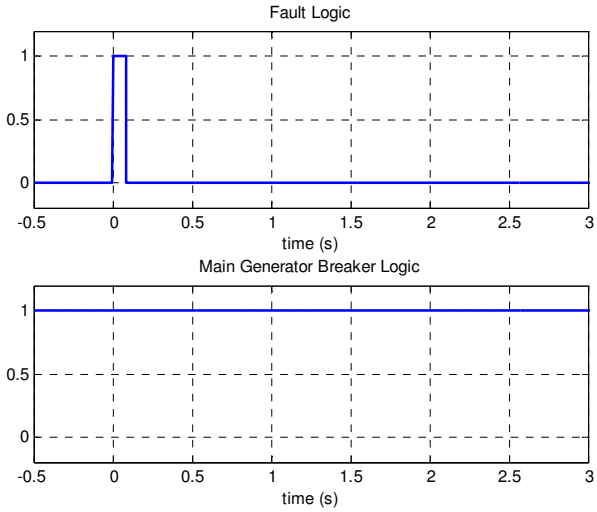

Figure 5.55. Fault and breaker logic during stable power swing condition.

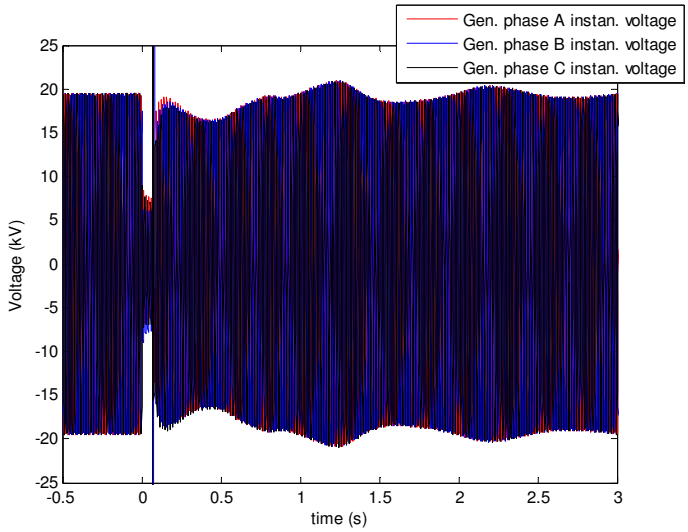

Figure 5.56. Generator instantaneous voltages during stable power swing condition.

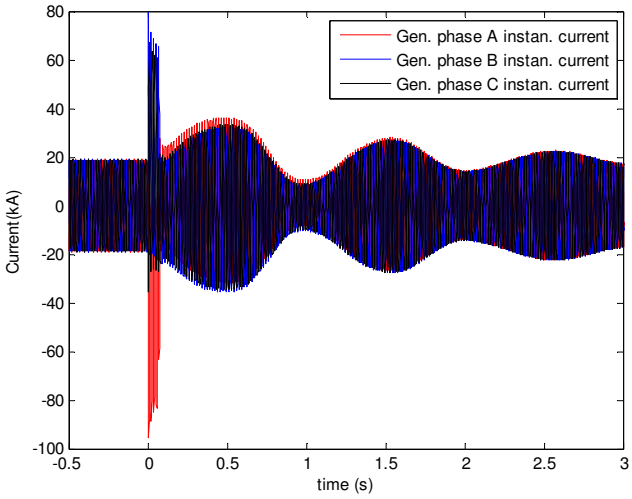

Figure 5.57. Generator instantaneous currents during stable power swing condition.

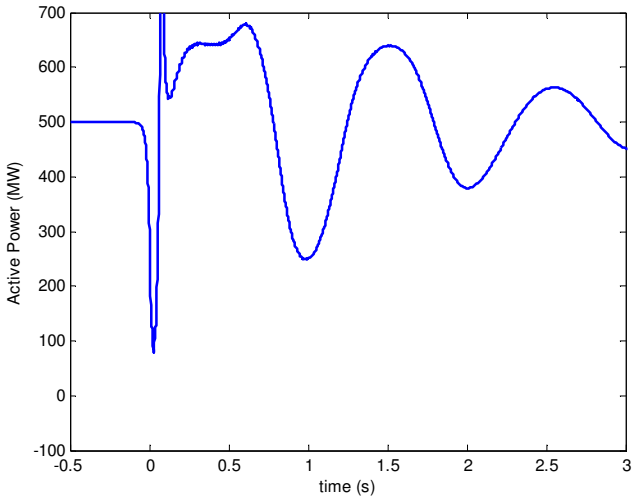

Figure 5.58. Active power output during stable power swing condition.

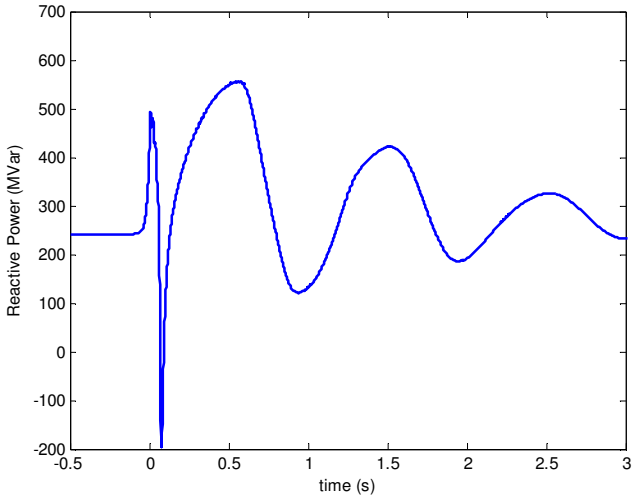

Figure 5.59. Reactive power output during stable power swing condition.

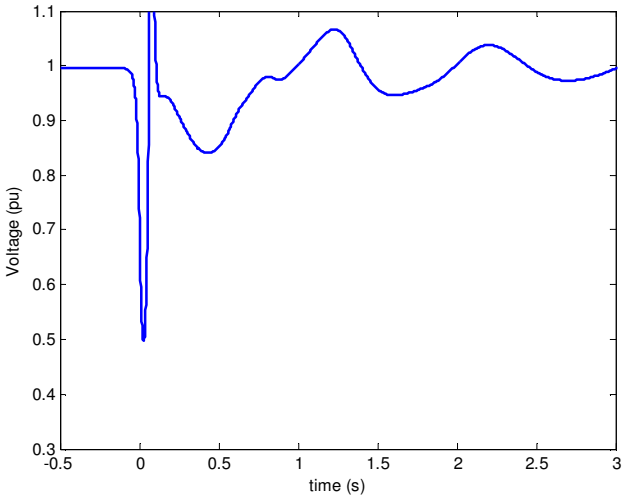

Figure 5.60. Generator terminal voltage during stable power swing condition.

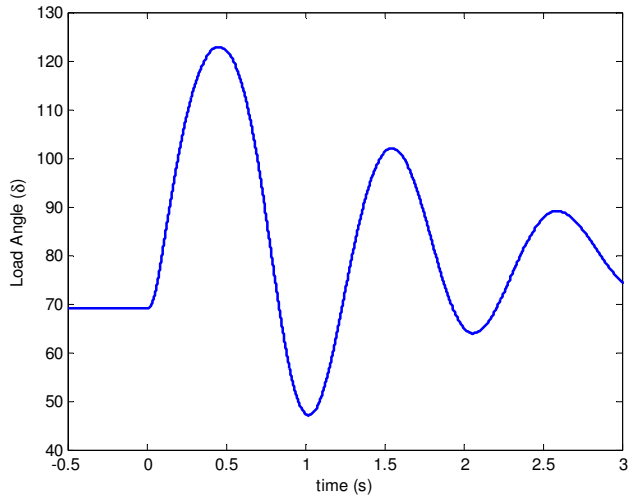

Figure 5.61. Generator load angle during stable power swing condition.

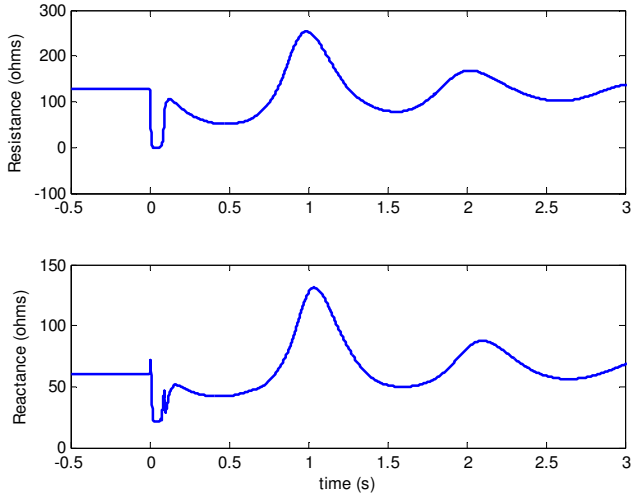

Figure 5.62. Positive sequence resistance and reactance during stable power swing condition.

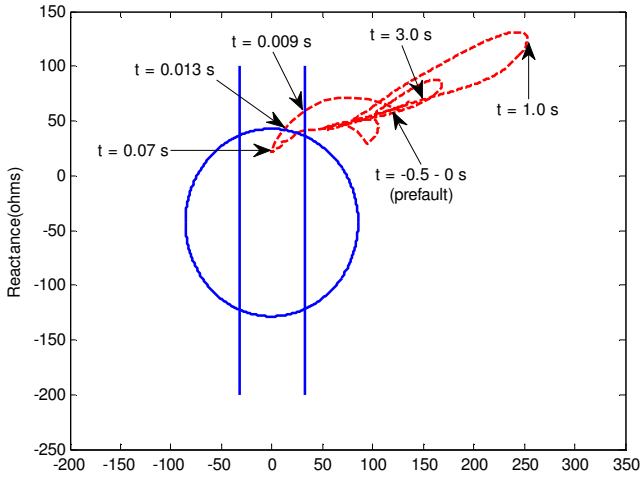

Figure 5.63. Impedance locus during stable power swing condition.

Figure 5.62 shows the positive sequence impedance versus time obtained from RSCAD's software generator protection relay model that was included in the simulation for the protection studies of the 78 element. In order to analyse how the 78 element of the SEL 300G relay responded to the swing condition, this measured apparent impedance was plotted together with the operating characteristic of the 78 element on the same R-X impedance plane as shown in Figure 5.63. From the plot in Figure 5.63, it is clear that the measured impedance travelled from right to left in the R-X plane, crossed the blinder on the positive side of the reactance axis and then passed further into the supervisory offset-mho circle during the system disturbance. However, as soon as the faulted transmission line was isolated, the measured impedance exited the operating characteristic of the 78 element from left to right without crossing the blinder on the negative side of the reactance axis. For this reason, the 78 element of the relay correctly identified that this was a stable swing condition and therefore did not issue a trip signal to isolate the protected generator.

5.4.1.2 Out-of-step condition after a system disturbance

Figures 5.64 to 5.70 show selected variables obtained from the real-time closed-loop study of the 78 element for an unstable generator swing condition (fault F1 cleared after 0.1 seconds). The test results indicate that the protected generator pole-slipped due to the prolonged system disturbance. After the protected generator pole-slipped, the measured generator voltages and currents exhibited large cyclic variations, with the frequency of these variations being a function of the rate of slip of its poles as shown in Figures 5.65 and 5.66 respectively. As a result of the out-of-step condition, the active and reactive power output of the generator also started to exhibit large-amplitude oscillations as seen in Figures 5.67 and 5.68 respectively.

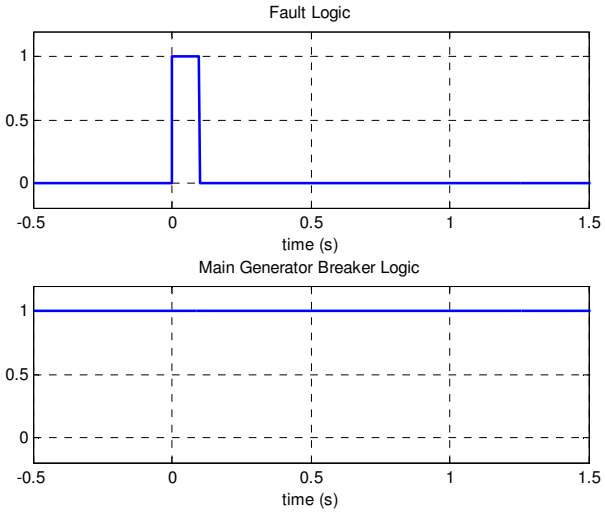

Figure 5.64. Fault logic during out-of-step condition.

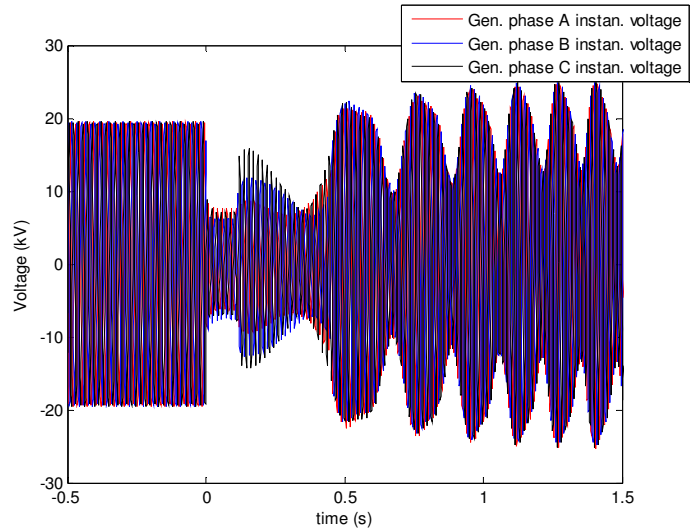

Figure 5.65. Generator instantaneous voltages during out-of-step condition.

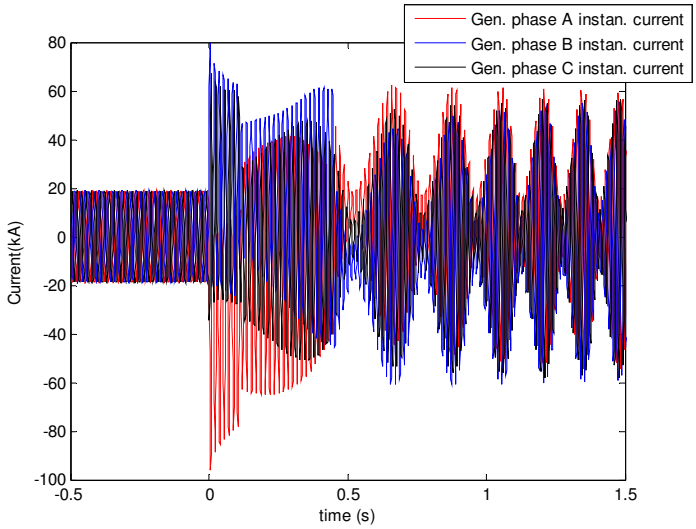

Figure 5.66. Generator instantaneous currents during out-of-step condition.

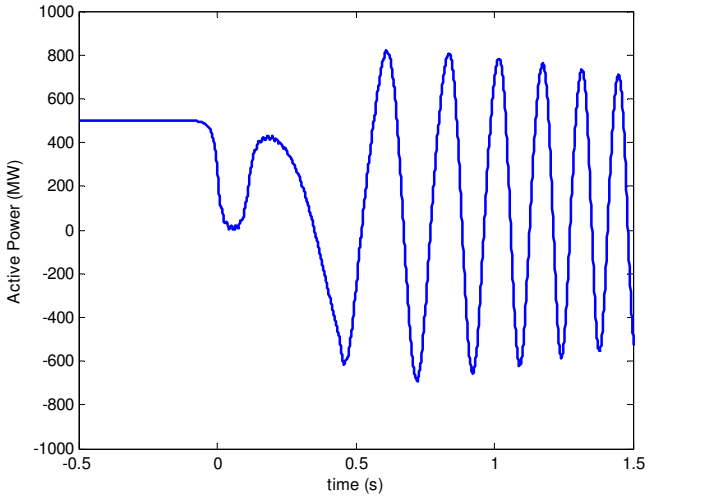

Figure 5.67. Active power output during out-of-step condition.

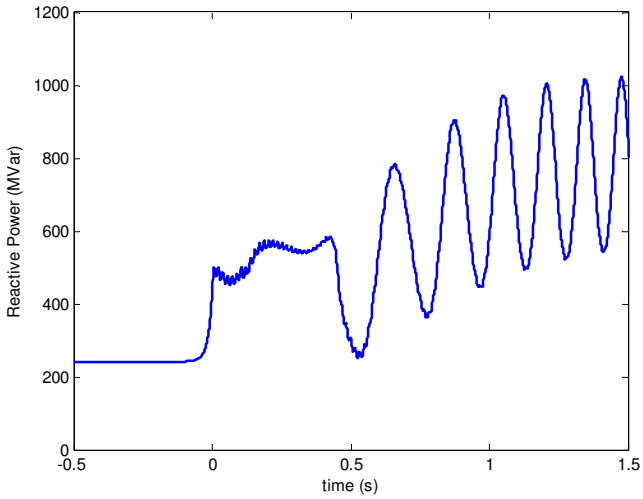

Figure 5.68. Reactive power output during out-of-step condition.

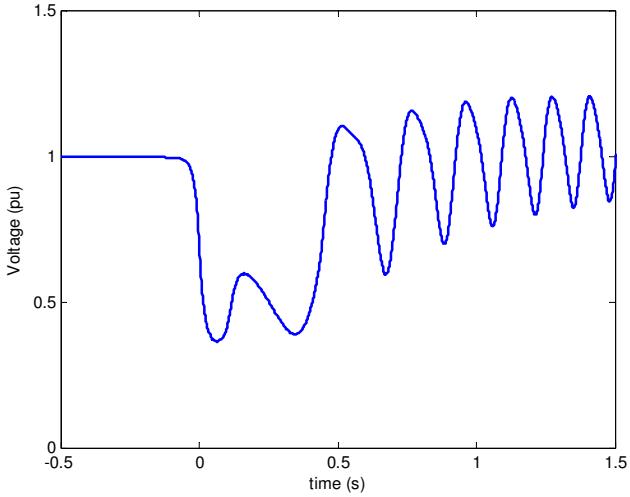

Figure 5.69. Generator terminal voltage during out-of-step condition.

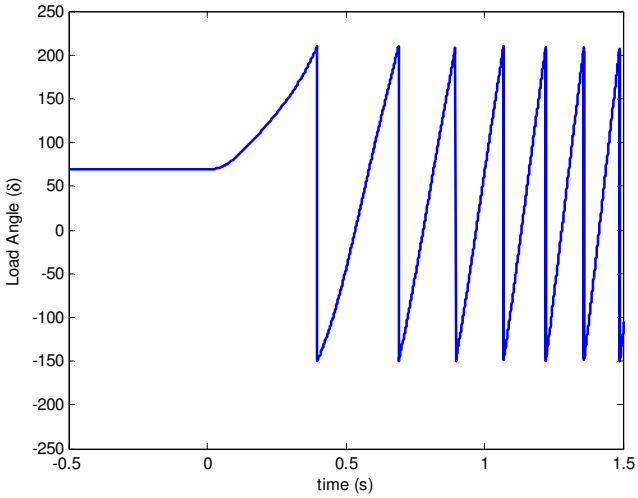

Figure 5.70. Generator load angle during out-of-step condition.

In order to be able to observe the behaviour of the affected generator during the out-of-step condition, the trip signal issued by the 78 element of the SEL 300G relay was initially blocked. The measured impedance locus during the out-of-step condition was plotted on the R-X impedance plane and overlaid onto the operating characteristic of the 78 element for further analysis. It is clear that the operating characteristic of the single blinder out-of-step protection scheme described in Chapter Four is able to detect the out-of-step condition in this case; In addition, if the unstable generator is not separated from the system during the out-of-step condition, the whole cycle may repeat itself as shown in Figure 5.72.

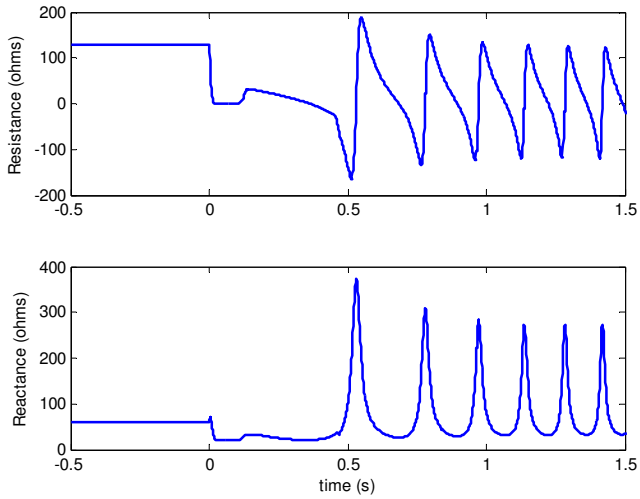

Figure 5.71. Positive sequence resistance and reactance during out-of-step condition (78 tripping blocked).

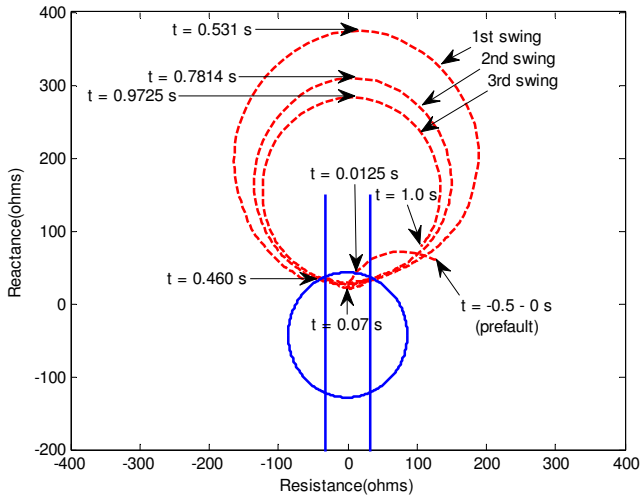

Figure 5.72. Impedance locus during out-of-step condition (78 tripping blocked).

Figures 5.73 and 5.74 show the real-time closed-loop test results when the 78 element of the SEL 300G relay was re-enabled. The SEL 300G relay issued a trip signal at $t = 0.4762$ seconds when an out-of-step condition was detected. As can be seen from Figure 5.74, the unstable generator was isolated from the system in less than one slip cycle.

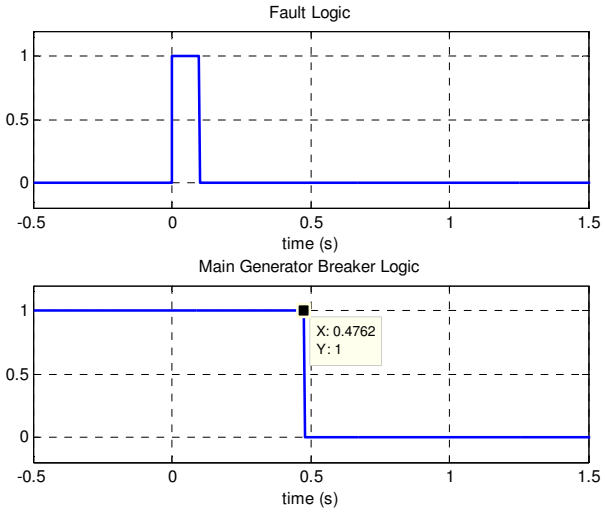

Figure 5.73. Fault and breaker logic during out-of-step condition (78 tripping enabled).

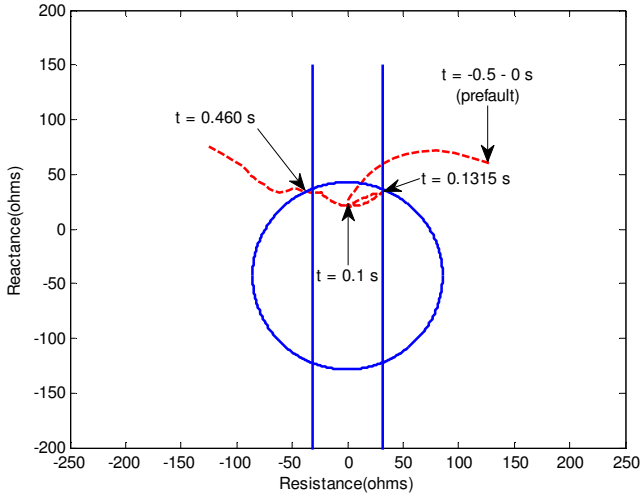

Figure 5.74. Impedance locus during out-of-step condition (78 tripping enabled).

5.4.2 Faults inside the power station

A further test was carried out to study the performance of the 78 element for more complex generator swing characteristics. In this particular case, the real-time closed-loop studies of the 78 element were conducted under the following system operating conditions: the particular generator under study was loaded to 90% of full load capacity and operated with 0.9 leading power factor. The remaining generators in the power station were loaded to 60% of full load capacity and operated with 0.8 lagging power factor. A solid three-phase fault was applied at point F2 (i.e. at the stator terminals of a neighbouring 555 MVA generator) in the modified study system shown in Figure 3.3. The fault was then cleared by opening the main circuit breaker of the neighbouring faulted generator at different time periods after the initiation of the fault in order to be able to investigate stable and unstable swings of the protected generator under the aforementioned fault

scenario. The test results for a stable and an unstable case are presented in Sections 5.4.2.1 and 5.4.2.2.

5.4.2.1 Stable swing after a system disturbance

Figure 5.75 shows the measured impedance locus following the system disturbance, overlaid onto both the loss-of-field and out-of-step operating characteristics in the R-X impedance plane, for a stable case (fault F2 cleared at t=0.3 seconds). It is clear that the 78 element of the relay did not issue a trip signal since the measured impedance did not pass into the supervisory offset-mho circle even though it crossed blinders on both sides of the reactance axis. In addition, it was observed that the measured impedance passed into the zone 2 mho characteristic of the loss-of-field protection scheme (40) for 0.113 seconds during the post-fault recovery swing following the system disturbance. In this case, the time delay of 0.5 seconds used with the zone 2 mho characteristic of the 40 element (as discussed in Chapter Four) did prevent relay misoperation during the stable recovery swing.

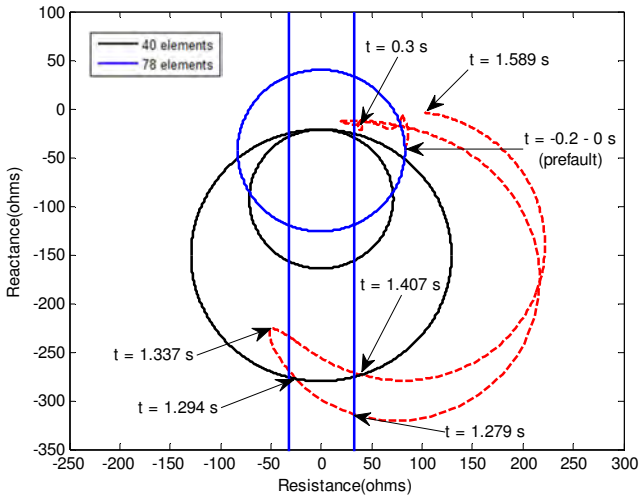

Figure 5.75. Impedance locus during stable power swing condition.

5.4.2.2 Out-of-step condition after a system disturbance

Figure 5.76 shows the measured impedance locus following the system disturbance, overlaid onto the single-blinder out-of-step operating characteristics in the R-X impedance plane, for an unstable case (fault F2 cleared at t = 0.7 seconds). As discussed in Chapter Four, if the ratio of the system voltages is smaller than one ($E_g/E_s < 1$) during an out-of-step condition, the impedance locus will be a circle with its centre located below the perpendicular bisector of the total system impedance characteristic. The impedance locus seen in Figure 5.76 is an example of the aforementioned case.

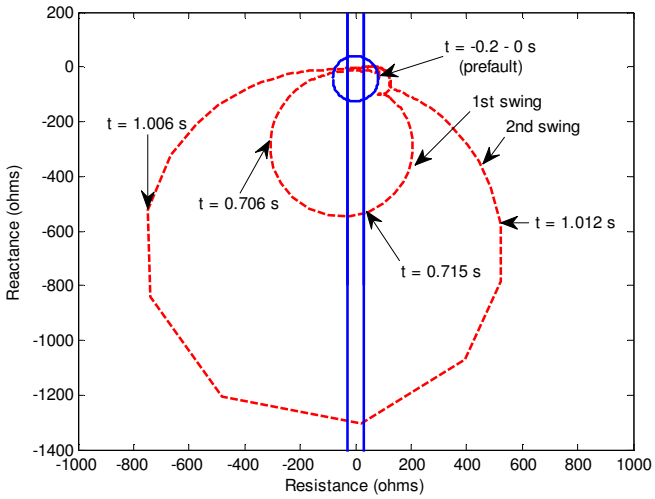

Figure 5.76. Impedance locus during out-of-step condition.

5.5 Conclusion

In this chapter, the performance of the phase percentage restrained differential protection scheme (87P) was investigated using the advanced faulted winding feature provided by the phase-domain synchronous machine model in RSCAD. The results obtained from the protection studies have confirmed that, as expected, the 87P element of the relay cannot detect stator-ground faults that occur at or near the generator neutral. It was explained that the protection coverage of the 87P element of the relay depends on both the selected resistance of the low-impedance grounding system and the practical settings of the 87P element.

Using the new phase-domain synchronous machine model that is available in RSCAD, different scenarios of circuit breaker failure during de-energization of the protected generator after a stator-ground fault were simulated, which in turn, allows the consequences of such events to be analysed using the real-time simulation results obtained during the studies. In addition, detailed and realistic contingencies were also simulated in the field circuit of the protected generator which allowed the performance of the loss-of-field protection scheme (40) to be examined.

The chapter further examined the performance of the single-blinder out-of-step protection scheme (78) of the SEL 300G relay. During one of the protection studies of the 78 element, it was discovered that the measured apparent impedance passed into the mho characteristic of the loss-of-field (40) element during the stable recovery swing following a system disturbance.

Chapter Six now presents the theory behind the particular 100% stator ground fault protection scheme (64G) available on the SEL 300G relay that would typically be employed to protect high-

impedance grounded generators. The results of real-time simulator tests of the SEL 300G's 64G element are then presented in Chapter Seven.

CHAPTER 6

100% STATOR GROUND PROTECTION FOR HIGH-RESISTANCE GROUNDED GENERATORS

6.1 Introduction

The previous chapter analysed the performance of specific generator protective functions employed to protect a particular low-resistance grounded generator represented in the real-time simulation model using the results obtained from real-time closed-loop studies of both hardware (SEL 300G) and software (generic model) generator protection relays.

This chapter reviews the theory and design of an alternative generator grounding approach, namely a high-resistance grounding scheme. Under this type of generator grounding scheme, the magnitude of stator winding to ground (stator-ground) fault currents can be limited significantly. However, due to the limited stator-ground fault currents, phase percentage restrained differential protection (87P) can no longer detect phase-to-earth faults on the generator stator winding. For this reason, alternative stator winding protection schemes for high-resistance grounded generators have been proposed, namely 100% stator ground fault protection (64G) and neutral injection schemes (64S).

The chapter then further discusses the theory of operation and setting calculations for the 64G element in particular, since it is the protection scheme available in the hardware generator protection relay (SEL 300G) being considered in the thesis. It is important to note that one of the 64G's sub-elements relies on measurements of the third-harmonic voltages in the generator stator windings in order to make its tripping decisions. However, as discussed in Chapter Two, the simplified version of the phase-domain synchronous machine model used in the work of this thesis does not represent phase-belt harmonics in the generator stator windings, and therefore it is not able to represent the third-harmonic voltages in these windings that are relied upon by one of the 64G's sub-elements to detect stator-ground faults. In order to examine the performance of the 64G element of the SEL 300G generator protection relay using the real-time closed-loop approach, an additional real-time simulation model had to be developed to supplement the characteristics of this simplified machine model.

Finally, the chapter discusses the development of the additional real-time simulation model that was used in the thesis to simulate the third-harmonic voltages produced in the generator stator windings, which in turn, allows testing of 100% stator ground fault protection schemes that rely on detection of third-harmonic voltages.

6.2 Review, theory and explanation of chosen method

There are two different approaches to implement high-resistance grounding schemes for generators. One of the approaches is to install a resistor with high-ohmic value directly between generator neutral and ground. Another approach is to utilize a single-phase distribution transformer as a grounding transformer with its primary winding connected between generator neutral and ground, while its secondary winding is loaded with a low-ohmic resistor [29]. Although both of the aforementioned grounding approaches ultimately achieve the same outcome, the latter grounding implementation is preferred in industry because of its rugged construction.

The purpose of implementing a high-resistance grounding scheme is to limit the maximum stator-ground fault current considerably to a small magnitude, typically between 5 to 15 amperes in the neutral path (depending on the chosen grounding resistor value) when a phase-to-earth fault occurs at the generator terminals [29]. Under this type of grounding arrangement, the possibility of causing severe physical damage to the generator during a stator-ground fault is greatly reduced due to the limited stator-ground fault current. Although a stator-ground fault that occurs on a high-resistance grounded generator does not pose as an immediate threat to either the power system's stability or to the generator itself, it is still highly recommended to remove the generator from service as soon as the fault is detected rather than to delay this tripping action. The reason for tripping immediately upon detection of a first stator-ground fault is to avoid the possibility of extremely high fault currents that would flow if a second stator-ground fault were to occur in the upper winding of the same phase [44],[45],[46].

In the past, a fundamental-frequency neutral overvoltage scheme (59GN) was employed to detect stator-ground faults on high-resistance grounded generators. The 59GN element comprises an overvoltage relay tuned to respond to the fundamental-frequency voltage measured across the grounding resistor. Under non-faulted conditions, if all three phases of the generator's stator windings are perfectly balanced, there will be no fundamental-frequency current flowing in the neutral path which results in zero fundamental-frequency voltage across the grounding resistor [46]. However, the fundamental-frequency voltage across the grounding resistor changes when a phase-to-earth fault occurs on one of the phases of generator stator windings. The magnitude of the fundamental-frequency voltage that appears across the grounding resistor is dependent on the location of stator-ground fault. For instance, when a stator-ground fault occurs at the generator terminals, the full-phase-to-neutral generator voltage at fundamental-frequency will appear across the grounding resistor. As the location of the stator-ground fault moves toward the generator neutral, the magnitude of the fundamental-frequency voltage that appears across the grounding resistor becomes smaller and eventually reduces to zero for the case when the fault is located

exactly at the generator neutral. For this reason, the 59GN element is not able to detect stator-ground faults that are located at or near the generator neutral. Nevertheless, the 59GN element does still provide reliable protection for the upper 90% to 95% of the generator stator windings depending on the sensitivity of the element [46].

Although the 59GN element is easy to implement and very reliable, there are two major disadvantages associated with it. Firstly, the 59GN element does not have self-monitoring capability and therefore it is not able to detect any contingencies on the grounding system (e.g. short-circuit or open-circuit of grounding resistor) [44],[45]. If a stator-ground fault occurs when the grounding resistor is short-circuited, the ground fault current is no longer limited by the high-resistance grounding system and consequently it can result extremely high fault current. Under this type of circumstance, the stator winding and stator core of the generator can be subjected to substantial damage. The second disadvantage of the 59GN element is the inability to detect stator-ground faults that are located at or near generator neutral due to insufficient sensitivity of the element. In the past, a small percentage of unprotected generator stator windings near the neutral end did not raise significant concern since it was considered unlikely to have a ground fault in this region due to low insulation stress [45]. However, one of Georgia Power Company's generator units was severely damaged due to the inability of a 59GN element to detect a turn-to-turn fault that occurred near the generator neutral. Due to the arcing nature of the original fault, an adjacent coil was damaged and consequently caused the original fault to evolve into a phase-to-phase fault that caused substantial current to flow in the stator windings [45]. Although it is important to provide protection for the upper 90% to 95% of generator stator windings, evidence suggests that it is equally important to provide protection for generator stator windings near the generator neutral.

Over the years, different types of protection scheme have been proposed to supplement the protection-blind region of the 59GN element. These protection schemes utilize a distinct practical characteristic of generators in order to detect the presence of stator-ground faults near the generator neutral, namely the non-sinusoidal components in their output voltages: generators typically produce harmonic voltages such as the 3^{rd}, 9^{th} and 15^{th} harmonic [32]. Of these harmonic voltages, the 3^{rd} harmonic voltage has the highest magnitude and it is the one chosen for use in the following generator protection schemes, namely third-harmonic undervoltage scheme (27H), third-harmonic overvoltage scheme (59T) and third-harmonic voltage differential scheme (59D). Before discussing the theory of operation of the aforementioned protection schemes, one needs to understand the distribution of third-harmonic voltages within generator stator windings under healthy and faulted generator operating conditions.

Figure 6.1 illustrates a simplified form of generator model that is constituted by a circuit of capacitances and a high-resistance grounding resistor. The grounding resistor R_n shown in Figure 6.1 is designed to limit the maximum stator-ground fault currents to approximately 5 to15 amperes and also to avoid high transient voltages during stator-ground faults [47]. A detailed discussion of the design procedure of high-resistance grounding systems is contained in Section 6.3.2. As can be seen from Figure 6.1, the total stray capacitance per phase of the generator stator winding is represented by two lumped capacitances, each equal to one-half of the total winding capacitance value ($C_g/2$), located at the ends of the generator stator winding. The additional capacitance (C_{add}) that is located at the generator terminals represents the combined capacitance-to-ground of equipment such as switchgear, cables and transformer windings [47]. Under healthy generator operating conditions, the third-harmonic voltage induced within the stator windings is divided between the generator neutral and stator terminals as a function of the zero-sequence impedance circuit [32].

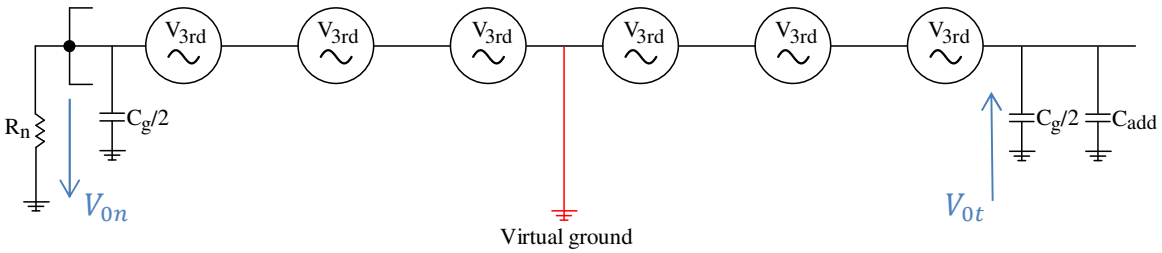

Figure 6.1. Simplified generator model.

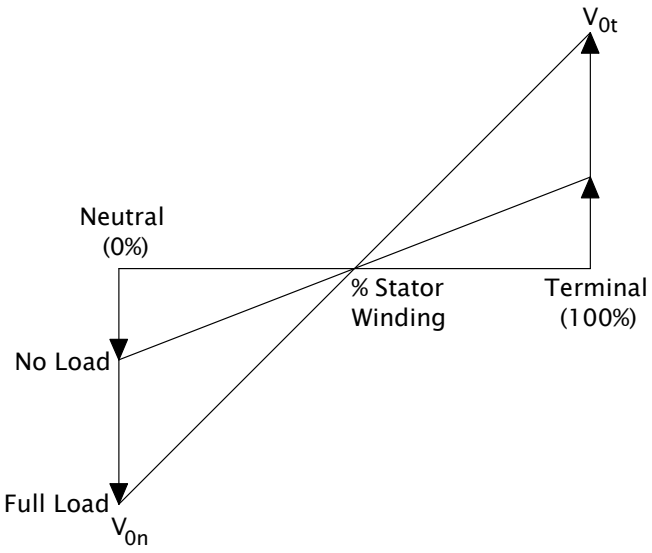

Figure 6.2. Third-harmonic voltage distribution under healthy generator operation.

Figure 6.2 illustrates the third-harmonic voltage distribution along the generator stator winding under healthy generator operating conditions at both no-load and full-load. As can be seen from Figure 6.2, there is a location on the generator stator winding that contains no third-harmonic

voltage potential relative to ground ($V_{3rd\_harmonic} = 0$). The location of this virtual ground (also known as a null point) varies depending on the values of the stray capacitances at each end of the generator stator windings and also depends on the value chosen for the grounding resistor.

When a stator-ground fault occurs on a high-resistance grounded generator, the magnitudes of the third-harmonic voltages at the neutral and stator terminal ends change. The location of the stator-ground fault determines how the third-harmonic voltage is re-distributed along the stator winding during the fault. Figure 6.3 illustrates the third-harmonic voltage re-distribution along the stator winding for the particular case when a stator-ground fault occurs at the generator terminals. As a result of this fault, the stray capacitance at the stator terminals is bypassed which causes the third-harmonic voltage at the stator terminal end to decrease to zero, while the third-harmonic voltage measured at the neutral end increases in magnitude, and now corresponds to the full magnitude of the third-harmonic voltage induced within the generator winding [32].

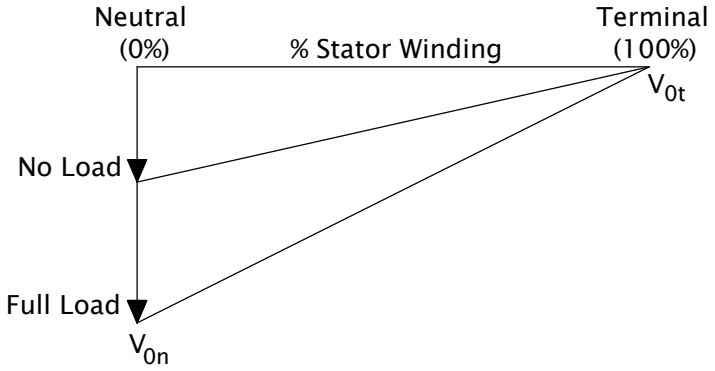

Figure 6.3. Third-harmonic voltage re-distribution during a stator-ground fault at the generator terminals.

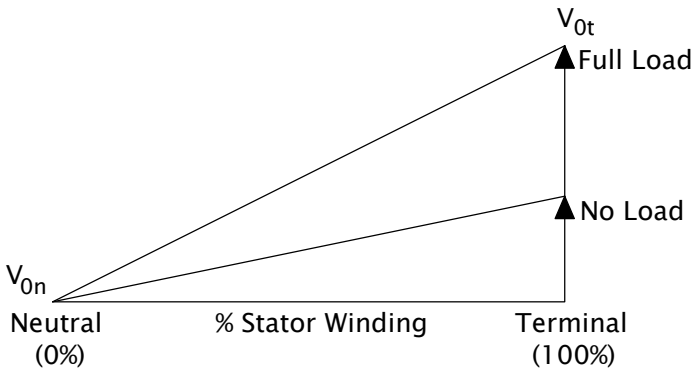

Figure 6.4. Third-harmonic voltage re-distribution during a stator-ground fault at the generator neutral.

Figure 6.4 illustrates the third-harmonic voltage re-distribution along the stator winding for a second case when a stator-ground fault occurs at the generator neutral. Under this fault scenario,

the external impedance in the neutral circuit (i.e. stray capacitance at the neutral end in parallel with the grounding resistor) is effectively bypassed which causes the third-harmonic voltage at the neutral end to decrease to zero, while the third-harmonic voltage measured at the generator terminals increases in magnitude, and corresponds to the full magnitude of the third-harmonic voltage induced within the generator winding.

By utilizing this unique characteristic of the third-harmonic voltage re-distribution shown in Figure 6.4, two types of protection scheme can be employed to protect generator stator windings against faults at or near the generator neutral, namely a third-harmonic undervoltage scheme (27H) and a third-harmonic overvoltage scheme(59T).

The 27H element comprises an undervoltage element that is tuned to respond to the third-harmonic voltage measured at the generator neutral. When a stator-ground fault occurs at or near the generator neutral, the third-harmonic voltage measured at the neutral end decreases to below the threshold setting of the undervoltage element and therefore causes the relay to trip. By employing the 27H element together with the 59GN element, the entire generator stator winding may, in theory, be protected without any protection-blind region. However, the third-harmonic voltage induced in the stator windings varies with different generator loading conditions as shown in Figure 6.2. Practically, it is a great challenge to find a reliable setting for the 27H element due to the load-dependent nature of the third-harmonic voltage variations in the stator windings. Under lightly-loaded or no-load conditions, the third-harmonic voltage measured at the generator neutral might be below the threshold setting of the undervoltage element. For this reason, the 27H element may have to be disabled under the aforementioned generator operating conditions in order to prevent relay misoperation [44]. As a result, the combination of the 27H element and the 59GN element can only provide full protection coverage for the stator windings under certain generator operating conditions.

The 59T element is another protection scheme that can be utilized to detect stator-ground faults at or near the generator neutral. This protection scheme comprises an overvoltage element that is tuned to respond to the zero-sequence third-harmonic voltage measured at the generator terminals. When a stator-ground fault occurs at or near the generator neutral, the zero-sequence third-harmonic voltage measured at the generator terminals increases above the threshold setting of the overvoltage element and therefore causes the relay to trip. By employing the 59T element and the 59GN element, it is also possible, in theory, to provide full protection coverage for the generator stator windings. The practical setting of the 59T element is typically chosen to be above the maximum zero-sequence third-harmonic voltage measured at the generator terminals under healthy generator operating conditions in order to prevent relay misoperation [32]. However, under lightly-

loaded or no-load conditions, a stator-ground fault that occurs at or near the generator neutral may not result in a sufficient increase in the zero-sequence third-harmonic voltage at the generator terminals to operate the 59T element. For this reason, in practice the combination of the 59T element and the 59GN element can only provide full protection coverage for the generator stator windings under certain generator operating conditions.

Since the 27H element and the 59T element can each only perform satisfactorily under certain generator loading conditions, an alternative protection scheme was proposed to overcome the load-dependent nature of the third-harmonic voltage variations in the stator windings, namely the third-harmonic voltage differential scheme (59D).

Several operational tests have been carried out on different generator units to investigate the variations in the third-harmonic voltage induced in the stator windings under different generator operating conditions. The results indicate that changes in generator reactive power output did not have a significant effect on the magnitude of the third-harmonic voltage induced in the stator windings, while changes in active power output altered the magnitude of the induced third-harmonic voltage. The results obtained from the operational tests also indicated that the third-harmonic voltage induced in the stator windings has a linear relationship with the active power output of the generators under study [45],[48],[49]. In other words, the third-harmonic voltage induced in the stator windings increases in direct proportion with an increase in generator active power output. During these operational tests, the ratio between the measured third-harmonic neutral voltage and the measured zero-sequence third-harmonic terminal voltage remained almost constant under all generator loading conditions [44],[46],[47],[50].

The 59D element incorporates this unique characteristic of the constant third-harmonic voltage ratio under healthy generator operating conditions to detect stator-ground faults on high-resistance grounded generators. Under healthy generator operating conditions, the measurements of the third-harmonic neutral voltage and the zero-sequence third-harmonic terminal voltage are utilized to calculate the constant third-harmonic voltage ratio using equation (6.1), since this ratio is required as one of the input settings of the 59D element.

$$k = \frac{|V_{0n}|}{|V_{0t}|} \tag{6.1}$$

Where V_{0n} = measured third-harmonic voltage at the generator neutral

V_{0t} = measured zero-sequence third-harmonic voltage at the generator terminals

By rearranging equation (6.1), equation (6.2) can be derived as follows.

$$k \times |V_{0t}| - |V_{0n}| = 0 \tag{6.2}$$

Ideally, under un-faulted conditions, the differential voltage calculated from the measurements of the third-harmonic neutral voltage and the zero-sequence third-harmonic terminal voltage would be zero under all generator loading conditions as shown in equation (6.2). However, the situation described above is somewhat idealized. In practice, it is possible to have slight variations in the third-harmonic voltage ratio under different generator loading conditions. For this reason, an operating margin V_{set} shown in equation (6.3) is introduced in the 59D element in order to increase the security of the protection scheme and therefore to prevent misoperation under healthy generator operating conditions.

$$V_{set} = k \times |V_{0t}| - |V_{0n}| \tag{6.3}$$

Where V_{set} = setting of the operating margin of the 59D element

k = constant third-harmonic voltage ratio under healthy generator operations

In general, if a stator-ground fault occurs on a high-resistance grounded generator, the ratio between the measured third-harmonic neutral voltage and the zero-sequence third-harmonic terminal voltage changes. The algorithm of the 59D element shows that if the differential voltage calculated from the measurements of the third-harmonic voltage exceeds the operating margin V_{set} under faulted generator conditions, the relay will operate and remove the faulted generator from service. However, it is important to note that the 59D element alone cannot provide full protection for the stator windings of high-resistance grounded generators since there will always be a lack of coverage over some internal portion of the winding. For instance, if a phase-to-earth fault occurs at or near the point where the third-harmonic voltage distribution along the stator winding crosses through zero as shown in Figure 6.2, the changes in the third-harmonic voltage ratio at the generator neutral and stator terminal ends will be insignificant. As a result, the differential voltage calculated from the measurements of the third-harmonic neutral voltage and zero-sequence third-harmonic terminal voltage is insufficient to operate the 59D element for such faults. For this reason, a 59D element is typically employed together with a 59GN element in order to provide full protection coverage of the generator stator windings since their respective protection-blind regions are located in different parts of the winding. In the SEL 300G generator protection relay, the 100% stator ground fault protection scheme (64G) that is typically employed to protect high-resistance grounded generators comprises a 59GN element and a 59D element. However, since both the 59GN element and the 59D element are considered sub-elements of the 64G element in the 300G relay, their device function numbers have been changed to 64G1 and 64G2 respectively in the

manufacturer's literature. The terms 64G1 and 64G2 are therefore used from this point on in the thesis to refer to these sub-elements.

It is important to note that the magnitude of the third-harmonic voltage induced within generator stator windings can vary considerably from one generator to another since these voltages are produced as a result of winding space harmonics and are therefore dependent on the machine's physical design. For this reason, operational tests must be carried out on the generator units in order to understand the characteristics of the induced third-harmonic voltages for each individual generator unit to be protected. In order to perform satisfactorily, the 64G2 element requires that the minimum magnitude of the third-harmonic voltage induced in the stator windings be 1% of the nominal generator voltage [47]. If the induced third-harmonic voltage is below 1% of the nominal generator voltage due to the machine's physical design, or if the third-harmonic voltage ratio varies dramatically under different generator loading conditions so that a secure operating margin V_{set} cannot be found, the 64G2 element is no longer suitable for protecting high-resistance grounded generators. In such cases, an alternative protection method, such as a neutral injection scheme (64S), can be considered.

6.3 Real-time modelling for 100% stator ground fault protection testing

In order to study the performance of the 100% stator ground fault protection scheme (64G) of the SEL 300G generator protection relay using the real-time closed-loop testing approach, a realistic RSCAD representation of the study system was required. As discussed in Chapter Three, the study system shown in Figure 3.1 was modified using a slightly different approach to lumping the multiple generators in the power station as shown in Figure 3.2 which, in turn, allows the SEL 300G relay connected to the real-time simulator in a hardware-in-loop configuration to protect one of the four generator units in the station. In addition, all four generator units were grounded through a high-resistance grounding system. With this modified study system, generator internal winding faults can be considered on the particular high-resistance grounded 555 MVA generator under study which allows the performance of the 64G element to be examined. The following sections describe the particular details that were required in the development and parameterisation of the real-time simulation model which was used for the protection studies of the 64G element. Section 6.3.1 reviews the choice of the system parameters (i.e. stray capacitances of the stator windings and auxiliary equipment) to be represented in the real-time simulation model. Section 6.3.2 demonstrates the design procedure of the practical high-resistance grounding approach described in [45]. Finally, Section 6.3.3 discusses the additional real-time model that was developed to simulate the third-harmonic voltages induced in the stator windings in order to supplement the characteristics of the simplified phase-domain synchronous machine model.

6.3.1 Review and choice of representative system parameters

As discussed in Section 6.2, for a given magnitude of induced third-harmonic voltage within the stator winding, the magnitudes of these voltages that appear between the terminals at each end of the stator winding and ground depend on the capacitances-to-ground at these terminals and the grounding resistance. Therefore it is important, especially in the protection studies of the 64G element, to represent the stray capacitances of the stator windings and auxiliary equipment correctly in the real-time simulation model. Figure 6.5 shows the schematic representation of the distributed capacitances-to-ground of the stator windings and auxiliary equipment that were included in the real-time model. However, due to the absence of parameter values for the stray capacitances in the study system shown in Figure 3.1, values from an actual generator of comparable size (MVA rating) and its auxiliary equipment were obtained from measurements presented in [45], as shown in Table 6.1, in order to allow the subsequent studies to be as representative as possible.

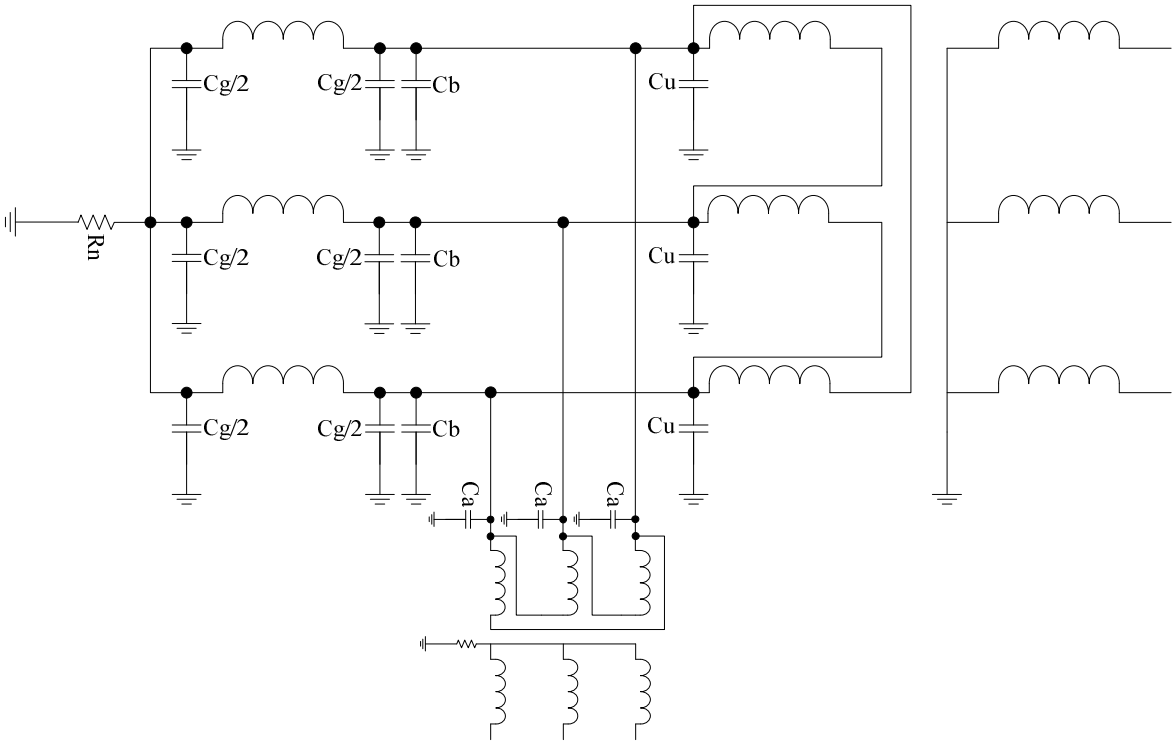

Figure 6.5. Schematic representation of the distributed capacitances-to-ground in a generator and its auxiliary equipment.

Table 6.1 shows the capacitances-to-ground of the stator windings and the auxiliary equipment obtained from one of the generation units of the Georgia Power Company that is rated at 25 kV, 789 MW [45].

Table 6.1. List of equipment in the diagram of Figure 6.5 with their capacitances-to-ground [45]

Equipment	Capacitance (μF)
Generator winding capacitance to ground per phase (C_g)	0.224
Lead capacitance to ground per phase (C_b)	0.002
GSU transformer capacitance to ground per phase (C_u)	0.020
Unit Auxiliary transformer phase-to-ground capacitance (C_a)	0.008
Total capacitance per phase ($C_{g\_total/phase}$)	0.254
Total capacitance for three phase (C_{g_total})	0.762

6.3.2 Practical design of representative grounding system parameters

As discussed in Section 6.2, there are two approaches to implement high-resistance grounding schemes for generators. In this section, the high-resistance grounding system that was designed and included in the neutral circuit of the particular 555 MVA generator under study comprises a single-phase distribution transformer used as a grounding transformer with its primary winding connected between the generator neutral and ground, and with its secondary winding loaded with a low-ohmic resistor. The design and ratings of the equipment in this grounding system were determined by closely following the guideline described in [29] in order to make the parameters of the grounding system as representative as possible. As explained earlier, the grounding resistance is selected to limit the maximum ground fault currents to between 5 to 15 amperes and also to prevent high transient voltages during stator-ground faults. In order to meet the aforementioned criteria when selecting the grounding resistance, the guideline shown in equation (6.4) was followed. The guideline states [29] that the selected grounding resistance must be less than or equal to the ohmic value of the total three-phase capacitance-to-ground. In other words, the ratio of the ohmic value of the total three-phase capacitance-to-ground ($X_{C_{g\_total}}$) over the grounding resistance (R_n) must be greater than or equal to one.

$$X_{C_{g\_total}}/R_n \geq 1 \tag{6.4}$$

As mentioned in Section 6.3.1, the actual values of stray capacitance shown in Table 6.1 were included in the real-time simulation model. Following the guideline shown in equation (6.4), the grounding resistance can be determined as follows.

The first step is to calculate the ohmic value of the total three-phase capacitance-to-ground at system frequency (which, in the case of the chosen study system, is 60 Hz).

$$X_{C_{g\_total}} = \frac{1}{\omega \cdot C_{g\_total}}$$

$$= \frac{1}{(2\pi * 60) * (0.762 * 10^{-6})} = 3481.08\ \Omega$$

The highest recommended grounding resistance can then be found by setting the ratio ($X_{C_{g\_total}}/R_n$) equal to one.

$$R_{primary} = X_{C_{g\_total}} = 3481.08\ \Omega$$

If the grounding approach is to connect a grounding resistor directly between the generator neutral and ground, the grounding resistance calculated above ($R_{primary}$) can be selected. However, a single-phase grounding transformer was used in this grounding scheme and therefore the calculated grounding resistance ($R_{primary}$) was referred to the secondary side of the transformer. The grounding transformer that was included in the neutral circuit of the particular generator under study has turns ratio of 14400:240, based on the nearest standard voltage on the primary winding above the generator nominal phase to neutral voltage.

$$R_{secondary} = R_{primary} / \left(\frac{V_{primary}}{V_{secondary}}\right)^2$$

$$= 3481.08 / \left(\frac{14400}{240}\right)^2 = 0.97\ \Omega$$

Under this grounding system, the maximum stator-ground fault current that flows through the primary winding of the grounding transformer can be calculated as follows.

$$I_{primary} = \frac{E_{Primary}}{R_{secondary} * \left(\frac{V_{primary}}{V_{secondary}}\right)^2}$$

$$= \frac{24/\sqrt{3} * 10^3}{0.97 * \left(\frac{14400}{240}\right)^2} = 3.97\ A$$

Where $E_{Primary}$ = rated nominal generator voltage per phase (This is the maximum voltage that can appear across the primary winding of the grounding transformer during stator-ground faults.)

From the above calculation, the maximum stator-ground fault current that flows through the secondary winding of the grounding transformer can be calculated using the turns ratio of the transformer.

$$I_{secondary} = I_{primary} * \left(\frac{V_{primary}}{V_{secondary}}\right)$$

$$= 3.97 * \left(\frac{14400}{240}\right) = 233.2\ A$$

The rating of the grounding transformer can then be determined as follows.

$$S = E_{Primary} * I_{primary} = \frac{24 * 10^3}{\sqrt{3}} * 3.97 = 55\ kVA$$

In practice, the grounding transformer will only be fully loaded when a stator-ground fault occurs at the stator terminals of the generator. In addition, the load on the transformer is not continuous since the faulted generator will be removed from service by its protection system as soon as a stator-ground fault is detected. For these reasons, it is justifiable to select a grounding transformer of a lower rating than the design value above. Table 6.2 shows different overload factors for grounding transformers under various overload durations. The overload duration on a grounding transformer is determined by the time required to remove a faulted generator when a stator-ground fault occurs.

Table 6.2. Permissible short-time overload factors for grounding transformers [29]

Duration of Overload	Multiple of Rated kVA
10 s	10.5
60 s	4.7
10 min	2.6
30 min	1.9
2 h	1.4

6.3.3 Real-time simulator modelling

As discussed in Chapter Two, the simplified version of the phase-domain synchronous machine model that is available for general use [13] does not represent phase-belt harmonics in the generator stator winding and therefore it is not able to represent the third-harmonic voltages in these windings that are relied upon by the 64G2 element to detect stator-ground faults. Nevertheless, the simplified version of the machine model does allow accurate representation of the internal stator winding faults, at least with respect to the fundamental frequency behaviour of the generator variables. For this reason, additional modelling effort was required in order to supplement the characteristics of this simplified version of the machine model to allow testing of the 64G2 element that relies on the measurement of third-harmonic voltages. Section 6.3.3.1 shows the real-time simulation model that is capable of representing the behaviour of the generator fundamental-frequency voltages while Section 6.3.3.2 shows an additional third-harmonic equivalent-circuit model that was designed to represent the behaviour of the third-harmonic voltages under healthy and faulted generator operating conditions.

6.3.3.1 Fundamental frequency

Figure 6.6 shows the real-time modelling details used to represent the fundamental-frequency behaviour of the particular high-resistance grounded 555 MVA generator under study.

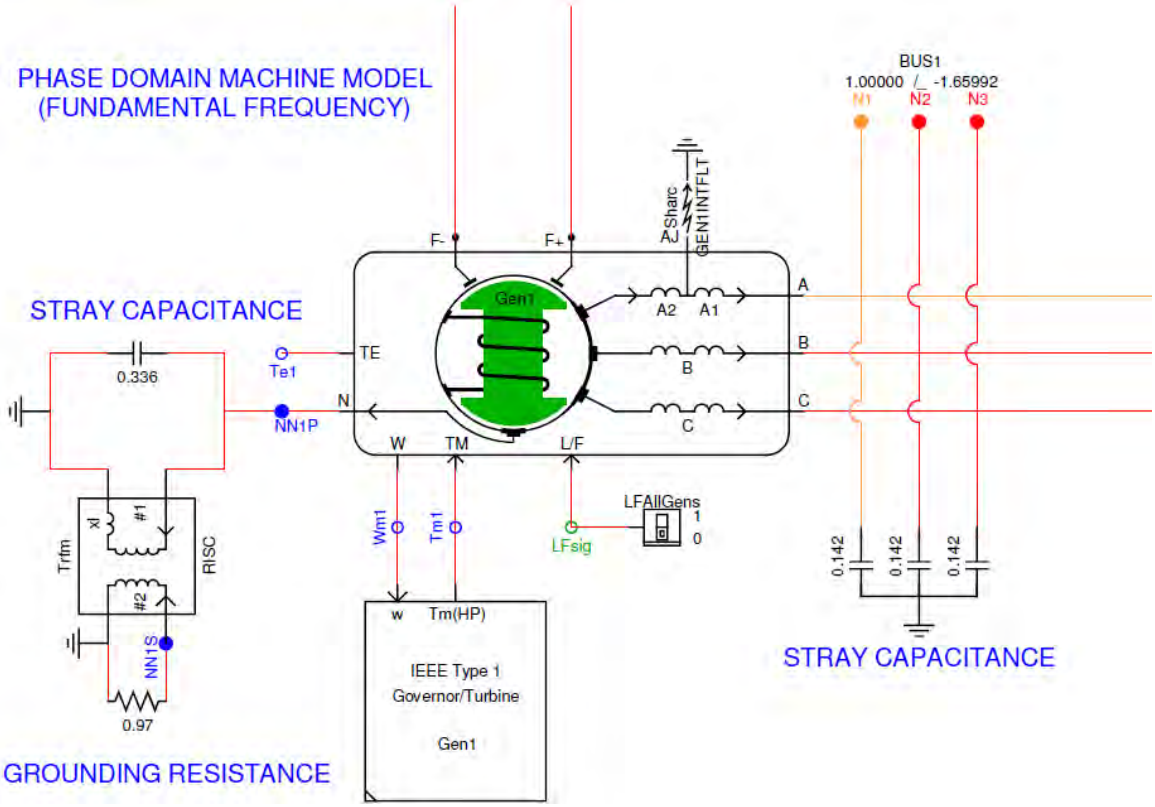

Figure 6.6. Real-time modelling details used to represent the particular generator under study.

The phase-domain synchronous machine model shown in Figure 6.6 allows phase to earth faults to be applied at different user-specified variable locations along the stator winding during the protection studies of the 64G element. Figure 6.6 further shows the stray capacitances included in the plant model that are defined in Figure 6.5 using the actual parameter values shown in Table 6.1. As can be seen from Figure 6.6, the high-resistance grounding approach described in Section 6.3.2 was represented in the real-time simulation model using the representative parameters calculated in the same section.

6.3.3.2 Equivalent circuit model for third harmonic voltages

This section discusses the implementation of the custom-designed real-time model used to simulate the behaviour of generator third-harmonic voltages that was included in the protection studies of the 64G element in order to supplement the characteristic of the simplified version of the phase-domain synchronous machine model. As discussed in Section 6.2, the magnitude of the induced third-harmonic winding voltage is dependent on generator loading conditions. Figure 6.7 shows the

design of real-time modelling elements that can be adapted to represent the known load-dependent characteristics of any generator's third-harmonic winding voltages. However, the coefficients of the model were configured in order to replicate the specific characteristics of the actual third-harmonic winding voltages of a comparably-rated large synchronous generator (Lambton generator unit No. 4, in Ontario Hydro's system, that is rated at 24kV, 500 MW [49]) for the particular studies carried out in this thesis. The specific characteristics of the aforementioned synchronous generator obtained from the operational testing results presented in [49] indicate that the induced third-harmonic winding voltage varies in the range from 2% to 9% of the generator's nominal phase-to-neutral voltage from no-load to full-load. The induced third-harmonic winding voltages were represented using voltage sources in each phase of the equivalent circuit representation shown in Figure 6.8 and the magnitude of which are dynamically adjusted by the model elements shown in Figure 6.7 based on any changes in generator loading conditions. The relative magnitude of the generated third-harmonic voltage sources on either side of the fault component in the equivalent circuit representation in Figure 6.8 are also adjusted according to the user-selected fault location chosen within the main, phase-domain synchronous generator model used to represent the fundamental frequency characteristics of the faulted generator (of Figure 6.6). By using the equivalent circuit model shown in Figure 6.8, the behaviour of the third-harmonic voltages at the neutral and stator terminals of the generator can therefore be represented under both healthy and faulted generator operating conditions.

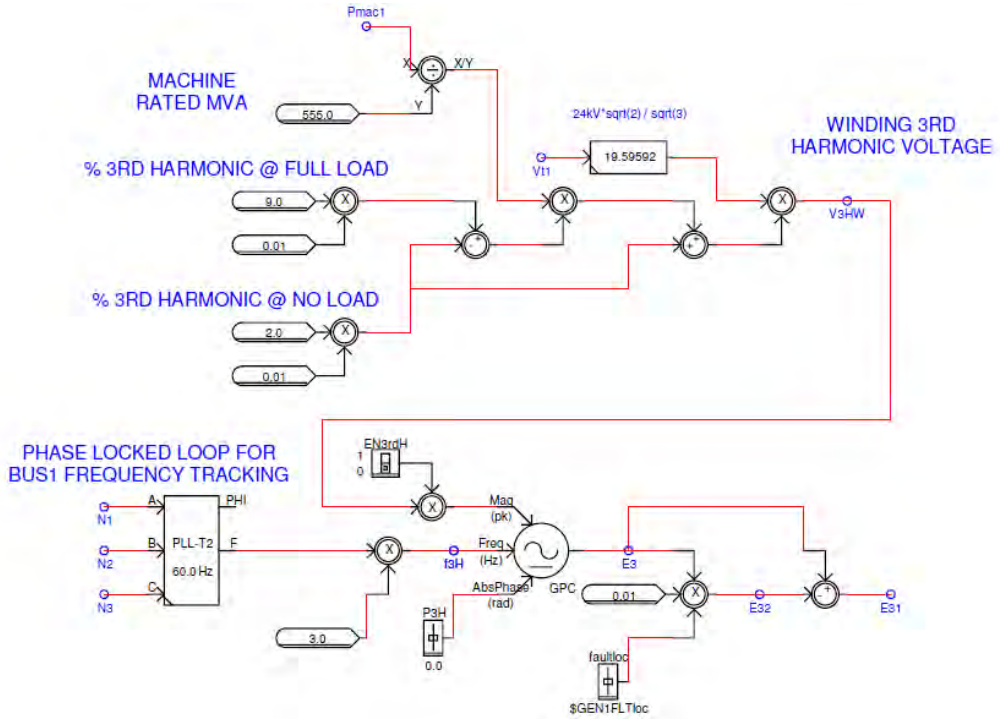

Figure 6.7. Modelling elements for representing the load-dependent characteristics of the generator's third-harmonic winding voltages in the equivalent circuit model.

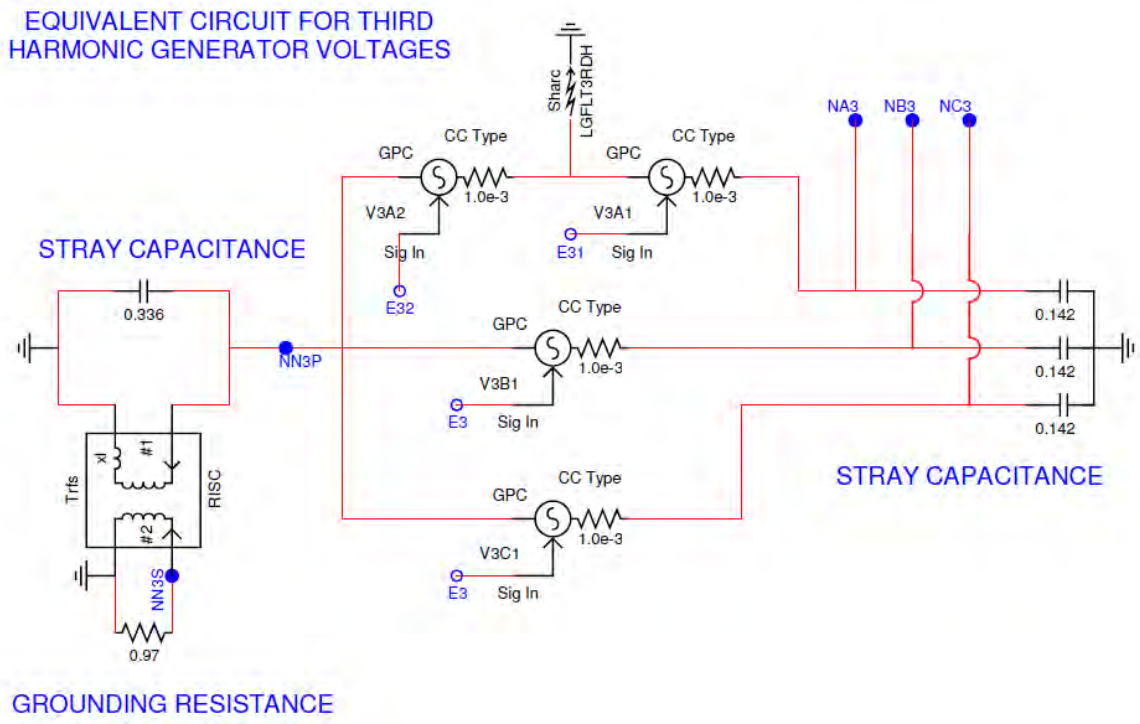

Figure 6.8. Equivalent circuit model for induced third harmonic voltages.

Finally, the fundamental-frequency voltages and the third-harmonic voltages measured at the neutral and stator terminals of the particular high-resistance grounded generator under study are combined within the real-time simulation model using the superposition principle. These composite voltage signals representing the fundamental and third-harmonic voltages measured at both ends of the generator stator winding are then exported to the SEL 300G generator protection relay under test in order for the 64G element to make tripping decisions (refer to Figure A.19 in Appendix A for further details).

6.3.3.3 Hardware-in-loop (HIL) connection

By using the same hardware-in-loop connection of the SEL 300G generator protection relay with the real-time simulation model described in Chapter Three, various protection studies were carried out in order to examine the performance of the relay's 64G element. As discussed in Section 6.2, the 64G element requires voltage measurements at the neutral and stator terminals of the particular high-resistance grounded 555 MVA generator under study in order to make tripping decisions. For this reason, two voltage transformers are included within the real-time simulation model in order to measure voltages at the neutral and stator terminals of the protected generator, and their secondary quantities are then injected into the normal measurement inputs of the SEL 300G relay under test. Since the measurements obtained from the voltage transformers are composite voltage signals which contain both fundamental-frequency and third-harmonic voltages, the SEL 300G relay performs a discrete Fourier transform (DFT) on the input voltage measurements in order to filter

the fundamental-frequency and third-harmonic voltages that are relied upon by the 64G's sub-elements to make tripping decisions. When the 64G element detects a stator-ground fault and makes a decision to trip the protected generator, the relay's trip signal is sent back to the real-time model in order to open the corresponding circuit breakers (i.e. the generator's main circuit breaker and field circuit breaker) to clear the fault.

6.4 Settings of the 64G element

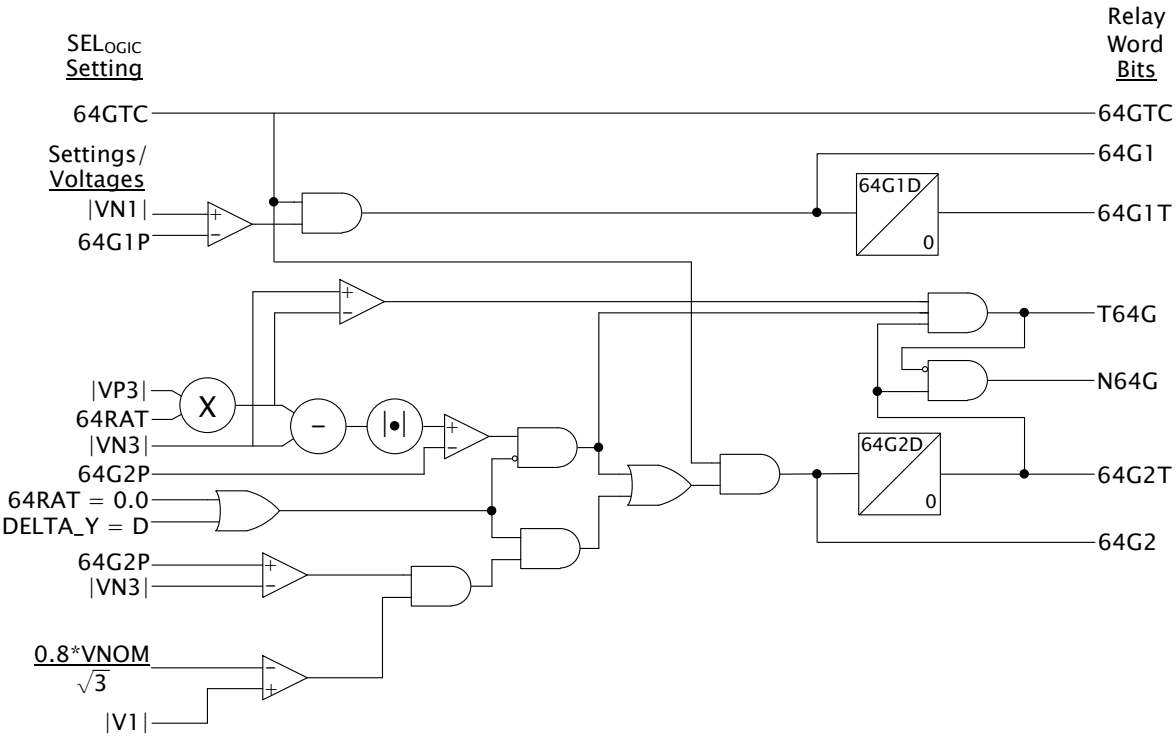

Figure 6.9. Logic diagram of 100% stator ground fault protection (reproduced from [31]).

The logic diagram shown in Figure 6.9 shows the algorithm implemented by the SEL 300G generator protection relay for the 100% stator ground fault protection scheme (64G). The theory of operation of the 64G's sub-elements (i.e. fundamental-frequency neutral overvoltage element (64G1) and third-harmonic voltage differential element (64G2)) has been discussed in detail in Section 6.2. The focus of this section is to demonstrate the practical setting calculations for the 64G's sub-elements based on the particular high-resistance grounded 555 MVA generator under study.

Setting calculation of the 64G1 element

The 64G1 element is set with a sufficient operating margin (typically 5% to 10% of the generator nominal phase-to-neutral voltage in secondary volts) to prevent undesirable misoperation if the generator stator windings are not perfectly balanced. As a result, 5% to 10% (depending on the set

operating margin) of the stator winding closest to the neutral end is not protected by the 64G1 element due to the insufficient sensitivity of the element.

In this study, the operating margin was set at 5% of the generator nominal phase-to-neutral voltage in secondary volts. The threshold setting of the 64G1 element (64G1P) was then calculated as follows.

$$64G1P = \left(\frac{5}{100}\right) * \left(\frac{V_{L-L} * 1000}{1.73 * PTRN}\right)$$

$$= \left(\frac{5}{100}\right) * \left(\frac{24 * 1000}{1.73 * 131}\right)$$

$$= 5.3\ V$$

Where V_{L-L} = generator nominal line-to-line voltage [kV]

PTRN = $Ngt * Nat$

Ngt = grounding transformer ratio (14400/240 in this particular case)

Nat = auxiliary transformer ratio (240/110 in this particular case)

Setting calculation of the 64G2 element

As discussed in Section 6.2, the ratio between the third-harmonic neutral voltage and the zero-sequence third-harmonic terminal voltage under healthy generator operating conditions is required as one of the input settings of the 64G2 element. In order to calculate the third-harmonic voltage ratio (64RAT) under un-faulted conditions, measurements of the third-harmonic voltages at the neutral and stator terminals of the protected generator under no-load and full-load operating conditions are required. Using the real-time monitoring feature provided by the SEL 300G generator protection relay shown in Figure 3.8c, the measurements of zero-sequence third-harmonic terminal voltage (VP3) and third-harmonic neutral voltage (VN3) under no-load and full-load operating conditions can be obtained while the relay is being injected with un-faulted waveforms from the real-time simulation model.

The following measurements were obtained under no-load generator operating conditions.

$VP3_{NL} = 2.0$ V

$VN3_{NL} = 1.1$ V

The following measurements were obtained under full-load generator operating conditions.

$VP3_{FL} = 8.9$ V

$VN3_{FL} = 5.0$ V

Using the third-harmonic voltage measurements obtained from no-load and full-load generator operating conditions, the third-harmonic voltage ratio (64RAT) can be calculated as follows.

$$64RAT = \frac{(VN3_{FL} + VN3_{NL})}{(VP3_{FL} + VP3_{NL})}$$

$$= \frac{5.0 + 1.1}{8.9 + 2.0} = 0.6$$

As discussed in Section 6.2, it is possible to encounter slight variations in the third-harmonic voltage ratio under different generator loading conditions. For this reason, an operating margin (64G2P) is introduced in the 64G2 element in order to increase security of this protection scheme and therefore to prevent misoperation under healthy generator operating conditions. In order to calculate a secure 64G2P setting, measurements of VP3 and VN3 at all anticipated load levels are required. By following the guideline shown below, the maximum calculated value of the setting 64G2P must be selected in order to avoid misoperation under non-fault conditions.

$$64G2P = 1.1 * (0.1 + |64RAT * VP3x - VN3x|)$$

$$= 1.1 * (0.1 + |0.6 * 8.9 - 5.0|)$$

$$= 0.5\ V$$

Table 6.3. Settings for the 64G element

Element	Description	Setting
E64	Enable 100% stator ground protection	Y
Zone 1 settings		
64G1P	Zone 1 neutral overvoltage pickup (V)	5.3
64G1D	Zone 1 time delay (seconds)	0.0
Zone 2 settings		
64G2P	Zone 2 differential voltage (V)	0.5
64G2D	Zone 2 time delay (second)	0.0
64RAT	Zone 2 ratio setting	0.6
64GTC	64G element torque control (SELogic Equation)	1

Table 6.3 summarizes the protection settings of the 64G's sub-elements calculated in this section. These settings were used to configure the SEL 300G generator protection relay when conducting real-time closed-loop studies of the 64G element in the subsequent chapter of this thesis.

6.5 Conclusion

This chapter has reviewed the background theory and standard design procedure of high-resistance grounding systems for generators. The chapter further discussed the theory of operation of different types of protection scheme that are typically employed to protect high-resistance grounded generators together with their advantages and disadvantages. It was concluded that, under all generator loading conditions, the particular form of 100% stator ground fault protection scheme (64G) that contains a fundamental-frequency neutral overvoltage element (64G1) and a third-harmonic voltage differential element (64G2) can provide protection coverage of the entire generator stator winding without any protection-blind region.

The chapter also discussed a detailed real-time simulation model representation of the modified study system that was developed based on representative parameters (i.e. stray capacitances) obtained from a comparably-rated generation unit to meet the specific requirements for carrying out protection studies of the 64G element. In addition, a custom-designed real-time model was developed to simulate the behaviour of the third-harmonic winding voltages that are relied upon by the 64G2 element to detect stator-ground faults since the simplified phase-domain synchronous machine model is not capable of representing any phase-belt harmonics. Once again, representative characteristics for the load-dependency of the generated third-harmonic voltages were obtained for the generator in the chosen study system from operational measurements on a comparably-rated generator reported in the literature.

Finally, the chapter demonstrated the setting calculations for the 64G element based on the particular high-resistance grounded 555 MVA generator under study and the practical settings were used to configure the SEL 300G relay for the real-time closed-loop studies. Using the aforementioned HIL configuration and the detailed real-time simulation model described in this chapter, the performance of the 64G element under different fault scenarios can be examined and the HIL testing results are presented in Chapter Seven.

CHAPTER 7

RESULTS OF HIL TESTING OF 100% STATOR GROUND FAULT PROTECTION SCHEME

7.1 Introduction

The previous chapter presented the background theory and setting calculations for a 100% stator ground fault protection scheme (64G) that is typically employed to protect high-resistance grounded generators. In addition, the chapter discussed an RSCAD representation of the modified study system that was developed including a high-resistance grounding system designed for the particular 555 MVA generator under study following standard guidelines, and using representative parameters (i.e. stray capacitance values) obtained from a comparably-rated generation unit. The chapter further discussed the custom-designed real-time model that was included for the protection studies of the 64G element in order to simulate the behaviour of third-harmonic winding voltages that are relied upon by the 64G2 element to detect stator-ground faults, once again using representative third-harmonic voltage characteristics from a comparably-rated generator.

By using the hardware-in-loop (HIL) configuration described in Chapter Six, the SEL 300G generator protection relay was connected to one of the four high-resistance grounded generators in the power station represented in the real-time simulation model. The aforementioned testing arrangement allows the impact of stator-ground faults to be considered on the particular 555 MVA generator under study, which in turn, allows the performance of the 64G element to be examined. This chapter presents the HIL test results of the 64G element under different fault scenarios in which the performance of the 64G's sub-elements were analysed individually in order to verify the test results against the theory presented in Chapter Six.

7.2 Results of HIL testing of 100% stator ground fault protection scheme

The 100% stator ground fault protection scheme (64G) provided by the SEL 300G relay contains two sub-elements, namely a fundamental-frequency neutral overvoltage element (64G1) and a third-harmonic voltage differential element (64G2). As discussed in Chapter Six, each of these two protection elements is expected to exhibit a lack of coverage over different sections of the stator winding. For instance, the 64G1 element of the scheme should provide protection coverage of approximately 95% of the stator winding, but is expected to be unable to detect stator-ground faults in the bottom 5% of the winding closest to the neutral terminal. By contrast, the 64G2 element of the scheme is expected to exhibit a lack of coverage over some internal section of the stator winding surrounding the location of the virtual ground in the third-harmonic voltage distribution. In addition, the size of this protection-blind region of the 64G2 element's coverage is expected to be

dependent on generator loading conditions. Nevertheless, by employing the 64G1 element together with the 64G2 element, the whole stator winding should be protected under all conditions since the protection-blind regions within the coverage of each element should always be complemented by the ability of the other element in the protection scheme to cover that part of the winding.

In order to examine the performance of the 64G scheme, various sets of test were carried out on the particular high-resistance grounded 555 MVA generator under study. Stator-ground faults were applied at locations along the entire length of one phase of the stator winding, using the detailed real-time simulation model shown in Chapter Six, at two different generator loading conditions (i.e. no-load and full-load), and the protection coverage of the 64G's sub-elements were documented as shown in Tables 7.1 and 7.2. These tables confirm that the 64G2 element, as expected, exhibits a lack of coverage in the middle part of the stator winding in this case, and that this gap in coverage is larger under no-load conditions than at full-load. In other words, the 64G2 element is more sensitive when the generator is operating at full-load. Nevertheless, in both cases the 64G2 element provides protection coverage of the bottom 5% of the winding in the region where the 64G1 element cannot detect stator-ground faults. The measured results shown in Tables 7.1 and 7.2 confirmed that the two complementary elements within the 64G scheme did in fact, between them, provide coverage of the entire winding for stator-ground faults.

Table 7.1. Response of SEL 300G relay's 100% stator ground protection elements at no load

FLT LOC	ELEMENTS	
%	64G1	64G2
100	Tripped	Tripped
95	Tripped	Tripped
⋮	⋮	⋮
59	Tripped	Tripped
58	Tripped	No trip
57	Tripped	No trip
56	Tripped	No trip
55	Tripped	No trip
54	Tripped	No trip
53	Tripped	No trip
52	Tripped	No trip
51	Tripped	No trip
50	Tripped	No trip
49	Tripped	No trip
48	Tripped	No trip
47	Tripped	No trip
46	Tripped	No trip
45	Tripped	No trip
44	Tripped	Tripped
⋮	⋮	⋮
5	Tripped	Tripped
0	No trip	Tripped

Table 7.2. Response of SEL 300G relay's 100% stator ground protection elements at full load

FLT LOC	ELEMENTS	
%	64G1	64G2
100	Tripped	Tripped
95	Tripped	Tripped
⋮	⋮	⋮
59	Tripped	Tripped
58	Tripped	Tripped
57	Tripped	Tripped
56	Tripped	Tripped
55	Tripped	Tripped
54	Tripped	No trip
53	Tripped	No trip
52	Tripped	No trip
51	Tripped	No trip
50	Tripped	No trip
49	Tripped	Tripped
48	Tripped	Tripped
47	Tripped	Tripped
46	Tripped	Tripped
45	Tripped	Tripped
44	Tripped	Tripped
⋮	⋮	⋮
5	Tripped	Tripped
0	No trip	Tripped

In order to further analyse the characteristics and protection coverage of the 64G scheme, detailed results were recorded for stator-ground faults located in the two parts of the stator winding that are not covered by both of its two complementary elements. Figures 7.1 to 7.4 show the results obtained from a real-time closed-loop study of a stator-ground fault applied at the generator neutral. Figure 7.1 shows that the SEL 300G relay sent a trip signal back to the real-time simulator at $t = 36.48\,ms$ to open the corresponding circuit breakers (i.e. generator's main circuit breaker and field circuit breaker) after the fault was detected. In Figure 7.3, under healthy conditions prior to the application of the fault, the generator neutral voltage consists predominantly of third-harmonic frequency, with very little fundamental-frequency component present (this can be seen more readily in the subsequent results shown in Figure 7.5). However, when the fault is applied at the generator neutral, the voltage at the neutral decreases to zero. For this reason, the 64G1 element is naturally unable to pick up for a stator-ground fault at this location. By contrast, the 64G2 element responds to changes in the relative third-harmonic voltage magnitudes at each end of the winding, and therefore this element is still able to detect stator-ground faults at or near the neutral despite the fact that the voltage measured at the neutral drops to zero for faults at this location.

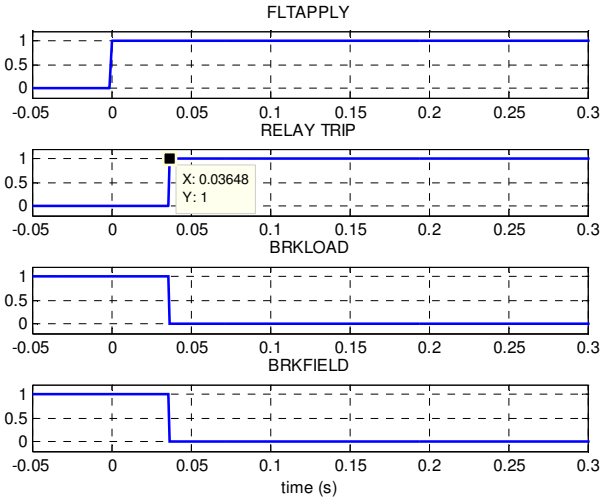

Figure 7.1. Binary logic variables for the case of a fault at the generator neutral.

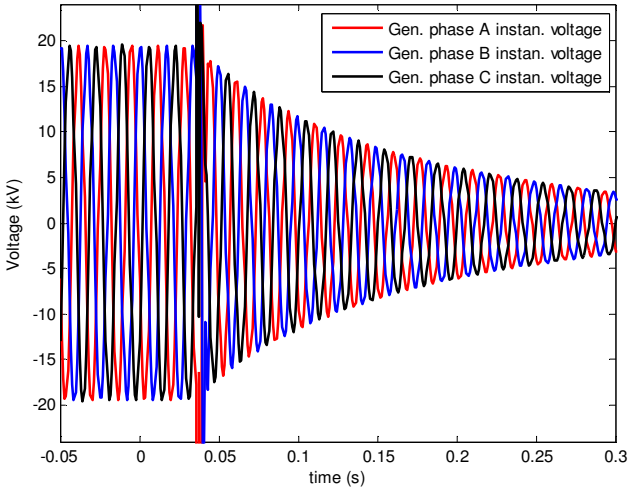

Figure 7.2. Generator stator voltages for the case of a fault at the generator neutral.

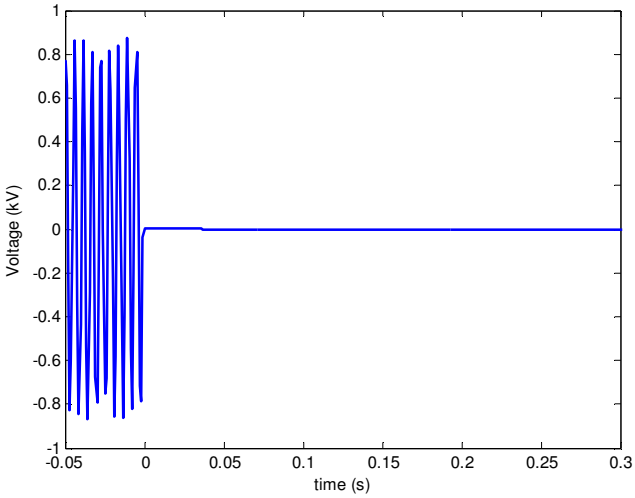

Figure 7.3. Generator neutral voltage for the case of a fault at the generator neutral.

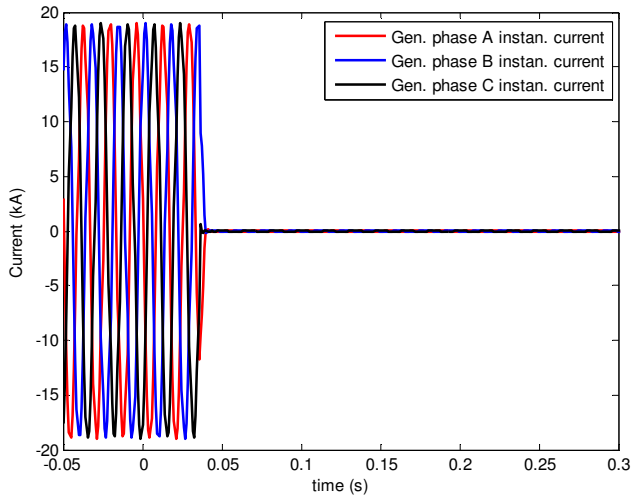

Figure 7.4. Generator stator currents for the case of a fault at the generator neutral.

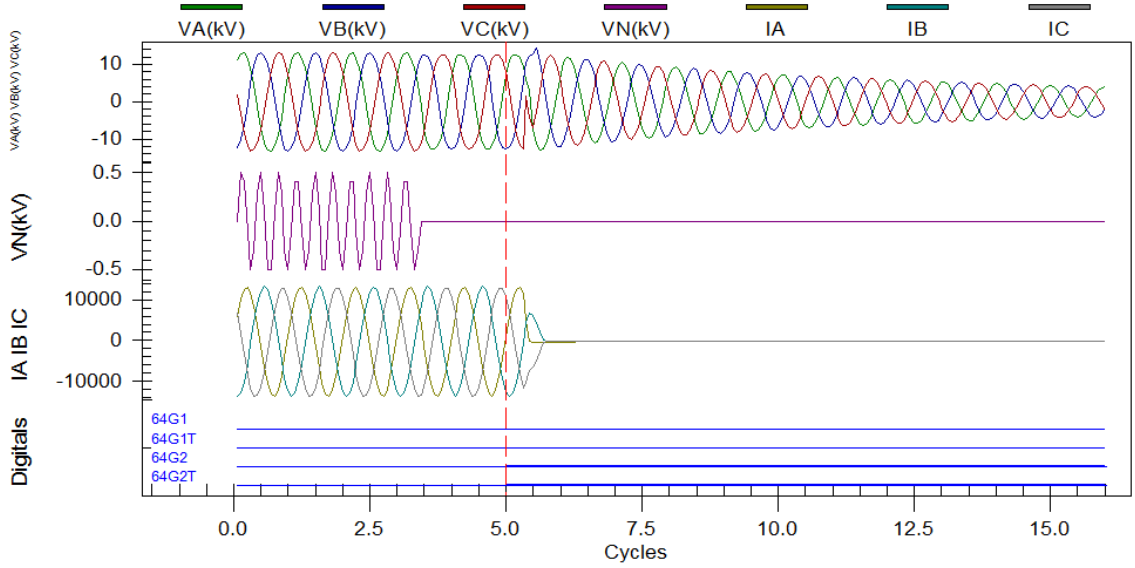

Figure 7.5. Variables recorded by the hardware relay's event recorder for the case of a fault at the generator neutral.

Figure 7.5 shows selected variables recorded by the SEL 300G relay's event recorder during the same fault study shown in Figures 7.1 to 7.4 which confirm that the 64G2 element of the relay detected this fault and was responsible for issuing the trip signal input to the real-time simulation model recorded in Figure 7.1. The purple trace in Figure 7.5 shows the predominance of third-harmonic frequency in the neutral voltage prior to the fault.

Figures 7.6 to 7.9 show the results obtained from a real-time closed-loop study of a stator-ground fault applied at a location 53% along the stator winding from the neutral end.

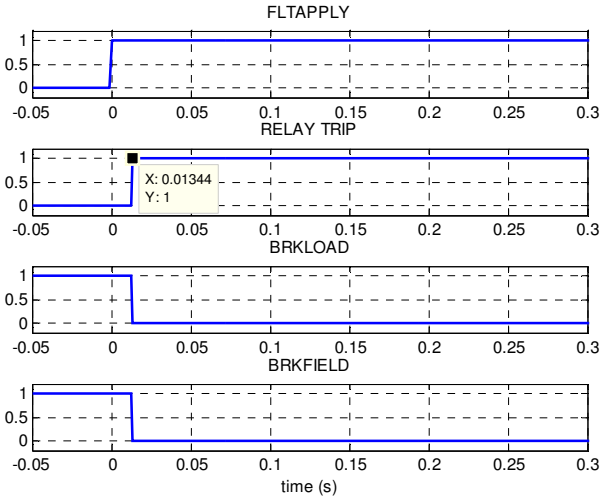

Figure 7.6. Binary logic variables for the case of a fault at 53% along the stator winding.

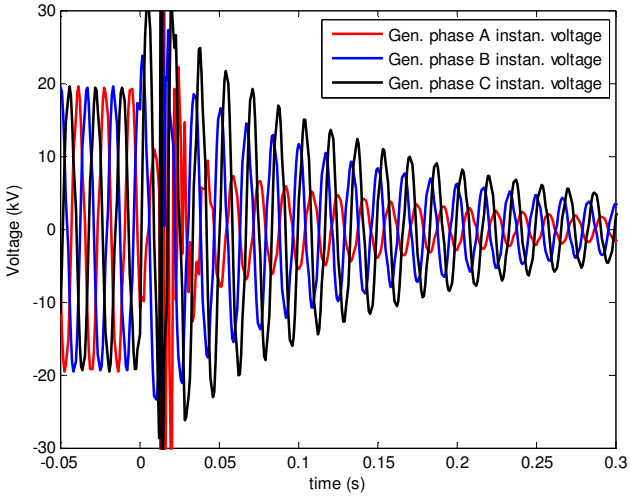

Figure 7.7. Generator stator voltages for the case of a fault at 53% along the stator winding.

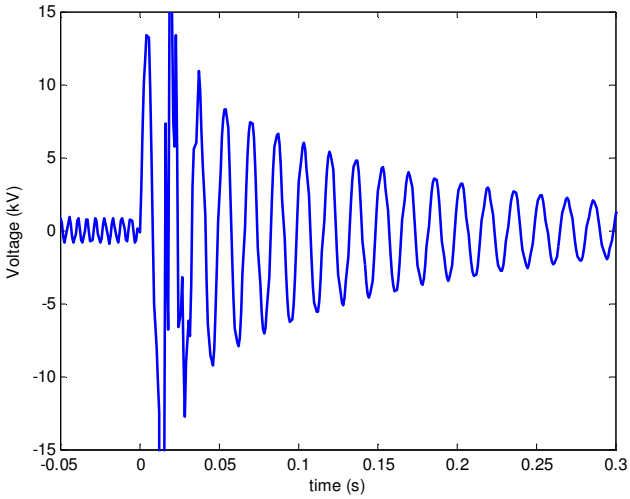

Figure 7.8. Generator neutral voltage for the case of a fault at 53% along the stator winding.

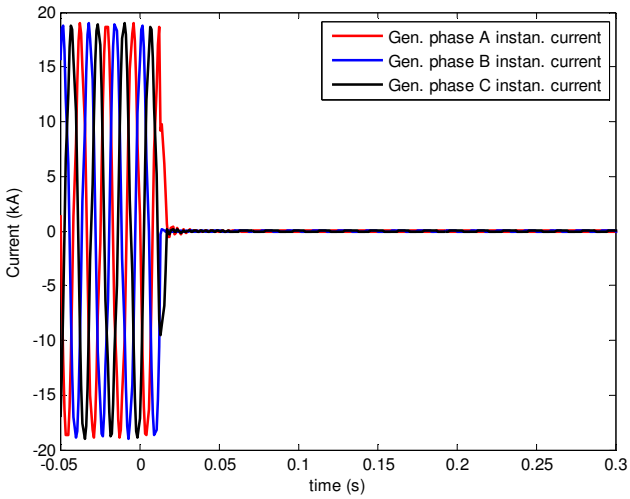

Figure 7.9. Generator stator currents for the case of a fault at 53% along the stator winding.

As discussed in Chapter Six, there is a null point within the stator winding at which the distribution of the induced third-harmonic winding voltage naturally passes through zero, and therefore shorting the winding to ground at this location has no effect on the third-harmonic voltages at the terminals at either end of the winding. For the high-resistance grounded generator in this study system, the null point is located at 53% along the winding from the neutral end, exactly at the chosen location for the fault in the results shown in Figures 7.6 to 7.9. For this reason, the 64G2 element did not respond to the fault at this location. However, Figure 7.8 clearly shows a significant increase in the fundamental-frequency component of the neutral voltage for this ground fault applied in the middle part of the stator winding.

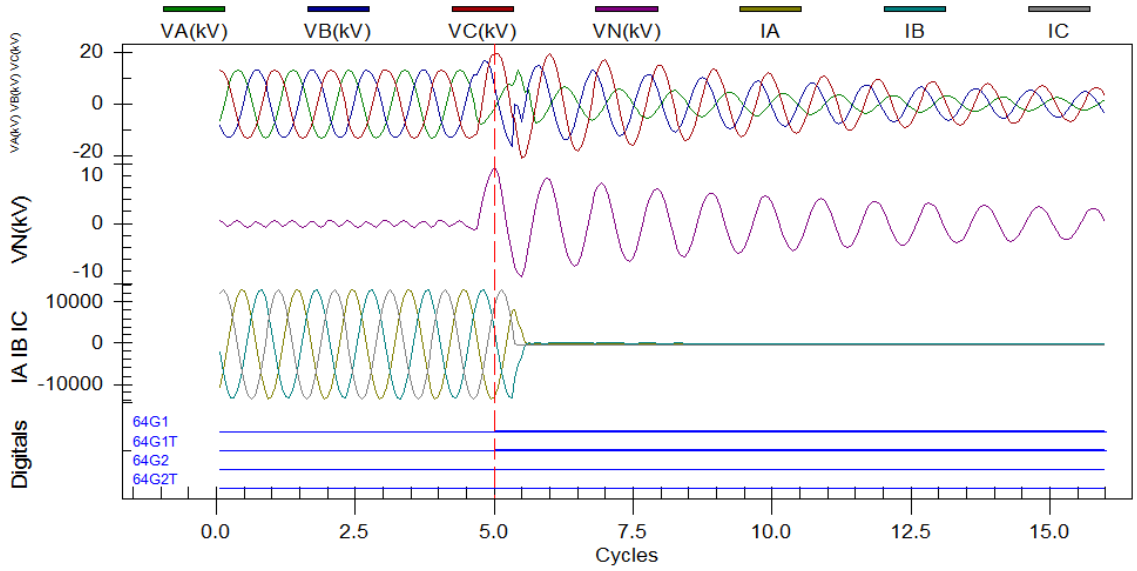

Figure 7.10. Variables recorded by the hardware relay's event recorder for the case of a fault at 53% along the stator winding.

Figure 7.10 once again shows selected variables recorded by the SEL 300G relay's event recorder during the ground fault located 53% along the stator winding. These recordings from the relay confirm that the trip signal issued in this case was as a result of the operation of the 64G1 element as expected. The behaviour of the purple trace in Figure 7.10 confirms the change in the characteristics of the neutral voltage from a small, predominantly third-harmonic voltage prior to the fault, to a large fundamental-frequency voltage during the fault.

7.3 Conclusion

This chapter has presented the results of HIL tests of the SEL 300G relay's 100% stator ground fault protection scheme (64G). In addition, the documented results were utilized to examine the performance of the 64G's sub-elements under different generator loading conditions. The results indicated that the performance of the 64G1 and 64G2 elements under different generator loading conditions corresponded with the theory presented in Chapter Six. For this reason, it was concluded that the modelling approach described in Chapter Six is suitable for protection studies of the 64G element.

Chapter Eight presents the conclusions for the research work carried out in this thesis as well as some suggestions for further research work that could be investigated in this area.

CHAPTER 8
CONCLUSION

8.1 Introduction

This thesis has evaluated the performance of a number of generator protection elements, namely phase percentage restrained differential protection (87P), loss-of-field protection (40), out-of-step protection (78) and 100% stator ground fault protection (64G), under various system contingencies and fault scenarios, using an actual hardware generator protection relay (SEL 300G) connected in a closed-loop configuration with a real-time simulation model of the study system. The results have shown that the performance of each generator protection function, and the most appropriate way to set these functions, can be better understood through real-time closed-loop studies as a result of the ability to test these functions in a realistic manner using the new phase-domain synchronous machine model. The validity of using the phase-domain synchronous machine model for hardware-in-loop testing of a generator protection relay has been confirmed in this thesis and therefore similar testing approaches can be followed for performance studies of industrial generator protection relays in the future. This chapter summarises the conclusions of each chapter in the thesis, and presents some suggestions for further research studies in this area in future.

8.2 Conclusions

Chapter One briefly discussed the advantages of utilizing the real-time, closed-loop testing approach to evaluate the performance of various power system controllers and protection relays. The chapter further explained certain limitations associated with hardware-in-loop testing of generator protection relays when using the conventional dynamic model of a synchronous generator to examine the performance of particular generator protection functions. Finally, the chapter discussed the advanced features of a recently-developed, phase-domain synchronous machine model and the motivation to carry out a thorough, research-based analysis of this new machine model and its applicability for testing generator protection and controls using an actual manufacturer's protection relay hardware (SEL 300G).

Chapter Two provided some background to the research topic by presenting a general review of power system protection together with a discussion of different protection philosophies and relaying technologies. The chapter further reviewed the particular protection functions commonly seen in industrial generator protection relays. In addition, the chapter discussed different approaches to modelling synchronous generators in the real-time simulation package RSCAD as well as different protection relay testing methodologies together with their advantages and disadvantages. This chapter concluded that a better understanding of the performance of specific

generator protection elements, and the most appropriate way to set them, can be obtained by means of the hardware-in-loop testing approach together with the new phase-domain synchronous machine model. Finally, the chapter discussed the particular generator protection functions to be focused on in the studies in this thesis, namely phase percentage restrained differential protection (87P), loss-of-field protection (40), out-of-step protection (78) and 100% stator ground fault protection (64G), as well as the motivation behind the focus on these particular elements.

Chapter Three presented an overview of a well-known study system that was adapted for the purposes of testing the particular generator protection functions of interest in this thesis. The chapter further discussed the reasons for certain modifications required in the representation of the generators in the system as well as the development of the real-time simulation models themselves, based on these modified study systems. In addition, the chapter provided an overview of the particular generator protection relay (SEL 300G) used in this research project as well as the details of the hardware-in-loop test set up and the closed-loop connections between the real-time simulator and the SEL 300G relay. Finally, the chapter explained that by utilizing RSCAD's generic, real-time model of a generator protection relay in parallel with the SEL 300G relay hardware during particular protection studies such as loss-of-field protection (40) and generator out-of-step protection (78), it is possible to gain further insight into the operation of these protection functions during various fault scenarios and system contingencies, which in turn, allows validation of the practical settings chosen for these protection elements.

Chapter Four presented the theory of operation of the particular generator protective functions (phase percentage restrained differential protection (87P), loss-of-field protection (40) and generator out-of-step protection (78)) to be considered during the hardware-in-loop tests for the case when low-resistance grounded generators were considered in the study system. The chapter further presented detailed practical settings calculations for the aforementioned protection functions based on the parameters of the particular generator and system under study. Various other settings considerations for these protection functions were also taken into account in order to prevent misoperation under healthy (un-faulted) generator operating conditions. The detailed settings determined for these protection elements were then used to configure the SEL 300G relay under test, prior to evaluating the performance of the particular protection functions using the real-time, closed-loop testing approach.

Chapter Five presented the results of the hardware-in-loop tests of the protection elements of the SEL 300G relay discussed in Chapter Four under different fault scenarios and system contingencies, and the test results were analysed and discussed. In particular, the performance of the phase percentage restrained differential protection scheme (87P) was evaluated when employed to protect

a particular low-resistance grounded generator represented in the real-time simulation model. The results confirmed that the 87P element is not able to detect stator-ground faults that occur at or near the generator neutral. It was concluded that the protection coverage of the 87P element depends on the grounding resistance of the particular generator being protected and the settings of the dual-slope differential characteristic of the 87P element. Additionally, since the new phase-domain model available in RSCAD allows detailed and realistic representation of the circuit supplying the field excitation to a synchronous generator, this chapter also considered the impact on the faulted generator of different field circuit breaker failure scenarios during attempts to clear a stator-ground fault. Using this advanced feature provided by the new phase-domain machine model, the performances of the loss-of-field element (40) under different types of field contingency were also evaluated. It was concluded that the trajectory of the measured positive sequence impedance during loss-of-field conditions depends on the relative rates of change of the generator internal voltage and rotor angle, which in turn, depend on the field circuit time constant and the initial generator loading condition.

Finally, Chapter Five investigated the performance of a single-blinder out-of-step protection scheme (78) using the highly-detailed, modified study system discussed in Chapter Three, in order to study its response to both stable power swings and out-of-step conditions caused by different system contingencies. The results have shown that the tripping characteristics of a properly-designed 78 element can discriminate between stable and unstable generator electromechanical swings following a system disturbance. The results also demonstrated that the trajectory of the positive sequence impedance measured by the relay may enter the tripping characteristics of its 40 (loss-of-field) element during a stable recovery swing following a severe system disturbance. However, since there was appropriate delay time introduced into the tripping characteristics of the 40 element, misoperation of the 40 element was prevented during the worst-case system disturbance.

Chapter Six reviewed the theory of high-resistance grounding schemes for generators and presented the design of a representative high-resistance grounding scheme for the studied generators following standard design procedures recommended in the technical literature. Additionally, the chapter discussed the theory of operation of various protection schemes that are typically employed to protect high-resistance grounded generators. It was concluded that the 100% stator ground fault protection scheme available on the SEL 300G relay (64G), which comprises a fundamental-frequency neutral overvoltage element (64G1) and a third-harmonic voltage differential element (64G2), is able to provide full stator winding protection for high-resistance grounded generators under all generator loading conditions. As discussed in Chapter Two, the publicly-available version of the phase-domain synchronous machine model used in the work of this thesis does not represent

phase-belt harmonics in the generator stator winding, and therefore it is not able to represent the third-harmonic voltages in these windings that are relied upon by the 64G2 element to detect stator-ground faults. Chapter Six therefore also presented an additional custom-designed, extension to the real-time simulation model of the generator that was developed in this thesis in order to be able to simulate the characteristics of the third-harmonic winding voltages that are relied upon by the 64G2 element to detect stator-ground faults. Finally, Chapter Six presented practical settings calculations for the 64G scheme based on the parameters of the particular high-resistance grounded generator under study, and the settings were used to configure the SEL 300G relay under test prior to evaluating the performance of the 64G scheme using the real-time, closed-loop testing approach.

Chapter Seven presented the results of the hardware-in-loop tests of the SEL 300G relay's 100% stator ground fault (64G) protection scheme. The results have shown that the 64G scheme can provide full stator winding protection for the particular high-resistance grounded generator studied, under both no-load and full-load generator operating conditions. The results were also able to demonstrate the performances of the individual elements making up the 64G scheme, namely the 64G1 and 64G2 elements. The protection coverage of both the 64G1 and 64G2 elements was confirmed during this particular protection study and the results were seen to correspond with the theory presented in Chapter Six regarding the protection-blind regions of these two protection elements.

The real-time simulation results have shown that by using the RSCAD's phase-domain synchronous machine model, together with some supplementary modelling to represent the third-harmonic voltages within the generator stator windings, it is possible to evaluate the performances of various generator protective functions which could not otherwise be achieved using conventional dynamic synchronous machine models. Furthermore, it is now possible to validate the settings of various generator protection elements under different realistic fault scenarios and system contingencies using similar hardware-in-loop, closed-loop testing procedures to those already widely adopted for other forms of power system protection.

Finally, some recommendations for further research that could be pursued as an extension of the work in this thesis are contained in the following section.

8.3 Suggestion for further work

The work presented in this thesis has confirmed the validity of using a real-time, phase-domain, synchronous machine model to directly test the performances of various generator protective functions using hardware-in-loop techniques.

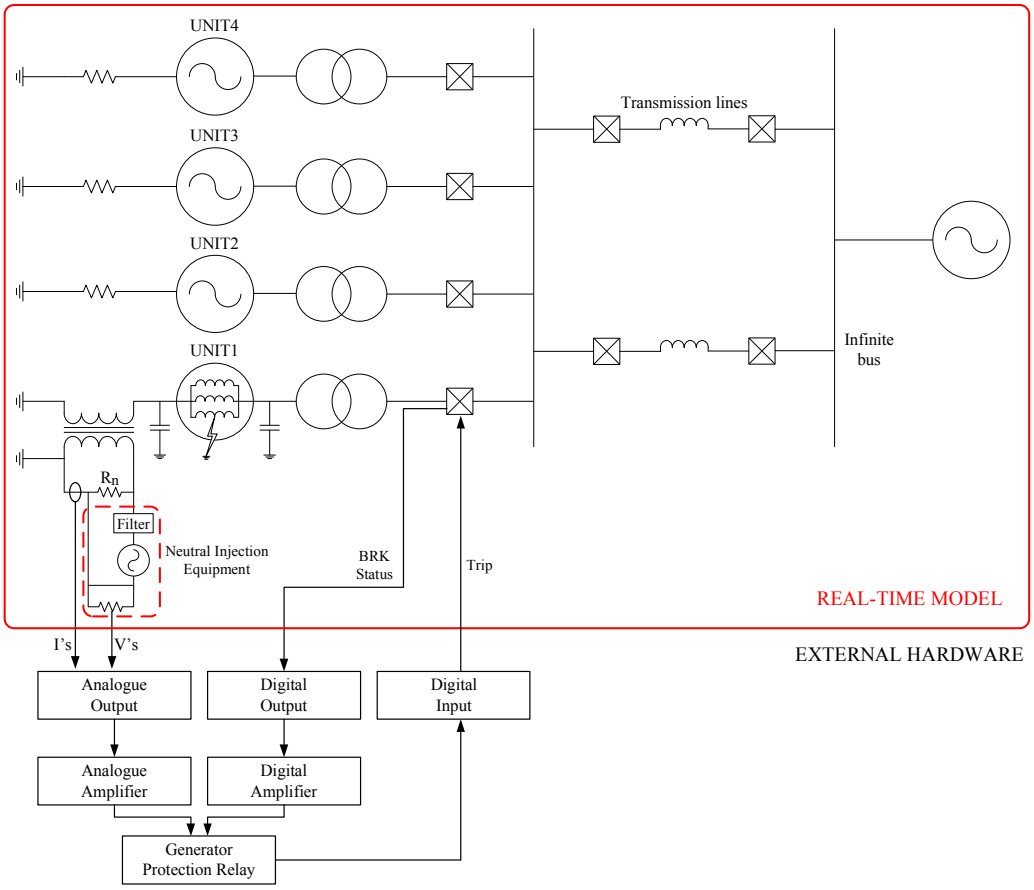

Figure 8.1. Schematic diagram showing proposed real-time, closed-loop testing of a neutral injection scheme (64S).

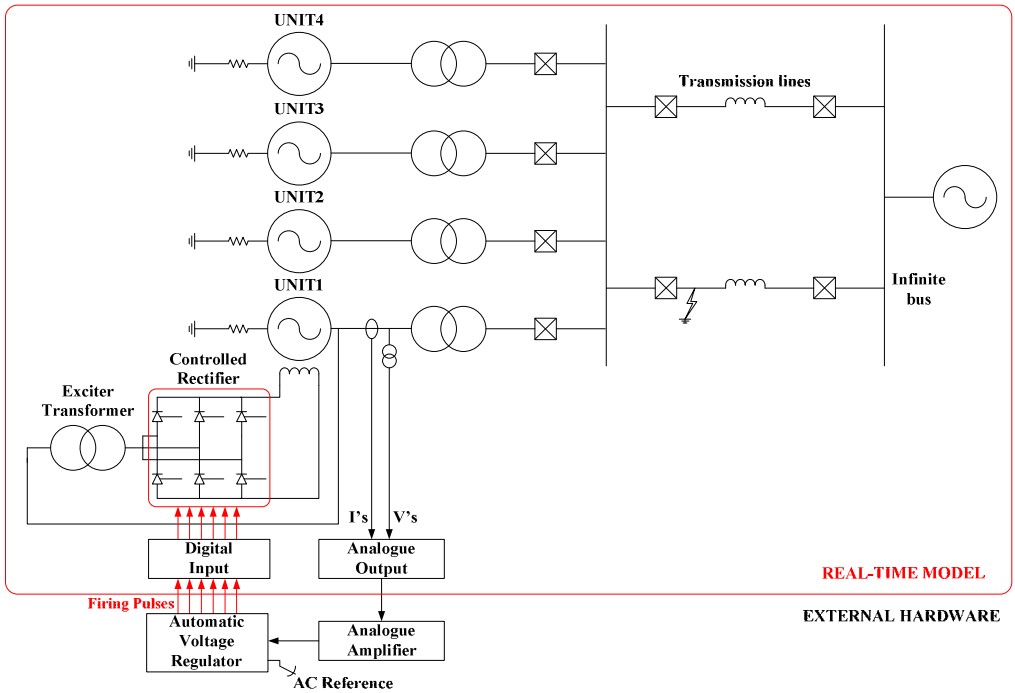

Figure 8.2. Schematic diagram showing real-time closed-loop testing of an automatic voltage regulator.

Following a similar hardware-in-loop testing approach, it should be possible to examine the performances of other stator winding protection schemes that were not considered in this thesis (e.g. ground differential protection (87N) or neutral injection (64S) schemes). Figure 8.1 shows a schematic diagram of how the performance of a 64S scheme could be evaluated using the real-time simulator, closed-loop testing approach. Using the kind of detailed and realistic real-time models of the generator plant described in Chapter Six, together with real-time models of the additional neutral injection equipment that forms part of such schemes, it should be possible to study the performance of a generator protection relay equipped with a 64S scheme under different fault scenarios.

Furthermore, because of the improved representation of the field winding in the real-time, phase-domain synchronous machine model, it is now possible to include detailed representations of the excitation system plant (including its power electronics) of a synchronous generator within a real-time simulation model. As a result, the effects of different types of practical fault scenarios within the power electronic devices of the excitation systems feeding the generator can now be studied. In addition, the performance of the actual controllers used for generator excitation system control can also be evaluated using hardware-in-loop techniques. Figure 8.2 is a schematic diagram showing how an automatic voltage regulator can be connected to a real-time model in a closed-loop configuration in order to conduct different studies for performance evaluation. With such a test set up, one could also study the effects of bus-fed and non-bus-fed excitation systems and their controls during a system disturbance, and the effects of such controls on generator protection systems.

APPENDIX A

DETAILED REAL-TIME SIMULATION MODELS FOR DIFFERENT PROTECTION STUDIES

Sections A1 to A3 provide further details of the specific real-time simulation models that were used for real-time closed-loop studies of particular protection elements of the SEL 300G generator protection relay, namely phase percentage restrained differential protection (87P), loss-of-field protection (40), out-of-step protection (78) and 100% stator ground fault protection (64G). In addition, the details of the real-time models within each hierarchy box in the various simulation cases are also presented in order to show the full scope of the modelling details required to conduct the aforementioned different protection studies.

A1. Real-time simulation model for protection studies of 87P and 40 elements

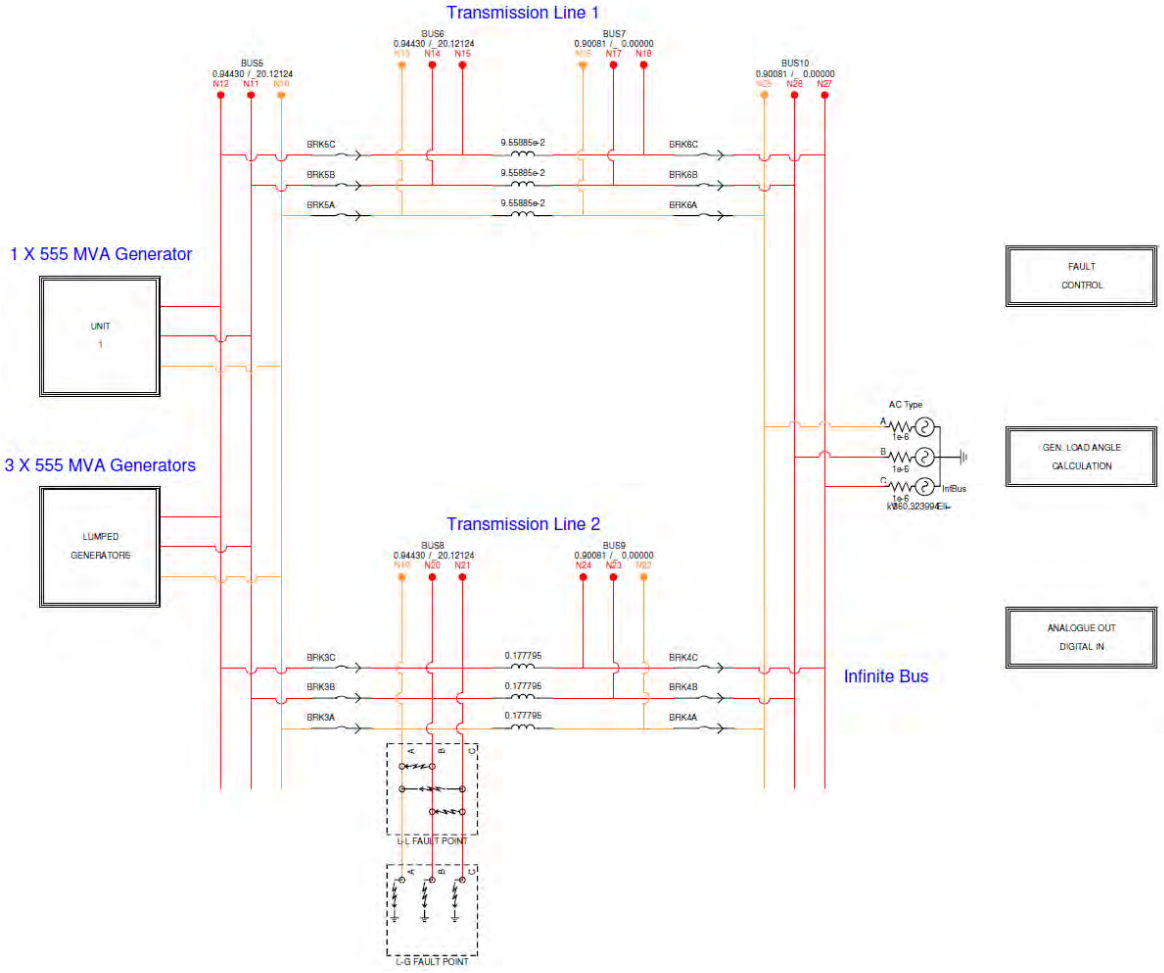

Figure A1. RSCAD representation of the modified study system for low-impedance grounding protection tests.

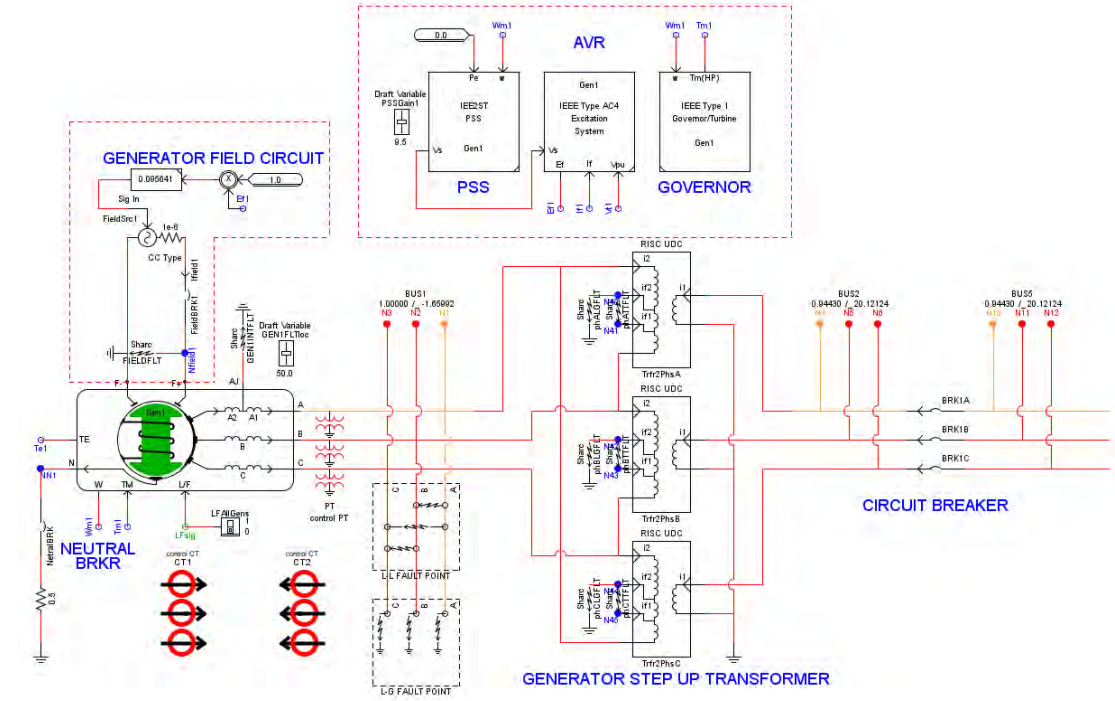

Figure A2. Real-time modelling details of the particular generator in the study system connected to protection relays for fault studies.

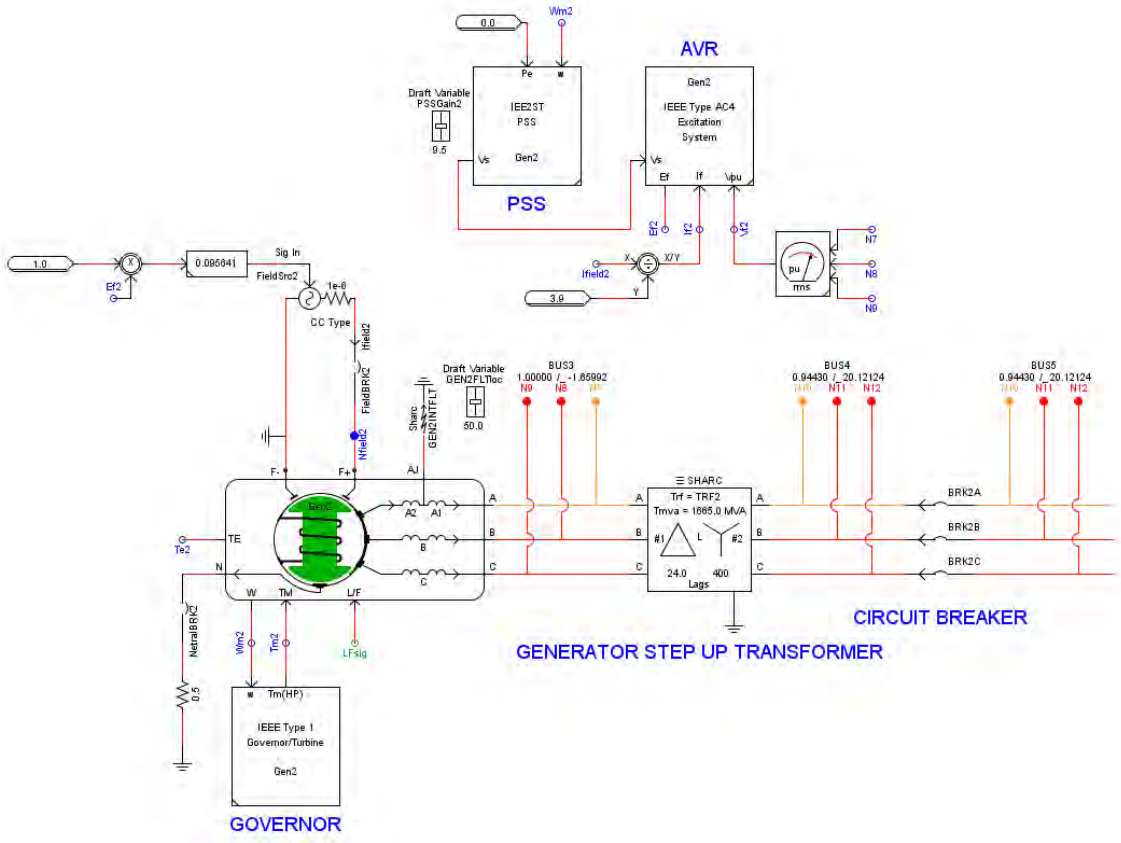

Figure A3. Real-time modelling details of the remaining (lumped) generators in the study system not connected to protection relays during the fault studies.

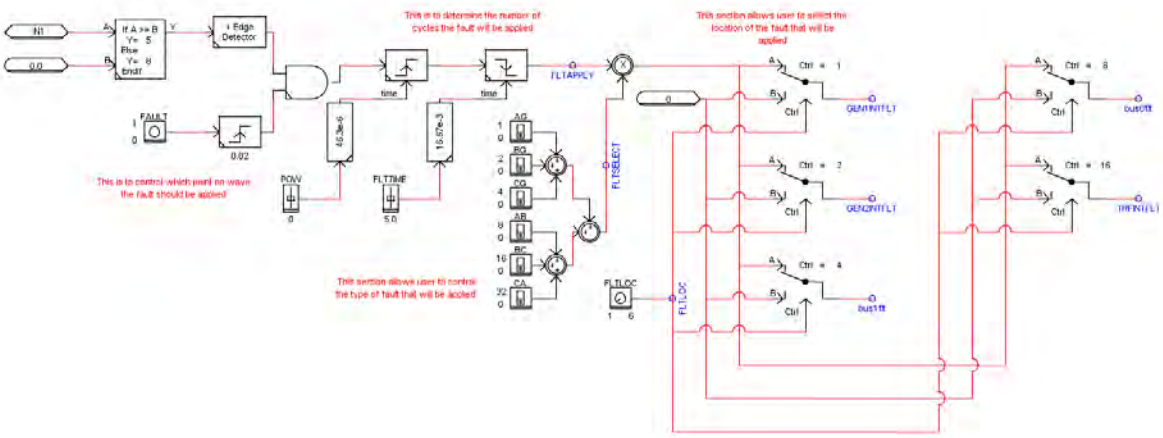

Figure A4. Fault control logic.

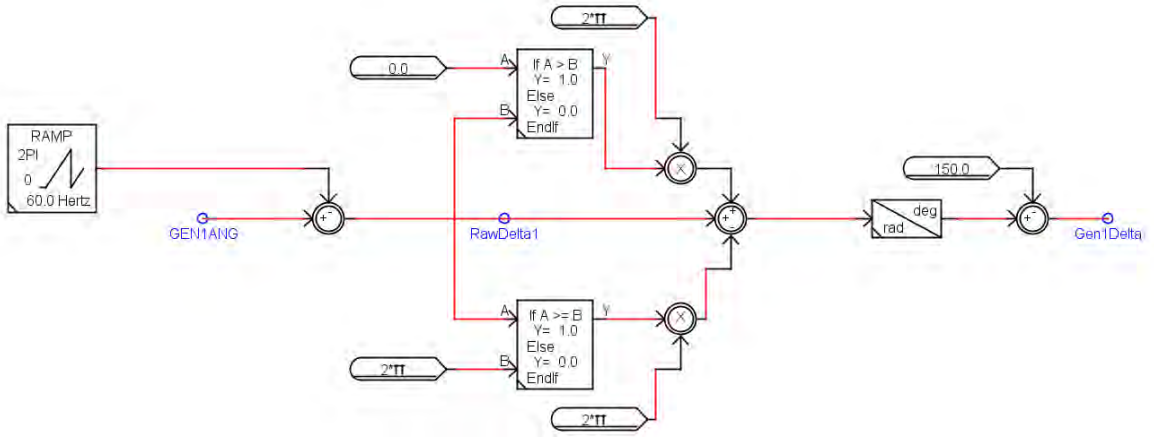

Figure A5. Rotor angle calculation.

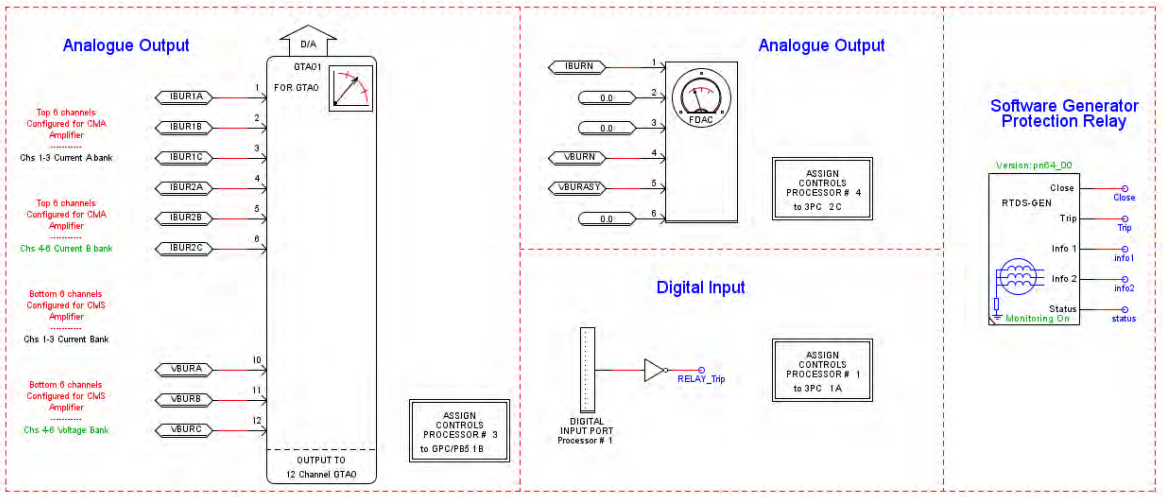

Figure A6. I/O signal interfacing between the real-time simulation model and the external SEL 300G relay hardware.

A2. Real-time simulation model for protection studies of 78 element

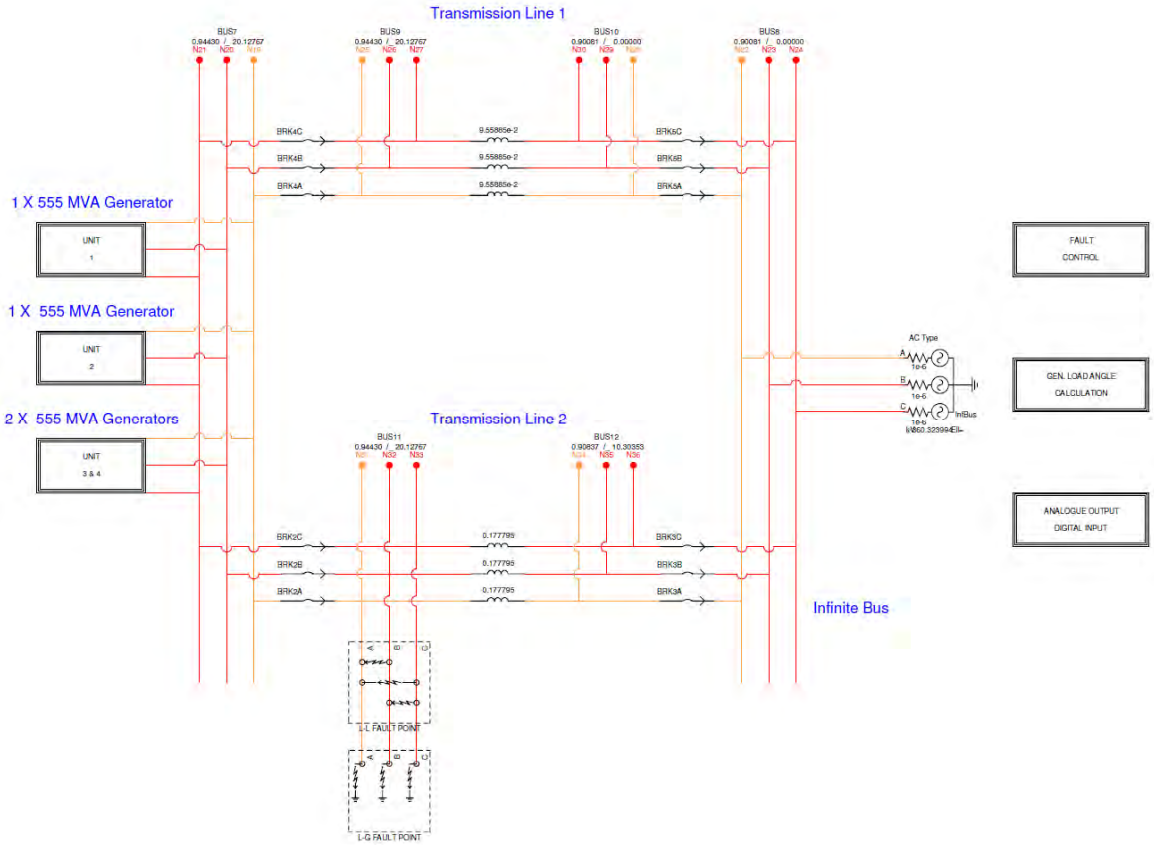

Figure A7. RSCAD representation of the modified study system for out-of-step protection tests.

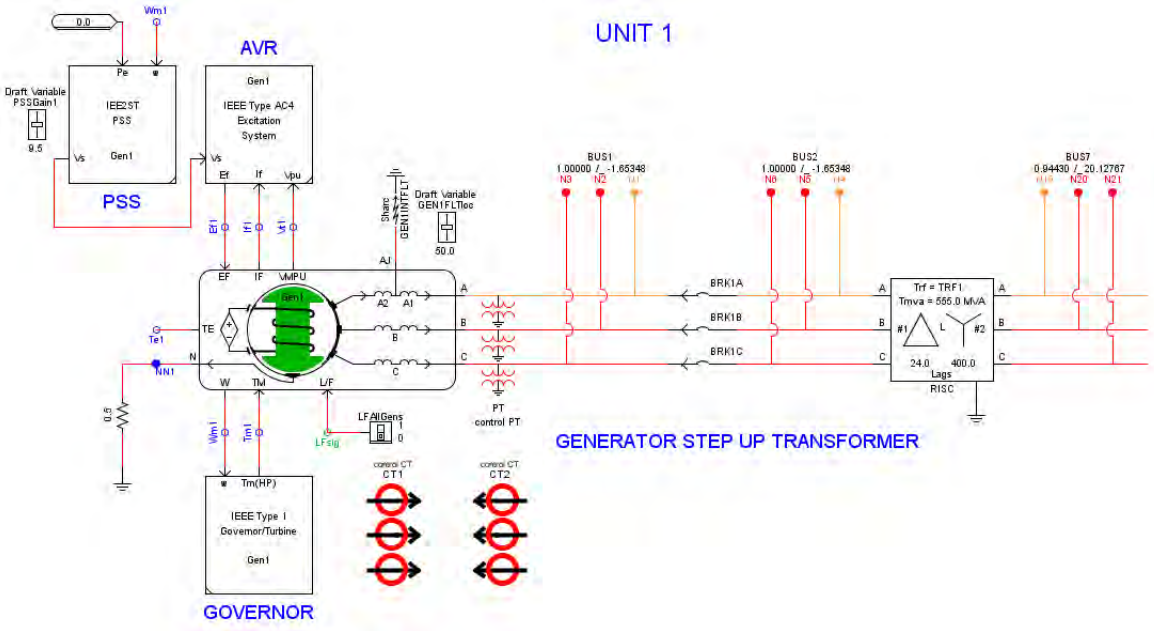

Figure A8. Real-time modelling details of the particular generator in the study system connected to protection relays for out-of-step tests.

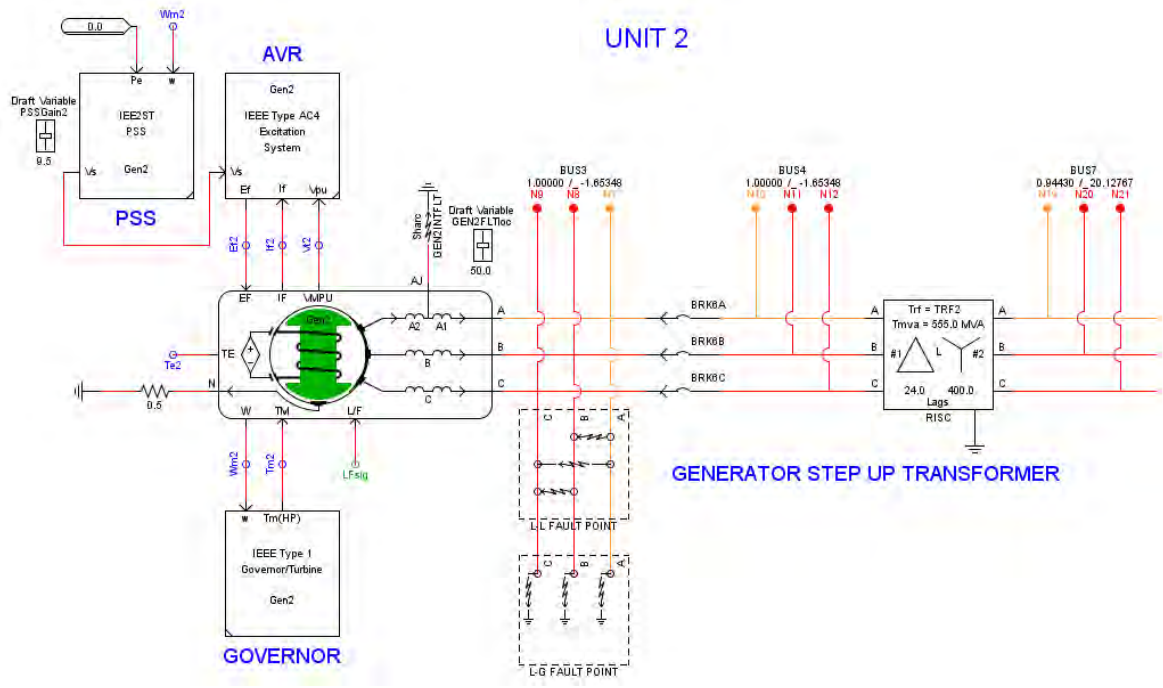

Figure A9. Real-time modelling details of the neighbouring generator represented as a single unit in the study system for out-of-step tests.

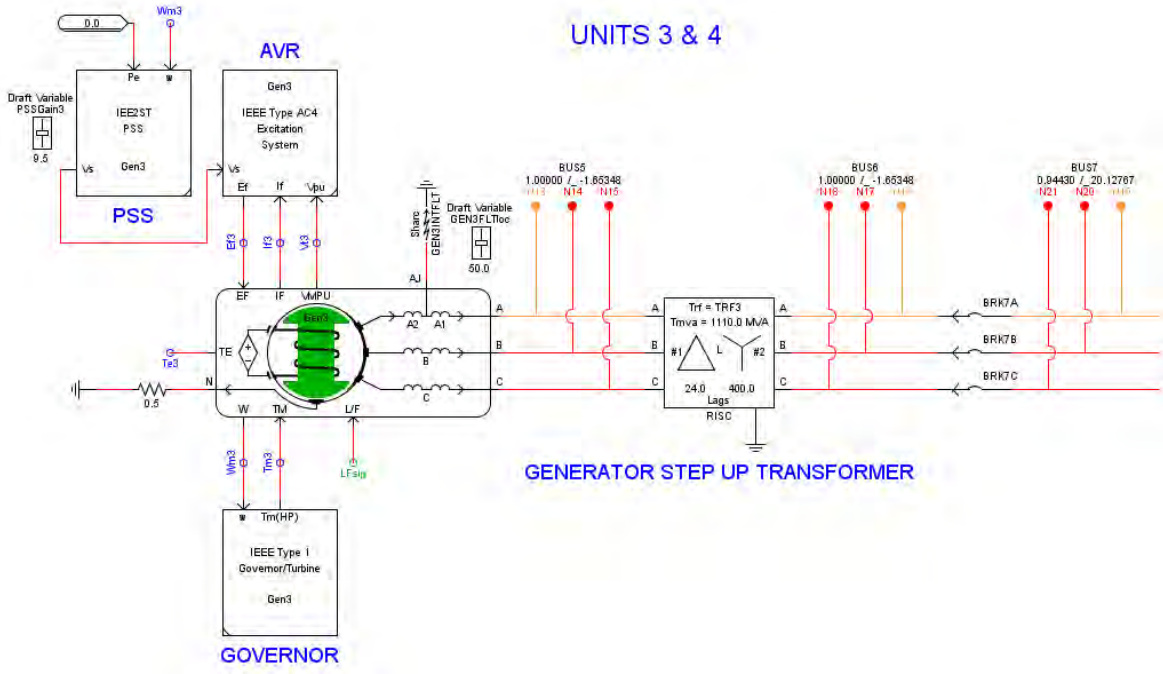

Figure A10. Real-time modelling details of the remaining neighbouring (lumped) generators in the study system for out-of-step tests.

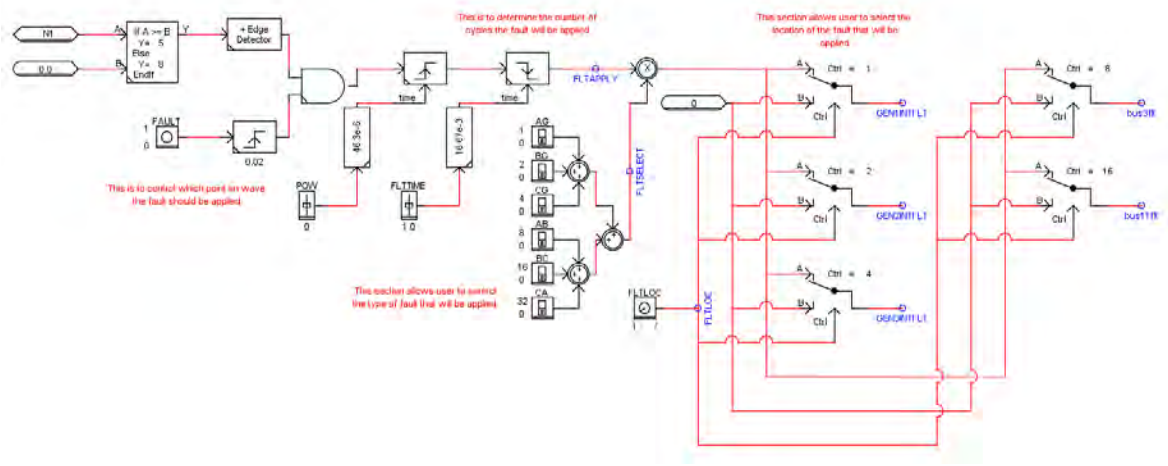

Figure A11. Fault control logic.

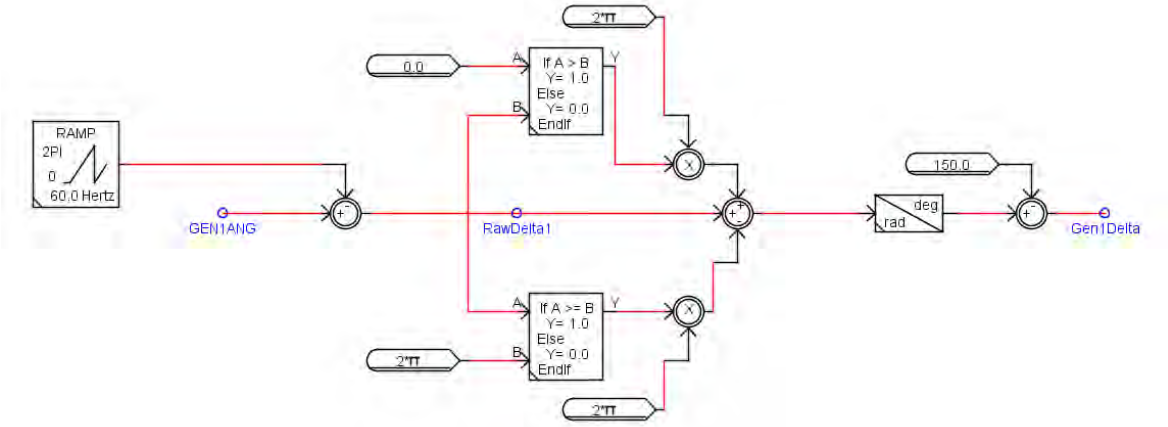

Figure A12. Rotor angle calculation.

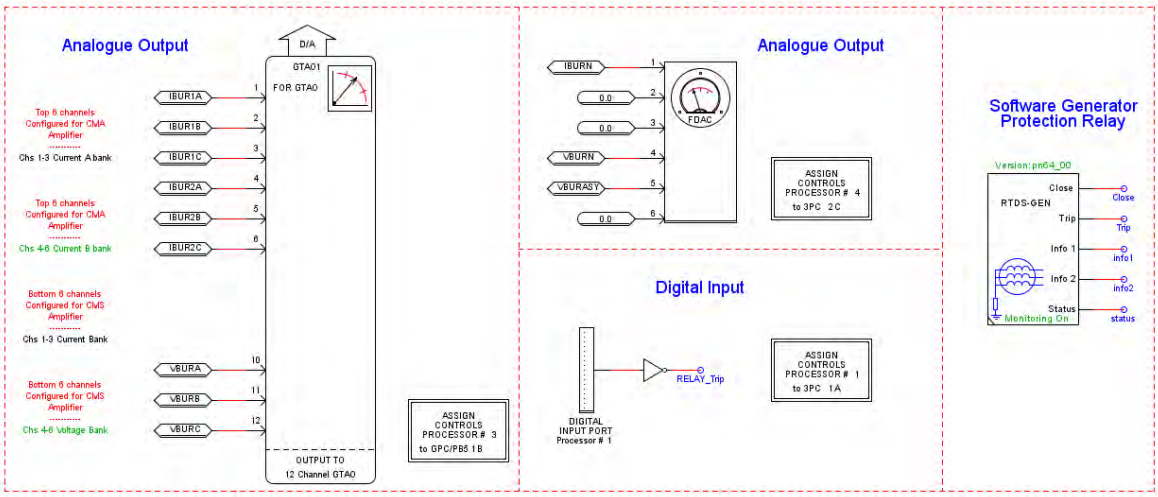

Figure A13. I/O signal interfacing between the real-time simulation model and the external SEL 300G relay hardware.

A3. Real-time simulation model for protection studies of 64G elements

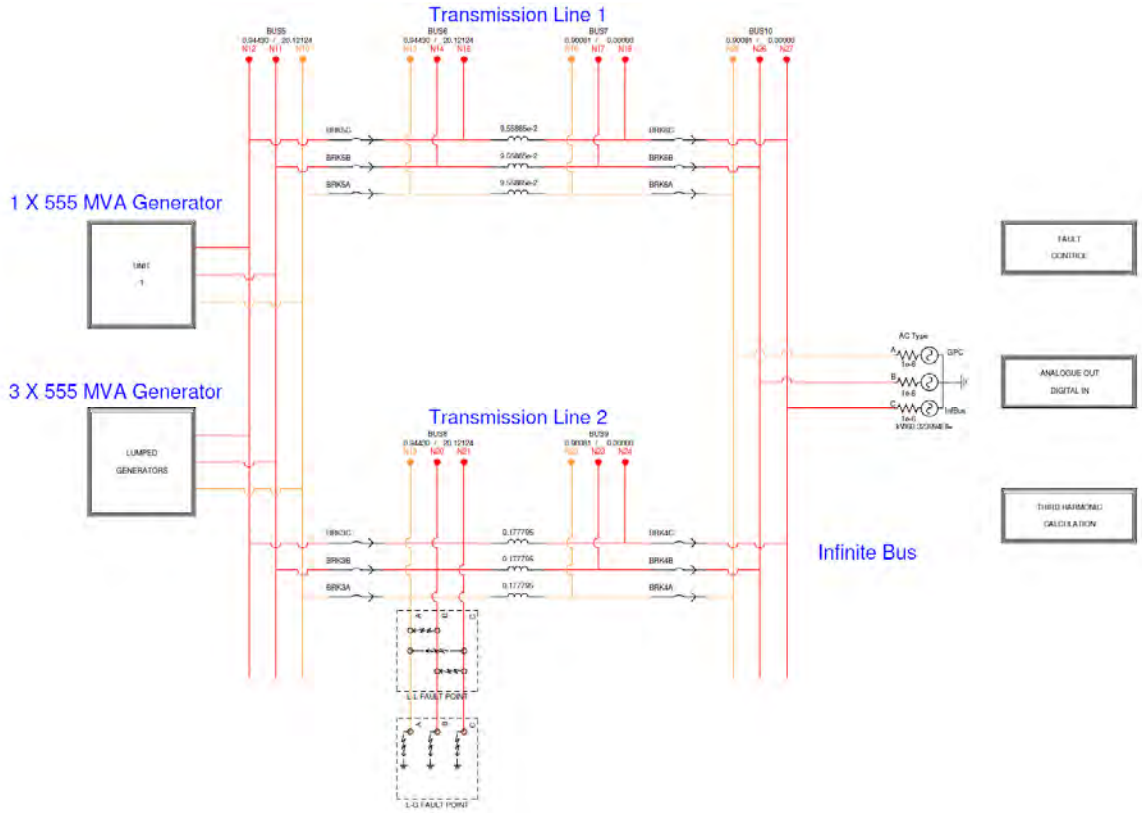

Figure A14. RSCAD representation of the modified study system for high-impedance grounding protection tests

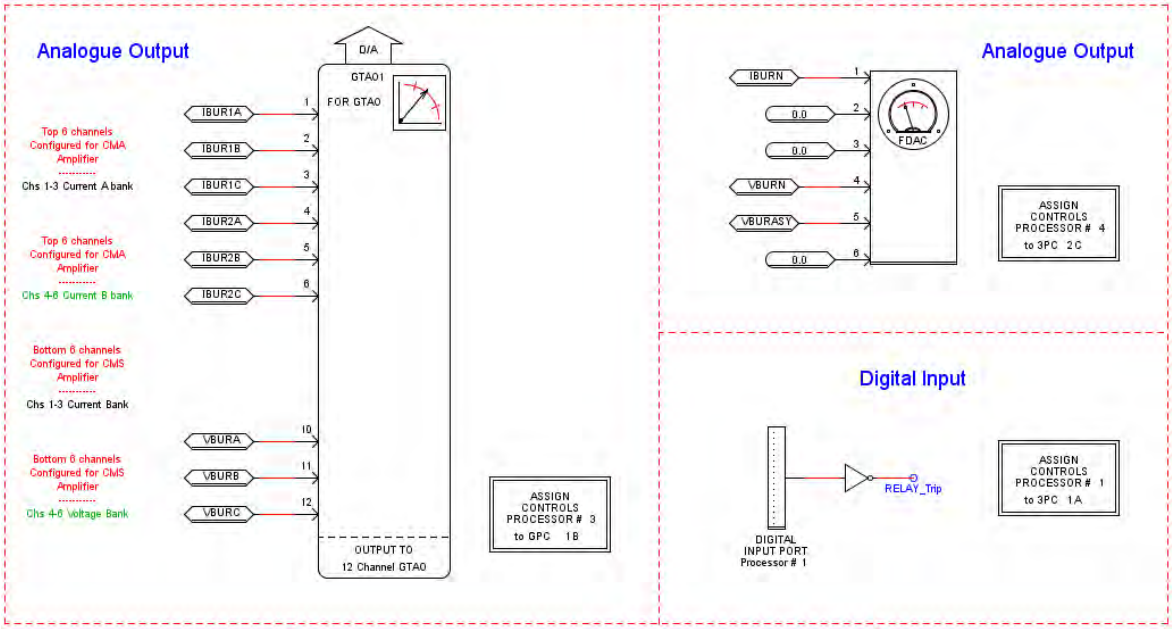

Figure A15. I/O signal interfacing between the real-time simulation model and the SEL 300G relay hardware.

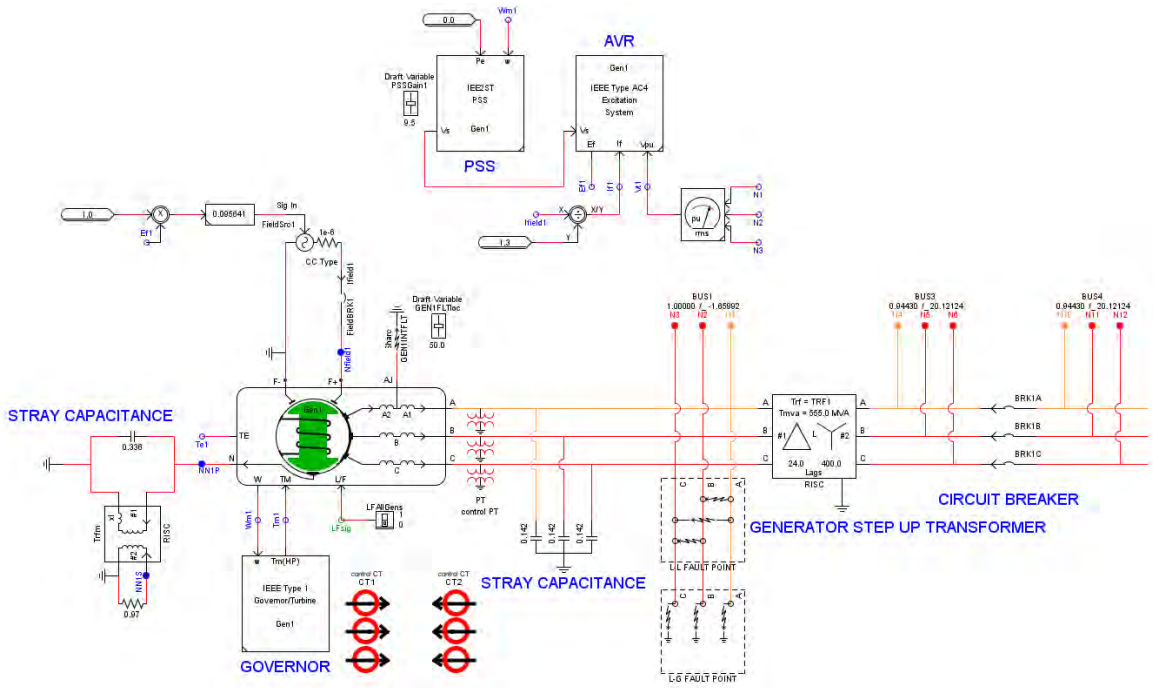

Figure A16. Real-time modelling details of the particular generator in the study system connected to protection relays for fault studies.

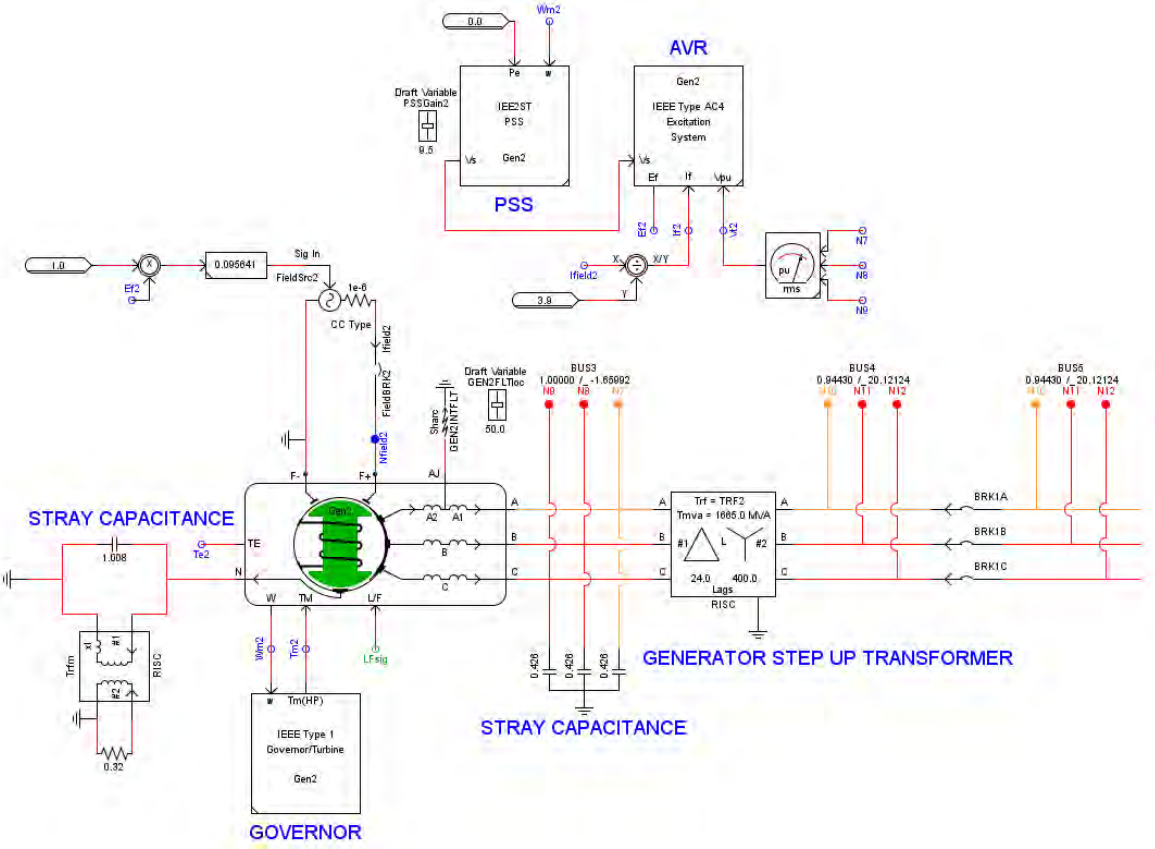

Figure A17. Real-time modelling details of the remaining (lumped) generators in the study system not connected to protection relays during the fault studies.

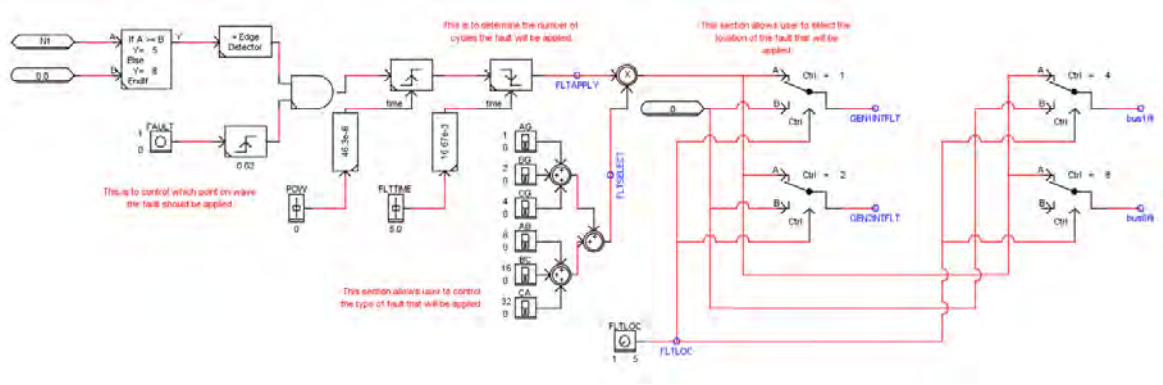

Figure A18. Fault control logic.

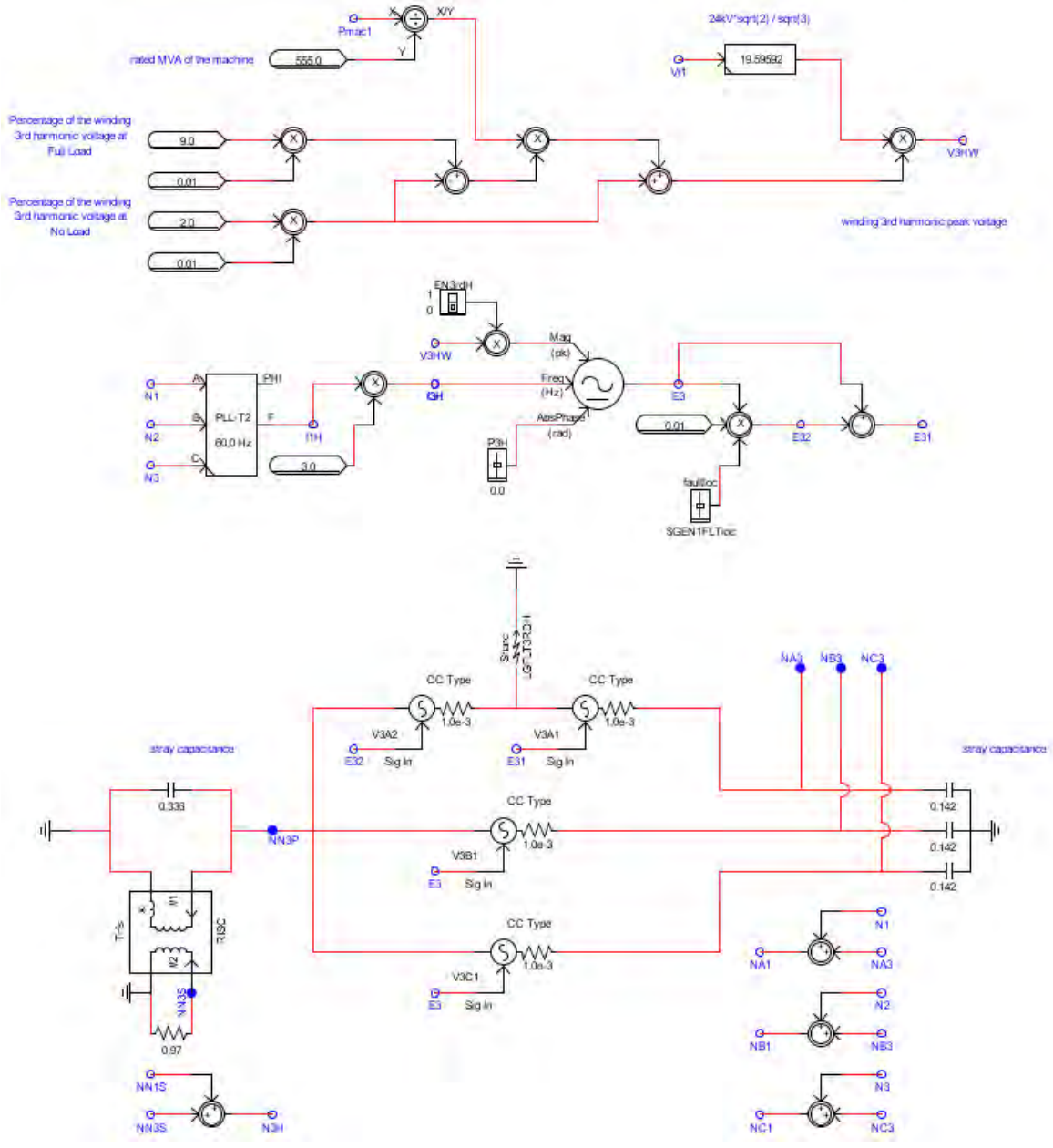

Figure A19. Real-time modelling details of third-harmonic winding voltages.

APPENDIX B

FULL DERIVATION FOR GENERATOR SWING CHARACTERISTICS

The generalized equation for generator swing characteristics shown in Chapter Four is the result obtained from the full derivation using the equivalent circuit diagram shown in Figure 4.6. Letting $n = E_g/E_s$ and $1\angle\delta = cos\delta + jsin\delta$, the step by step derivation using the equivalent circuit diagram shown in Figure 4.6 is shown as follows.

$$Z_R = \frac{V_R}{I} = \frac{E_g\angle\delta - \dfrac{E_g\angle\delta - E_s}{X_g + X_{TR} + Z_{sys}} \cdot X_g}{\dfrac{E_g\angle\delta - E_s}{X_g + X_{TR} + Z_{sys}}}$$

$$= \frac{E_g\angle\delta}{E_g\angle\delta - E_s} \cdot \left(X_g + X_{TR} + Z_{sys}\right) - X_g$$

$$= \frac{E_g \cdot cos\delta + jE_g \cdot sin\delta}{E_g \cdot cos\delta + jE_g \cdot sin\delta - E_s} \cdot \left(X_g + X_{TR} + Z_{sys}\right) - X_g$$

$$= \frac{\dfrac{E_g}{E_s} \cdot cos\delta + j\dfrac{E_g}{E_s} \cdot sin\delta}{\dfrac{E_g}{E_s} \cdot cos\delta + j\dfrac{E_g}{E_s} \cdot sin\delta - 1} \cdot \left(X_g + X_{TR} + Z_{sys}\right) - X_g$$

$$= \frac{n \cdot cos\delta + jn \cdot sin\delta}{n \cdot cos\delta + jn \cdot sin\delta - 1} \cdot \left(X_g + X_{TR} + Z_{sys}\right) - X_g$$

$$= \frac{(n \cdot cos\delta + jn \cdot sin\delta) \cdot (n \cdot cos\delta - 1 - jn \cdot sin\delta)}{(n \cdot cos\delta - 1 + jn \cdot sin\delta) \cdot (n \cdot cos\delta - 1 - jn \cdot sin\delta)} \cdot \left(X_g + X_{TR} + Z_{sys}\right) - X_g$$

$$= \frac{n^2 \cdot cos^2\delta + jn^2 \cdot sin\delta \cdot cos\delta - n \cdot cos\delta - jn \cdot sin\delta - jn^2 \cdot sin\delta \cdot cos\delta + n^2 \cdot sin^2\delta}{(n \cdot cos\delta - 1)^2 + n^2 \cdot sin^2\delta}$$

$$\cdot \left(X_g + X_{TR} + Z_{sys}\right) - X_g$$

$$= \frac{(n^2 \cdot cos^2\delta + n^2 \cdot sin^2\delta) - n \cdot cos\delta - jn \cdot sin\delta}{n^2 \cdot cos^2\delta - 2n \cdot cos\delta + 1 + n^2 \cdot sin^2\delta} \cdot \left(X_g + X_{TR} + Z_{sys}\right) - X_g$$

$$= \frac{n^2 - n \cdot cos\delta - jn \cdot sin\delta}{n^2 - 2n \cdot cos\delta + 1} \cdot \left(X_g + X_{TR} + Z_{sys}\right) - X_g$$

$$= \frac{n \cdot (n - cos\delta) - jn \cdot sin\delta}{(n^2 - 2n \cdot cos\delta + cos^2\delta) + 1 - cos^2\delta} \cdot \left(X_g + X_{TR} + Z_{sys}\right) - X_g$$

$$= n \cdot \frac{(n - cos\delta) - jsin\delta}{(n - cos\delta)^2 + sin^2\delta} \cdot \left(X_g + X_{TR} + Z_{sys}\right) - X_g$$

When the special case in which $E_g = E_s \quad (n = 1)$ is evaluated, the equation becomes

$$Z_R = \frac{V_R}{I} = \frac{(1 - cos\delta) - jsin\delta}{(1 - cos\delta)^2 + sin^2\delta} \cdot \left(X_g + X_{TR} + Z_{sys}\right) - X_g$$

$$= \frac{(1 - cos\delta) - jsin\delta}{1^2 - 2 \cdot cos\delta + cos^2\delta + sin^2\delta} \cdot \left(X_g + X_{TR} + Z_{sys}\right) - X_g$$

$$= \frac{(1 - cos\delta) - jsin\delta}{2 - 2 \cdot cos\delta} \cdot \left(X_g + X_{TR} + Z_{sys}\right) - X_g$$

$$= \left(\frac{1 - cos\delta - jsin\delta}{1 - cos\delta}\right) \cdot \frac{\left(X_g + X_{TR} + Z_{sys}\right)}{2} - X_g$$

$$= \left(1 - \frac{jsin\delta}{1 - cos\delta}\right) \cdot \frac{\left(X_g + X_{TR} + Z_{sys}\right)}{2} - X_g$$

$$= \left(1 - j\frac{\sqrt{sin^2\delta}}{1 - cos\delta}\right) \cdot \frac{\left(X_g + X_{TR} + Z_{sys}\right)}{2} - X_g$$

$$= \left(1 - j\frac{\sqrt{1 - cos^2\delta}}{1 - cos\delta}\right) \cdot \frac{\left(X_g + X_{TR} + Z_{sys}\right)}{2} - X_g$$

$$= \left(1 - j\frac{\sqrt{(1 - cos\delta) \cdot (1 + cos\delta)}}{1 - cos\delta}\right) \cdot \frac{\left(X_g + X_{TR} + Z_{sys}\right)}{2} - X_g$$

$$= \left(1 - j\frac{\sqrt{1 + cos\delta}}{\sqrt{1 - cos\delta}}\right) \cdot \frac{\left(X_g + X_{TR} + Z_{sys}\right)}{2} - X_g$$

$$= \left(1 - j\frac{\frac{\sqrt{1 + cos\delta}}{2}}{\frac{\sqrt{1 - cos\delta}}{2}}\right) \cdot \frac{\left(X_g + X_{TR} + Z_{sys}\right)}{2} - X_g$$

$$= \left(1 - j\frac{cos\left(\frac{\delta}{2}\right)}{sin\left(\frac{\delta}{2}\right)}\right) \cdot \frac{\left(X_g + X_{TR} + Z_{sys}\right)}{2} - X_g$$

$$= \left(1 - jcot\left(\frac{\delta}{2}\right)\right) \cdot \frac{\left(X_g + X_{TR} + Z_{sys}\right)}{2} - X_g$$

REFERENCES

[1] Power System Relaying Committee: “Performance of Generator Protection During Major System Disturbances”, IEEE Transactions in Power Delivery, 2003.

[2] Power System Relay Committee: “Coordination of Generator Protection with Generator Excitation Control and Generator Capability”, IEEE Power Engineering Society General Meeting, 2007.

[3] Power System Relaying Committee: “Voltage Collapse Mitigation”, Report to IEEE power System Relaying Committee, December 1996.

[4] P.G. McLaren, R. Kuffel, R. Wierckx, J. Giesbrecht, L. Arendt: “A Real Time Digital Simulator for Testing Relays”, IEEE Transactions on Power Delivery, Vol. 7, No.1, January 1992.

[5] R. Kuffel, J. Giesbrecht, T. Maguire, R.P. Wiercks, P. McLaren: “RTDS – A Fully Digital Power System Simulator Operating in Real Time”, WESCANEX 95, Communications, Power, and Computing Conference Proceedings, IEEE Vol. 2, May 1995, pp. 300 – 305.

[6] Paul Forsyth, Trevor Maguire, Rick Kuffel: “Real Time Digital Simulation for Control and Protection System Testing”, IEEE Power Electronics Specialists Conference, Vol. 1, June 2004, pp. 329 – 335.

[7] R. Kuffel, P. McLaren, M. Yalla, X. Wang: “Testing of the Beckwith Electric M-0430 Multifunction Protection Relay Using a Real-Time Simulator (RTDS)”, Conference Proceedings of ICDS, College Station, Texas, USA, April 1995, pp. 49 – 54.

[8] R.J. Marttila: “Testing of Integrated Multifunction Protection Systems on the Real-Time Digital Simulator, Conference Proceedings of ICDS, Montreal, Canada, May 1997, pp. 177 – 182.

[9] T. Badelt, M. Claus, B. Friedrich, D. Retzmann, S. Boshoff, P. Davel, P. Forsyth, T.L. Maguire: “Advanced SVC Testing using a Real Time Digital Simulator, Conference Proceedings of ICDS, Montreal, Canada, May 1997, pp. 265 – 270.

[10] A.B. Dehkordi, Prabhakar Neti, A.M. Gole, T.L. Maguire: “Development and Validation of a Comprehensive Synchronous Machine Model for a Real-Time Environment”, IEEE Trans. Energy Conversion, Vol. 25, No. 1, 2010, pp. 34 – 48.

[11] Prabha Kundur: Power System Stability and Control, McGraw-Hill Inc., New York, 1994.

[12] P.G. McLaren, E.N. Dirks, R.P. Jayasinghe, G.W. Swift, Z. Zhang: "Using a Real Time Digital Simulator to Develop an Accurate Model of a Digital Relay", Conference Proceedings of ICDS, College Station, Texas, USA, April 1995, pp. 173 – 178.

[13] "Real-Time Digital Simulator Power System Users Manual", RTDS Technologies, Winnipeg, Manitoba, Canada, November 2006.

[14] H. Duchen, M. Lagerkvist, R. Kuffel, R. Wierckx: "HVDC Simulation and Control Testing using a Real Time Digital Simulator (RTDS), Conference Proceedings of ICDS, College Station, Texas, USA, April 1995, pp. 213 – 218.

[15] R. Kuffel, R. Wierckx, P. Forsyth, H. Duchen, M. Lagerkvist, P. Holmberg, X. Wang: "Expanding an Analogue Simulator's Modelling Capability Using a Real-Time Digital Simulator", Conference Proceedings of ICDS, College Station, Texas, USA, April 1995, pp. 199 – 204.

[16] K. Bergmann, K. Braun, G. Kuhn, D. Retzmann, I. Baran, F. Pereira, P. Forsyth, T.L. Maguire: "Advanced Fully Digital TCSC Real-Time Simulation in Comparison with Computer Studies and On-site Testing, Conference Proceedings of ICDS, Vasteras, Sweden, May 1999.

[17] Dean S. Ouellette, Rudi P. Wierckx, Peter G. McLaren: "Using a Multi-threaded Time Step to Model a Multi-function Relay in a Real Time Digital Simulator", Developments in Power System Protection (DPSP 08), Glasgow, March 2008.

[18] A.B. Dehkordi, D.S. Ouellette, P.A. Forsyth: "Protection Testing of A 100% Stator Ground Fault Using A Phase Domain Synchronous Machine Model in Real Time", IET International Conference on Developments in Power System Protection, January 2010.

[19] Y-T Huang, B S Rigby, A B Dehkordi: "Using a new faulted synchronous machine model for hardware-in-loop testing of a generator protection relay", Southern African Power System Protection Conference, 2012.

[20] Y-T Huang, B S Rigby: "Design and Real-Time Simulator Testing of Generator Protection Schemes for Low- and High-Impedance Grounding Methods", PAC World Conference, Cape Town, 2013.

[21] J. Lewis Blackburn, Thomas J. Domin: Protective Relaying Principles and Applications, Third Edition, Taylor and Francis Group, LLC, 2007.

[22] Antonio Gomez-Exposito, Antonio J. Conejo, Claudio Canizares: Electric Energy Systems Analysis and Operation, Taylor and Francis Group, LLC, 2009.

[23] P.M. Anderson: Power System Protection, John Wiley & Sons, Inc., New York, 1999.

[24] Stanley H. Horowitz, Arun G. Phadke: Power System Relaying, Third Edition, John Wiley & Sons, Ltd., England, 2008.

[25] A.R. van C. Warrington, "Protective Relays", Vol.1, Chapman & Hall, 1968.

[26] Moketjema Clarence Leoaneka: "Dynamic Performance of Numerical Distance Protection Relays in Heavily Series Compensated Networks", University of KwaZulu-Natal, 2009.

[27] R.E. Cosse: "Turbine/Generator Governor Droop/Isochronous Fundamentals – A Graphical Approach", Petroleum and Chemical Industry Conference, September 2011.

[28] Alexander Murdoch, Robert W. Delmerico, Sundar Venkataraman, Rodney A. Lawson, James E. Curran, William R. Pearson: "Excitation System Protective Limiters and Their Effect on Volt/Var Control – Design, Computer Modelling, and Field Testing", IEEE Transactions on Energy Conversion, Vol. 15, No. 4, December 2000.

[29] Surge Protective Devices Committee, "IEEE Guide for the Application of Neutral Grounding in Electrical Utility Systems, Part II – Grounding of Synchronous Generator Systems", IEEE C62.92-1989.

[30] Substation Committee: "IEEE Standard Electrical Power System Device Function Numbers", IEEE Std C37.2-1991.

[31] "SEL-300G Multifunction Generator Relay Instruction Manual", Schweitzer Engineering Laboratories, Inc., 2007.

[32] Donald Reimert: Protective Relaying for Power Generation Systems, Taylor & Francis Group, New York, 2006.

[33] L.G. Hewitson, Mark Brown and Ramesh Balakrishnan: Power System Protection, pp.207-225, Elsevier Ltd, 2005.

[34] Power System Relaying Committee: "IEEE Guide for AC Generator Protection", IEEE Std C37.102-1995.

[35] G.J. Lloyd, H.T. Yip, G. Millar: "Operation, Design and Testing of generator 100% Stator Earth Fault Protection Using Low Frequency Injection", IET 9th International conference on Developments in Power System Protection, 2008.

[36] Rotating Machinery Protection Subcommittee: “Loss-of-Field Relay Operation during System Disturbances”, IEEE Transactions on Power Apparatus and Systems, Vol. PAS-94, No. 5, September/October 1975.

[37] Charles R. Arndt, McClennon Rogers: “A Study of Loss-of-Excitation Relaying and Stability of a 555 MVA Generator on the Detroit Edison System”, IEEE Transactions on Power Apparatus and Systems, Vol. PAS-94, No. 5, September/ October 1975.

[38] Rotating Machinery Protection Subcommittee: “Out of Step Relaying for Generators”, IEEE Transactions on Power Apparatus and Systems, Vol. PAS-96, No. 5, September/October 1977.

[39] Electric Machinery Committee: “IEEE Standard for Cylindrical-Rotor 50 Hz and 60 Hz Synchronous Generators Rated 10 MVA and Above”, IEEE/ANSI C50.14, 2006.

[40] Power System Relaying Committee: “IEEE Guide for Abnormal Frequency”, IEEE Std C37.106-1987.

[41] Rationalized User Specification: “Electricity Supply – Quality of Supply, Part 2: Voltage Characteristics, Compatibility Levels, Limits and Assessment Methods”, Technology Standardization Department (TSD), Eskom, 1993.

[42] U.A. Bakshi, M.V. Bakshi: “Protection and Switchgear”, Technical Publications Pune, India, 2006.

[43] “Differential Protection SPAD 346 C3 Application and Setting Guide”, ABB, 2005.

[44] J.W. Pope , “A comparison of 100% Stator Ground Fault Protection Schemes for Generator Stator Windings”, IEEE Transactions on Power Apparatus and Systems, Vol. PAS-103, No. 4, April 1984, pp. 832 -840.

[45] C.H. Griffin, J.W. Pope, “Generator Ground Fault Protection Using Overcurrent, Overvoltage, and Undervoltage Relays”, IEEE Transactions on Power Apparatus and Systems, Vol. PAS-101, No. 12, December 1982, pp. 4490 – 4501.

[46] R.L. Schlake, G.W. Buckley, G. McPherson, “Performance of Third Harmonic Ground Fault Protection Schemes for Generator Stator Windings”, IEEE Transactions on Power Apparatus and Systems, Vol. PAS-100, No. 7, July 1981, pp. 3195 – 3202.

[47] N. Salomon, “New Experiences in the Application of 100% Stator Earth Fault Protection Relays Evaluating the 3rd Harmonic of the Generator Voltage”.

[48] M. Fulczyk, R. Mydlikowski, “Influence of Generator Load Conditions on Third-Harmonic Voltages in Generator Stator Winding”, IEEE Transactions on Energy Conversion, Vol. 20, No. 1, March 2005, pp. 158 – 165.

[49] R.J. Marttila, “Design Principles of A New Generator Stator Ground Relay for 100% Coverage of the Stator Winding”, IEEE Transactions on Power Delivery, Vol. PWRD-1, No. 4, October 1986, pp. 41 – 51.

[50] L. Pazmandi, “Stator Earth-Leakage Protection for Large Generators”, IEEE Transactions on Power Apparatus and Systems, Vol. PAS-94, No. 4, July/August 1975, pp. 1436 – 1439.